UNIVERSIDAD AUTÓNOMA DE MADRID

Programa de Doctorado en Microbiología

Role of the interferon-stimulated gene 15 (ISG15) as a regulator of macrophage metabolism after *Vaccinia virus* infection

Manuel Albert Sola

Tesis doctoral

Madrid, 2022

UNIVERSIDAD AUTÓNOMA DE MADRID

Programa de Doctorado en Microbiología

Departamento de Medicina Preventiva, Salud Pública y Microbiología

Facultad de Medicina

Role of the interferon-stimulated gene 15 (ISG15) as a regulator of macrophage metabolism after *Vaccinia virus* infection

Memoria de tesis doctoral presentada por el Graduado en Biología

Manuel Albert Sola

para optar al título de Doctor por la Universidad Autónoma de Madrid

Directora de tesis: **Dra. Susana Guerra García**

Madrid, 2022

A mi madre, a mi padre.

A mi familia y amigos.

A Celia.

“Si no conozco una cosa, la investigaré”

Louis Pasteur

AGRADECIMIENTOS

El hecho de estar escribiendo estas palabras supone que una etapa importante ha llegado a su fin. El fin de la tesis doctoral. Una aventura en la que siempre tuve claro que me embarcaría, motivado por mi curiosidad y mi afán investigador. Un camino tan arduo como gratificante, a lo largo del cual las personas que te rodean son fundamentales para mantener el ritmo, no tropezar y llegar sano y salvo a destino. Yo he llegado. Por tanto, solo queda agradecer.

A mi directora de tesis, Susana. Gracias por abrirme las puertas del laboratorio allá por 2016, permiténdome adentrarme de lleno en el apasionante (y agotador) mundo de ISG15. Gracias por tu trabajo y esfuerzo durante estos años, por siempre ofrecerme oportunidades para mejorar profesionalmente y, sobre todo, por tus ánimos y motivación cuando afloraba mi lado más pesimista.

A mis compañeros de laboratorio a lo largo de esta etapa. A los que están, y a los que estuvieron. A Michela, Martina, Carlitos, Rocío, Celine, Ana, Diego. Gracias por vuestra ayuda, vuestros consejos y vuestro apoyo. Gracias por los momentos vividos, dentro y fuera del laboratorio. Sois parte de esta tesis. Gracias también a todas aquellas personas cuya estancia en el laboratorio ha sido menos duradera. De algún modo u otro, habéis contribuido a que este trabajo sea posible.

A mis compañeros del Departamento de Bioquímica. A Diego, Marta Celorio, Ángela, Raúl, Pablo, Marta Paz, Omar, y un largo etcétera. Conoceros supuso un antes y un después en mi doctorado. Gracias a vosotros he disfrutado esta etapa.

A la gente del Instituto de Biología y Genética Molecular de Valladolid. Al profesor Jesús Balsinde y a la Dra. María Ángeles Balboa por acceder a colaborar con nosotros. A Laura y a Clara, así como al resto del equipo. Gracias por acogerme desde el minuto uno y por ayudarme siempre que lo he necesitado.

A la gente de UCLA. Gracias al profesor Marc Liesa por darme la oportunidad de pasar un maravilloso verano en su laboratorio, por compartir sus ideas y ayudarme en todo lo posible. Gracias al profesor Orian Shirihai por hacerme sentir uno más del equipo desde el primer momento. Gracias a Rebeca por portarse tan bien conmigo allá donde hemos coincidido. Gracias a Cynthia, Lucía, Jenny, Michaela, Vince, Anton, Siyouneh, y demás personas que conocí durante mi estancia en UCLA. Ha sido una experiencia inolvidable.

A la gente del CNIC. Al Dr. Miguel Sánchez-Álvarez y a la Dra. Irene Fernández-Delgado por ayudarme aportando ideas y reactivos.

Por último, quiero dar las gracias a las personas que han estado a mi lado desde siempre.

A Carlos, mi hermano de otra madre. Gracias por estar ahí siempre que lo he necesitado. Tenerte cerca ha sido fundamental, aunque sé que puedo contar contigo en la distancia. Ambos sabemos que lo que unió el *garbanzo* jamás podrá separarse.

A mis amigos de Alicante, mi familia por elección, los *pollis*. Alex, Raquel, Alberto, Andrea, Vicky, Lorena, Guille. Gracias por todo, hay poco más que decir.

A mis padres y a mi familia por confiar en mi, por todo su amor y su apoyo.

A Celia. Gracias por estar a mi lado todos estos años, por ayudarme, motivarme e impulsarme a ser mejor. Especialmente, gracias por tu paciencia y tu apoyo en esta última etapa, la más dura con diferencia. Por muchos más momentos juntos.

ABSTRACT

RESUMEN

ABSTRACT

The production of interferons (IFNs) is one of the most relevant and best known antiviral strategies of the innate immune response. IFNs induce the expression of a wide variety of IFN-stimulated genes (ISGs), being *Isg15* one of the most highly expressed ISGs. *Isg15* encodes the protein ISG15, a ubiquitin-like protein that modulates the cell proteome through non-covalent and covalent interactions with target proteins. ISG15 is also secreted out of the cell, acting as a cytokine that regulates immune cell functions. ISG15 was first identified as an antiviral molecule, but research along the last two decades has demonstrated that ISG15 participates in the regulation of diverse cellular pathways, from genome replication to energy metabolism. In this work, we explored the role of ISG15 in the regulation of macrophage metabolism, as well as the relevance of ISG15 in the interaction between macrophages and *Vaccinia virus* (VACV) from a metabolic point of view. For that purpose, we used a proteomics and lipidomics-based approach, which revealed alterations in mitochondrial and lipid metabolism in *Isg15-/-* bone marrow-derived macrophages (BMDM). Our results demonstrated that *Isg15-/-* BMDM display impaired OXPHOS and ROS production, increased mitochondrial fusion, and defective mitophagy, concomitant with accumulation of mitochondrial proteins. Regarding lipid metabolism, *Isg15-/-* BMDM showed increased levels of proteins involved in lipid hydrolysis and oxidation compared with *Isg15+/+* BMDM, consistent with a strong decrease in neutral lipid levels, reflected by reduced lipid droplet number and size. Such changes, however, were not linked to increased fatty acid oxidation. VACV provoked a marked inhibition of both *Isg15* expression and ISG15 conjugation to target proteins, causing similar mitochondrial alterations to those observed in *Isg15-/-* BMDM. As well, VACV-infected BMDM showed increased levels of proteins involved in lipid uptake and storage, consistent with higher neutral lipid content compared with uninfected cells. The alterations on lipid metabolism caused by VACV were stronger in *Isg15-/-* BMDM, suggesting that ISG15 is required to restrict the metabolic reprogramming induced by VACV infection. Furthermore, both the absence of ISG15 and VACV infection of BMDM led to the development of a mixed activation phenotype, showing features of both M1 and M2 polarization. Last, we investigated the role of ISG15 in the regulation of VACV morphogenesis and spread in mouse embryonic fibroblasts (MEF), and detected a reduction in actin tail formation and extracellular virus release in *Isg15-/-* MEF. This was consistent with the accumulation of intracellular virus particles, the abrogation of comet-shaped plaques, and changes in the virion proteome of viruses purified from *Isg15-/-* or *Isg15+/+* MEF. Overall, this work introduces ISG15 as a novel regulator of macrophage metabolism, and highlights its importance in the interplay between VACV and the host.

RESUMEN

La producción de interferones (IFNs) es una de las estrategias antivirales más importantes y mejor conocidas de la respuesta inmunitaria innata. Los IFNs inducen la expresión de una gran variedad de genes estimulados por IFN (ISGs), siendo *Isg15* uno de los ISGs más expresados. *Isg15* codifica la proteína ISG15, una proteína de tipo ubiquitina que modula el proteoma celular a través de interacciones covalentes y no covalentes con sus proteínas diana. ISG15, además, es secretado fuera de la célula, donde actúa como una citoquina modulando las funciones de las células del sistema inmunitario. Inicialmente, ISG15 fue identificado como una molecula antiviral, pero investigaciones a lo largo de las dos últimas décadas han demonstrado que ISG15 participa en la regulación de diversos procesos celulares, desde la replicación del ADN hasta el metabolismo energético. En este trabajo exploramos el papel de ISG15 en la regulación del metabolismo del macrófago, así como su importancia en la interacción entre el macrófago y el virus *Vaccinia* (VACV) desde un punto de vista metabólico. Para ello, empleamos un abordaje basado en técnicas proteómicas y lipidómicas, que revelaron alteraciones en el metabolismo mitocondrial y lipídico en macrófagos de médula ósea de ratón (BMDM) *Isg15-/-*. Nuestros resultados demostraron que los BMDM *Isg15-/-* muestran defectos en la fosforilación oxidativa y la producción de especies reactivas de oxígeno, así como un aumento en la fusión mitocondrial y defectos en la mitofagia, de acuerdo con una acumulación de proteínas mitocondriales. En cuanto al metabolismo lipídico, los BMDM *Isg15-/-* mostraron un aumento en los niveles de proteínas implicadas en hidrólisis y oxidación de lípidos, en línea con una marcada reducción en el contenido de lípidos neutros, que se vió reflejada en un menor número y tamaño de gotas lipídicas. Sin embargo, estas alteraciones no estaban asociadas a un aumento de la oxidación de ácidos grasos. VACV provocó una marcada inhibición tanto de la expresión de *Isg15* como de la conjugación de ISG15 a proteínas diana, causando alteraciones mitocondriales similares a las observadas en BMDM *Isg15-/-*. Además, BMDM infectados con VACV mostraron mayores niveles de proteínas implicadas en captación y almacenamiento de lípidos, de acuerdo con mayores niveles de lípidos neutros en comparación con células no infectadas. Las alteraciones en el metabolismo lipídico causadas por VACV fueron más acusadas en BMDM *Isg15-/-*, lo que sugiere que ISG15 es necesario para limitar la reprogramación metabólica inducida por VACV. Asimismo, tanto la ausencia de ISG15 como la infección por VACV de los BMDM condujeron al desarrollo de un fenotipo de activación mixto, mostrando características tanto de polarización M1 como de M2. Por último, investigamos el papel de ISG15 en la regulación de la morfogénesis y diseminación de VACV en fibroblastos embrionarios de ratón (MEF), y detectamos una reducción en la formación de colas de actina y en la liberación de virus extracelular. Esto fue consistente

con una acumulación intracelular de partículas virales, la abolición de la formación placas de tipo cometa, y cambios en el proteoma de viriones purificados de MEF *Isg15-/-* o *Isg15+/+*. En conjunto, este trabajo presenta a ISG15 como un nuevo regulador del metabolismo del macrófago, y resalta su importancia en la interacción entre VACV y su hospedador.

INDEX

INDEX

ABBREVIATION KEY

ABBREVIATION KEY

25HC	25-hydroxycholesterol
ABC	ATP binding cassette subfamily (protein)
ACAC	Acetyl-CoA carboxylase
ACAD	Acyl-CoA dehydrogenase
ACAT	Acyl-CoA:cholesterol acyltransferase
AMP	Adenosine monophosphate
AMPK	AMP-activated protein kinase
APOA1	Apolipoprotein A1
ARG1	Arginase 1
ATG	Autophagy-related gene
ATGL	Adipose triglyceride lipase
ATP	Adenosine triphosphate
BMDM	Bone marrow-derived macrophages
C/EBP	CCAAT/enhancer binding protein
CARD	Caspase-recruitment domain
CD	Cluster of differentiation
CE	Cholesterol ester
CEV	Cell-associated enveloped virus
cGAS	Cyclic GMP-AMP synthase
CH25HC	Cholesterol-25-hydroxylase
CI	Mitochondrial respiratory complex I
CII	Mitochondrial respiratory complex II
CIII	Mitochondrial respiratory complex III
CIV	Mitochondrial respiratory complex IV
CLR	C-type lectin receptor
CoA	Coenzyme A
COVID-19	*Coronavirus* disease 19
CPT	Carnitine palmitoyl transferase
CV	Mitochondrial respiratory complex V
DAG	Diacylglycerol
DAMP	Danger-associated molecular pattern
DAPI	2-(4-amidinophenyl)-1H -indole-6-carboxamidine
DGAT	Diacylglycerol acyltransferase
DMEM	Dulbecco's Eagle Modified Medium
DNA	Deoxyribonucleic acid
DRP1	Dynamic-related protein 1
ECAR	Extracellular acidification rate
EGFR	Epidermal growth factor
eIF2	Eukaryotic translation initiation factor 2
ER	Endoplasmic reticulum
ERK	Extracellular signal-regulated kinase
ERR	Estrogen-related receptor
ESCRT	Endosomal sorting complex required for transport
ETC	Electron transport chain
EV	Extracellular virus
FA	Fatty acid
$FADH_2$	Flavin adenine dinucleotide (reduced)
FAO	Fatty acid oxidation
FAS	Fatty acid synthesis
FASN	Fatty acid synthase

FBS	Fetal bovine serum
FCCP	Carbonyl cyanide-p-trifluoromethoxyphenylhydrazone
FDPS	Farnesyl pyrophosphate synthase
FIS1	Fission protein 1
FPP	Farnesyl pyrophosphate
G3P	Glycerol-3-phosphate
GAS	Gamma activated sequence
GPAT	Glycerol-3-phosphate acyltransferase
GTP	Guanosine triphosphate
HBV	*Hepatitis B virus*
HCMV	*Human Cytomegalovirus*
HCV	*Hepatitis C virus*
HDL	High-density lipoprotein
HIF1α	Hypoxia-inducible factor 1
HMGCR	3-hydroxy-3-methyl glutaryl-CoA reductase
HMGCS	3-hydroxy-3-methyl-glutaryl-CoA synthase
HPV	*Human Papilomavirus*
HSL	Hormone-sensitive lipase
HSV	*Human Herpesvirus*
IAV	*Influenza A virus*
IBV	*Influenza B virus*
IFN	Interferon
IFNAR	Interferon α receptor
IFNGR	Interferon γ receptor
IFNLR	Interferon λ receptor
IHD-J	International Health Department-J (VACV strain)
IL	Interleukin
IMM	Inner mitochondrial membrane
IMS	Intermembrane space
iNOS	Inducible nitric oxide synthase
INSIG	Insulin-induced gene protein
IPA	Ingenuity Pathway Analysis
IRF	Interferon regulatory factor
ISG	Interferon-stimulated gene
ISGF	Interferon-stimulated gene factor
ISRE	Interferon-stimulated response element
JAK	Janus kinase
LCFA	Long-chain fatty acid
LC-MS/MS	Liquid chromatography-tandem mass spectrometry
LD	Lipid droplet
LDAH	Lipid droplet-associated lipase
LDL	Low-density lipoprotein
LDLR	Low-density lipoprotein receptor
LFA-1	Lymphocyte function-associated antigen 1
LIPA	Lysosomal acid lipase
LPAT	Lysophosphatidate acyltransferase
LPS	Lipopolysaccharide
LXR	Liver X receptor
MAG	Monoacylglycerol
MAPK	Mitogen-activated protein kinase
MAVS	Mitochondrial antiviral signaling protein
MDA5	Melanoma differentiation-associated gene 5
MEF	Mouse embryonic fibroblast
MFF	Mitochondrial fission factor
MFN	Mitofusin

MGLL	Monoglyceride lipase
MM	Mitochondrial matrix
MOI	Multiplicity of infection
mtDNA	Mitochondrial DNA
mTOR	Mammalian target of rapamycin
mtUPR	Mitochondrial unfolded protein response
MV	Mature virus
NADH	Nicotinamide adenine dinucleotide (reduced)
NCEH1	Neutral cholesterol ester hydrolase 1
NF-κB	Nuclear factor-*kappa* B
NK	Natural killer (cell)
NL	Neutral lipid
NLR	NOD-like receptor
NLRP3	NOD-, LRR- and pyrin domain containing 3 (protein complex)
NO	Nitric oxide
NOD	Nucleotice-binding and oligomerization domain
NRF	Nuclear respiratory factor
OA	Oleic acid
OCR	Oxygen consumption rate
OMM	Outer mitochondrial membrane
OPA1	Optic atrophy 1 protein
OPLS	Orthogonal partial least-squares to latent structures
OXPHOS	Oxidative phosphorylation
PA	Phosphatidic acid
PaCSC	Pancreatic cancer stem cell
PAGE	Polyacrylamide gel electrophoresis
PAMP	Pathogen-associated molecular pattern
PBS	Phosphate buffered saline
PC	Phosphatidylcholine
PCA	Principal component analysis
PE	Phosphatidylethanolamine
PFA	Paraformaldehyde
PFU	Plaque-forming units
PG	Phosphatidylglycerol
PGC	PPAR *gamma* coactivator
PI	Phosphatidylinositol
PINK1	PTEN-induced kinase 1
PK	Proteinase K
PKB	Protein kinase B
PKR	Protein kinase R
PL	Phospholipid
PLIN	Perilipin
PLpro	Papain-like protease
PPAR	Peroxisome proliferation-activated receptor
PPP	Pentose phosphate pathway
PRR	Pattern-recognition receptor
PS	Phosphatidylserine
RIG-I	Retinoic acid-inducible gene I
RLR	RIG-I-like receptor
RNA	Ribonucleic acid
RNS	Reactive nitrogen species
ROR	Retinoic acid receptor-related orphan receptor
ROS	Reactive oxygen species
RT	Room temperature
RXR	Retinoid X receptor
SARS-CoV-2	Severe acute respiratory syndrome *Coronavirus* 2
SC	Supercomplex (mitochondrial)

SCAP	SREBP-cleavage activating protein
SDS	Sodium dodecyl sulphate
SOAT	Sterol-O-acyltransferase
SOD2	Superoxide dismutase 2
SREBP	Sterol regulatory element-binding protein
STAT	Signal transducer and activator of transcription
STING	Stimulator of interferon genes
TAG	Triacylglycerol
TBK1	TRAF binding kinase 1
TBS	Tris buffered saline
TCA	Tricarboxylic acid
TEM	Transmission electron microscopy
TF	Transcription factor
TFAM	Mitochondrial transcription factor
TFB	Mitochondrial transcription factor B
TLR	Toll-like receptor
TNF	Tumor necrosis factor
TOM	Translocase of outer membrane
TRAF	TNF receptor-associated factor
TSG101	Tumor susceptibility gene 101
TYK	Tyrosine kinase
UHPLC	Ultra-high performance liquid chromatography
UPR	Unfolded protein response
USP18	Ubiquitin-specific protease 18
VACV	*Vaccinia virus*
VDAC	Voltage-dependent anion channel
VGF	Viral growth factor
VLDL	Very low-density lipoprotein
WR	Western Reserve (VACV strain)
WV	Wrapped virus

INTRODUCTION

1. INTRODUCTION

1.1 The innate immune response

The innate immune response is the first line of defense against an invading pathogen or a potential danger. Immune cells can recognize pathogen- and danger-associated molecular patterns (PAMPs and DAMPs, respectively) through specific molecules known as pattern-recognition receptors (PRRs), and thus develop an adequate response to avoid damage (Brubaker, Bonham, Zanoni, & Kagan, 2015). Different PRRs exist, which are classified in five main classes: Toll-like receptors (TLRs), retinoic acid-inducible gene-I (RIG-I)-like receptors (RLRs), nucleotide-binding and oligomerization domain (NOD)-like receptors (NLRs), C-type lectin receptors (CLRs), and cytosolic sensors of deoxyribonucleic acid (DNA). The activation of these receptors triggers different signaling pathways that lead to the production of interferons (IFNs), proinflammatory cytokines and chemokines, which aid to establish an antiviral state (Geijtenbeek & Gringhuis, 2009; Kumar, Kawai, & Akira, 2011) (Figure 1).

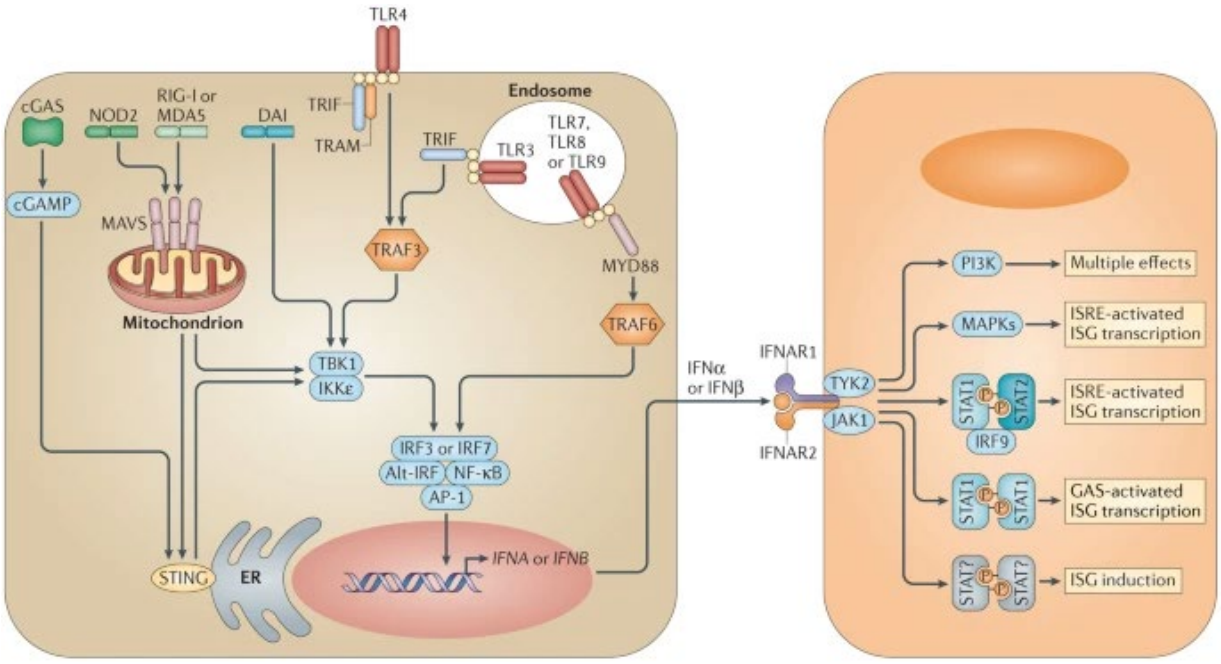

Figure 1. PAMP recognition and type I IFN signaling. PAMPs and DAMPs are sensed through intracellular and membrane-associated PRRs, which include membrane-associated receptors (e.g., TLRs) and citoplasmic nucleic acid sensors (e.g., STING, RIG-I). The detection of PAMPs and DAMPs triggers intracellular signaling cascades that culminate in the production of type I IFNs, which are secreted out of the cell. Binding of type I IFNs to IFNAR activates the JAK-STAT signaling pathway, enhancing the expression of IFN-stimulated genes (ISGs), which play diverse roles that contribute to set up an effective immune response. Adapted from (McNab, Mayer-Barber, Sher, Wack, & O'Garra, 2015).

1.1.1. Interferons

In the early 1950s, experiments with animal viruses revealed the existence of a substance that interfered with viral infections (Henle, 1950). A few years later, in 1957, Isaacs and Lindenmann used the term “interferon” to describe that unknown substance able to interfere with *Influenza virus* (Isaacs & Lindenmann, 1957; Isaacs, Lindenmann, & Valentine, 1957). In the following decades, IFNs were identified as not one protein, but a family of small proteins, produced and secreted by cells in response to different stimuli, and responsible for a wide range of immune and regulatory functions (Lengyel, 1982).

IFNs are classified in three types, based on their genetic, structural, and functional features (S. F. Li et al., 2018). Type I IFNs were the first to be discovered, and comprise 8 groups: IFN-α, IFN-β, IFN-δ, IFN-ε, IFN-κ, IFN-τ and IFN-ω (Mazewski, Perez, Fish, & Platanias, 2020). Type I IFNs bind to IFN-α receptor (IFNAR), a heterodimeric protein complex consisting of IFNAR1 and IFNAR2 subunits. This class of IFNs is present in almost every cell, and exerts a wide range of functions, from antiviral signaling to immunomodulation (Schneider, Chevillotte, & Rice, 2014). Type II IFN is only represented by IFN-γ, and its production is restricted to immune cells, principally natural killer (NK) cells (A. J. Lee & Ashkar, 2018). It forms a homodimer and binds to the IFN-γ receptor (IFNGR) complex, formed by two IFNGR1 subunits and two additional IFNGR2 subunits. Its main function is the development of cellular immunity by connecting and regulating innate and adaptive immune responses (Schneider et al., 2014). The third type of IFNs includes IFN-λ1, IFN- λ2, IFN- λ3, also known as interleukin (IL)-29, IL-28-A and IL-28B, respectively (Kotenko et al., 2003), and the recently identified IFN- λ4 (Prokunina-Olsson et al., 2013). Type III IFNs bind to a heterodimeric protein formed by the IFN-λ receptor 1 (IFNLR1) and the IL-10 receptor 2 (IL-10R2). IFNLR1 shows high affinity for type III IFNs, but its expression is limited to epithelial cells and a subset of immune cells. However, IL-10R2 is widely distributed and, despite its lower affinity, it broadens the range of action of this type of IFNs (Sommereyns, Paul, Staeheli, & Michiels, 2008; Stanifer, Guo, Doldan, & Boulant, 2020). Type III IFNs are structurally different to type I IFNs, but both types share components of the intracellular signaling cascade; therefore, their functions are similar, and even induce many of the same genes (Schneider et al., 2014; Stanifer et al., 2020).

1.1.2. Interferon signaling: the JAK-STAT pathway

Binding of IFNs to their specific receptors in the cell membrane starts a rapid intracellular signaling cascade that results in the transcriptional activation and expression of hundreds of IFN-stimulated genes (ISGs) (Schneider et al., 2014). This signaling pathway, known as the JAK-STAT pathway, is mediated by Janus kinases (JAK) and signal transducer and activator of transcription (STAT) proteins (Darnell, Kerr, & Stark, 1994).

1.1.2-A. Janus kinases (JAK) and signal transducer and activator of transcription (STAT) proteins

Four kinases form the JAK family in mammals: JAK1, JAK2, JAK3 and tyrosine kinase 2 (TYK2). Of the four, JAK1, JAK2 and TYK2 participate in IFN-mediated signaling, while JAK3 is mainly involved in signaling of γc cytokines (Gadina et al., 2020). JAK kinases are constitutively associated to intracellular domains of IFN receptors, but remain inactive in terms of signal transduction, although they contribute to the stability, localization and trafficking of these receptors (Haan, Kreis, Margue, & Behrmann, 2006). The STAT family includes seven STAT proteins in mammals (STAT1, STAT2, STAT3, STAT4, STAT5a, STAT5b and STAT6), being STAT1 and STAT2 the most relevant in IFN signaling (Schneider et al., 2014). STATs are cytoplasmic proteins with a dual role, both transducing signals from cytokines and growth factors through the cytoplasm, and activating transcription of numerous genes in the nucleus (Levy & Darnell, 2002).

1.1.2-B. Type I interferon signaling pathway

The JAK-STAT signaling pathway can be defined as essential. Not only IFNs, but more than 50 cytokines and growth factors depend on this route (Villarino, Kanno, & O'Shea, 2017). Hence, different mechanisms participate in its regulation to ensure proper functioning (Shuai & Liu, 2003). Signaling through the JAK-STAT pathway requires roughly three steps: 1) binding of cytokines to their cell surface receptors; 2) signal transduction by the sequential activation of cytoplasmic proteins; and 3) translocation of transcription factors (TFs) to the nucleus and modulation of gene expression (Kisseleva, Bhattacharya, Braunstein, & Schindler, 2002). Despite the wide array of cytokines that signal through this pathway, here type I IFN signaling will be briefly described.

The detection of PAMPs and DAMPs by specific PRRs starts downstream signaling pathways that culminate in the activation of TFs such as nuclear factor-*kappa* B (NF-κB), IFN regulatory factor (IRF)-3 and IRF-7. Once activated, these factors promote transcription and production of type I IFNs (Kawasaki & Kawai, 2014) (Figure 1). Secreted type I IFNs act as both autocrine and paracrine cytokines and bind to IFNAR receptors at the cell surface. Upon binding of IFNs, IFNAR1 and IFNAR2 subunits oligomerize and the JAK proteins JAK1 and TYK2, (associated to

IFNAR1 and IFNAR2, respectively) approximate to each other, allowing their activation by transphosphorylation (Platanias, 2005). Once activated, JAKs phosphorylate key tyrosine residues located in the cytoplasmic domains of IFNARs, which act as binding sites for STAT proteins (Morris, Kershaw, & Babon, 2018). STATs are then recruited and activated by JAK-mediated phosphorylation, what leads to STAT dimerization. Type I IFNs can induce the formation of STAT1 homodimers and STAT1/STAT2 heterodimers. On one hand, STAT1/STAT2 heterodimers bind to IRF9 and form the IFN-stimulated gene factor 3 (ISGF3). ISGF3, once in the nucleus, binds to IFN-stimulated response elements (ISRE) in the DNA and promotes the expression of ISGs. On the other hand, STAT1 homodimers translocate to the nucleus and stimulate the production of ISGs by binding to the consensus gamma activated sequences (GAS) (Mazewski et al., 2020; Platanias, 2005) (Figure 1). Altogether, these signals result in the production of ISGs and proinflammatory cytokines to set up an efficient antiviral state.

1.2. Interferon-stimulated gene 15 (ISG15)

1.2.1. The ISG15/ISGylation system

The *interferon-stimulated gene 15* (*Isg15*) codifies the protein ISG15, a 15-kDa small ubiquitin-like modifier consisting of two ubiquitin-like domains connected by a polypeptide “hinge” region (Narasimhan et al., 2005) (Figure 2A). It is one of the most highly induced ISGs in response to type I IFN (Der, Zhou, Williams, & Silverman, 1998), but its expression is also stimulated by type II and type III IFNs (Cai et al., 2017; J. L. Taylor, D'Cunha, Tom, O'Brien, & Borden, 1996; Tecalco Cruz & Mejia-Barreto, 2017), viral and bacterial infections (Radoshevich et al., 2015; Yuan & Krug, 2001), lipopolysaccharide (LPS) (O. Malakhova, Malakhov, Hetherington, & Zhang, 2002), retinoic acid (Pitha-Rowe, Hassel, & Dmitrovsky, 2004), aging (Lou et al., 2009) and genotoxic stressors (Jeon, Park, & Chung, 2017). ISG15 has been found only in vertebrates and it shows high sequence variability between species. Some authors suggest that this variability implies functional diversity, while others argue that only specific regions of ISG15 need to be conserved to serve its functions (Dzimianski, Scholte, Bergeron, & Pegan, 2019).

As a ubiquitin-like protein, ISG15 is capable of binding proteins through a process termed ISGylation (D. Zhang & Zhang, 2011) (Figure 2B). The expression of ISG15 results in the synthesis of a 17-kDa precursor, which is proteolytically processed into a 15-kDa mature form. This cleavage exposes a carboxy-terminal LRLRGG motif essential for ISGylation, as conjugation of ISG15 and target proteins takes place through the formation of a covalent bond between the last glycine residue of ISG15 and a lysine residue of the target protein (Durfee & Huibregtse, 2012; Potter, Narasimhan, Mende-Mueller, & Haas, 1999). Like ubiquitylation, ISGylation occurs

in three sequential steps, in which participate activation (E1), conjugation (E2) and ligation (E3) enzymes (Figure 2B). UBE1L is the enzyme responsible for binding and activating ISG15, with the consumption of adenosine triphosphate (ATP) (Yuan & Krug, 2001). ISG15 is then transferred to UBCM8 (mouse) or UBCH8 (human), that act as conjugation enzymes (K. I. Kim, Giannakopoulos, Virgin, & Zhang, 2004). In the third and last step, ISG15 is covalently bound to target proteins by the ligation enzymes HERC5 or HERC6 (mouse or human, respectively), TRIM25 and ARIH1 (D. Zhang & Zhang, 2011).

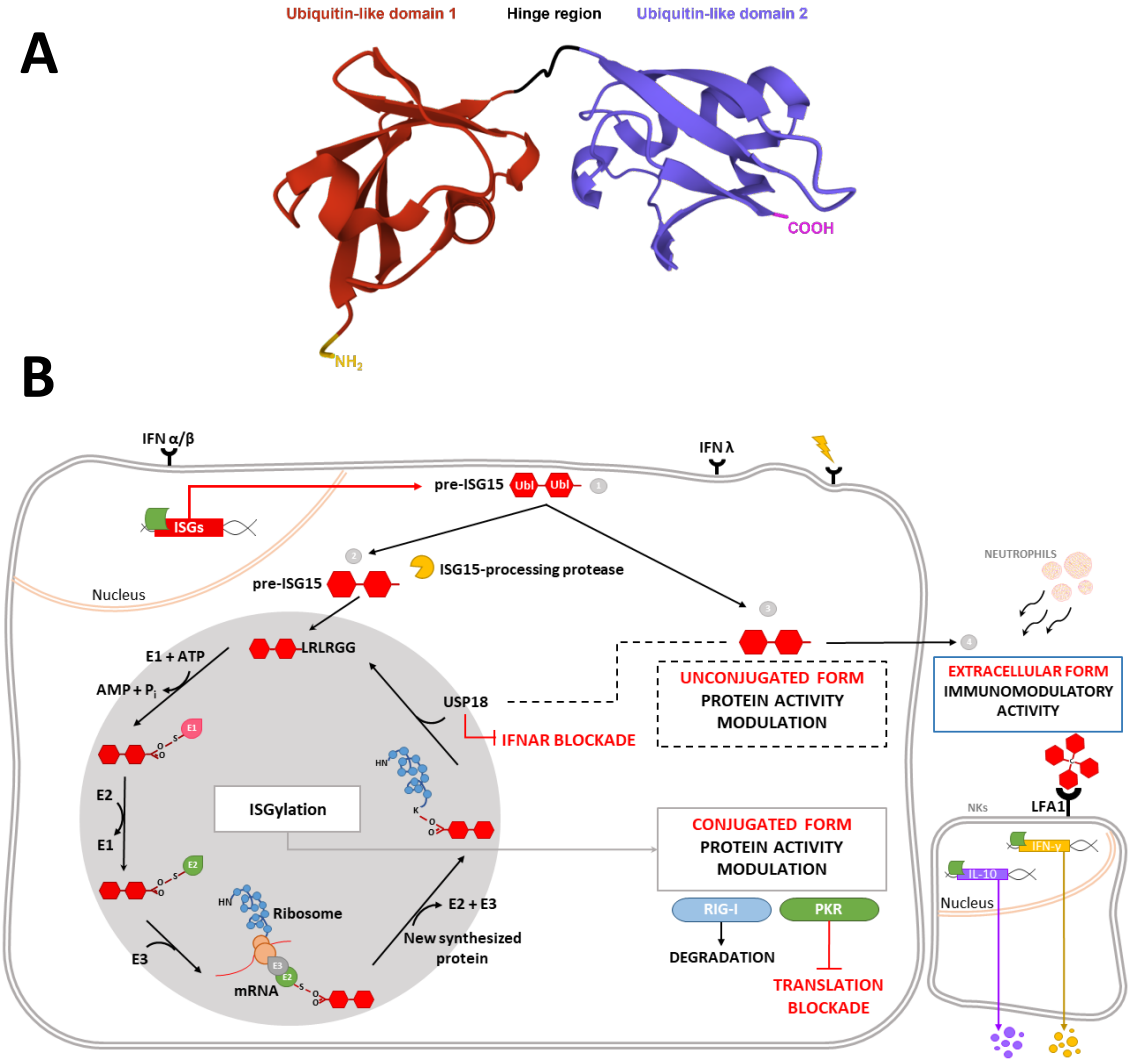

Figure 2. ISG15 and the ISGylation system. A) ISG15 tertiary structure, representing the two ubiquitin-like domains (red and blue) connected by the 'hinge region' (black). N- and C-terminus are represented (yellow and pink, respectively). Source: rcsb.org. B) The ISG15/ISGylation system. IFNs and stressors stimulate the synthesis which undergoes proteolytic processing. Inside the cell, mature ISG15 can be conjugated to target proteins through ISGylation, or remain as a free molecule, modulating protein activity

and turnover. Secreted extracellular ISG15 acts as a cytokine and exerts diverse immunomodulatory functions. Reproduced from (Albert, Becares, Falqui, Fernandez-Lozano, & Guerra, 2018).

One key feature of ISGylation is that ISG15 is conjugated to *de novo* synthesized proteins in a co-translational manner (Durfee, Lyon, Seo, & Huibregtse, 2010), and only to a small fraction of the total pool of a target protein (C. Zhao, Denison, Huibregtse, Gygi, & Krug, 2005). Even so, the effects of such small changes are enormous, what remarks the relevance of ISG15. Furthermore, it was demonstrated that ISG15 dimerizes through cysteine residues of the hinge region, and that disruption of dimerization regulates ISGylation levels (F. Okumura, Lenschow, & Zhang, 2008). Another important aspect of ISGylation is that it is a reversible process. USP18, an ISG15-specific protease, cleaves the covalent bond and releases ISG15 from its targets (Malakhov, Malakhova, Kim, Ritchie, & Zhang, 2002) (Figure 2B). Interestingly, USP18 not only acts as a deconjugase, but also binds to IFNAR, interfering with JAK proteins and negatively regulating type I IFN signaling (O. A. Malakhova et al., 2006). In this way, USP18 regulates the expression of ISG15 and the ISGylation machinery, including USP18 itself, as all these proteins are induced by type I IFN (Durfee & Huibregtse, 2012). Moreover, USP18 is involved in numerous immunological processes, such as autoimmunity, cancer development and infection control (Honke, Shaabani, Zhang, Hardt, & Lang, 2016).

1.2.2. ISG15, a multifunctional regulator of cell homeostasis

The number of functions carried out by ISG15 is continuously increasing. Early studies identified ISG15 as an immunomodulator of NK- and T-cell-mediated immune responses (D'Cunha, Knight, Haas, Truitt, & Borden, 1996). Later on, diverse studies reported ISG15 as an antiviral molecule against a wide array of viruses, both *in vitro* and *in vivo* (Morales & Lenschow, 2013), with the exception of *Hepatitis C virus* (HCV) and *Hepatitis B virus* (HBV), whose replication was impaired in the absence of ISG15 (Broering et al., 2010; Chua et al., 2009; Y. Li et al., 2016). In the recent years, research has linked ISG15 to numerous pathways, including cancer (Han, Moon, & Jeon, 2018), genome stability (Sandy, da Costa, & Schmidt, 2020), intracellular trafficking (Villarroya-Beltri et al., 2016), autophagy (Bhushan et al., 2020; Desai, Reed, Babu, & Lorio, 2013; Falvey et al., 2017), vascular remodeling (Gonzalez-Amor et al., 2021), and energy metabolism (Alcala et al., 2020; Baldanta et al., 2017; Kespohl et al., 2020; S. Yan et al., 2021; Y. Zhang et al., 2019). This ample variety of functions is possible thanks to the versatility in the mode of action of ISG15, as it acts both conjugated to target proteins and as a free molecule, either intracellularly or extracellularly.

1.2.2-A. Roles of protein ISGylation

The identification of ISG15 conjugation targets has always been one of the main challenges in the field. Along the past two decades, great efforts have been made to identify and characterize ISGylated host and pathogen proteins, although the effect of ISGylation remains elusive for the majority of the proteins identified. ISGylation of host proteins has been shown to modulate protein synthesis, activity and turnover. For example, ISGylation of the double-stranded RNA-activated protein kinase (PKR) enhances its activity and downregulates protein translation (F. Okumura et al., 2013). Binding of ISG15 to STAT1 and IRF3 sustains their activation, while conjugation to RIG-I promotes its degradation, thus modulating IFN signaling (Ganesan, Poluektova, Tuma, Kharbanda, & Osna, 2016; M. J. Kim, Hwang, Imaizumi, & Yoo, 2008; Shi et al., 2010). ISGylation also regulates proteins from the ubiquitin-proteasome system, including the ubiquitinases UBC13 and UBCH6, supressing their activity; the ubiquitin ligase PARKIN, promoting its activation and activity; or ubiquitin, whose ISGylation interferes with the turnover of ubiquitylated proteins (Fan et al., 2015; Im, Yoo, Hyun, Shin, & Chung, 2016; Takeuchi, Iwahara, Saeki, Sasajima, & Yokosawa, 2005; Takeuchi & Yokosawa, 2005). Proteins involved in the control of cell cycle and tumorigenesis have also been identified as ISGylation targets, such as p53, PCNA, β-catenin and HIF-1α, whose modification by ISG15 has antitumorigenic outcomes (Huang, Wee, Gunaratne, Lane, & Bulavin, 2014; J. H. Lee et al., 2010; J. H. Park et al., 2016; J. M. Park et al., 2014; Yeh, Yang, Hsieh, Yeh, & Li, 2013).

Pathogen proteins are also targets of ISGylation, being viruses primarily affected. The rapid induction of ISG15 upon virus detection and the increased production of viral components during infection create the ideal conditions for ISGylation of viral proteins. Some well-known examples are the NS1 protein of *Influenza A virus* (IAV), whose ISGylation inhibits its translocation to the nucleus and, therefore, avoids the shut-off of the host antiviral response (Tang et al., 2010; C. Zhao, Hsiang, Kuo, & Krug, 2010); the *Influenza B virus* (IBV) nucleoprotein (NP), that cannot oligomerize when ISGylated, resulting in impaired viral RNA synthesis and virus replication (C. Zhao et al., 2016); and the *Human Papilomavirus* (HPV) capsid protein L1, whose ISGylation interferes with the structure of the viral capsid and results in the production of defective viral progeny (Durfee et al., 2010). It is important to note that the antiviral activity of ISGylation is the result of both the direct effects of the modification of viral proteins, and the indirect effects derived from the modulation of host proteins involved in numerous immune-related pathways (Perng & Lenschow, 2018).

1.2.2-B. Role of unconjugated ISG15

As mentioned earlier, ISG15 not only exerts its functions through conjugation to target proteins, but also as a free molecule, inside the cell or secreted as a cytokine (Dos Santos & Mansur, 2017). Free intracellular ISG15 modulates protein activity and function via non-covalent interactions. Unconjugated ISG15 has been shown to interact with the autophagy mediators HDAC6 and SQSTM1/p62, modulating the autophagic clearance of ISGylated proteins (Nakashima, Nguyen, Goins, & Chiocca, 2015). Non-covalent binding of ISG15 and the ubiquitin E3 ligase NEDD4 disrupts the interplay between NEDD4 and ubiquitin E2 conjugating enzymes, impairing NEDD4-mediated protein ubiquitylation, a necessary process for *Ebolavirus* budding (A. Okumura, Pitha, & Harty, 2008). Interestingly, human ISG15 interacts with USP18, and the interaction leads to the stabilization of USP18 by avoiding its ubiquitination and subsequent degradation by the ubiquitin-26S proteasome system (Tokarz et al., 2004). This sustains USP18-mediated downregulation of type I IFN signaling, avoiding overamplification and autoinflammation events (X. Zhang et al., 2015). As this interaction only occurs in humans, ISG15 deficiency in humans leads to enhanced resistance to viral infections due to increased IFN production (Speer et al., 2016), contrary to what occurs in mice.

Outside the cell, ISG15 is an immunomodulatory cytokine, acting as a chemotactic factor for neutrophils, stimulating maturation of dendritic cells and promoting proliferation of NK cells and IFN-γ secretion (Bogunovic et al., 2012; D'Cunha et al., 1996; Owhashi et al., 2003; Padovan et al., 2002). In addition, ISG15-containing microparticles released from infected macrophages have been shown to stimulate macrophage proinflammatory responses (Hare et al., 2015). Lymphocyte function-associated antigen 1 (LFA-1), also known as CD11a/CD18 integrin, has been identified as an ISG15 receptor, and binding of ISG15 is known to stimulate IFN-γ and IL-10 secretion (Swaim, Scott, Canadeo, & Huibregtse, 2017) (Figure 2B). In this sense, patients with ISG15 deficiency show increased susceptibility to mycobacterial infections, as IFN-γ is an essential component in the restriction of intracellular pathogens (Bogunovic et al., 2012). Interestingly, it was demonstrated that the cystein residues through which ISG15 dimerizes are necessary for the induction of IL-1β secretion by $CD8^+$ dendritic cells, but not for the LFA-1-mediated stimulation of IFNγ secretion by NK cells (Napolitano et al., 2018), suggesting that additional molecules may also act as ISG15 receptors.

How ISG15 is released to the extracellular milieu is still under investigation. Several studies have reported different mechanisms for ISG15 secretion, mainly apoptosis, neutrophil granule secretion and exosomes (Dos Santos & Mansur, 2017; Sun et al., 2016). Recent work

demonstrated that ISG15 is also released from virus-infected macrophages in an autophagy-dependent manner, via an LC3-dependent unconventional secretory pathway (Munnur et al., 2021).

1.2.3. Viral strategies against ISG15 and ISGylation

Viruses have developed different strategies to neutralize the antiviral effects of ISG15 signaling. Some viruses, such as *Human cytomegalovirus* (HCMV) and HCV, inhibit ISG15 expression at the transcriptional level (Foy et al., 2005; Y. J. Kim et al., 2016). Other viruses prevent protein ISGylation. For example, *Vaccinia virus* (VACV) uses its protein E3 to bind ISG15 and block ISGylation, in a similar way that HMCV does via its protein pUL26 (S. Guerra, Caceres, Knobeloch, Horak, & Esteban, 2008; Y. J. Kim et al., 2016). Another mechanism is the sequestration of ISGylated proteins. IBV makes use of its NS1 protein to bind ISGylated NP monomers, avoiding their incorporation in NP oligomers and the disruption of viral RNA synthesis (C. Zhao et al., 2016). Finally, some viruses encode proteins with deISGylase activity, such as ovarian tumor (OTU) domain proteases of nairoviruses and arteriviruses (Frias-Staheli et al., 2007), or the papain-like proteases (PLpro) of coronaviruses, including the novel coronavirus SARS-CoV-2, cause of the current COVID-19 pandemic. Recently, it was demonstrated that the SARS-CoV-2 PLpro preferentially cleaves ISG15 from ISGylated proteins, what increases the levels of free intracellular and extracellular ISG15. This phenomenon positively regulates ISG15-mediated signaling and likely contributes to the cytokine storm reported during SARS-CoV-2 infection (Munnur et al., 2021; Shin et al., 2020; Swaim et al., 2020).

1.3. Immunometabolism, where metabolism meets immune responses

Recent technological advances have led to the development of sophisticated tools that allow the study of metabolic features in great detail. In consequence, the precise metabolic characterization of immune cells has revealed the existence of a close relationship between energy metabolism and immune responses, the so-called immunometabolism. Signaling cascades induced by intracellular and extracellular stimuli regulate metabolic pathways, which are coupled to immune functions through the production of metabolic intermediates with immunomodulatory or antipathogenic effects. Moreover, many of these products are shared between different metabolic pathways, creating an interconnected system that determines cell survival, proliferation and function (O'Neill, Kishton, & Rathmell, 2016).

1.3.1. Mitochondria, the coordinators of immunometabolism

Virtually every cell component has a role in the complex immunometabolic network, but if only one has to be attributed an outstanding relevance, it is the mitochondrion. Mitochondria have

myriad functions in the cell, although they are best known for being the main productors of energy in the form of ATP. To accomplish such an essential task, mitochondria are metabolic hubs where distinct metabolic pathways converge, as well as a source of numerous molecules that serve as metabolic intermediates, confering these organelles the role of regulators of central metabolism.

1.3.1-A. Mitochondrial structure and metabolic functions

Mitochondrial functions are strictly dependent on its structural organization. Mitochondrial structure can be divided in outer mitochondrial membrane (OMM), inner mitochondrial membrane (IMM), the intermembrane space (IMS) between OMM and IMM, and mitochondrial matrix (MM), the innermost compartment. The OMM is smooth and contains transport proteins such as porins (e.g., voltage-dependent anion chanel, VDAC), that allow the free difusion of ions and small, uncharged molecules between mitochondria and the cytoplasm, and specific translocases (e.g., translocase of outer membrane (TOM) complex) responsible for the transport of larger molecules (Neupert & Herrmann, 2007). The IMM is folded into cristae, and it is best known for being the structure where the electron transport chain (ETC) and ATP synthase protein complexes are located (Papa et al., 2012); as well, the IMM harbors translocases that control the molecular trafficking into and out of the MM (Wiedemann & Pfanner, 2017). Last, the MM is the compartment where replication of mitochondrial DNA (mtDNA) and numerous metabolic processes, such as the tricarboxylic acid (TCA) cycle, fatty acid oxidation (FAO), and synthesis of diverse of biomolecules, take place (Friedman & Nunnari, 2014; O'Neill et al., 2016) (Figure 3).

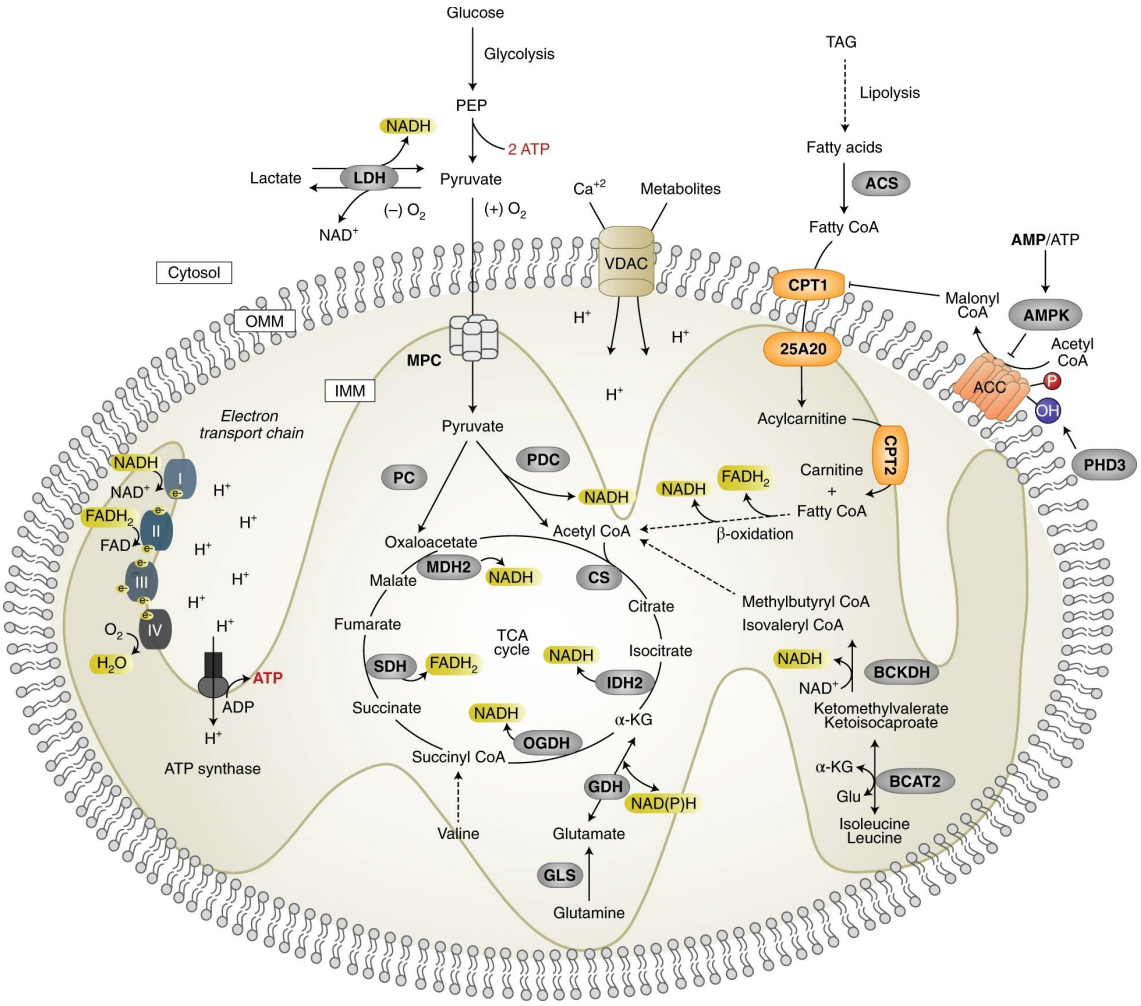

Figure 3. Schematic overview of mitochondrial structure and metabolism. Mitochondrial structure is divided, outside in, in OMM, IMS, IMM and MM. Numerous molecules and metabolites from diverse metabolic pathways are transported across mitochondrial membranes to the matrix, where the main mitochondrial metabolic processes (e.g., the TCA cycle, FAO) occur. These processes generate metabolic intermediates and redox equivalents. Intermediates are used for biosynthesis and immune signaling. Redox equivalents provide the ETC with electrons for ATP synthesis through OXPHOS. Adapted from (Spinelli & Haigis, 2018).

As hubs of cell metabolism and main productors of energy, mitochondria are the destination of a great variety of molecules originated in many different metabolic pathways. These molecules, once in the mitochondrion, converge on an essential mitochondrial process: the TCA cycle. The TCA cycle, also known as the Krebs cycle or the citric acid cycle, consists of a loop of enzymatic reactions that take place in the MM. It starts with the condensation of acetyl coenzyme A (acetyl-CoA) with oxaloacetate to form citrate, by the action of citrate synthase. Citrate then undergoes a series of oxidative reactions that culminate in the generation of oxaloacetate which, again,

enters the cycle (O'Neill et al., 2016). Each round results in the complete oxidation of one molecule of acetyl-CoA to CO_2, and the generation of 3 molecules of reduced nicotinamide adenine dinucleotide (NADH), 2 molecules of reduced flavin adenine dinucleotide ($FADH_2$), and one molecule of guanosine triphosphate (GTP), which can be converted to ATP (Martinez-Reyes & Chandel, 2020). The source of acetyl-CoA is diverse, as it is synthesized in the mitochondrion by descarboxylation of glycolysis-derived pyruvate, or by oxidation of fatty acids (FAs) (Figure 3). On one hand, pyruvate, the end-product of glycolysis, is transported from the cytosol into the MM where it is oxidized to acetyl-CoA by the action of the enzyme pyruvate dehydrogenase (Zangari, Petrelli, Maillot, & Martinou, 2020). On the other hand, FAs are first activated in the cytoplasm by conjugation with CoA, resulting in the formation of acyl-CoAs. Acyl-CoAs are then esterified to carnitine by the carnitine palmitoyl transferase 1 (CPT1) and transported as acylcarnitines across the mitochondrial membranes into the MM, where CPT2 removes carnitine to form acyl-CoAs again. Acyl-CoAs in the MM are then oxidized by the action of acyl-CoA dehydrogenases (ACAD) and the mitochondrial trifunctional protein (Adeva-Andany, Carneiro-Freire, Seco-Filgueira, Fernandez-Fernandez, & Mourino-Bayolo, 2019). This process results in the production of acetyl-CoA and an acyl-CoA molecule two carbon atoms shorter than the starting molecule, which enters the cycle again (Houten, Violante, Ventura, & Wanders, 2016). However, this is a symplistic view of the TCA cycle, as acetyl-CoA is not the only molecule that enters the cycle. Intermediates of the TCA cycle are used as precursors for the synthesis of diverse biomolecules, such as citrate for FA synthesis (FAS), or malate for gluconeogenesis. This requires that products from different metabolic pathways are incorporated into the cycle to replenish intermediates (e.g., glutamine as a source of α-ketoglutarate) and sustain the TCA cycle. This flux of biomolecules into and out of the cycle (also termed anaplerosis and cataplerosis, respectively) has a dual role, supporting both anabolic and catabolic processes, and is a good example of the relevance of mitochondria in the control of whole cell metabolism (Martinez-Reyes & Chandel, 2020; Owen, Kalhan, & Hanson, 2002).

Catabolic pathways such as glycolysis and the TCA cycle generate ATP (or GTP), although the number of molecules produced is not sufficient to sustain cell functions when high amounts of energy are required. However, these processes, together with FAO, generate great amounts of NADH and $FADH_2$, which are used for ATP synthesis via OXPHOS. OXPHOS is an essential mitochondrial process by which most of the ATP is produced, thanks to the orchestrated action of the ETC and ATP synthase protein complexes, located in the IMM. The ETC consists of four protein complexes (NADH:ubiquinone oxidorreductase, complex I (CI); succinate dehydrogenase, complex II (CII); cytochrome c (cyt c) oxidoreductase, complex III (CIII); Cyt c

oxidase, complex IV (CIV)), and two electron carriers (coenzyme Q and cyt c). NADH and $FADH_2$ are oxidized by redox centers in CI and CII, respectively, and the electrons are transported across the ETC to CIV, where electrons reduce O_2 to H_2O. This electron transport is coupled to pumping of protons from CI, CIII and CIV to the IMS, generating a proton motive force that is used by the ATP synthase, also named complex V (CV), to generate ATP by phosphorylation of adenosine diphosphate (ADP) (Yin & O'Neill, 2021). The structure of the OXPHOS machinery is essential for its correct function; therefore, the assembly of the OXPHOS complexes is a sophisticated process subjected to a tight regulation to ensure an efficient respiration (Signes & Fernandez-Vizarra, 2018; Szczepanowska & Trifunovic, 2021). Furthermore, CI, CIII and CIV have been shown to associate into supercomplexes, also known as respirasomes. This association confers stability and reduces electron leak and the formation of reactive oxygen species (ROS), thus maximizing the efficiency of the process (Letts, Fiedorczuk, & Sazanov, 2016).

1.3.1-B. Mitochondrial dynamics and turnover

Mitochondria are highly dynamic organelles that continuously undergo fusion and fission events to meet specific metabolic requirements and to adapt to the ever-changing cellular environment. The process of mitochondrial fusion and fission, also known as motochondrial dynamics, is mediated by GTPases of the dynamin family. Dynamin-related protein 1 (DRP1) is the main responsible for mitochondrial fission. When mitochondrial fission is needed, DRP1 is recruited from the cytoplasm to form spiral structures around mitochondria that constrict and divide these organelles, with the assistance of adaptor proteins such as mitochondrial fission factor (MFF) and mitochondrial fission protein 1 (FIS1) (H. Lee & Yoon, 2016; Loson, Song, Chen, & Chan, 2013). Mitochondrial fusion is mediated by mitofusin 1 (MFN1), MFN2, and OPA1. Mitofusins are required for fusion of the OMM, while OPA1 is responsible for fusion of the IMM and the maintenance of cristae structure (Meeusen et al., 2006; Schrepfer & Scorrano, 2016) (Figure 4A). Mitochondrial dynamics regulates mitochondrial number, morphology, activity and turnover (Friedman & Nunnari, 2014). There is a close relationship between energetic balance, mitochondrial dynamics and mitochondrial metabolism. It has been demonstrated that mitochondrial fusion/elongation is associated with increased ATP synthesis in response to starvation and stressful situations in which the energetic demand is high. Conversely, nutrient abundance is associated with mitochondrial fragmentation and reduced mitochondrial respiration (Liesa & Shirihai, 2013). In this line, defects in proteins such as MFN2, OPA1 and DRP1 have been associated with alterations in mitochondrial membrane potential and the ETC structure, with detrimental effects in mitochondrial respiration that contribute to the development of a wide range of diseases (Sebastian, Palacin, & Zorzano, 2017).

Mitochondrial dynamics also impacts on mitochondrial turnover. It was demonstrated that mitochondrial fission is required for isolation of defective mitochondria from the mitochondrial network, thus facilitating their elimination by autophagic mechanisms (Twig et al., 2008). Autophagy is a catabolic process in which cellular components are engulfed by a double-membrane structure, the autophagosome, and further degraded in the lysosome. This process is mediated by an ample number of autophagy-related (ATG) genes, and serves to provide nutrients, to recycle damaged, old and spare organelles, and to eliminate harmful content such as protein aggregates (Levine & Kroemer, 2019; Wong et al., 2012; Yang & Klionsky, 2010). Non-selective and cargo-specific autophagic processes have been identified, the latter including the selective clearance of mitochondria, known as mitophagy. Different mechanisms of mitophagy exist but, in mammalian cells, PINK1/PARKIN-mediated mitophagy is the main process for mitochondrial turnover (Youle & Narendra, 2011) (Figure 4B). PTEN-induced kinase 1 (PINK1) is a Ser/Thr kinase which contains a mitochondrial targeting sequence. Upon recruitment to healthy mitochondria, PINK1 is transported through the TOM complex to the IMM, where it interacts with the translocase of inner membrane (TIM) complex and suffers a double cleavage by mitochondrial proteases. The cleaved form of PINK1 is degraded and mitophagy does not occur. In contrast, when recruited to damaged mitochondria, PINK1 remains in the OMM due to depolarization of mitochondria, leading to oligomerization and activation of PINK1. PINK1 then recruits and activates PARKIN, an E3 ubiquitin ligase that mediates ubiquitylation of diverse mitochondrial substrates. Ubiquitylated mitochondrial proteins then recruit cytosolic factors, such as p62/SQSTM1, which mediate the initiation and progression of mitophagy (Eiyama & Okamoto, 2015; Jin & Youle, 2012). Mitophagy depends on both mitochondrial dynamics and autophagy. It is an essential mechanism to maintain a healthy and functional mitochondrial network and, therefore, defects in mitophagy are the origin of severe conditions such as Parkinson's and Alzheimer's disease (Kerr et al., 2017; Malpartida, Williamson, Narendra, Wade-Martins, & Ryan, 2021).

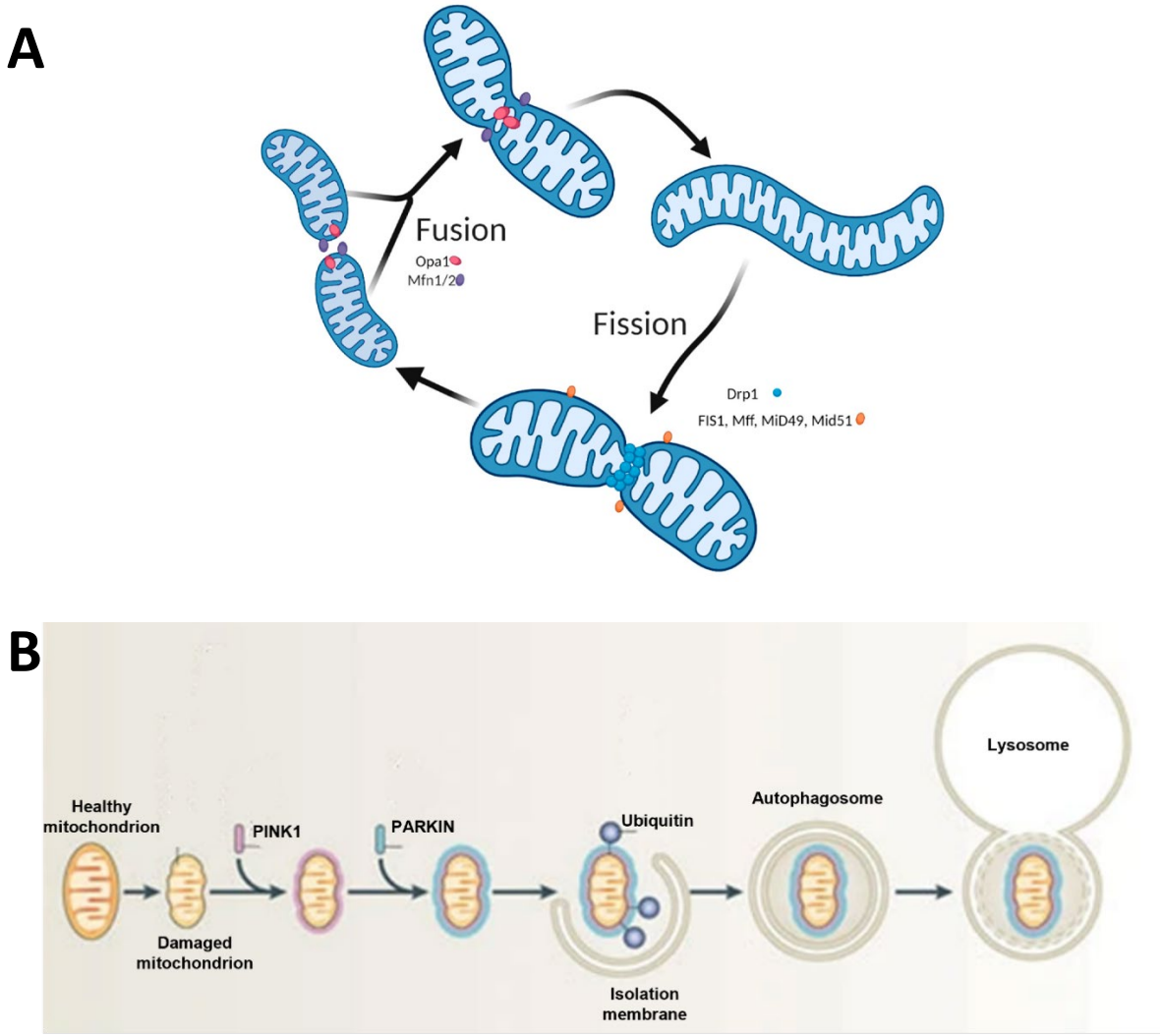

Figure 4. Mitochondrial dynamics and mitophagy. A) Mitochondrial fusion and fission. Mitochondria continuously fuse and divide to adapt to the changing conditions of the cellular environment. Mitofusins mediate fusion between OMMs, while OPA1 is responsible for fusion of IMMs as well as the maintenance of cristae integrity. DRP1 mediates mitochondrial fission, together with assistant proteins such as FIS1. Adapted from (Leduc-Gaudet, Hussain, Barreiro, & Gouspillou, 2021). **B)** PINK1/PARKIN-mediated mitophagy. After mitochondrial damage, healthy mitochondria are depolarized, what favors the accumulation of PINK1 at the surface. This triggers the recruitment of PARKIN to damaged mitochondria. PARKIN ubiquitylates mitochondrial proteins, what acts as a signal for the formation of an autophagosome that isolates damaged mitochondria. The autophagosome fuses with a lysosome to degrade dysfunctional mitochondria. Modified from (Youle & Narendra, 2011).

1.3.1-C. Mitochondria, key players in immune responses

The close relationship between metabolism and immune responses gives mitochondria a pivotal role in immunity. Mitochondrial immune functions include the production of molecules with

antimicrobial and immunomodulatory functions, the participation in immune signaling pathways, the release of mitochondrial DAMPs that activate immune responses, and metabolic reprogramming of immune cells. All mentioned functions are intimately related and complement each other, creating an interconnected system that ensures an efficient immune response.

Molecules derived from mitochondrial metabolism, primarily the TCA cycle and OXPHOS, play a broad range of immune functions. OXPHOS is an important source of ROS, oxygen-derived molecules with high oxidative capacity. ROS are generated by association of O_2 with leaked electrons from the ETC (mainly CI and CIII) or electrons transported by CI in a reverse direction (towards the MM) (Scialo, Fernandez-Ayala, & Sanz, 2017). This process generates superoxide anions ($O_2^{\bullet-}$), precursors of other ROS molecules, such as hydrogen peroxide (H_2O_2) or hydroxyl radicals ($^{\bullet}OH$) (Al Ghouleh et al., 2011). ROS cause oxidative damage on lipids, proteins and DNA, and show bactericidal activity by directly damaging bacterial biomolecules. In addition, ROS increase the intraphagosomal pH, modulating the activity of proteases involved in bacterial killing and promoting the elimination of bacteria (Al Ghouleh et al., 2011; Rybicka, Balce, Khan, Krohn, & Yates, 2010). Apart from antibacterial functions, ROS also play essential roles in antiviral signaling. For example, ROS have been shown to modulate RIG-I-like receptor (RLR) signaling and type I IFN production (Tal et al., 2009). This mitochondrial antiviral mechanism is mediated by the mitochondrial antiviral signaling protein (MAVS), an adaptor molecule crucial for RLR signaling (Seth, Sun, Ea, & Chen, 2005). MAVS is an OMM protein that interacts with the RLRs RIG-I and melanoma differentiation-associated gene 5 (MDA5) through their caspase-recruitment domains (CARDs). This interaction leads to the activation of NF-κB and IRF signaling pathways and the subsequent production of proinflammatory cytokines and type I IFN (Kawai et al., 2005; Seth et al., 2005) (Figure 5).

The TCA cycle is also a source of molecules with antimicrobial and immunomodulatory functions. Some examples include acetyl-CoA, which has been shown promote histone acetylation and the epigenetic modulation of genes involved in IFN production, as well as activation of macrophages and dendritic cells (Infantino, Iacobazzi, Palmieri, & Menga, 2013; Peng et al., 2016); succinate, involved in the regulation of ROS levels and the production of IL-1β (Chouchani et al., 2014; Tannahill et al., 2013); and itaconate, a metabolite derived from cis-aconitate which has shown antibacterial activity in macrophages and exerts diverse roles in the regulation of inflammation (Peace & O'Neill, 2022).

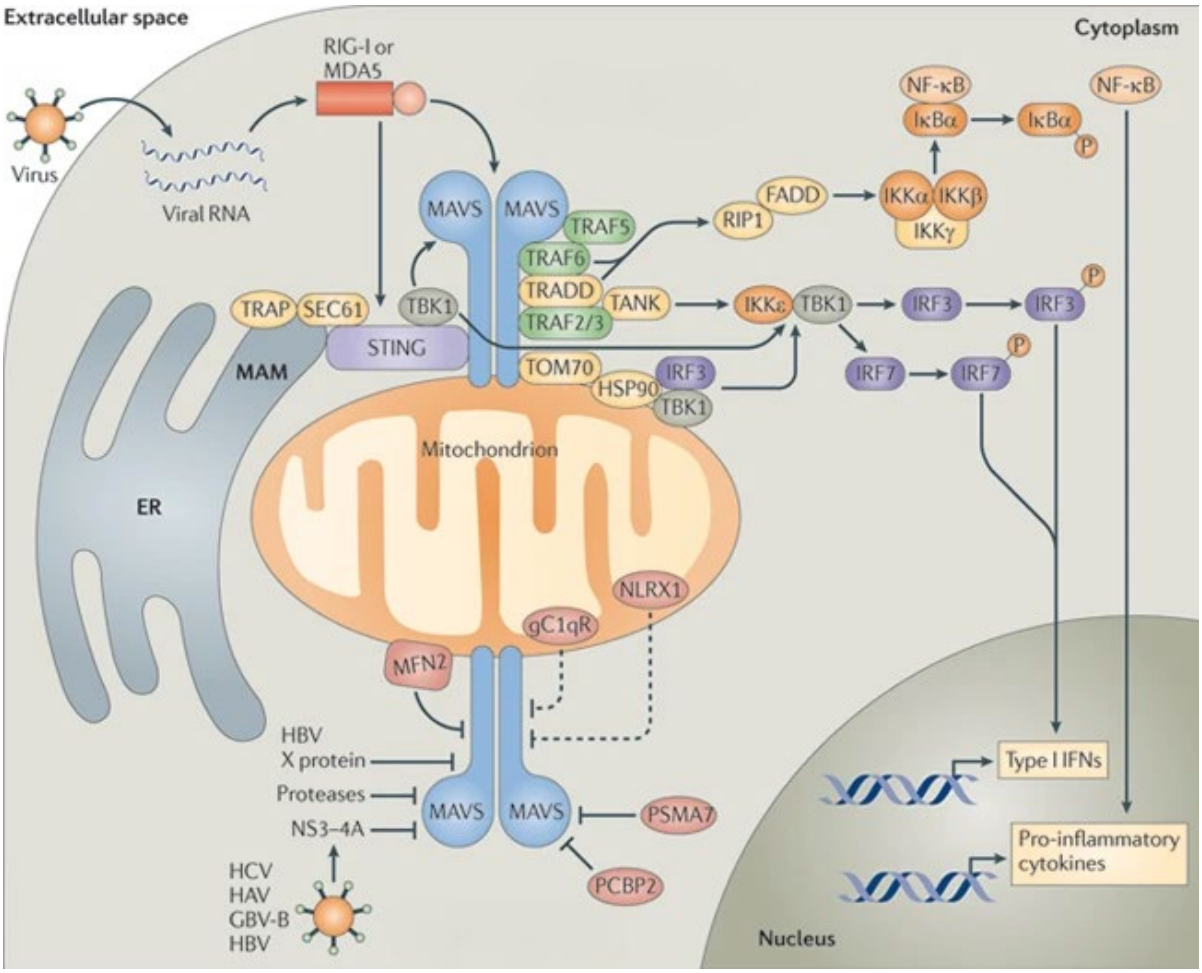

Figure 5. MAVS signaling. During infection of RNA viruses, dsRNA molecules are generated and detected by the RLRs RIG-I and MDA5, which interact with MAVS through their CARD domains. This interaction activates MAVS, which recruits numerous signaling molecules (e.g., TNF receptor-associated factor (TRAF) proteins), leading to the activation of NF-κB signaling and the production of type I IFNs and proinflammatory cytokines. MAVS also interacts with other cytosolic DNA sensors such as STING, activating IRF-mediated responses. As well, MAVS signaling is inhibited by host factors, which modulate its activity, and by viral proteins, limiting the antiviral response. Adapted from (West, Shadel, & Ghosh, 2011).

Mitochondria originated from bacteria and, therefore, contain molecules with specific features that can be recognized as DAMPs by the innate immune system. These molecules include mtDNA, N-formylated proteins, the mitochondrial transcription factor A (TFAM) and cardiolipin, among others (Nakahira, Hisata, & Choi, 2015). The production of type I IFN and proinflammatory cytokines through TLR9, NF-κB and cGAS/STING signaling pathways, the activation of apoptosis, the modulation of calcium fluxes, and the stimulation of ROS production, are some of the

outcomes of mitochondrial DAMP release (Nakahira et al., 2015). Among these mechanisms, the activation of the NOD-, LRR-, and pyrin domain containing 3 (NLRP3) inflammasome is common to several mitochondrial DAMPs. The NLRP3 inflammasome consists of a protein complex whose activation triggers the activation of caspase-1 and the subsequent production of IL-1β and IL-18, as well as gasdermin D, key effectors in inflammatory responses and pyroptotic cell death, respectively (Swanson, Deng, & Ting, 2019; West et al., 2011).

1.3.1-D. Transcriptional regulation of mitochondrial functions

Mitochondria are involved in a plethora of functions that determine cell survival, and rapidly respond to changes in the cellular environment, what requires a fine regulation of mitochondrial gene expression. Owing to their endosymbiotic origin, mitochondria contain their own genome, a single ~16-kb circular DNA which encodes 13 mitochondrial proteins (all constituents of OXPHOS complexes), 2 ribosomal RNAs, and 22 transfer RNAs; the rest of mitochondrial proteins are encoded by nuclear DNA (Pearce et al., 2017). Consequently, the transcriptional regulators of mitochondrial genes act on both mtDNA and nuclear DNA, although all of them are encoded by nuclear genes (Scarpulla, 2008). TFAM and the two isoforms of the mitochondrial transcription factor B (TFB1M and TFB2M) bind to specific regions of mtDNA and regulate the expression of genes encoded by the mitochondrial genome. In addition, TFAM also binds to mtDNA in a non-specific manner, contributing to its maintenance and stability (Scarpulla, 2008). The expression of mitochondrial genes encoded by nuclear DNA is controlled by a wide variety of transcriptional regulators, which include the nuclear respiratory factor-1 (NRF-1) and NRF-2, estrogen-related receptors (ERRs), peroxisome proliferator-activated receptors (PPARs), and the PPARγ coactivator-1 (PGC-1) family of coactivators, among others (Hock & Kralli, 2009). NRF-1 and NRF-2 stimulate the expression of genes encoding OXPHOS proteins, mitochondrial transport proteins, as well as the genes for TFAM, TFB1M and TFB2M. ERRs modulate the transcription of genes encoding components of numerous mitochondrial processes, such as OXPHOS, the TCA cycle, mitochondrial dynamics, mitochondrial transport, and FAO. PPARs are regulators of lipid homeostasis, actin as lipid sensors that modulate FAO and mitochondrial uncoupling proteins involved in thermogenesis, as well as proteins responsible for lipid uptake and storage. In addition, PPARs are also regulators of mitochondrial biogenesis in specific tissues, such as skeletal muscle or alternatively activated macrophages. Finally, PGC-1 coactivators modulate and interact with the mitochondrial TFs mentioned above. PGC-1 coactivators sense and integrate numerous stimuli, such as changes in energetic balance and metabolic needs (e.g., starvation, exercise), or activation of immune cells, that require mitochondrial biogenesis and

changes in mitochondrial metabolism (Hock & Kralli, 2009; C. Luo, Widlund, & Puigserver, 2016; Scarpulla, 2008; Shao et al., 2010; Sonoda et al., 2007; Tripathi, Yen, & Singh, 2020) (Figure 6).

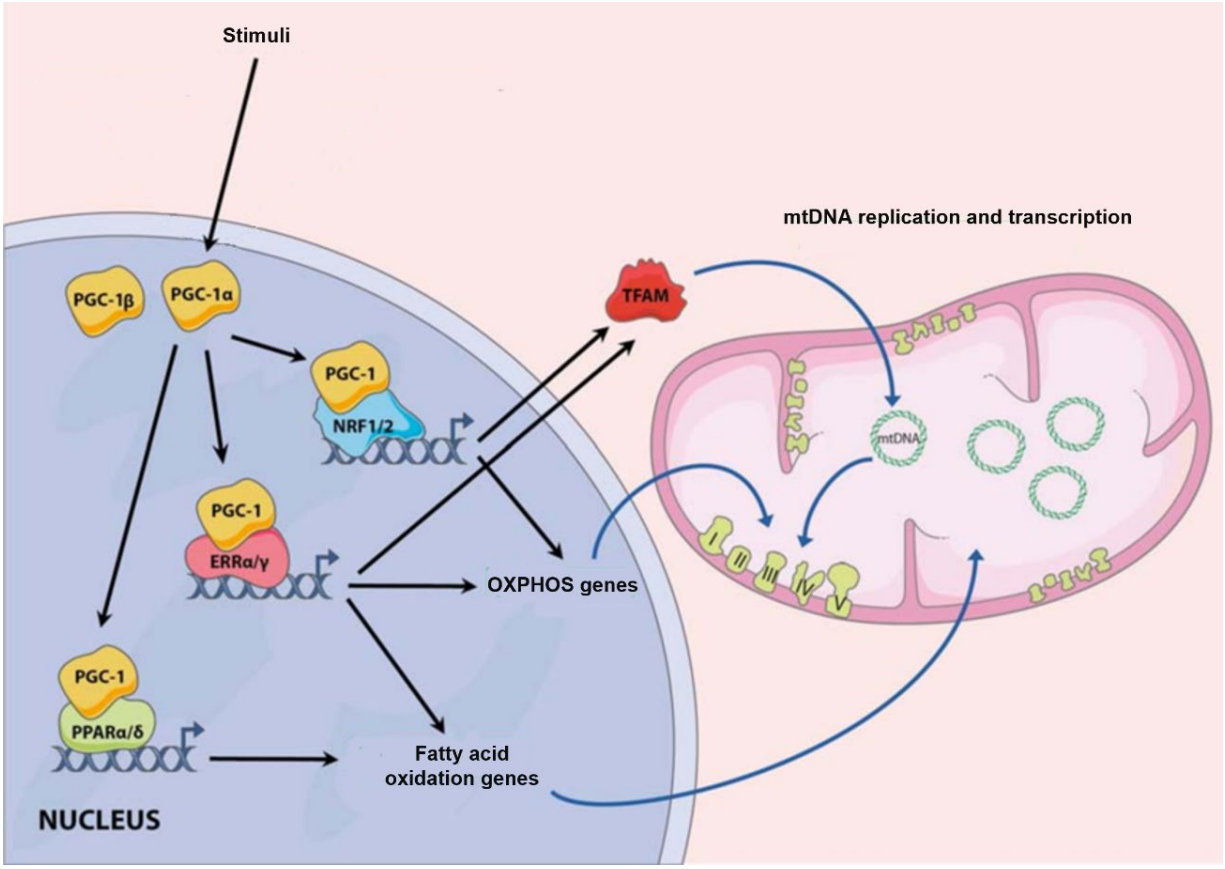

Figure 6. Transcriptional regulation of mitochondrial genes. Several situations require increased mitochondrial activity, such as exercise, cold exposure, fasting, or immune cell activation, which generate stimuli that activate the expression of PGC-1 coactivators. PGC-1 coactivators bind to and modulate the activity of different transcription factors involved in mitochondrial biogenesis, such as NRFs, ERRs and PPARs. The activation of these transcription factors enhances the expression of nuclear genes encoding mitochondrial proteins, as well as the expression of mitochondrial transcription factors (e.g., TFAM) that activate the replication and transcription of the mitochondrial genome. These regulatory mechanisms promote the synthesis of mitochondrial proteins involved in key processes such as OXPHOS and FAO, and increment mitochondrial activity (Zamora & Villena, 2014).

1.3.2. Lipid metabolism and lipid-mediated immune responses

Lipids are hydrophobic or amphiphilic biomolecules essential for life. Lipids comprise a wide variety of molecules that carry out a broad range of physiological functions, such as membrane formation, energy storage and signaling. Lipid homeostasis is a requisite for the adequate performance of cellular functions and, therefore, alterations in lipid composition are the cause of

numerous diseases. Furthermore, lipids are intimately related with immunity, acting as signaling molecules and modulators of protein functions that determine the effectiveness of immune responses (Cockcroft, 2021).

1.3.2-A. Fatty acid synthesis

Lipids are highly diverse in structure and composition, but almost all lipid species contain fatty acids (FAs) as building blocks or as components of their structure. FAs consist of a carboxylic acid with a hydrocarbon chain which varies in length (number of carbon atoms) and degree of saturation (number of double bonds between carbon atoms) (Cockcroft, 2021). FA synthesis (FAS) occurs in the cytoplasm and is closely linked to mitochondrial metabolism. Citrate derived from the TCA cycle is transported to the cytoplasm and converted into acetyl-CoA and oxaloacetate by ATP-citrate lyase. Acetyl-CoA is then converted into malonyl-CoA by acetyl-CoA carboxylases (ACACs) through a highly regulated process, as malonyl-CoA levels determine the balance between FAS and FAO (Foster, 2012). The following steps involve the condensation of 7 malonyl-CoA molecules and an acetyl-CoA by the action of the fatty acid synthase (FASN) multifunctional enzymatic complex. This process requires large amounts of reduced nicotinamide adenine dinucleotide phosphate (NADPH), which is produced through the pentose phosphate pathway (PPP) (Stincone et al., 2015). The result is the generation of a 16-carbon saturated FA known as palmitate, which acts as precursor of a wide variety of FAs with different lengths and degrees of saturation, such as the 18-carbon monounsaturated FA oleic acid (OA). In addition, some FAs (e.g., linoleic acid) cannot be synthesized by mammals and their incorporation through the diet is essential (Cockcroft, 2021; O'Neill et al., 2016; Rohrig & Schulze, 2016). The next steps of lipid synthesis occur in different subcellular locations, mainly the endoplasmic reticulum (ER), although some lipid species are synthesized in mitochondria and the Golgi apparatus (Cockcroft, 2021). The incorporation of FAs into different molecular backbones generates three main lipid classes: glycerolipids, sterols and sphingolipids. Here, we put our focus on glycerolipids and cholesterol.

1.3.2-B. Glycerolipids

Glycerolipids consist of a glycerol backbone to which FAs, or a combination of FAs and a phosphate ion, are esterified. When FAs are esterified to hydroxyl groups at *sn-1* and *sn-2* positions of glycerol-3-phosphate, the resulting molecules are glycerophospholipids or phospholipids (PLs). This step is mediated by glycerol-3-phosphate acyltransferases (GPATs) and lysophosphatidate acyltransferases (LPATs), generating phosphatidic acid (PA). PA is the simplest PL and the precursor of phosphatidylinositol (PI), as well as the glycerolipids

diacylglycerols (DAGs) by the action of PA phosphatases or lipins. The rest of PLs are synthesized by modification of DAG, generating phosphatidylcholine (PC) and phosphatidylethanolamine (PE), which can be converted into phosphatidylserine (PS) (Cockcroft, 2021) (Figure 7). PLs are the building blocks of cell membranes, being PC the most abundant PL in mammals, but PLs also play relevant roles in signaling and energy homeostasis (van der Veen et al., 2017; Vance, 2015). Moreover, the PL composition of organelle membranes is critical for their function. For example, the levels of cardiolipin, a mitochondria-specific PL derived from phosphatidylglycerol (PG) determines the proper functioning of mitochondria (Paradies, Paradies, Ruggiero, & Petrosillo, 2019).

FAs can also be esterified to DAG by the action of DAG acyltransferases (DGATs), generating the glycerolipids triacylglycerols (TAGs), the main form in which FAs are stored in lipid droplets (LDs). The process is reversible by the action of specific lipases (e.g., adipose triglyceride lipase (ATGL), hormone-sensitive lipase (HSL)), which generate DAGs from TAGs, as well as monoacylglycerols (MAGs) from DAGs (Ruggles, Turkish, & Sturley, 2013). TAGs, DAGs, and MAGs are classified as non-polar or neutral lipids (NLs), and play important roles in energy storage, signaling and maintenance of lipid homeostasis (Eichmann & Lass, 2015; H. Wang, Airola, & Reue, 2017).

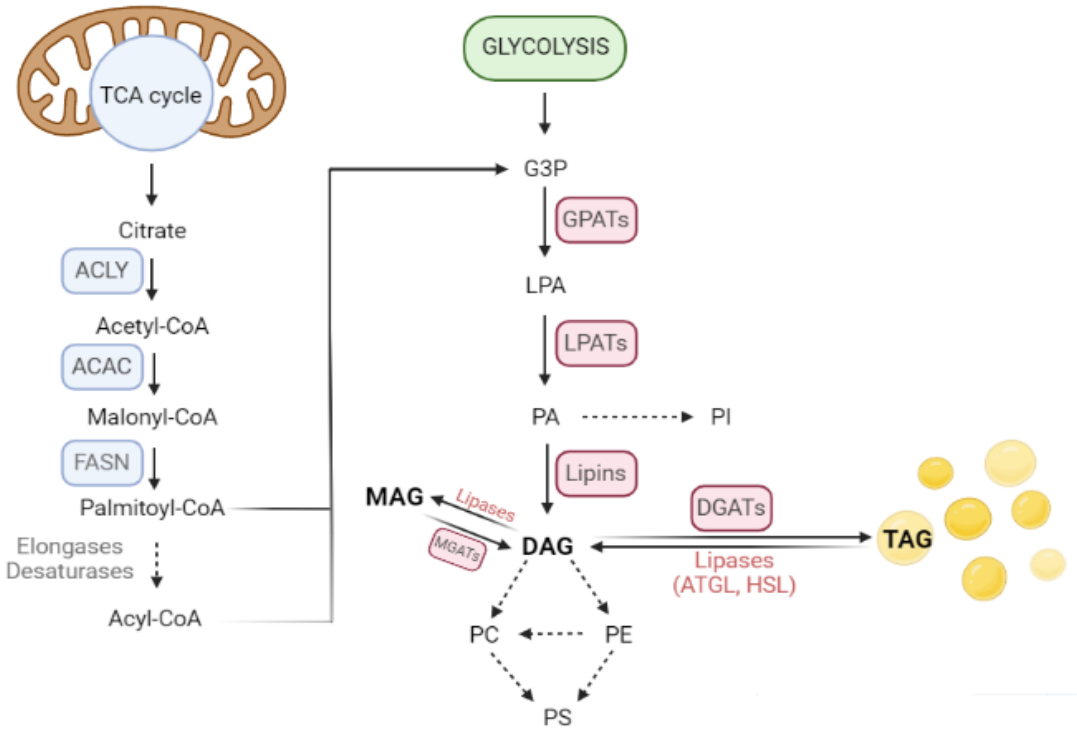

Figure 7. Schematic overview of FAS and glycerolipids synthesis. *De novo* fatty acid biosynthesis occurs in the cytoplasm, and results in the synthesis of palmitoyl-CoA from TCA cycle-derived citrate. Palmitoyl-CoA is further modified to synthesize numerous FAs of varying length and saturation degree. FAs are esterified to glycolysis-derived G3P, which acts as backbone for PL synthesis. Subsequent enzymatic reactions lead to the formation of PA and DAGs, precursors of PLs. DAGs can also be synthesized by esterification of FAs to MAGs. Likewise, TAGs are synthesized by esterification of FAs to DAGs. Both TAGs and DAGs can be hydrolyzed by lipases, generating free FAs and their respective precursor molecules (DAGs and MAGs, respectively). Image created with BioRender.com.

Glycerolipids play relevant roles in immune responses, as they are the source of numerous bioactive lipid mediators that participate in immune signaling and inflammation. PLs are targets of phospholipases, which remove FAs from PLs to produce molecules such as lysoPLs, oxylipins, oxidized PLs, phosphoinositides, etc., which act as signaling molecules and activators of immune cells (O'Donnell, Rossjohn, & Wakelam, 2018). For example, phospholipase A_2 subtypes generate arachidonic acid, which activates cyclooxygenase-mediated production of prostaglandins, key inflammatory molecules (Balsinde, Winstead, & Dennis, 2002). As well, phospholipase C subtypes cleave target PLs generating DAG and the phosphorylated PL headgroup, which activate pathways involved in T cell, granulocyte, and macrophage functions (O'Donnell et al., 2018).

1.3.2-C. Cholesterol

Sterols consist of a sterane nucleus, formed by 3 cyclohexane rings and 1 cyclopentane ring, and a hydrocarbon tail esterified at the C-17 position. Sterols are present in eukaryotes and a few prokaryotes, and their composition varies depending on the organism (Nes, 2011). In mammals, the main sterol is cholesterol, an essential molecule which plays numerous roles in the cell, including membrane formation and control of membrane fluidity, modulation of protein activity, synthesis of vitamins and hormones, transport, and signaling (Incardona & Eaton, 2000; A. H. Payne & Hales, 2004). Cholesterol is synthesized through a complex process involving more than 20 chemical reactions, which can be divided in two pathways. The first one is known as the mevalonate pathway, in which citrate-derived acetyl-CoA is converted to mevalonate, which subsequently undergoes a series of reactions until its conversion in farnesyl pyrophosphate (FPP). The synthesis of mevalonate is mediated by the enzyme 3-hydroxy-3-methyl glutaryl-CoA reductase (HMGCR), and it is the rate-limiting step of the whole process. Another important step in this pathway is the synthesis of FPP by the FPP synthase (FDPS). In the second pathway, FPP is converted to squalene, which is further modified until its conversion in cholesterol (B. Guerra et al., 2021; Korber, Klein, & Daum, 2017). In addition to *de novo* biosynthesis, cholesterol is also

obtained from the diet. It is absorbed in the intestines and processed in the liver. Any excess of cholesterol in the liver is distributed to peripheral tissues bound to very-low density lipoproteins (VLDL). VLDL is released into the bloodstream, where it is converted to low-density lipoprotein (LDL). LDL binds to membrane proteins such as LDL receptor (LDLR), CD36 and scavenger receptor class A type 1 (SR-A1), which mediate the uptake of LDL by endocytosis. LDL is then processed in the lysosomes and free cholesterol is released and transported to cell membranes or diverse organelles. If in excess, membrane proteins such as ATP binding cassette subfamily A member 1 (ABCA1), ABCG1 and SR-B1 mediate the efflux and transfer of cholesterol to high-density lipoprotein (HDL) and apolipoprotein A1 (ApoA1), which reintroduce cholesterol into circulation (Y. M. Park, 2014; Phillips, 2014; Shen, Azhar, & Kraemer, 2018). Furthermore, excess cholesterol can also be esterified to FAs by the action of acyl-CoA:cholesterol acyltransferases (ACATs), also known as sterol O-acyltransferases (SOATs), forming the NLs cholesterol esters (CE), which act as storage molecules for both FAs and cholesterol in LDs (Korber et al., 2017). When necessary, CE hydrolases such as neutral CE hydrolase 1 (NCEH1) and HSL break down CE stored in LDs and release free cholesterol (Ghosh, 2012; Sakai et al., 2014) (Figure 8).

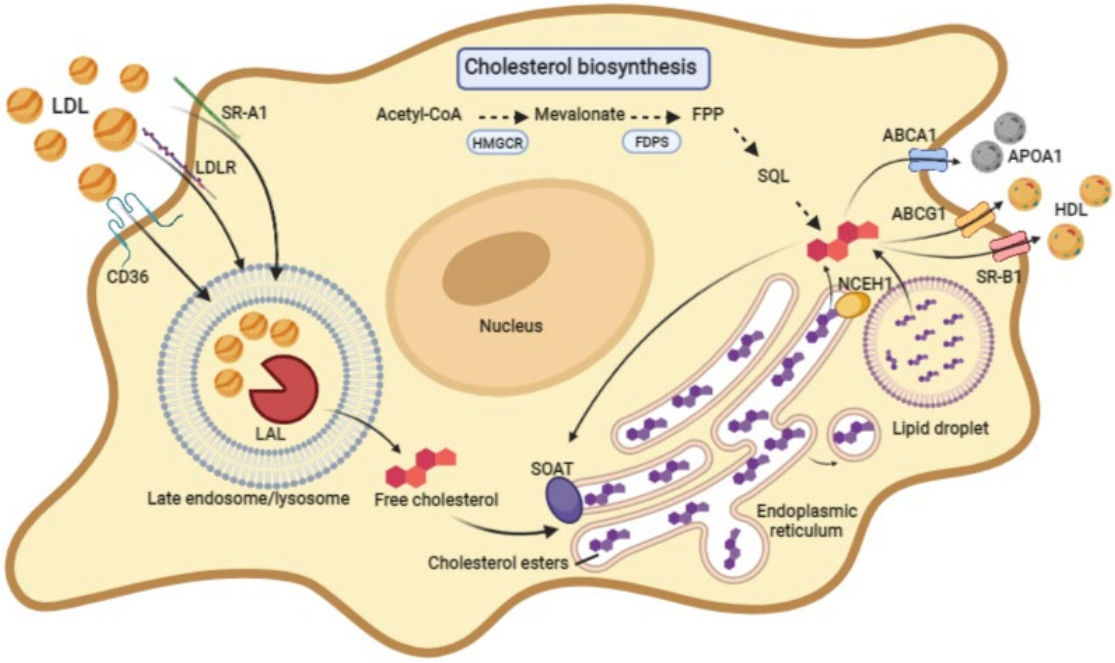

Figure 8. Cholesterol metabolism. Cholesterol can be obtained via *de novo* biosynthesis through a complex process that take places in the cytoplasm and the ER and involves more than 20 enzymatic reactions. Also, cholesterol can be acquired from the extracellular milieu by endocytosis of LDL particles, which are eventually degraded in the lysosome by lysosomal acid lipases, releasing free cholesterol. If in excess, sterol acyltransferases generate CEs in the ER, which are stored in LDs. CEs can be hydrolyzed

by CE hydrolases, releasing free cholesterol. As well, excess cholesterol can be transported out of the cell through specific membrane-associated transporters. Extracellular cholesterol is captured by lipoproteins such as HDL and APOA1, which reintroduce cholesterol into the circulation. Image created with BioRender.com.

Cholesterol homeostasis and immunity are closely related. Membrane cholesterol levels have been shown to modulate the activity of proteins involved in immune signaling. For example, accumulation of cholesterol in plasma membrane enhances TLR4 signaling (Yvan-Charvet et al., 2008). As well, cholesterol levels in the ER membrane determine the production of type I IFN via STING/TBK1/IRF3 signaling axis (York et al., 2015) which, in turn, modulates cholesterol biosynthesis (Robertson & Ghazal, 2016). Not only cholesterol, but also cholesterol derivatives are important immune effectors. 25-hydroxycholesterol (25HC) is synthesized by cholesterol-25-hydroxylase (CH25H), an enzyme induced in response to IFN stimulation. 25HC has been shown to regulate membrane cholesterol pools, affecting bacterial and viral pathogenesis (Blanc et al., 2013; Dang, Madhani, & Vance, 2020; S. Y. Liu et al., 2013). Furthermore, oxysterols and cholesterol crystals activate inflammatory pathways, such as the NLRP3 inflammasome, leading to the production of proinflammatory cytokines and the activation of cell death processes (Tall & Yvan-Charvet, 2015).

1.3.2-D. Lipid droplets

LDs are ubiquitous intracellular organelles consisting of a neutral lipid (NL) core surrounded by a PL monolayer in association with a wide variety of proteins. The accumulation of NLs (mainly TAG and CE) in LDs serves as lipid storage for membrane formation, energy generation and synthesis of lipid-derived molecules (e.g., steroid hormones), as well as a mechanism to avoid lipotoxicity, damage caused by accumulation of excess FAs and sterols, which results in numerous cell alterations and apoptosis (Listenberger et al., 2003). The biogenesis of LDs has been a matter of debate for decades, and different models have been proposed; however, all models concur in the ER as the site of LD formation, as the enzymes of NL synthesis localize in this organelle (Buhman, Chen, & Farese, 2001). The most accepted model for LD biogenesis describes the process in 4 sequential steps: 1) the synthesis and accumulation of NLs in the lumen of the ER; 2) the formation of a NL lens in the ER membrane that separates the lipid bilayer; 3) the spontaneous and/or protein-mediated budding of the nascent LD into de cytosol; and 4) the expansion of cytosolic LDs by *in situ* lipid synthesis, carried out by LD-associated enzymes such as GPATs and DGATs (Saka & Valdivia, 2012; Walther, Chung, & Farese, 2017) (Figure 9). LDs are surrounded by a great diversity of proteins that control their biogenesis, stability, dynamics, and functions (Bersuker & Olzmann, 2017). These LD-associated proteins mainly remain at the

surface of the LD membrane, although some proteins have been shown to localize in the lipid core (Robenek, Robenek, & Troyer, 2005). Perilipins (PLINs) are some of the most abundant LD-associated proteins. This family includes 5 members in mammals, from PLIN1 to PLIN5, being PLIN2 and PLIN3 ubiquitously expressed. PLIN1 and PLIN2 are specific of LDs, while the rest can be found in the cytoplasm associated to lipoprotein particles. Every LD contains at least two PLIN member, which modulate LD features such as LD size, and act as mediators in the interaction between LDs and other organelles (Kimmel & Sztalryd, 2016; Sztalryd & Brasaemle, 2017). Apart from PLINs, proteins involved in lipid synthesis and hydrolysis, membrane trafficking, signaling, immune response, and protein degradation, among other functions, are also associated to LDs, indicating that the biological roles of LDs are far beyond lipid storage (S. Xu, Zhang, & Liu, 2018).

The role of LDs in immune responses has gained relevance in the recent years. LDs participate in immunity at different levels. They are sources of lipids which act as immune signaling molecules and mediators of inflammatory responses (Jarc & Petan, 2020). In addition, LDs act as scaffolds for antimicrobial proteins (e.g., viperin) and establish direct contact with pathogens to facilitate their elimination (Bosch et al., 2020). Finally, LDs interact with organelles such as mitochondria, modulating cell metabolism and, therefore, immune functions (Bosch & Pol, 2022). However, LDs play a dual role in immune responses, as they can also promote viral infections acting as scaffold structures for virus assembly and as a source of energy for viral replication (Dias et al., 2020; Filipe & McLauchlan, 2015).

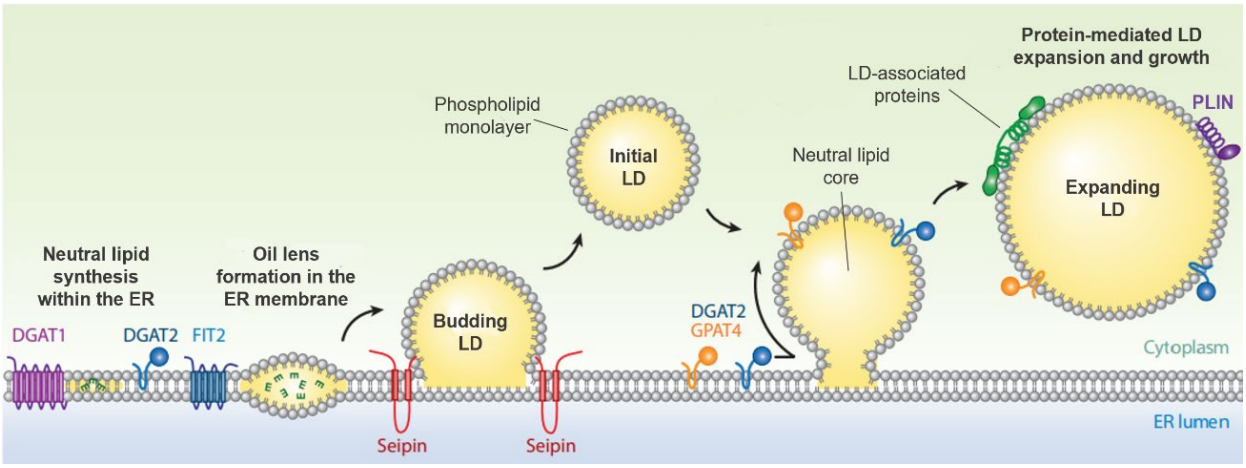

Figure 9. Lipid droplet biogenesis and structure. LD biogenesis starts with the synthesis and accumulation of NLs in the ER. Increasing NL levels generate a lipid lens between the two leaflets of the ER membrane, which increases in size to form a nascent LD that buds off the ER. Budding occurs spontaneously or via protein-mediated mechanisms. Newly synthesized LDs consist of a NL core

surrounded by a phospholipid monolayer, in which diverse proteins are embedded. These proteins contribute to LD stability and growth, as well as diverse functions such as immune signaling. Adapted from (Walther et al., 2017).

1.3.2-E. Transcriptional regulation of lipid metabolism

The complexity and relevance of lipid metabolism requires the fine regulation of every pathway involved. Therefore, the expression of lipid metabolism genes is under the control of different TFs, which include the liver X receptors (LXRs), PPARs, sterol regulatory element-binding proteins (SREBPs), and CCAAT/enhancer binding proteins (C/EBPs). Not only TFs, but also microRNAs such as miR-33 participate in the transcriptional regulation of lipid metabolism (Adeva-Andany et al., 2019). Here, LXRs, PPARs and SREBPs will be briefly described.

The LXR family is formed by the isotypes LXRα and LXRβ. The former is predominantly expressed in metabolically active tissues (e.g., liver, macrophages), while the latter is ubiquitously expressed (Repa et al., 2000). LXRs dimerize with retinoid X receptors (RXRs) and bind to LXR response elements in the DNA, modulating the expression of lipid metabolism genes. LXR-RXR complexes activate gene expression when bound to lipid ligands (e.g., cholesterol derivatives), but in the absence of ligands LXR-RXRs bind co-repressors and repress the expression of target genes (B. Wang & Tontonoz, 2018). LXRs are known regulators of cholesterol metabolism, promoting efflux of excess cholesterol, and inhibiting cholesterol biosynthesis and uptake through the indirect modulation of SREBP2 activity (L. Zhang et al., 2017; Y. Zhang et al., 2012). Moreover, LXR are important regulators of FA and PL metabolism, stimulating lipogenesis by inducing SREBP1c (Schultz et al., 2000), and modulating membrane PL composition as a protective mechanism against lipid stress (Rong et al., 2013).

PPARs are ligand-dependent TFs and major regulators of lipid metabolism. To date, 3 PPAR subtypes have been identified: PPARα, PPARγ and PPARβ/δ. PPARs, like LXRs, form heterodimers with RXRs and bind to PPAR response elements in target genes, increasing or decreasing their expression depending on the interaction of PPARs with co-activators (e.g., PGC-1α) or co-repressors (Gearing, Gottlicher, Teboul, Widmark, & Gustafsson, 1993; Kang & Fan, 2020; Qi, Zhu, & Reddy, 2000). PPARα and PPARβ/δ are highly expressed in oxidative tissues and are involved in the regulation of lipid uptake, transport, esterification, and oxidation. PPARγ, in contrast, promotes FA transport, lipid synthesis and energy storage (Christofides, Konstantinidou, Jani, & Boussiotis, 2021). PPARs are closely linked to mitochondrial metabolism, as they enhance the expression of PGC-1 coactivators and promote mitochondrial biogenesis

and mitochondrial lipid metabolism (Hock & Kralli, 2009). This makes PPARs indirect regulators of whole cell metabolism, what impacts on immune functions.

SREBPs are regulators of lipid synthesis. The SREBP family is comprised of SREBP1 (isoforms *a* and *c*) and SREBP2. SREBP1 isoforms regulate global lipid synthesis and storage, while SREBP2 is involved in cholesterol metabolism (Shimano & Sato, 2017). SREBPs reside in the ER and require an activation process to exert their functions. The activation of SREBP2 is well characterized. In the ER, SREBP2 is associated with SREBP cleavage-activating protein (SCAP) which, in turn, interacts with insulin-induced gene proteins (INSIGs). When cholesterol levels are adequate, INSIGs retain the SREBP2-SCAP complex in the ER. However, when cholesterol levels drop below a certain threshold, INSIGs are degraded and the SREBP2-SCAP complex is transported to the Golgi. In the Golgi, specific proteases cleave the complex and generate an active SREBP2 product, which enters the nucleus and activates the expression of genes involved in cholesterol biosynthesis by binding to sterol regulatory element sequences (J. Luo, Yang, & Song, 2020). SREBPs are regulated at different levels, including transcriptional and post-translational mechanisms, in which participate TFs such as LXRs, as well as metabolic regulators such as adenosine monophosphate (AMP)-activated protein kinase (AMPK), mammalian target of rapamycin (mTOR) and protein kinase B (PKB/Akt) (Shimano & Sato, 2017), thus modulating lipid metabolism in response to changes in energy demands. As well, SREBPs are expressed in response to inflammatory signals, leading to metabolic reprogramming and activation of inflammatory target genes (Kusnadi et al., 2019).

1.4. Macrophages, key players in innate immune responses and homeostasis

Macrophages were first identified by Metchnikoff in the 19th century as cells with high phagocytic capacity. Since then, research has evidenced that macrophages are essential cells for the innate immune response against pathogens, as well as for the normal functioning of a great variety of physiological processes (Murray & Wynn, 2011; Wynn, Chawla, & Pollard, 2013). It would not be precise to talk about macrophages as a single cell type, as functionally diverse macrophage subpopulations exist in different anatomical locations (Gordon & Taylor, 2005). This is the result of a complex ontogeny, which involves both the establishment of tissue-specific macrophage populations during the embryonic development, and the differentiation of macrophages from bone marrow-derived monocytes released into the circulation (Epelman, Lavine, & Randolph, 2014). Macrophages are highly plastic cells that continuously sense and adapt to their microenvironment to offer an effective response to homeostatic imbalances. This is achieved thanks to a wide repertoire of receptors that recognize exogenous and endogenous signals, leading to metabolic

reprogramming and activation (P. R. Taylor et al., 2005). Depending on the signal, macrophages undergo different activation states, a process known as macrophage polarization, that implies phenotypic changes and determines macrophage functions. Attending to their activation state, macrophages can be classified as “classically activated”/M1, or “alternatively activated”/M2. M1 macrophages are induced in response to proinflammatory molecules such as IFNγ, LPS and tumor necrosis factor-α (TNF-α). In contrast, anti-inflammatory cytokines such as IL-4 and IL-13 induce macrophage polarization towards an M2 phenotype (Cassetta, Cassol, & Poli, 2011). Macrophage polarization is accompanied by substantial metabolic changes (Figure 10).

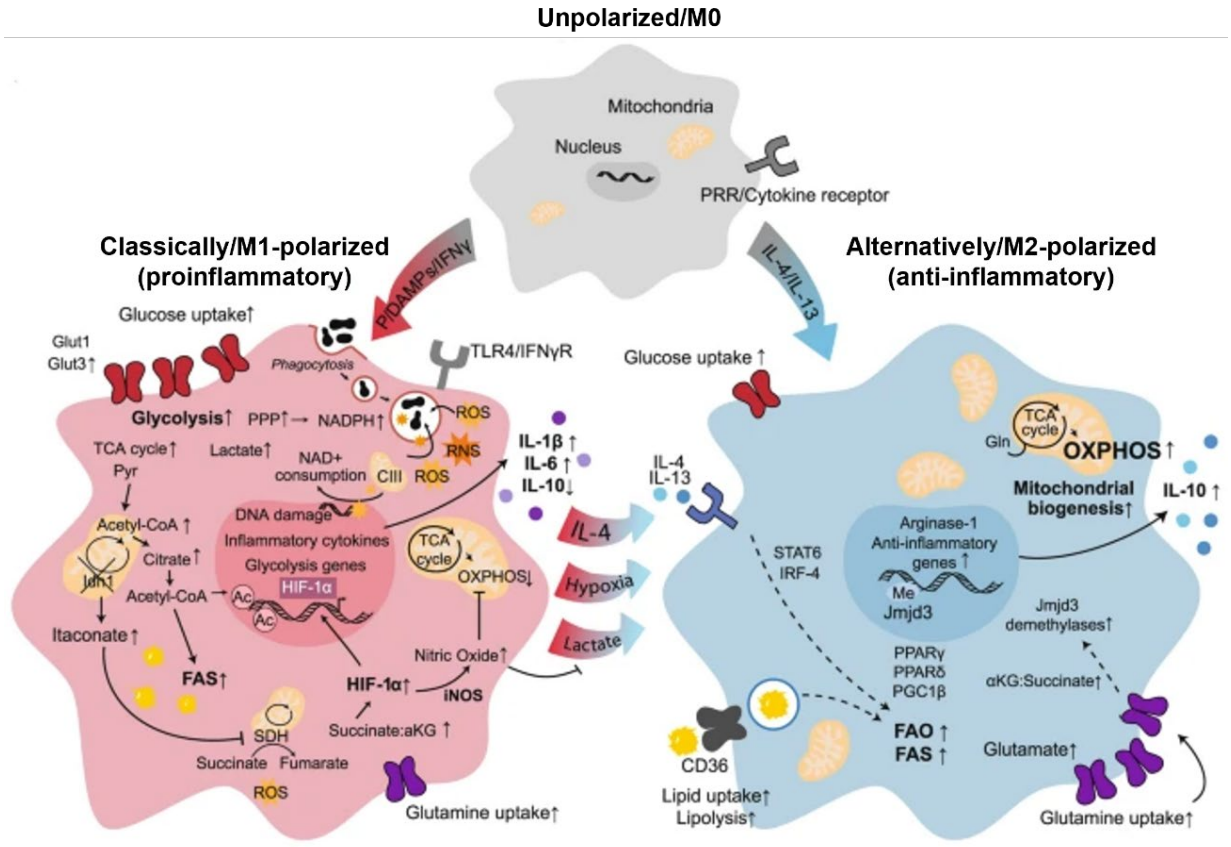

Figure 10. Macrophage polarization. Macrophages are highly plastic cells that adapt to changes in their environment to offer and adequate response. Sensing of specific stimuli triggers macrophage activation. Molecules such as PAMPs, LPS and IFNγ activate macrophages to proinflammatory/M1 phenotype, whereas cytokines such as IL-4 and IL-13 drive activation towards an anti-inflammatory/M2 phenotype. Activation involves metabolic reprogramming. Roughly, M1 macrophages display increased glycolysis, a ‘broken’ TCA cycle and increased FAS, what allows the rapid obtention of ATP and the synthesis of numerous microbicidal and proinflammatory molecules. M2 macrophages show increased mitochondrial biogenesis and lipid uptake, rely on the TCA cycle and OXPHOS to generate ATP, and are involved in the resolution of inflammation and tissue regeneration. Of note, a switch from M1 to M2 can occur along the

inflammatory process, and intermediate phenotypes can be acquired. Modified from (Wculek, Dunphy, Heras-Murillo, Mastrangelo, & Sancho, 2022).

M1 macrophages have enhanced glycolytic metabolism and reduced OXPHOS, breaks in the TCA cycle after citrate and succinate which contribute to anabolism and production of proinflammatory molecules, and increased activity through FAS and PPP pathways. In addition, the conversion of arginine in nitric oxide (NO) and citrulline by inducible NO synthase (iNOS) is characteristic of this phenotype (Van den Bossche, O'Neill, & Menon, 2017). These metabolic features support cell growth and the production of proinflammatory cytokines, ROS, and reactive nitrogen species (RNS), resulting in strong microbicidal and tumoricidal activity (Sica & Mantovani, 2012). Conversely, M2 macrophages rely on OXPHOS to obtain ATP, have an intact TCA cycle, present increased FAO and, in these cells, arginine is converted into ornithine and urea by arginase-1 (ARG1) (Van den Bossche et al., 2017). As a result, M2 macrophages display high phagocytic and scavenging capacity, what makes these cells important effectors in tissue remodeling and immune responses against helminth parasites (Sica & Mantovani, 2012). However, this is a simplistic classification that does not fully cover the broad spectrum of macrophage activation states. As well, the metabolic pathways characteristic of M1 and M2 are not unique of each type. For example, glycolysis is crucial for M2 activation, as well as FAO contributes to the production of proinflammatory cytokines in M1 macrophages (Moon et al., 2016; Tan et al., 2015). Thus, macrophage functions depend on their metabolic state, being mitochondrial and lipid metabolism main contributors (Jones & Divakaruni, 2020; J. Yan & Horng, 2020).

1.5. Viruses, hijackers of cell metabolism

Viruses lack their own metabolism and, hence, depend on host metabolic processes to complete their replicative cycles. However, virus-host interactions are not passive, as viruses encode proteins that modulate host metabolism for their own benefit (Thaker, Ch'ng, & Christofk, 2019). In general terms, viruses induce a metabolic shift towards enhanced glycolysis and lactate production even in the presence of oxygen, a phenomenon known as the Warburg effect, which is also characteristic of cancer cells and activated immune cells (Icard et al., 2021). In addition, most viruses also stimulate glutaminolysis to fuel the TCA cycle. These changes serve to rapidly generate ATP, as well as reducing equivalents and metabolic intermediates to support nucleotide and lipid synthesis (Sanchez & Lagunoff, 2015). Each virus uses specific proteins and mechanisms to modulate host metabolism, offering a wide variety of strategies to ensure a successful infection. Here, we will focus on poxviruses, and specifically, VACV.

1.5.1. The Poxviridae family

The *Poxviridae* family comprises large, enveloped, double-stranded DNA (dsDNA) viruses that replicate entirely in the cytoplasm of host cells and have a unique barrel-shaped morphology (Lefkowitz, Wang, & Upton, 2006). Poxviruses infect both invertebrate and vertebrate animals, including humans. *Variola virus* is the cause of smallpox, one of the deadliest diseases in human history, and the first disease ever eradicated thanks to a global vaccination campaign (Meyer, Ehmann, & Smith, 2020). Nowadays, poxviruses are still significant to public health due to the possibility of emergence of novel poxviruses able to infect humans. A good example is the monkeypox outbreak detected in May 2022, which involved 12 non-endemic countries worldwide (World Health Organization, 2022). As well, the risk of re-emergence of smallpox from old stocks or the use of *Variola virus* as a biological weapon are also important threats to public health (McCarthy, 2014; Petersen et al., 2019). However, the importance of poxviruses does not fall only on their potential to become a global health concern. Poxviruses have been and are used by researchers to understand virus-host interactions and the molecular basis of viral infections, as well as to develop biotechnological tools and novel therapies against infectious and non-infectious diseases (Yang, Gray, & Winter, 2021). In this sense, the Modified Virus Ankara strain of VACV is a well-established vector system for the development of vaccines against a wide variety of viruses (Boudewijns et al., 2022; Perdiguero et al., 2019).

1.5.1-A. Vaccinia virus (VACV) infection and dissemination

VACV is the prototype virus of the *Orthopoxvirus* genus of the *Poxviridae* family. VACV is the live vaccine used for the eradication of smallpox, and one of the most extensively studied poxviruses (Meyer et al., 2020). Like all poxviruses, VACV is a large, enveloped, dsDNA virus with a complex infectious cycle that occurs entirely in the cytoplasm of host cells (Figure 11). The lifecycle of VACV starts with the binding of virions to the cell surface, after which two entry mechanisms can take place: 1) the fusion of the virion membrane with the cell membrane and the penetration of the virion core into the cytoplasm (Carter, Law, Hollinshead, & Smith, 2005); or 2) the endocytic capture of virions by macropinocytosis and the posterior release of the virion core into the cytoplasm (Mercer & Helenius, 2008). Once in the cytoplasm, VACV cores are transported on microtubules to perinuclear regions called factories, where DNA transcription and replication begins (Carter et al., 2003; Moss, 2013). As expected from a virus that replicates in the cytoplasm, VACV synthesizes its own set of proteins involved in genome replication. Of these proteins, those involved in the transcription of early genes are carried within the virion, together with the 185-200 kbp linear dsDNA genome, which encodes approximately 200 proteins (Bahar et al., 2011; Moss, 2013). First, early genes are expressed, synthesizing proteins responsible for genome replication

and immune evasion (Smith et al., 2013). After that, the progeny DNA molecules serve as templates for the expression of intermediate and late genes (Broyles, 2003; Moss, 2013). Then, a complex morphogenetic process commences with the generation of crescent-shaped and spherical structures consisting of a lipid bilayer and proteins, which enclose viral content and form the immature virion (Moss, 2015; Roberts & Smith, 2008). VACV genome is then packed into immature virions, forming the intracellular mature virus (IMV or MV), which accumulates intracellularly until cell lysis (Roberts & Smith, 2008). However, the lifecycle of VACV does not end with the IMV, as poxviruses have developed effective strategies for dissemination that involve the formation of different virion forms. Some MVs are wrapped by additional membranes derived from the endosomal system or the trans-Golgi network (Schmelz et al., 1994; Tooze, Hollinshead, Reis, Radsak, & Kern, 1993), forming the intracellular enveloped virus (IEV) or wrapped virus (WV). WVs are then transported on microtubules to the cell periphery, where they fuse with the cell membrane and exit the cell. Enveloped virus that remains attached to the cell surface is called cell-associated enveloped virus (CEV), whereas enveloped virus completely released out of the cell is called extracellular enveloped virus (EEV or EV) (Roberts & Smith, 2008). Apart from exocytosis, EVs can also form by budding of MVs through the cell membrane (Meiser, Sancho, & Krijnse Locker, 2003).

The last step of VACV infectious cycle is the dissemination to neighboring cells or within the host. *In vitro*, cell-to-cell spread occurs by different mechanisms: 1) cell lysis and liberation of IMVs (Roberts & Smith, 2008); 2) EV release and dissemination through convection currents, forming characteristic comet-shaped plaques (L. G. Payne, 1980); 3) actin tail formation, consisting of polymerization of actin beneath CEVs and propulsion of virions to adjacent cells (Cudmore, Cossart, Griffiths, & Way, 1995). During infection, a percentage of WVs is not released as EVs and remains attached to the cell surface as CEVs, what triggers intracellular signaling pathways that result in the polymerization of actin underneath the CEVs, pushing the virus out of the cell surface (Roberts & Smith, 2008). Moreover, actin tails are also formed when EVs contact previously infected cells, thus avoiding superinfection and favoring the infection of adjacent cells (Doceul, Hollinshead, Breiman, Laval, & Smith, 2012; Doceul, Hollinshead, van der Linden, & Smith, 2010). *In vivo*, EVs are the main form of VACV dissemination, as free virions or associated to cells such as macrophages (Byrd et al., 2014). Moreover, EVs are effective forms of dissemination within the host due to their relative resistance to complement and antibody-mediated neutralization (Law & Smith, 2001; Vanderplasschen, Mathew, Hollinshead, Sim, & Smith, 1998).

Virion protein composition is determinant for the correct progression of VACV infectious cycle, and many different viral proteins participate in each step of infection. Interestingly, protein composition differs between the distinct virus forms found throughout infection. The proteins A25 and A26, involved in the regulation of virus entry, are only found in MV (Ulaeto, Grosenbach, & Hruby, 1996), while the proteins B5, A33, A34, A36, A56, F12, F13, K2 and E2 are exclusive of WV (Bidgood & Mercer, 2015). These proteins are essential for MV wrapping (B5 and F13), WV transport (A36, E2 and F12), actin tail formation (A33, A34 and A36), and prevention of superinfection (A56 and K2), highlighting the importance of WV in viral spread (Bidgood & Mercer, 2015).

1.5.1-B. VACV strategies to counteract the IFN-mediated antiviral response

As mentioned earlier, IFNs are the first line of defense against viral infections, being produced by many different pathways upon detection of viral molecules. The cytoplasmic replication of VACV might be advantageous in terms of independency and immediacy, but it leads to diverse cellular alterations and to the generation of PAMPs that rapidly activate the innate immune response and the production of IFNs. However, VACV encodes a plethora of immunomodulatory genes that are expressed early and throughout the infection to counteract IFN signaling (Assarsson et al., 2008). The mechanisms by which VACV evades the antiviral action of IFN have been recently reviewed (Smith, Talbot-Cooper, & Lu, 2018). Briefly, VACV interferes with IFN at four different steps of the IFN signaling cascade. First, VACV prevents the production of IFN through the inhibition of translation of host proteins (Strnadova et al., 2015), the reduction in the generation and sensing of viral nucleic acid PAMPs (Meade et al., 2018; Scutts et al., 2018), and the blockage of downstream signaling molecules that enhance the production of IFN, such as IRF3 and NF-κB (Smith et al., 2013). Second, VACV synthesizes soluble proteins (B8 and B18) that bind IFN, preventing the recognition of IFN by its receptor and the activation of IFN signaling (Alcami, Symons, & Smith, 2000; Hernaez et al., 2018; Symons, Alcami, & Smith, 1995). Third, VACV blocks the production of ISGs through the inhibition of the IFN signaling cascade by preventing STAT1 and STAT2 activation (Mann et al., 2008; Najarro, Traktman, & Lewis, 2001). Last, VACV has also developed strategies to counteract the action of diverse ISGs, preventing their activation, as in the case of PKR, OAS and eIF2α (Chang, Watson, & Jacobs, 1992; Langland & Jacobs, 2002), or interfering with their function, as in the case of ISG15 (S. Guerra et al., 2008). Of note, VACV not only modulates IFN signaling, but also diverse host defense mechanisms such as the production of proinflammatory cytokines and apoptosis (Bahar et al., 2011), what makes VACV an efficient evader of immune responses.

1.5.1-C. VACV and cell metabolism

As every other virus, VACV depends on the cellular metabolic state to complete its infectious cycle, although each type of virus has specific requirements. VACV has been shown induce a pseudo-hypoxic state early after infection through the stabilization of hypoxia-inducible factor (HIF)-1α (Mazzon et al., 2013). This shifts glycolytic flux towards lactate production and inhibits the TCA cycle (J. W. Kim, Tchernyshyov, Semenza, & Dang, 2006). To overcome this situation, VACV has been shown to sustain the TCA cycle through increased glutamine consumption (Fontaine, Camarda, & Lagunoff, 2014). This allows the generation of citrate to synthesize FAs, which are oxidized in the mitochondrion to fuel OXPHOS-linked ATP production (Greseth & Traktman, 2014; Pant, Dsouza, Cao, Peng, & Yang, 2021). Lipids also play a relevant role during VACV infection, apart from its function as an energy source. Cholesterol content on membrane lipid rafts is important for fusion of VACV and cell membranes, what determines virus entry and egress (Chung, Huang, & Chang, 2005). In addition, several VACV proteins require FA acylation (e.g., palmitoylation, myristoylation) for proper function (Grosenbach, Ulaeto, & Hruby, 1997; Lorenzo, Sanchez-Puig, & Blasco, 2012). As well, as an enveloped virus, alterations in the cellular lipid content impact on VACV membrane generation and composition (Krijnse Locker, Chlanda, Sachsenheimer, & Brugger, 2013). Therefore, the efficiency of VACV infection is expected to be dependent on the mitochondrial and lipid status of host cells.

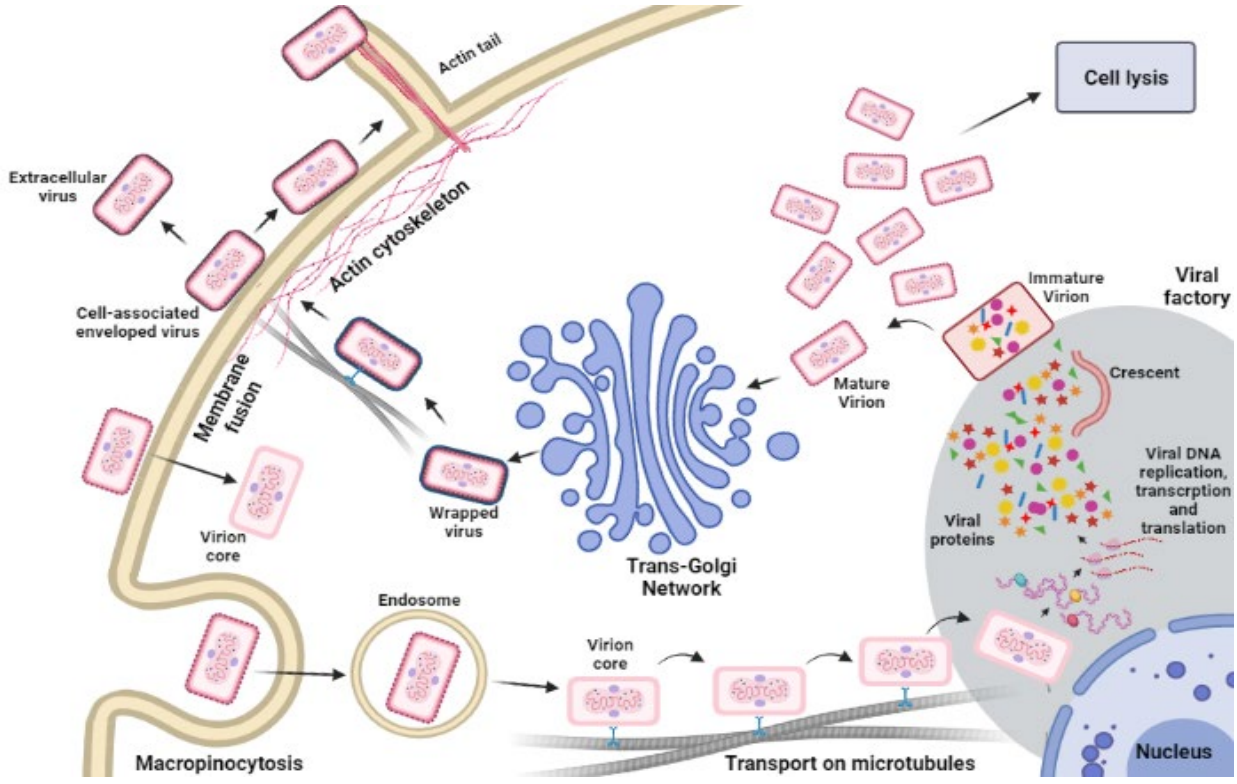

Figure 11. VACV infectious cycle. VACV virions enter the cell through membrane fusion or via macropinocytosis. Once inside, viral genome replication and viral protein synthesis occur in cytoplasmic viral factories. Then, viral content is enclosed within membranes, eventually forming the mature virion. Mature virions accumulate inside the cell until cell lysis, or undergo wrapping in the trans-Golgi network, forming wrapped virions. Wrapped virions are released out of the cell, forming extracellular virus. Wrapped virions that remain attached to the cell surface are named cell-associated enveloped virions, which can be pushed out of the cell by actin tails. Image created with BioRender.com.

OBJECTIVES

2. OBJECTIVES

Previous work from our research group demonstrated that ISG15 plays an important role in the regulation of macrophage functions and intracellular trafficking, significantly affecting the macrophage-mediate antiviral response. This prompted us to investigate whether the absence of ISG15 has an impact on macrophage homeostasis in the context of VACV infection. For that purpose, we performed a proteomic analysis of uninfected and VACV-infected BMDM that directed our project towards the following specific objectives, focused on the host (1-6) and on the virus (7 and 8):

1. To evaluate the presence of ISG15 and ISGylated proteins throughout the mitochondrial structure.
2. To investigate the effect of the absence of ISG15 on mitochondrial respiratory function and dynamics.
3. To study whether ISG15 participates in macrophage polarization.
4. To assess the impact of ISG15 on the macrophage lipid profile, focusing on neutral lipids.
5. To examine the role of ISG15 in the regulation of neutral lipid mobilization and storage on lipid droplets.
6. To elucidate the regulatory network by which ISG15 governs macrophage metabolism.
7. To determine the role of ISG15 as a regulator of VACV morphogenesis and dissemination.
8. To analyze the protein signature of VACV virions grown in the presence or absence of ISG15.

MATERIALS AND METHODS

3. MATERIALS AND METHODS

3.1. Antibodies

Table M1. Antibodies used for western blot and confocal microscopy analyses. Table list: Antibody target (column A); Dilution of stock at use (column B); Source of the antibody (column C).

Antibody	Dilution of stock	Source
β-ACTIN	1:3000	Cell Signaling #3700
ISG15	1:1500	Invitrogen (14-5758-82)
SOD2	1:1000	Abcam ab68155
TOMM20	1:1000	Abcam ab186735
TIMM23	1:1000	Abcam ab230253
CORE2	1:1000	Abcam ab203832
NDUFA9	1:1000	Abcam ab14713
SDHA	1:1000	Abcam ab14715
iNOS	1:1000	Cell Signaling #2982
ARG1	1:1000	Cell Signaling #93668
eIF2A	1:1000	Cell Signaling #9722
SQSTM1	1:1000	Abcam ab109012
COX4	1:1000	Cell Signaling #4850
VDAC1	1:1000	Abcam ab14734
PARKIN	1:500	Santa Cruz Biotechnology sc-32282
NCEH1	1:1000	Sigma-Aldrich SAB4301148
VACV proteins	1:3000	Kindly provided by Dr. Mariano Esteban
VACV A27	1:1000	Kindly provided by Dr. Mariano Esteban
VACV F13	1:1000	Kindly provided by Dr. Rafael Blasco
VACV E3	1:1000	Kindly provided by Dr. Bertrand L. Jacobs
Anti-rabbit IgG-peroxidase	1:10000	Sigma-Aldrich A0545
Anti-mouse IgG-peroxidase	1:10000	Sigma-Aldrich A9044
Anti-Armenian hamster IgG-peroxidase	1:10000	Sigma-Aldrich SAB3700454
Anti-mouse IgG AlexaFluor488	1:1000	Invitrogen #A28175

Anti-rabbit IgG AlexaFluor488	1:1000	Invitrogen #A-11008
Anti-rabbit IgG AlexaFluor 594	1:1000	Invitrogen #A-11012

3.2. Primers

Table M2. Murine primers used in RT-qPCR analysis of mRNA expression. Table list: Target gene (column A); Forward primer sequence (5'-3') (column B); Reverse primer sequence (5'-3') (column C).

Gene	Forward primer (5'-3')	Reverse primer (5'-3')
Abcg1	CCTTCCTCAGCATCATGCG	CCGATCCCAATGTGCGA
Acadl	TCTTGCGATCAGCTCTTTCA	GGTACATGTGGGAGTACCCG
Acadm	AGCTCTAGACGAAGCCACGA	GCGAGCAGAAATGAAACTCC
Acads	AGCTGGACAGGGAGCATCT	ACTCAGCTCCTCTGGCACAT
Cd36	GCGACATGATTAATGGCACA	CCTGCAAATGTCAGAGGAAA
Cpt1a	GATGAACTTCTTCTTCCAGGAGTGC	ATGGCAGAGGCTCACCAAGC
Fasn	AAGTTGCCCGAGTCAGAGAACC	ATCCATAGAGCCCAGCCTTCCATC
Hmgcr	CTTGTGGAATGCCTTGTGATTG	AGCCGAAGCAGCACATGAT
Hmgcs	GCCGTGAACTGGGTCGAA	GCATATATAGCAATGTCTCCTGCAA
Hprt	GATTAGCGATGATGAACCAGGTT	CCTCCCATCTCCTTCTTCATGACA
Isg15	TGACTGTGAGAGCAAGCAGC	CCCCAGCATCTTCACCTTTA
Lxra	TGAGAGCATCACCTTCCTCA	TGGAGAACTCAAAGATGGGG
mtDNA	CTAGAAACCCCGAAACCAAA	CCAGCTATCACCAAGCTCGT
Nceh1	CGGTATTTCTGGAGACAGTGCTG	GGTGTGTTGAAGTCCAAAGCCTG
Nr1h3/Lxra	TGAGAGCATCACCTTCCTCA	TGGAGAACTAAAGATGGGG
Plin2	CCCGTATTTGAGATCCGTGT	CAATTTGTGGCTCCAGCTTC
Ppara	GCGGCCCCATACAGGAGAGCAG	CTAACCTTGGGCCACACCTTGACT
Pparg	TCGCTGATGCACTGCCTATG	GAGAGGTCCACAGAGCTGATT
Ppargc1a	TATGGAGTGACATAGAGTGTGCT	CCACTTCAATCCACCCAGAAAG
Ppargc1b	TGCGGAGACACAGATGAAGA	GGCTTGTATGGAGGTGTGGT
Scap	ATTTGCTCACCGTGGAGATGTT	GAAGTCATCCAGGCCACTACTAATG
Soat1	AGCCCAGAAAAATTTCATGGACACATACAG	CCCTTGTTCTGGAGGTGCTCTCAGATCTTT

Srebf2	GCGTTCTGGAGACCATGGA	ACAAAGTTGCTCTGAAAACAAATCA
Tfam	AATTGCAGCCATGTGGAGGGA	GCTCTCAGGTGGGATGCAG
VACV	CATCATCTGGAATTGTCACTACTAAA	ACGGCCGACAATATAATTAATGC

3.3. Cell culture

BSC40 cells (African green monkey kidney cells, American Type Culture Collection (ATCC), Cat. No. CRL-2761), immortalized *Isg15+/+* and *Isg15-/-* mouse embryonic fibroblasts (MEF), and primary *Isg15+/+* and *Isg15-/-* mouse bone marrow-derived macrophages (BMDM) were used. Cells were grown in Dulbecco's Modified Eagle's Medium (DMEM) 1X supplemented with fetal bovine serum (FBS; 5% for BSC40, 10% for MEF and BMDM), 2 µg/mL glutamine (Sigma, Cat. No. G7513), 1X non-essential amino acids (Sigma, Cat No. M7145), 1X Penicillin Streptomycin (Gibco, Cat. No. 15140-122), and 1 µg/mL amphotericin B (Gibco, Cat. No. 15290-018). Cells were incubated in a humidified incubator at 37ºC and 5% CO_2. Incubation times and additional treatments are specified elsewhere.

3.4. Isolation and culture of bone marrow-derived macrophages

Female mice from the C57BL/6J (*Isg15+/+*) and B6.129P2-*Isg15*^{tm1Kpk}/J (*Isg15-/-*) strains were used to isolate BMDM. Mice between 12 and 25 weeks of age were selected to obtain the cells. The protocol followed for BMDM isolation is based on a well-established method for mouse bone marrow extraction (Toda, Yamauchi, Kadowaki, & Ueki, 2021; X. Zhang, Goncalves, & Mosser, 2008), with some modifications. Mice were euthanized following the appropriate methods approved by the institution and soaked with 70% ethanol before dissection. The tibia and femur bones were obtained by dislocation of their respective joints. When possible, the ilium (pelvic bone) was also extracted. The muscles that remained attached to the bones were removed by scraping with a scalpel. Once the bones were completely clean, the epiphyses were cut off and the bones were placed in a 0.5 mL centrifuge tube with a hole at the bottom. The tubes containing the bones were placed into 1.5 mL centrifuge tubes, and the bone marrow was extracted by centrifugation at 2000 ^{x}g for 10 s. Bone marrow pellets were resuspended in 1 mL BMDM culture medium, consisting of DMEM 1X containing 10% FBS and 10 ng/mL of recombinant murine macrophage-colony stimulating factor (rM-CSF; PeproTech Cat. No. 315-02), and the cell suspension was transferred to a 50 mL tube containing the appropriate amount of BMDM culture medium. Cells were seeded on 100 mm cell culture dishes, 6-well, 12-well or 24-well tissue-culture plates depending on the requirements of the experiment, following the ratio of 4 plates per mouse. Plates were then placed in a humidified incubator at 37ºC and 5% CO_2 and incubated for

6 days. After 6 days of differentiation, BMDM attached to the surface of the plate were washed with PBS and the adequate volume of DMEM 1X containing 10% FBS was added. Specific treatments are indicated in the corresponding sections.

3.5. Immunofluorescence

Cells growing on 12 mm coverslips were washed twice with PBS and fixed with 300 µL of fixation buffer (4% paraformaldehyde [PFA] in PBS) for 20 min at RT. After fixation, PFA was aspirated, and cells were washed twice with PBS. Cells were then incubated with 300 µL of permeabilization buffer (0.2% Triton X-100 in PBS) for 20 min at RT, washed twice with PBS and incubated with blocking buffer (10% FBS in PBS) for 30 min at RT. After blocking, cells were incubated with the desired primary antibodies in binding buffer (PBS containing 5% FBS and 0.2% Triton X-100) for 1 h at 37ºC. Cells were washed 5 times with PBS and incubated with the appropriate secondary antibodies for 30 min at 37ºC in the dark. Concentrations of primary and secondary antibodies are specified in figure legends. After incubation, cells were washed 5 times with PBS, incubated with 1 µg/mL of 2-(4-amidinophenyl)-1H -indole-6-carboxamidine (DAPI) for 20 min at RT and dark, and washed another 5 times with PBS. Finally, coverslips were mounted on glass slides using ProLong™ Diamond mounting medium (Invitrogen, ThermoFisher Scientific, Cat. No. P36961), incubated overnight at RT in the dark and stored at 4ºC until analysis.

3.6. Generation and purification of a viral stock

BSC-40 cells (African green monkey kidney cells, American Type Culture Collection (ATCC), Cat. No. CRL-2761) or immortalized *Isg15-/-* and *Isg15+/+* MEF were propagated in 150 mm tissue-culture dishes and scaled up to 20-25 dishes, following the specified culture conditions. When 80% of confluence was reached, cells were infected with *Vaccinia virus* (VACV) wild-type Western Reserve strain (VACV WR) or International Health Department-J (IHD-J) strain at 0.01 PFU/cell for 48 h, following the protocol described in section *3.7. Viral infection*. At 48 hpi, infected cells were harvested with a cell scraper, and cell suspension was transferred to sterile 50 mL tubes. Cells were pelleted by centrifugation at 250 ^{x}g and 4ºC for 10 min, and the supernatant was discarded. Pellets were resuspended in 10 mL of 10 mM Tris-HCl pH 9.0, and cell suspensions were sonicated in a water bath using a Branson Ultrasonics™ Sonifier 450; sonication was continuous at 50% amplitude until cell clumps were completely homogenized. After sonication, homogenized cell suspension was transferred to 15 mL tubes and centrifuged for 5 min at 400 ^{x}g and 4ºC. Virus-containing supernatants were transferred to new 50 mL tubes, and cell pellets were resuspended in 10 mL of 10 mM Tris-HCl pH 9.0, sonicated again in the same conditions

described above, and centrifuged for 5 min at 400 ˣg and 4ºC. Virus-containing supernatants were mixed with the supernatants previously obtained.

A sucrose cushion was prepared by adding 20 mL of cold 45% sucrose in 10 mM Tris-HCl pH 9.0 in an ultracentrifuge tube (Ultra-Clear Centrifuge Tubes, Beckman Coulter, Cat. No. 344058). Virus-containing supernatant was slowly dispensed on top of the sucrose cushion, ultracentrifuge tubes were placed into the rotor buckets and equilibrated with the appropriate volume of 10 mM Tris-HCl pH 9.0 before ultracentrifugation. Supernatants were ultracentrifuged for 1 h at 72100 ˣg and 4ºC using a Beckman SW28 Ti Swinging-Bucket Aluminium rotor. After ultracentrifugation, supernatants were carefully discarded, and virus pellets were resuspended in 5 mL of 10 mM Tris-HCl pH 9.0 and frozen at -80ºC.

To obtain a highly purified virus stock a further purification step was carried out. A sucrose gradient was prepared by adding 16 mL of 45% sucrose in 10 mM Tris-HCl pH 9.0 in an ultracentrifuge tube, and carefully dispensing 16 mL of 20% sucrose in 10 mM Tris-HCl pH 9.0 on top. The sucrose mixture was frozen at -80ºC for at least 5 h and thawed overnight at 4ºC, causing the formation of a sucrose gradient. Virus suspension was thawed on ice, carefully pipetted over the sucrose gradient, and ultracentrifuged for 20 min at 40000 ˣg and 4ºC using a Beckman SW28 Ti Swinging-Bucket Aluminum rotor. After ultracentrifugation, the virus-containing white band in the middle of the sucrose gradient was recovered by aspiration with a glass pipette and dissolved in 10 mM Tris-HCl pH 9.0. Virus suspension was ultracentrifuged for 45 min at 72100 ˣg and 4ºC using a Beckman SW28 Ti Swinging-Bucket Aluminum rotor. Finally, supernatant was discarded, virus pellet was resuspended in 1 mL of 10 mM Tris-HCl pH 9.0, and 100 µL aliquots were prepared and stored at -80ºC.

3.7. Viral infection

Frozen viral stocks were placed on ice until complete thawing. Prior to infection, viral stocks were sonicated in a water bath to dismantle virus aggregates, using a Branson Ultrasonics™ Sonifier 450. The sonication protocol consisted of 3 cycles of 10 s of continuous sonication followed by 10 pulses at 50% amplitude. Next, viral dilutions were prepared in FBS-free DMEM 1X to match the desired MOI. Cells were washed with PBS and infected with the appropriate inoculum volume, being 3 mL, 1.5 mL, 600 µL, 300 µL and 150 µL for 150 mm tissue-culture dishes, 100 mm tissue-culture dishes, 6-well, 12-well and 24-well tissue-culture plates, respectively. Infected plates were incubated for 1 h to promote virion adsorption to the cell surface, gently shaking the plates every 15 min to distribute the inoculum. After the adsorption time the inoculum was removed, cells were washed with PBS and the infection was restricted with the appropriate volume of DMEM 1X

containing 2% FBS. Infected plates were incubated for the desired infection times. At the convenient post-infection times, cell supernatants were recovered to analyze the extracellular virus production and stored at 4ºC. For the analysis of intracellular virus production, cells were washed with PBS and scraped with a micropipette tip in the appropriate volume of DMEM 1X containing 2% FBS, and samples were stored at -20ºC until sample processing.

3.8. Virus titration by plaque assay

BSC40 cells were seeded in 12-well plates 24 h prior to titration, in a 1:3 passage ratio to allow the formation of a cell monolayer; 1 mL of cell suspension was added to each well. Samples were subjected to 3 cycles of freezing in dry ice and thawing at 37ºC before titration to extract intracellular virus particles. Then, cell debris was pelleted by centrifugation at 250 ^{x}g for 5 min, and the virus-containing supernatants were recovered and transferred to new 1.5 mL tubes. Extracellular virus samples (supernatants of infected cells) were centrifuged at 250 ^{x}g for 5 min to pellet dead cells and cell debris in suspension, and the clean supernatants were transferred to a new 1.5 mL tubes.

Processed samples were sonicated in a water bath to dismantle virus aggregates, using a Branson Ultrasonics™ Sonifier 450. The sonication protocol consisted of 3 cycles of 10 s of continuous sonication followed by 10 pulses at 50% amplitude. After sonication, serial 1:10 dilutions of the samples were prepared in 1.5 mL tubes using FBS-free DMEM. Finally, BSC40 monolayers were infected with 300 µL of the appropriate dilution of the samples. Infected plates were incubated at 37ºC and 5% CO_2 for 1 h to promote virion adsorption to the cell surface, gently shaking the plates every 15 min to distribute the inoculum. After the adsorption time the inoculum was removed, and 1 mL of overlay medium was added to each well. When titrating VACV WR-infected cells, DMEM 1X containing 2% FBS was used as liquid overlay; for VACV IHD-J-infected cells, medium also contained 1% agarose to form a semisolid overlay. Finally, plates were incubated at 37ºC and 5% CO_2 for 48 h in a humidified incubator.

After 48 h plates were fixed and stained for plaque quantification. For VACV WR strain-infected samples fixation and staining were simultaneous, by adding 0.5 mL per well of 10% formaldehyde in PBS containing 0.2% crystal violet and incubating for 30 min at room temperature (RT). VACV IHD-J strain-infected samples were first fixed through the semisolid overlay with 0.5 mL per well of 10% formaldehyde in PBS, incubating for 20 min at RT. Afterwards, formaldehyde and the overlay were removed and 0.5 mL of 10% formaldehyde in PBS containing 0.2% crystal violet was added to each well, incubating for 20 min at RT. Fixation solution was then recovered, and plates were rinsed twice with water before plaque quantification.

Virus plaques were counted and virus plaque forming units (PFU) per mL were quantified using the equation:

$$\frac{PFU}{mL} = Mean\ plaque\ number * Dilution\ counted * (\frac{Sample\ volume}{Inoculum\ volume})$$

3.9. Interferon treatment

Cells were washed with PBS and treated for 16 or 24 h with the appropriate volume of DMEM 1X containing 10% FBS and 500 U/mL of Universal Type I Interferon (PBL Assay Science, Cat. No. 11200-2), at 37ºC and 5% CO_2 in a humidified incubator.

3.10. Ethics statement

All animals were handled in strict accordance with good animal practice defined by the pertinent local, national and/or international welfare bodies, following the guidelines defined by the Spanish Royal Decree (RD 53/2013) and the European Union Directive (2010/63/UE), relative to the protection of animals used for scientific purposes. The Ethics Committee of Animal Experimentation of Universidad Autónoma de Madrid (UAM) approved all animal experimental procedures. Animals were bred and housed under conventional conditions. The projects' license numbers assigned by the Ethics Committee are PROEX 041/15 and PROEX 184.3/20.

3.11. Immunoblot

Cells were homogenized in lysis buffer (50 mM Tris, 150 mM NaCl, 1% NP-40) supplemented with protease inhibitors cocktail (cOmplete Mini, Roche, Cat. No. 11836153001) and phosphatase inhibitors cocktail (Pierce™ Phosphatase Inhibitor Mini Tablets, Thermo Scientific, Cat. No. A32957). To ensure a complete homogenization and protein extraction, samples underwent 3 cycles of freezing in dry ice and thawing at 37ºC and resulting cell debris was pelleted by centrifugation at 21000 ^{x}g for 20 s. Protein-containing supernatants were transferred to new centrifuge tubes, and protein concentration was determined by Bradford assay using the Protein Assay Dye Reagent Concentrate (BioRad, Cat. No. 500-0006) and measuring absorbance at 595 nm wavelength.

Protein samples were mixed with SDS sample buffer (Laemmli buffer [recipe]) and boiled at 95ºC for 5 min. Proteins were separated by 12% or 10% SDS-PAGE at an intensity of 40 mA per gel, using handcast gels and Tris-Glycine running buffer (25 mM Tris, 152 mM Glycine, 3.5 mM SDS, pH 8.5). Protein Marker VI (10-245) prestained (PanReac AppliChem, ITW Reagents, Cat. No. A8889) was used as marker for protein molecular weight. Proteins in the gel were transferred to

a 0.45 µm PVDF membrane (Merck Millipore, Cat. No. IPVH00010) in a semi-dry immunoblot transfer system (Trans-Blot SD Semi-Dry Transfer Cell, BioRad, Cat. No. 1703940) at 15 V for 45 min. After transfer, membranes were blocked with 5% skimmed milk in Tris-Buffered Saline pH 7.5 (TBS) with 0.1% Tween-20 (TBS-T), for 1 h at RT and agitation. Blocked membranes were incubated with the desired primary antibodies overnight at 4ºC and agitation. Incubation with primary antibodies was followed by 3 washing steps of 5 min with TBS-T, and incubation with the appropriate HRP-conjugated secondary antibodies for 1 h at RT and agitation. Primary and secondary antibodies were prepared in 0.5% skimmed milk in TBS-T, and the concentrations are specified in figure legends. Finally, membranes were washed 3 times TBS-T (5 min each) and developed by incubating with chemiluminescence substrate (Clarity Western ECL Substrate, BioRad, Cat. No. 1705061) for 1 min in agitation in the dark. Imaging was performed using a ChemiDoc™ MP Imaging System (BioRad, Cat. No. 1708280) and Image Lab™ Software (BioRad, Cat. No. 1709690).

3.12. Analysis of mRNA expression by two-step quantitative reverse transcription PCR (RT-qPCR)

Total RNA was extracted using NucleoZOL (Macherey-Nagel, Cat. No. 740404.200), following the manufacturer's instructions. RNA pellets were resuspended in DEPC-treated RNase-free water (ThermoFisher Scientific, Cat. No. J70783.K2) and RNA concentration was measured using a Maestrogen MaestroNano Spectrophotometer (MaestroGen). 1 µg of RNA was reverse-transcribed using the High-Capacity cDNA Reverse Transcription Kit (Applied Biosystems™, Cat. No. 4368814). For mRNA quantification, reactions were prepared with 10 µL of 2X qPCRBIO SyGreen Mix Hi-ROX (PCR Biosystems, Cat. No. PB20.12-05), 400 nM of forward and reverse primers (see Table X), 25 ng of template cDNA and the adequate volume of DEPC-treated RNase-free water up to a final volume of 20 µL. The analysis was performed in StepOnePlus™ Real-Time PCR System (ThermoFisher Scientific, Cat. No. 4376600) following the protocol: pre-incubation 2 min at 95ºC (1 cycle); denaturation at 95ºC for 5 s, annealing and extension at 60ºC for 30 s (40 cycles), and melt curve analysis: melting at 95ºC for 15 s, 65ºC for 60 s and 95ºC for 15 s, step and hold (1 cycle), followed by a step of cooling at 4ºC for 30 s. HPRT gene was used as housekeeping gene (see Table M2), and the relative gene expression was calculated by the $2^{-\Delta\Delta Ct}$ method.

3.13. Quantitative proteomic analysis of BMDM

Protein extracts from *Isg15+/+* and *Isg15-/-* BMDM, treated with type I IFN (500 U/mL, 24 h), were obtained after cell lysis in extraction buffer (50 mM Tris-HCl, 1 mM EDTA, 1.5% SDS, pH 8.5).

Samples digested in trypsin, and the resulting peptides were subjected to 4-plex isobaric labeling (iTRAQ) and separated into 8 fractions by cation exchange chromatography using Waters Oasis MCX cartridges (Waters Corp, Milford, MA, USA) and graded concentrations of ammonium formate, pH 3.0 (AF3) in acetonitrile (ACN). The tryptic peptide fractions were subjected to nanoLC-MS/MS. High-resolution analysis was performed on a nano-HPLC Easy nLC 1000 liquid chromatograph (Thermo Scientific, San Jose, CA, USA) coupled to an Orbi-trap Fusion mass spectrometer (Thermo Scientific). Protein identification was performed using the SEQUEST HT algorithm integrated in Proteome Discoverer 1.4 Software (Thermo Scientific). MS/MS scans were matched against a mouse database (UniProtKB/Swiss-Prot 2015_11 Release). Peptides were identified from MS/MS data using the probability ratio method (Martinez-Bartolome et al., 2008). False discovery rate of peptide identifications was calculated by the refine method (Bonzon-Kulichenko, Garcia-Marques, Trevisan-Herraz, & Vazquez, 2015; Navarro & Vazquez, 2009). Quantitative information was extracted from the MS/MS spectra of iTRAQ-labeled peptides. For comparative analysis of protein abundance changes, the Weighted Scan-Peptide Protein (WSPP) statistical workflow was applied (Garcia-Marques et al., 2016; Navarro et al., 2014). The quantified proteins were functionally annotated using the Ingenuity Knowledge Database (Calvano et al., 2005; Ficenec et al., 2003) and DAVID, a repository that includes 13 functional databases, including Panther, KEGG and Gene Ontology (Huang da et al., 2009).

3.13.1. Bioinformatic analysis of BMDM proteomics

The proteins identified in the proteomic analysis of BMDM and the ratio fold-change between *Isg15-/-* and *Isg15+/+* cells were used to analyze the differences in the proteome related to the absence of ISG15. Ingenuity Pathway Analysis software (IPA, Qiagen) was used to explore the main pathways and regulators affected by the lack of ISG15. The Canonical Pathway Analysis identified the pathways from the IPA library that were most significant to our dataset. The statistical significance of the association between identified pathways and our data was determined by Fisher's exact test, for which the significance threshold was set at 0.05 (Codrea & Nahnsen, 2016). The Upstream Regulator Analysis identifies proteins, present or not in the dataset, that are potential master regulators of the different pathways represented in the dataset. This tool sets an overlap p-value to evaluate the enrichment of proteins in the dataset related to a given master regulator from the database.

The STRING Database V11.5 (Szklarczyk et al., 2021) was used to generate protein-protein interaction networks and to classify proteins by their function. In this analysis, only proteins with a ratio fold-change equal or higher than +2, and equal or lower than -2, were used. Functional

and physical protein associations were analyzed, and the minimum required interaction score was set to 0.9 (highest confidence).

3.14. Confocal microscopy and image analysis

Confocal microscopy analyses were performed using Leica TCS SP5, Leica TCS SP8 and Zeiss LSM 880 Airyscan Super-resolution confocal microscopes. Processing of microscopy images was performed with Fiji software (Schindelin et al., 2012), and Fiji and Aivia AI Image Analysis software (https://www.aivia-software.com) were used for image analysis.

3.15. Cell fractionation and isolation of mitochondria

BMDM subcellular fractionation and isolation of mitochondria was performed as described elsewhere (Garaude et al., 2016). 10^7 BMDM were harvested in PBS containing 5 mM EDTA, pelleted by centrifugation at 250 ^{x}g for 5 min, washed with PBS and pelleted again. Pellets were frozen at -80ºC to increase cell breakage and were homogenized in a tightly fitting glass-teflon homogenizer with 10 volumes of buffer A (83 mM sucrose, 10 mM MOPS, pH 7.2). An equal volume of buffer B (250 mM sucrose, 30 mM MOPS, pH 7.2) was added and the mixture was centrifuged at 1000 ^{x}g for 5 min. Supernatants were transferred to new 1.5 mL centrifuge tubes and pellets corresponding to the nuclear fraction were stored at -80ºC. Collected supernatants were centrifuged at 12000 ^{x}g for 2 min and the resulting supernatants corresponding to the cytoplasmic fraction were recovered and stored at -80ºC. Mitochondria pellets were washed with buffer C (320 mM sucrose, 1 mM EDTA, 10 mM Tris-HCl, pH 7.4) and mitochondria were pelleted by centrifugation at 12000 ^{x}g for 2 min. Mitochondria pellets were resuspended in an appropriate volume of PBS and stored at -80ºC.

3.16. Determination of mitochondrial location of ISG15 and ISGylated proteins by proteinase K digestion

Isolated mitochondria (25 µg) from type I IFN-treated *Isg15*+/+ BMDM were resuspended in 50 µL of assay buffer (20 mM Tris pH 7.2, 15 mM KH_2PO_4, 20 mM $MgSO_4$, 0.6 M sorbitol). Proteinase K (Roche, Cat. No. 3115836001) was added at a final concentration of 50 or 250 µg/mL to constitute digestion buffer, and samples were incubated for 15 min on ice. Alternatively, digestion buffer was used in combination with increasing concentrations of digitonin or osmotic shock buffer (25 mM sucrose, 10 mM MOPS-KOH, pH 7.2) in the presence or not of 1% Triton-X100 to disrupt mitochondrial membranes and allow the digestion of proteins at different mitochondrial locations. Addition of PMSF to a final concentration of 5 mM was used to stop the reaction. Finally, digested mitochondria were centrifuged at 6800 ^{x}g for 3 min at 4ºC, the pellet was resuspended in SDS

sample buffer and proteins were analyzed by Western Blot following the protocol described in section *3.11. Immunoblot*.

3.17. Analysis of mitochondrial respiratory parameters

Real-time oxygen consumption rate (OCR) and extracellular acidification rate (ECAR) were assessed for *Isg15+/+* and *Isg15-/-* BMDM using both Seahorse XF-96 and XF-e96 Extracellular Flux Analyzer platforms (Agilent). 6 x10^4 BMDM/well in five wells were used per condition. Measurements were performed in XF Base Medium (Agilent) supplemented with 5 mM glucose, 2 mM glutamine, 1 mM sodium pyruvate, 50 µM palmitate, 100 µg/mL penicillin, and 100 µg/mL streptomycin. Where indicated, cells were treated with type I IFN (500 U/mL) 24 h before the analysis. In addition, to assess specific metabolite demands, cells were treated with etomoxir (5 µM final concentration) for 30 min before the analysis started. The ETC inhibitors oligomycin (oligo; 2 µM final), Carbonyl cyanide-p-trifluoromethoxyphenylhydrazone (FCCP) (2.85 µM final), rotenone (Rot; 1 µM final) and antimycin A (AA; 2 µM final) were used to assess the different mitochondrial respiratory parameters. Basal respiration was defined as OCR in the absence of inhibitors. Maximal respiration was defined as the OCR after addition of oligomycin and FCCP. The protocol consisted of: 5 measurements at basal conditions → oligo injection → 3 measurements → first FCCP injection → 3 measurements → second FCCP injection → 3 measurements →injection of Rot+AA → 3 measurements. Measurements lasted 3 min and were preceded by 2 min of mixing. Once finished, cells were fixed with 4% PFA for 10 min at RT, washed with PBS and stained with 0.5 ng/mL Hoechst Stain solution (Sigma, Cat. No. H6024) for 15 min at RT in the dark. Cell counts were determined by fluorescence microscopy using an Operetta® CLS™ High-Content Analysis System (PerkinElmer), and results were normalized to cell numbers. Data were analyzed using the Wave Software (Agilent).

3.18. Citrate synthase activity assay

The activity of citrate synthase was determined in total extracts from IFN-treated *Isg15-/-* and *Isg15+/+* BMDM by measuring the production of SH-CoA from oxaloacetate, using a Beckman DU-650 spectrophotometer. Protein concentration was measured by the Lowry's method for normalization. Citrate synthase activity is represented as nmol x min^{-1} x mg $protein^{-1}$. All measurements were performed with 3 biological replicates.

3.19. ATP synthesis assay

ATP synthesis was determined in permeabilized BMDM by kinetic luminescence assay as described in (Vives-Bauza, Yang, & Manfredi, 2007). BMDM (2 x10^6 cells) were resuspended in

160 µL of buffer A (150 mM KCl, 25 mM Tris-HCl, 2 mM EDTA, 0.1% BSA FA, 10 mM K-phosphate, 0.1 mM $MgCl_2$, pH 7.4) at RT, and 50 µg/mL of digitonin was added. Samples were mixed gently for 1 min, and the reaction was stopped by addition of 1 mL of buffer A. Cells were centrifuged at 850 ^{x}g for 2 min at RT, and pellets were resuspended in 160 µL of buffer A and transferred to a 96-well luminescence reading plate (Corning® Costar, Cat. No. 3917). Substrate cocktail (50 µL) and 20 µL of buffer B (0.5 M Tris-acetate pH 7.75, 0.8 mM luciferine, 20 µg/mL luciferase) were added, and luminescence was measured over 1 min. Substrate cocktails were composed of 6 mM diadenosine pentaphosphate and 6 mM ADP supplemented with 1 mM glutamate and 1 mM malate for determination of mitochondrial complex I activity, or with 1 M succinate for complex II activity. ATP production rate is expressed as nmol of ATP/min/mg of protein. All measurements were performed in triplicate.

3.20. Blue native PAGE

Mitochondria isolated from *Isg15+/+* and *Isg15-/-* BMDM, treated or not with type I IFN (500 U/mL, 16 h) were mixed with 10 µL of sample buffer (5% Blue G-250, 5% glycerol in AA Buffer [500 mM 6-aminohexanoic acid, 50 mM imidazole, 1 mM EDTA, pH 7.0]). Samples were separated according to their indicated masses on a linear 3.5%→16% acrylamide gradient gel for BN-PAGE, as described in (Wittig, Braun, & Schagger, 2006). Next steps were performed as described in section *3.11. Immunoblot.*

3.21. Quantification of mitochondrial DNA by quantitative PCR (qPCR)

Mitochondrial DNA (mtDNA) content was determined by absolute quantification using real time PCR as described in (Malik, Czajka, & Cunningham, 2016). Primers for mouse mtDNA (see Table M2) were used to amplify the respective products from mouse genomic DNA. Mitochondria DNA copy numbers per cell were determined from template DNA by performing a quantitative PCR (qPCR) in a total volume of 10 µL, containing 5 µL of QuantiFast SYBR Master Mix (Qiagen, Cat. No.04054), 400 nM of forward and reverse primers, 2 µL of template DNA and 2 µL of DNase-free water. The reactions were performed in Roche LightCycler (LC) 480 following the protocol: pre-incubation 5 min at 95ºC (1 cycle); denaturation at 95ºC for 10 s, annealing and extension at 60ºC for 30 s (40 cycles); and melt curve analysis: melting at 95ºC for 5 s, 65ºC for 60 s and 95ºC for 15 s, continuous (1 cycle), followed by a step of cooling at 4ºC for 30 s.

3.22. Analysis of mitochondrial reactive oxygen species (ROS) production

BMDM were seeded on 8-well chamber slides (µ-Slide 8 Well, ibidi, Cat. No. 80826) at a density of 2 x10^5 cells per well. The culture medium was replaced with medium supplemented with 10 µM

MitoSOX™ Red Mitochondrial Superoxide Indicator (Invitrogen™, Thermo Fisher Scientific, Cat. No. M36008) and incubated a 37ºC and 5% CO_2 for 1 h in the dark. After incubation, cells were washed with PBS, replenished with fresh medium, and analyzed by confocalmicroscopy. Images were taken every hour during 6 h and analyzed with Fiji Software (Schindelin et al., 2012). Fluorescence was measured in several fields in each well and results were expressed as relative fluorescence per cell.

3.23. Analysis of NO production

Nitric oxide (NO) production was determined by the Griess assay, a method for the indirect determination of NO by measuring nitrites in cell supernatants (Bryan & Grisham, 2007). BMDM supernatants were combined with an equal volume of 10 mM sulfanilamide (Sigma-Aldrich, Cat. No. S9251) and 10 mM N-(1 napththyl) ethylenediamine dihydrochloride (Sigma-Aldrich, Cat. No. N5889), and incubated at room temperature for 10 min. After incubation, absorbance was measure at 490 nm wavelength in a microplate reader. A standard curve of known concentrations of sodium nitrite was used to determine nitrite levels in samples.

3.24. Determination of arginase activity

Arginase activity was assessed by measuring urea production with the Arginase Activity Assay Kit (Sigma-Aldrich, Cat. No. MAK112), following the manufacturer's instructions. Arginase activity was expressed in arbitrary units, where 1 unit is equivalent to the amount of enzyme needed to convert 1 micromole of L-arginine to ornithine and urea per minute at pH 9.5 and 37ºC.

3.25. Lipidomic analysis of BMDM

3.25.1. Sample obtention

BMDM from *Isg15+/+* and *Isg15-/-* mice (4 mice per genotype) were isolated and cultured as described in *3.4. Isolation and culture of bone marrow-derived macrophages*. After 6 days, cells were treated with type I IFN (500 U/mL) for 24 h or infected with VACV WR at 1 PFU/cell for 16 h. BMDM were then collected and pelleted by centrifugation at 250 ^{x}g for 10 min, and pellets were frozen at -80ºC until they were processed for lipidomic analysis at the Center for Cooperative Research in Biosciences (CIC bioGUNE, Derio, Basque Country, Spain).

3.25.2. Metabolite extraction

Metabolite extraction was accomplished by fractionating the BMDM into pools of species with similar physicochemical properties, using appropriate combinations of organic solvents. Cell pellets were resuspended in cold water and vortexed. Proteins were precipitated from the lysed cell samples by adding methanol, followed by addition of chloroform after a brief vortex. Both

extraction solvents were spiked with metabolites not detected in unspiked cell extracts (internal standards). Samples were incubated at -20ºC for 30 min and, after vortexing, 500 µL were collected for liquid chromatography-tandem mass spectrometry (LC-MS/MS) analysis.

3.25.3. Sample preparation

Cell extracts were mixed with ammonium hydroxide in water (pH 9.0), vortexed and incubated for 1 h at -20ºC. Samples were centrifuged at 18000 ^{x}g and 4ºC for 15 min and the organic phase was collected and dried under vacuum. Dried extracts were reconstituted in acetonitrile:isopropanol (1:1), resuspended by agitation for 10 min, centrifuged at 18000 ^{x}g and 4ºC for 5 min, and transferred to plates for UHPLC-MS analysis (Y. Y. Zhao, Wu, Liu, Zhang, & Lin, 2014).

Additionally, two different types of quality control (QC) samples were used to assess the data quality (van der Kloet, Bobeldijk, Verheij, & Jellema, 2009). The QC samples are reference serum samples, which were evenly distributed over the batches and extracted and analyzed together with the individual samples. A QC calibration sample was used to correct the different response factors between and within batches, and a QC validation sample was used to assess how well data pre-processing procedure improved data quality.

3.25.4. UHPLC-MS analysis

For this analytical platform, randomized sample injections were performed, with each of the QC samples uniformly interspersed throughout the entire batch run. The overall quality of the procedure was monitored using repeat extracts of the QC samples. Retention time stability throughout the run is generally < 6 s variation (injection-to-injection) and mass accuracy is generally < 5 ppm for mass-to-charge ratio (*m/z*) 400-1000, and < 1.2 mDa for *m/z* 50-400.

3.25.5. Data pre-processing

All data were processed using the TargetLynx^{TM} Application Manager for MassLynx^{TM} 4.1 Software (Waters Corp., Milford, USA). A set of predefined retention time-*m/z* pairs (Rt-*m/z*) corresponding to metabolites included in the analysis was fed to the program. Associated extracted ion chromatograms (mass tolerance window = 0.05 Da) were then peak-detected and noise-reduced in both the LC and MS domains so that only true metabolite-related features were processed by the software. A list of chromatographic peak areas was generated for each sample injection.

3.25.6. Data normalization and quality control

Normalization factors were calculated for each metabolite by dividing their intensities in each sample by the recorded intensity of and appropriate internal standard in the same sample, following the procedure described in (Martinez-Arranz et al., 2015). The most appropriate internal standard for each variable was defined as that which resulted in a minimum relative standard deviation after correction, as calculated from the QC calibration samples over the analysis batches. In addition, robust linear regression was used to estimate any intra-batch drift not corrected by internal standard correction in the QC calibration samples. Following normalization, response values were assessed. Where coefficients of variation higher than 30% were found, corresponding sample injection data automatically generated by the software were manually revised, and modifications were performed where appropriate. Any variable with zero values in the corrected dataset were replaced with missing values before forming the final dataset and performing the statistical analyses.

3.25.7. Statistical analysis

Once normalized, the dimensionality of the complex data set was reduced to enable easy visualization of any metabolic clustering of the different groups of samples. This was achieved by multivariate data analysis, including the non-supervised principal component analysis (PCA) and/or supervised orthogonal partial least-squares to latent structures (OPLS) approaches (Checa, Bedia, & Jaumot, 2015).

To examine potential metabolic differences between *infected* vs. *uninfected* samples of the same genotype, and *Isg15-/-* vs. *Isg15+/+ uninfected* samples, we performed univariate statistical analyses. Group percentage changes and paired *Student's t-test p-value* were calculated, and *Welch's t-test* was performed where unequal variances were found. When comparing *Isg15-/-* vs. *Isg15+/+ infected* samples, and to avoid the differences per mouse, data were first normalized by dividing the data of each metabolite obtained for *infected* samples per the data obtained for *uninfected* samples for the same mouse. Then, univariate statistical analyses (*Student's t-test p-value* and *Welch's t-test p-value*) were performed.

3.26. Statistical analysis

Statistical analyses were performed with GraphPad Prism V 9.0 software (GraphPad Software, San Diego, CA, USA, http://www.graphpad.com). Comparisons of two groups were analyzed applying the two-tailed unpaired *Student's t-test*, or the *Welch's t-test* when variances were unequal. Equality of variances was tested with the *F-test*. When necessary, two-way ANOVA and Tukey post-hoc tests were performed. A $p\text{-value} < 0.05$ was considered statistically significant.

3.27. OA-FBS conjugation

Oleic acid (OA) (Sigma-Aldrich, Cat. No. O1383) was dissolved in ethanol to a final concentration of 400 mM. Aliquots of FBS were prepared and placed in a water bath at 57ºC. OA was added to the FBS aliquots to constitute a 2 mM OA solution. A total of 10 OA additions were done, while vortexing; the first 6 additions were followed by 20 min incubations at 57ºC in a water bath, increasing the incubation time to 30 min in the last 4 additions. Vehicle control solutions were prepared by adding the appropriate volume of ethanol to FBS. Once prepared, solutions were aliquoted and stored at -80ºC.

3.28. LD analysis by confocal microscopy

BMDM were seeded on coverslips in 12-well or 24-well plates at a density of 2 $x10^5$ or 1 $x10^5$ cells per well, respectively. Cells were washed with PBS and treated or not with type I IFN in DMEM 1X containing 10% FBS. LD synthesis was induced incubating cells with DMEM 1X containing 10% FBS and 100 µM OA, together with type I IFN treatment. Incubations were done for 24 h in a humidified incubator at 37ºC and 5% CO_2. For LD staining, BMDM were washed twice with PBS and incubated with DMEM 1X containing 10% FBS and BODIPY 493/503 to a final concentration of 1 µg/mL, for 30 min in a humidified incubator at 37ºC and 5% CO_2. After staining, cells were washed twice with PBS and processed for confocal microscopy analysis as described in section *3.5. Immunofluorescence*.

3.29. Analysis of lipid mobilization by confocal microscopy

BMDM were seeded on 8-well chamber slides (µ-Slide 8 Well, ibidi, Cat. No. 80826) at a density of 1.5 $x10^5$ cells per well. The culture medium was replaced with DMEM 1X containing 10% FBS and 1 uM BODIPY 558/568 C12, and cells were incubated for 16 h at 37ºC and 5% CO_2. After incubation, cells were washed 3 times with growth medium and fresh medium was added. Cells were incubated for 1 h at 37ºC and 5% CO_2 and, 2 h after incubation (or 3 h after medium was replaced), cells were subjected to confocal microscopy analysis with live cells with a Leica TCS SP5 confocal microscope. Microscopy images were processed and analyzed with Fiji.

3.30. Comet-like plaque formation assays

Immortalized *Isg15-/-* and *Isg15+/+* MEF were seeded in 6-well plates. MEF monolayers were infected with WR or IHD-J at approximately 0.0001 PFU/cell. After 1 h of adsorption, the inoculum was replaced with DMEM 1X containing 2% FBS, and plates were incubated at 37°C and 5% CO_2 for 48 h (for IHD-J) or 72 h (for WR). After the indicated incubation times, plates were fixed and stained for comet visualization following the protocol described in *3.8. Virus titration by plaque assay*.

3.31. Transmission electron microscopy

Isg15-/- and *Isg15*+/+ BMDM were isolated and cultured in 100 mm cell culture dishes, and processed for TEM analysis. Immortalized *Isg15-/-* and *Isg15*+/+ MEF were seeded in 100 mm cell culture dishes. MEF monolayers were infected at 2 PFU/cell with the strain IHD-J of VACV. At 9 hpi, when the cytopathic effect was evident, the supernatant was removed and MEF were processed for TEM analysis. Cells were fixed with a solution of 2.5% glutaraldehyde containing 1% tannic acid, 0.4 M HEPES in PBS. After fixation, cells were carefully scraped, centrifuged to eliminate the fixative, and processed for embedding in the epoxy-resin EML-812 as previously described (Rodríguez, Esteban, & Rodríguez, 1995). Electron micrographs were taken using a transmission electron microscope (JEOL JEM-1011; Centro Nacional de Biotecnología, Spain) equipped with a ES1000W Erlangshen charge-coupled-device (CCD) camera (Gatan Inc.) at an acceleration voltage of 40 to 100 kV. Micrographs were analyzed with Fiji. Fifty low-magnification micrographs were analyzed per genotype. Cells which kept integrity were considered for the analysis. In the case of MEF, non-infected cells were excluded from the analysis, and the number of intracellular viral particles per cell was quantified in more than 110 cells per genotype.

3.32. Quantitative proteomic analysis of purified virions

Isg15-/- and *Isg15*+/+ MEF were infected with IHD-J (0.01 PFU/cell, 48 h), and intracellular virions were purified following the protocol described in *3.6. Generation and purification of a viral stock*. Purified virions were processed for LC-MS/MS analysis.

3.32.1. In-solution Digestion

Protein samples were individually digested with trypsin using a standard protocol. Briefly, 20 µg of protein of each sample were resuspended and denatured in 20 µL of 7 M urea, 2 M thiourea, 100 mM TEAB (triethylammonium bicarbonate), reduced with 2 µL of 50 mM Tris 2-carboxyethyl phosphine (TCEP) (AB SCIEX, Foster City, CA, USA), pH 8.0, at 37 °C for 60 min and followed by cysteine-blocking reagent chloroacetamide (CAA). Samples were diluted up to 60 µL with 50 mM TEAB to reduce the concentration of urea. One µg of sequence grade-modified trypsin (Pierce) was added to each sample (ratio 1:20 enzyme:sample), which were then incubated at 37 °C overnight on a shaker. After digestion, samples were dried in a SpeedVac (Thermo Scientific, Waltham, MA, USA).

3.32.2. Tagging with TMT 6plex™ reagent

The resulting tryptic peptides were subsequently labelled using TMT-6plex Isobaric Mass Tagging Kit (Thermo Scientific, Rockford, IL, USA) according to the manufacturer's instructions as follows: 126: WT-R1; 127: WT-R2; 128: WT-R3; 129: KO-R1; 130: KO-R2; 131: KO-R3). After labelling,

the samples were pooled, evaporated to dryness, and stored at -20°C until the LC−MS analysis. Three biological replicates of each condition were analyzed.

3.32.3. Liquid chromatography and mass spectrometry analysis (LC-ESI-MS/MS)

Before MS analysis, we determined the amount of peptide in the combined sample by Qubit™ Fluorometric Quantitation (Thermo Fisher Scientific). A 1 µg aliquot of each fraction was subjected to 1D-nano LC ESI-MS/MS (Liquid Chromatography Electrospray Ionization Tandem Mass Spectrometric) analysis using an Ultimate 3000 nano HPLC system (Thermo Fisher Scientific) coupled online to an Orbitrap Exploris 240 mass spectrometer (Thermo Fisher Scientific). Peptides were eluted onto a 50 cm × 75 µm Easy-spray PepMap C18 analytical column at 45°C and were separated at a flow rate of 300 nL/min using a 120 min gradient ranging from 2 % to 35 % mobile phase B (mobile phase A: 0.1% formic acid (FA); mobile phase B: 80 % acetonitrile (ACN) in 0.1% FA). The loading solvent was 2 % ACN) in 0.1 % FA and injection volume was 5 µL. Data acquisition was performed using a data-dependent top-20 method, in full scan positive mode, scanning 375 to 1200 m/z. Survey scans were acquired at a resolution of 60,000 at m/z 200, with Normalized Automatic Gain Control (AGC) target (%) of 300 and a maximum injection time (IT) in AUTO. The top 20 most intense ions from each MS1 scan were selected and fragmented via Higher-energy collisional dissociation (HCD). Resolution for HCD spectra was set to 45,000 at m/z 200, with AGC target of 100 and a maximum ion injection time in AUTO. Isolation of precursors was performed with a window of 0.7 m/z, exclusion duration (s) of 45 and the HCD collision energy was 30. Precursor ions with single, unassigned, or six and higher charge states from fragmentation selection were excluded. Raw instrument files were converted to MGF files and MS/MS spectra searched using OMSSA 2.1.9, X!TANDEM 2013.02.01.1, Myrimatch 2.2.140 and MS-GF+ (Beta v10072) against a composite target/decoy database built from the *Mus musculus* reference proteome sequences and the Vaccinia virus (strain Western Reserve) proteome downloaded from UniprotKB. Search engines were configured to match potential peptide candidates with mass error tolerance of 25 ppm and fragment ion tolerance of 0.02 Da, allowing for up to two missed tryptic cleavage sites and a maximum isotope error (13C) of 1, considering fixed carbamidomethyl modification of cysteine and variable oxidation of methionine, pyroglutamic acid from glutamine or glutamic acid at the peptide N-terminus, and modification of lysine and peptide N-terminus with TMT 6-plex reagents. Score distribution models were used to compute peptide-spectrum match p-values, and spectra recovered by a false discovery rate (FDR) ≤ 0.01 (peptide-level) filter were selected for quantitative analysis. Approximately 5% of the signals with the lowest quality were removed prior to further analysis. Differential regulation was

measured using linear models, and statistical significance was measured using q-values (FDR). All analyses were conducted using a software from Proteobotics (Madrid, Spain).

RESULTS

4. RESULTS

4.1. ISG15 is a regulator of mitochondrial functions in BMDM

4.1.1. The absence of ISG15 alters the mitochondrial proteome of BMDM

The relevance of ISG15 in macrophages and the impact of ISG15 induction on a wide array of proteins prompted us to investigate whether there were significant differences between the proteomes of *Isg15-/-* and *Isg15+/+* BMDM. To answer our questions, we analyzed the total proteomes of type I IFN-treated *Isg15-/-* and *Isg15+/+* BMDM by quantitative proteomics, in collaboration with the group of Dr. Jesús Vázquez, at the Spanish Center for Cardiovascular Research (CNIC, Madrid, Spain). The proteomic analysis of BMDM identified and annotated 7154 proteins. Of the total, 2199 proteins were considered significantly differentially expressed between genotypes, as their *Zq* values (standardized log2 [*Isg15-/-* /*Isg15+/+*] ratio at the protein level) were higher or lower than +2 and -2, respectively. 983 proteins were significantly upregulated (*Zq* ≥ +2), while 1216 proteins were significantly downregulated (*Zq* ≤ -2). These proteins were subjected to bioinformatic analyses using the Ingenuity Pathway Analysis (IPA) software. The IPA Canonical Pathway Analysis tool identified numerous pathways that were altered in the absence of ISG15, some of which are depicted in Figure R1.

Interestingly, pathways related to endocytosis and phagosome formation, intracellular trafficking and apoptosis signaling appeared to be altered in *Isg15-/-* BMDM, in line with previous studies (Jeon et al., 2009; Villarroya-Beltri et al., 2016; D. Xu et al., 2015; Yanguez et al., 2013). However, it is to note that several of the pathways reported were related to mitochondria. Mitochondrial dysfunction, OXPHOS, the TCA cycle, FAO and mitochondrial ROS production were reported as affected by the absence of ISG15, indicating that many essential mitochondrial functions were dysregulated in *Isg15-/-* BMDM. Moreover, not only mitochondrial activity, but signaling pathways that regulate mitochondria, such as ERR signaling, sirtuin signaling, and NRF2-mediated oxidative response (Dinkova-Kostova & Abramov, 2015; Lombard, Tishkoff, & Bao, 2011; Vernier & Giguere, 2021), were also altered in *Isg15-/-* BMDM. As introduced earlier, mitochondria are master regulators of cellular metabolism and serve as major coordinators of innate immunity (West et al., 2011). As well, macrophage functions are strictly dependent on their metabolic state, which is directly or indirectly associated with mitochondria (P. S. Liu & Ho, 2018; Tur, Vico, Lloberas, Zorzano, & Celada, 2017). Therefore, given the critical role of mitochondria in the regulation of macrophage-mediated immune responses, we put our focus on these organelles.

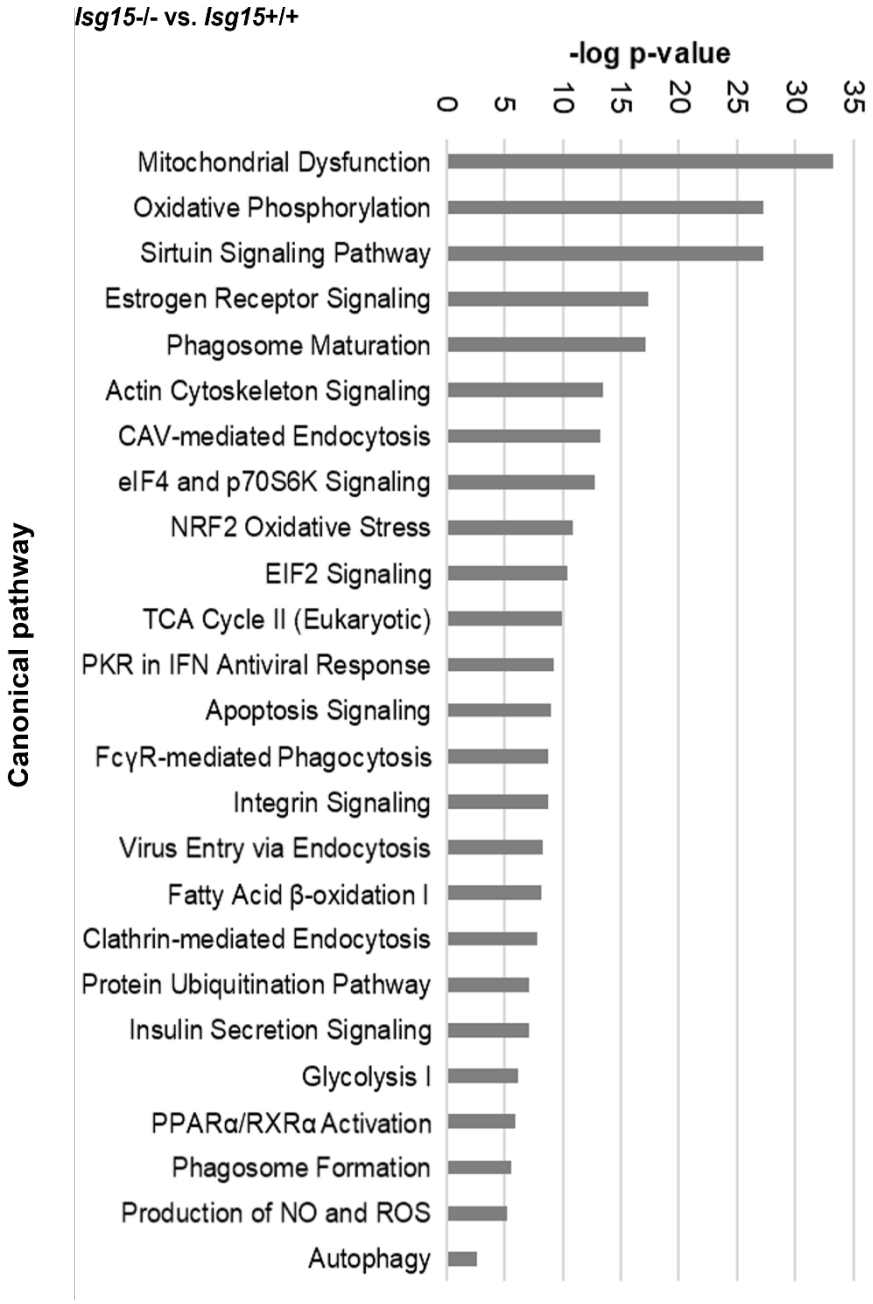

Figure R1. Differentially expressed canonical pathways between IFN-treated *Isg15-/-* and *Isg15+/+* BMDM. Data from the proteomic analysis of IFN-treated *Isg15-/-* and *Isg15+/+* BMDM were subjected to the IPA Canonical Pathway Analysis. Top differentially expressed pathways between genotypes are listed. Pathways are classified according to the *p-value* of the comparison *Isg15-/-* vs. *Isg15+/+* BMDM.

4.1.2. Mitochondria contain ISG15 and ISGylated proteins

Our first aim was to validate the presence of ISG15 and ISGylated proteins in mitochondria of BMDM. *Isg15*+/+ BMDM were treated or not with type I IFN for 16 h and subjected to subcellular fractionation. The presence of free and conjugated ISG15 in total protein extracts and protein extracts from the cytosolic and mitochondrial fractions was analyzed by western blot. As shown in Figure R2-A, IFN treatment strongly induced ISG15 expression and ISGylation in BMDM, making possible to detect both free and conjugated ISG15 in the total homogenate and in all the fractions evaluated. These results confirmed previous observations of ISG15 and ISGylated proteins in mitochondria (Giannakopoulos et al., 2005), and make feasible that the absence of ISG15 results in mitochondrial dysfunction.

4.1.3. ISG15 and ISGylated proteins are found throughout the mitochondrion

Proteins from all submitochondrial locations (OMM, IMM, IMS and MM) were reported as altered in the proteomic analysis, so we decided to evaluate the presence of ISG15 and ISGylated proteins throughout the mitochondrial structure. For that purpose, isolated mitochondria from IFN-treated *Isg15*+/+ BMDM were subjected to digestion with proteinase K (PK) alone or in combination with varying concentrations of detergents. The different conditions allowed the selective disruption of mitochondrial structure and the access of the PK to the different submitochondrial locations. Afterwards, the presence of ISG15 and ISGylated proteins was analyzed by western blot.

Results of the PK assay are represented in Figure R2-B. In the absence of any treatment (lane 1), ISG15 and ISGylated proteins could be detected in mitochondrial extracts, as well as the proteins TOMM20, TIMM23 and SOD2, used as controls for OMM, IMM and MM, respectively. The addition of PK (lane 2) caused the degradation of OMM proteins, as PK cannot penetrate the OMM. Consequently, TOMM20 was no longer detected; however, there was only a slight reduction in ISGylated proteins, while free ISG15 could still be detected. The addition of a low concentration of the detergent digitonin (lane 3) disrupted the OMM, making possible the digestion of IMS and IMM proteins by PK. Accordingly, TIMM23 disappeared, and so did monomeric ISG15 and the majority of ISGylated proteins. Higher concentrations of digitonin (lane 4) disrupted all mitochondrial membranes, permitting the PK to degrade MM proteins. In consequence, SOD2 and the remaining ISGylated proteins were degraded. These results indicated that ISG15 and ISGylated mitochondrial proteins are mainly located in the IMS and IMM, although they can also be found in the OMM and the MM, validating the results of the proteomic analysis.

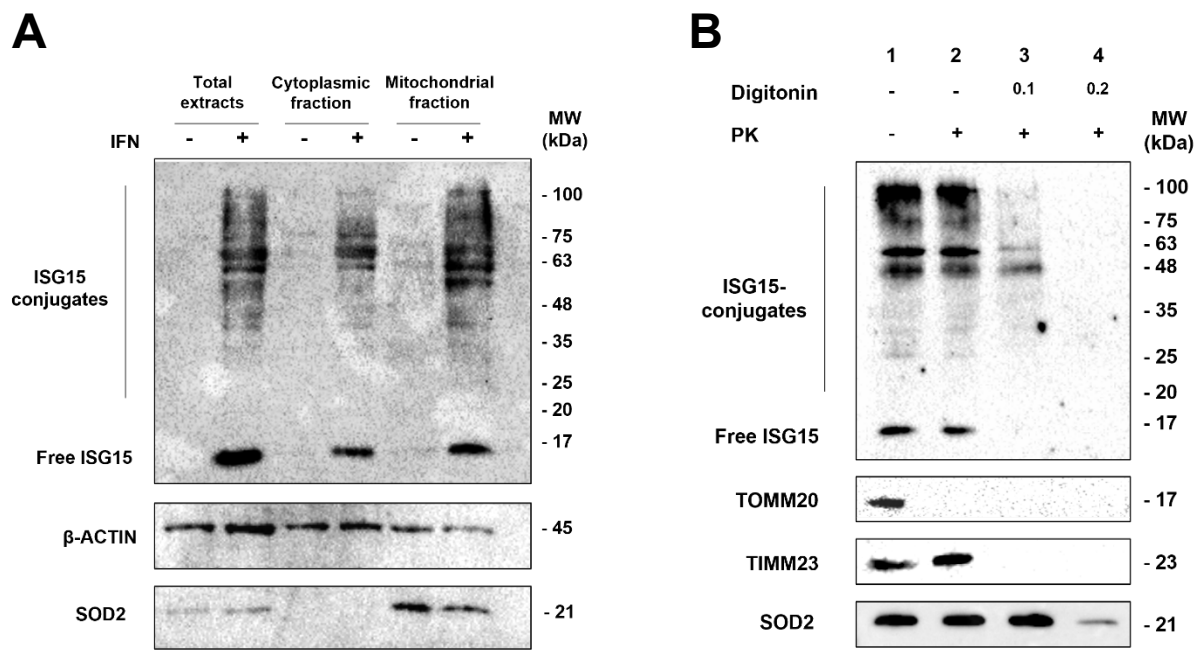

Figure R2. Subcellular and submitochondrial localization of ISG15 and ISGylated proteins. (A) Detection of ISG15 and ISGylated proteins in total protein extracts, and in cytoplasmic and mitochondrial fractions of untreated and IFN-treated *Isg15+/+* BMDM. 20 µg of protein were subjected to 12% SDS-PAGE and analyzed by western blot. Antibodies against ISG15, β-actin (cytoplasmic control) and SOD2 (mitochondrial control) were used. **(B)**. Detection of ISG15 and ISGylated proteins throughout the mitochondrial structure. Isolated mitochondria from IFN-treated *Isg15+/+* BMDM were subjected to proteinase K (50 µg/mL) digestion combined with digitonin permeabilization. Protein extracts were subjected to 12% SDS-PAGE and analyzed by western blot. Antibodies against ISG15, TOMM20 (OMM control), TIMM23 (IMM control) and SOD2 (MM control) were used. Molecular weights (MW) are indicated in kilodalton (kDa) in each case.

4.1.4. ISG15 modulates the organization of the mitochondrial ETC

Our results pointed to a role of ISG15 in the control of mitochondrial respiration. As demonstrated, ISG15 and ISGylated proteins mainly localize in the IMS and IMM, where the ETC is located and OXPHOS takes place. Moreover, our proteomic analysis reported increased expression of proteins of the five mitochondrial respiratory complexes in *Isg15-/-* BMDM (Figure R3-A). Specifically, 54 OXPHOS proteins were detected, all of which were upregulated in cells lacking ISG15 (Table 1). The assembly of the ETC complexes is a sophisticated process subjected to a tight regulation (Signes & Fernandez-Vizarra, 2018; Szczepanowska & Trifunovic, 2021); therefore, a dysregulation in the levels of its components could result in alterations in the ETC structure. To test this hypothesis, we analyzed the organization of the ETC respiratory complexes

by Blue-Native-PAGE (BN-PAGE) with isolated mitochondria from untreated and IFN-treated *Isg15+/+* and *Isg15-/-* BMDM (Figure R3-B). Observing the organization of the ETC complexes analyzed, three changes were found in *Isg15-/-* BMDM compared with *Isg15+/+* cells: 1) the absence of free complex I (CI) (red arrowhead); 2) the presence of an upper band close to the supercomplex (SC) formed by one unit of CI and two units of complex III (CIII) (I+III2s) (black arrowhead); 3) a clear upper band close to the complex II (CII) (blue arrowhead). It is important to note that these alterations were not affected by increased ISGylation, as no variations were observed in IFN-treated *Isg15+/+* BMDM compared with untreated cells. However, these changes were more evident in *Isg15-/-* BMDM after type I IFN treatment, likely due to an increase in the synthesis of OXPHOS proteins in response to type I IFN, in line with the results of the proteomic analysis. Collectively, our results demonstrated that the absence of ISG15 causes a reorganization of mitochondrial ETC supercomplexes, as well as an increase in the protein levels of the ETC complexes in response to type I IFN, suggesting a role of ISG15 in the regulation of the ETC structure and components.

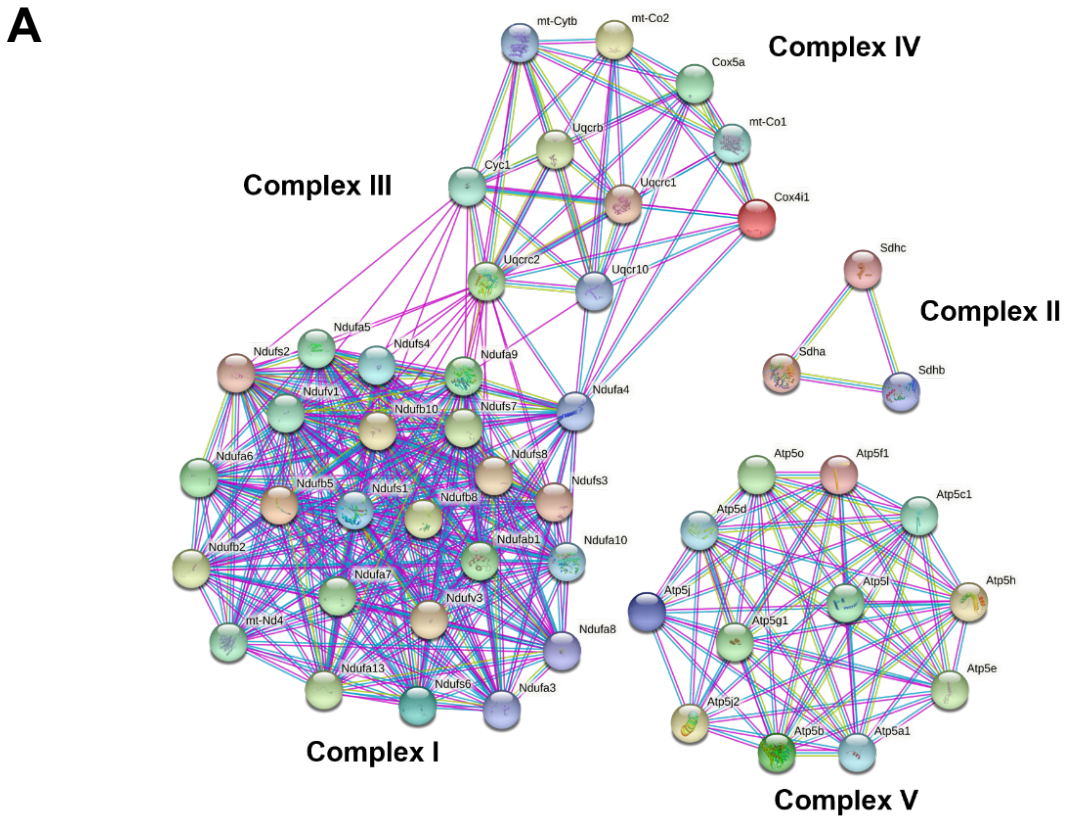

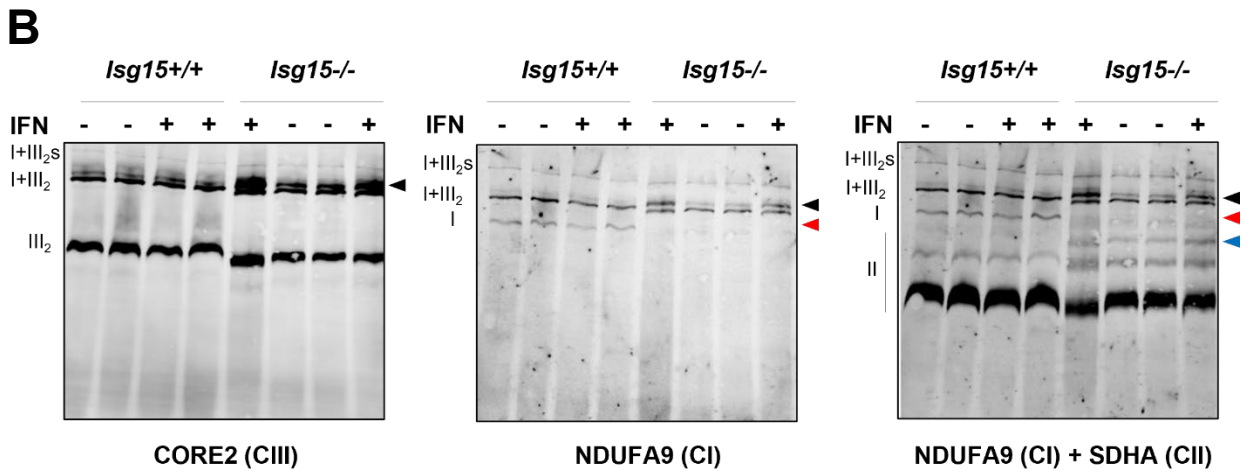

Figure R3. Differences in OXPHOS proteins and ETC organization between *Isg15-/-* and *Isg15+/+* BMDM. (A). Proteins from all five OXPHOS complexes are enriched in IFN-treated *Isg15-/-* BMDM. Functional and physical association of OXPHOS proteins detected in the quantitative proteomic analysis were analyzed with STRING Database V11.5. The minimum required interaction score was set at 0.9 (high confidence. Lines represent functional and physical relationships between protein. Names of the mitochondrial OXPHOS complexes are indicated. **(B).** The organization of ETC complexes and supercomplexes differs between *Isg15-/-* and *Isg15+/+* BMDM. Isolated mitochondria from untreated or IFN-treated *Isg15-/-* and *Isg15+/+* BMDM were subjected to BN-PAGE and resolved by western blot. Antibodies against CI (NDUFA9), CII (SDHA) and CIII (CORE2) were used to analyze the presence of each complex. Complexes and supercomplexes which bands belong to are indicated. Black, red, and blue arrows indicate the main differences between genotypes (see main text).

Table R1. Differences in OXPHOS protein abundances between IFN-treated *Isg15-/-* and *Isg15+/+* BMDM, and between IFN-treated, VACV-infected vs. uninfected *Isg15+/+* BMDM. Table list (from left to right): Mitochondrial location (OXPHOS complex) (column A); Protein ID (UniProt code) (column B); Gene name (column C); Standardized log2 fold change in protein abundance between the comparisons indicated (columns D and E). Targets of ISGylation are highlighted in blue.

		Gene	*Isg15-/-* vs. *Isg15+/+*	*Isg15+/+*
Complex I	Q9CPU2	Ndufb2	40.54	0
	Q99LC3	Ndufa10	5.38	6.95
	Q91VD9	Ndufs1	4.80	11.44
	Q9DCT2	Ndufs3	4.76	8.50
	Q8BK30	Ndufv3	4.71	2.84
	Q8K3J1	Ndufs8	4.61	7.76

	Q9CR21	Ndufab1	4.53	5.64
	Q91YT0	Ndufv1	3.81	8.57
	Q9CPP6	Ndufa5	3.65	5.62
	P52503	Ndufs6	3.41	3.81
	Q9ERS2	Ndufa13	3.38	6.12
	Q91WD5	Ndufs2	3.29	8.25
	Q7GIP3	Nd5	3.14	4.99
	M1VMU3	Nd2	3.11	3.13
	Q9DC70	Ndufs7	3.01	5.17
	Q9CXZ1	Ndufs4	2.96	5.17
	Q9DCS9	Ndufb10	2.92	7.09
	P03911	Mtnd4	2.89	4.51
	Q9CQZ5	Ndufa6	2.61	5.06
	Q9CQH3	Ndufb5	2.58	6.80
	Q9Z1P6	Ndufa7	2.57	5.20
	Q9CQ91	Ndufa3	2.40	2.81
	Q9D6J5	Ndufb8	2.38	4.17
	Q9DCJ5	Ndufa8	2.16	4.37
	Q9DC69	Ndufa9	2.10	6.01
Complex II	Q9CQA3	Sdhb	9.34	9.41
	Q8K2B3	Sdha	8.30	7.28
	Q9CZB0	Sdhc	3.97	4.16
Complex III	Q9CZ13	Uqcrc1	5.74	11.18
	Q9D855	Uqcrb	5.73	9.72
	Q9DB77	Uqcrc2	5.15	13.10
	Q9DB77	Uqcrq	5.15	13.10
	Q8R1I1	Uqcr10	4.69	6.50
	Q9D0M3	Cyc1	3.40	8.60
	P00158	Mt-Cyb	3.10	5.21
Complex IV	Q62425	Ndufa4	4.52	4.49
	P00405	Mtco2	4.16	12.68
	P12787	Cox5a	2.83	12.38
	P00397	Mtco1	2.60	3.39
	P19783	Cox4I1	2.13	12.48
Complex V	Q03265	Atp5a	8.15	19.92
	P56480	Atp5b	7.48	19.33
	Q91VR2	Atp5c	6.74	14.48
	P97450	Atp5J2	4.90	9.85
	Q9CQQ7	Atp5f1	4.59	9.44
	Q9DB20	Atp5o	4.51	12.79
	Q9DCX2	Atp5h	4.24	13.81

	Q9CPQ8	Atp5l	2.89	5.32
	P56135	Atp5j2	2.28	5.53
	Q9CR84	Atp5g1	2.09	2.49
	P56382	Atp5e	2.07	6.63
	Q9D3D9	Atp5d	2.06	4.21

4.1.5. ISG15 modulates mitochondrial respiration and mitochondrial ATP production

Considering the dysregulation of OXPHOS proteins and the reorganization of ETC supercomplexes observed in *Isg15-/-* BMDM, we hypothesized that these cells might suffer alterations in mitochondrial respiration. To prove it, we analyzed the mitochondrial respiratory function of untreated and IFN-treated *Isg15+/+* and *Isg15-/-* BMDM using a Seahorse Biosciences XF96 Extracellular Flux Analyzer platform, in collaboration with the group of Dr. José Antonio Enríquez (CNIC). We measured the oxygen consumption rate (OCR) and extracellular acidification rate (ECAR) at basal conditions and after treating cells with different inhibitors of mitochondrial respiratory complexes, to assess the different respiratory parameters. Furthermore, we evaluated the production of ATP by kinetic luminescence assay, as an impairment in OXPHOS would be reflected in alterations in ATP production, and our data also suggested alterations in the ATP synthase complex.

Basal OCR is an indicator of the normal respiration rate in physiological conditions, associated to ATP synthesis and proton leak events, while maximal OCR represents the capacity of the cells to respond to an increase in energy demands (Divakaruni, Paradyse, Ferrick, Murphy, & Jastroch, 2014). In untreated cells, basal OCR was similar between all conditions. However, after IFN treatment, there was a significant increase in basal OCR in *Isg15+/+* cells, that did not occur in *Isg15-/-* BMDM (Figure R4-A, upper left panel). Similar results were obtained for maximal OCR (Figure R4-A, upper right panel), with no significant differences between untreated cells, but a significant increase after IFN treatment only in *Isg15+/+* BMDM. In line with the reduction in mitochondrial respiration, changes in ATP production were only detected in IFN-treated cells, with a significant reduction in *Isg15-/-* BMDM compared with their *Isg15+/+* counterparts (Figure R4-A, lower left panel).

ECAR is an indicator of glycolytic flux and lactate production, processes in which the release of protons causes the acidification of the extracellular medium (Divakaruni et al., 2014). There were no significant differences in ECAR between all conditions (Figure R4-A, lower right panel), indicating that glycolytic activity was similar in *Isg15+/+* and *Isg15-/-* BMDM. Moreover, these

results suggested that the reduction in ATP production observed in *Isg15-/-* BMDM could be attributed to a deficiency in OXPHOS, as glycolysis-derived ATP levels should not be altered.

Finally, to confirm that changes in mitochondrial respiration were not the result of differences in mitochondrial content, we measured citrate synthase activity and quantified mtDNA, as indicators of mitochondrial content (Larsen et al., 2012) (Figure R4-B). We did not detect significant differences in citrate synthase activity and mtDNA levels between genotypes, indicating that differences in OCR resulted from impaired mitochondrial respiration.

Altogether, our analysis of mitochondrial respiratory parameters indicated that the absence of ISG15 alters mitochondrial functions, decreasing OXPHOS and ATP synthesis.

4.1.6. The production of mitochondrial ROS is reduced in Isg15-/- BMDM

Mitochondria play key roles in the regulation of energy metabolism, but also in the coordination of immune responses. Both functions are closely related, and the production of mitochondrial ROS is a good example of it (Dan Dunn, Alvarez, Zhang, & Soldati, 2015). ROS production was one of the affected pathways in *Isg15-/-* BMDM according to the proteomic analysis (Figure R1). In this line, we reported alterations in the ETC organization and mitochondrial respiration in BMDM lacking ISG15. Given the close relationship between the ETC, mitochondrial respiration and ROS, we analyzed the generation of ROS in our cells by confocal microscopy using the MitoSOX superoxide indicator. Attending to untreated cells, ROS production did not significantly change between all conditions (Figure R4-C). However, ROS significantly increased in response to IFN treatment, although ROS levels were significantly lower in the absence of ISG15. These results suggested that the alterations in the ETC and OXPHOS due to the absence of ISG15 affect ROS production, what has detrimental effects not only on the effectiveness of immune responses, but also on the regulation of numerous signaling pathways in which ROS are important mediators (Dan Dunn et al., 2015).

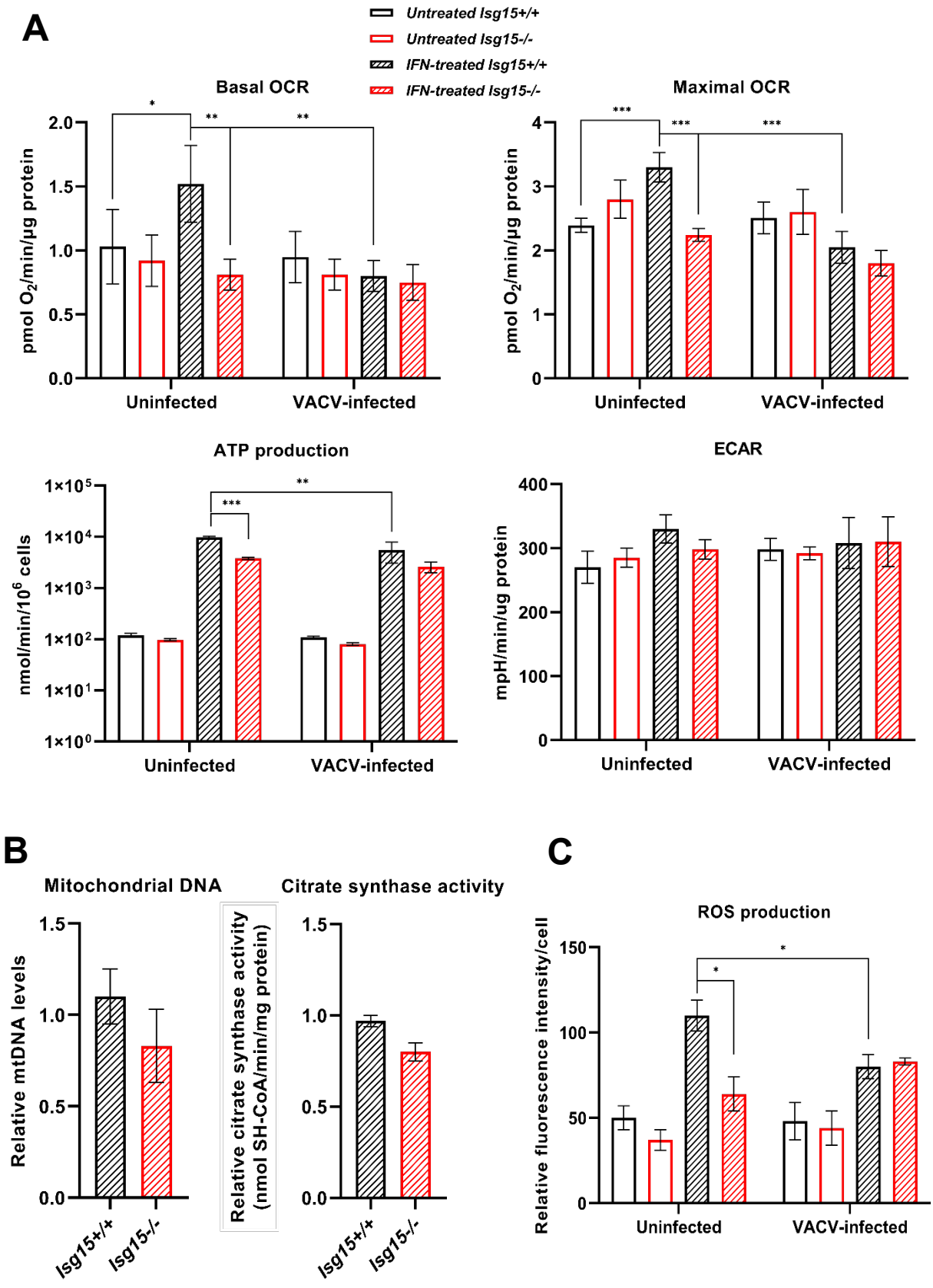
A
Untreated Isg15+/+
Untreated Isg15-/-
IFN-treated Isg15+/+
IFN-treated Isg15-/-
Basal OCR
pmol O2/min/µg protein
Uninfected
VACV-infected
Maximal OCR
ATP production
nmol/min/10^6 cells
ECAR
mpH/min/ug protein
B
Mitochondrial DNA
Relative mtDNA levels
Isg15+/+
Isg15-/-
Citrate synthase activity
Relative citrate synthase activity (nmol SH-CoA/min/mg protein)
C
ROS production
Relative fluorescence intensity/cell

Figure R4. Evaluation of mitochondrial respiration and ROS production of uninfected and VACV-infected *Isg15-/-* and *Isg15+/+* BMDM. (A). Analysis of mitochondrial respiratory parameters and ECAR. *Isg15-/-* and *Isg15+/+* BMDM were treated or not with type I IFN (500 U/mL), and infected or not with VACV (1 PFU/cell, 2 h). Basal and maximal OCR and ECAR were analyzed using a Seahorse Biosciences XF96 Extracellular Flux Analyzer platform. ATP levels were determined in permeabilized BMDM by kinetic luminescence assay. Mean ± SD of 4 biological replicates is represented. **(B).** Analysis of mitochondrial content indicators. Mitochondrial DNA content and citrate synthase activity were assessed by qPCR and spectrophotometry, respectively, as described in sections *3.21.* and *3.18.* of Materials and Methods, respectively. Mean ± SD of 3 biological replicates is represented. **(C).** Analysis of ROS production. *Isg15-/-* and *Isg15+/+* BMDM were treated or not with type I IFN (500 U/mL), and infected or not with VACV (1 PFU/cell, 2 h). ROS production was measured by confocal microscopy using MitoSOX™ Red Mitochondrial Superoxide Indicator. Images were analyzed with Fiji. Student's T-test was performed for the appropriate comparisons. * *p-value < 0.05; ** p-value < 0.01: *** p-value <0.001.*

4.1.7. VACV infection and the absence of ISG15 have similar effects on mitochondrial respiratory metabolism

VACV has been shown to modulate mitochondrial metabolism by stimulating mitochondrial FAO and OXPHOS to obtain energy during infection (Greseth & Traktman, 2014). Moreover, research from our group demonstrated that VACV counteracts the effect of ISG15 via its E3 protein, modulating the antiviral response (Eduardo-Correia, Martinez-Romero, Garcia-Sastre, & Guerra, 2014). Thus, we explored the impact of VACV infection on the macrophage mitochondrial metabolism. For that purpose, we first subjected the data from a previous proteomic analysis of IFN-treated, VACV-infected *Isg15+/+* BMDM to the IPA Canonical Pathway Analysis and observed that mitochondrial dysfunction and OXPHOS were the most altered pathways in response to VACV infection (Figure R5). As well, several pathways related to mitochondria, such as the TCA cycle, FAO and ROS production were also affected. Interestingly, the profile obtained with infected *Isg15+/+* BMDM was very similar to that of uninfected *Isg15-/-* BMDM, with increased levels of mitochondrial proteins (Table 2). Given the changes in the mitochondrial proteome observed in response to infection, we evaluated mitochondrial respiration of VACV-infected BMDM (1 PFU/cell, 2 and 6 h), as we did for uninfected BMDM (see section *4.1.5. ISG15 modulates mitochondrial respiration and mitochondrial ATP production*). Attending to OCR, both basal and maximal OCR were significantly reduced by VACV infection only in *Isg15+/+* BMDM, while VACV did not significantly affect these parameters in *Isg15-/-* BMDM, which were already reduced (Figure R4-A, upper panels). As a result of impaired OXPHOS, VACV caused a significant reduction ATP production in *Isg15+/+* BMDM, but not in *Isg15-/-* BMDM, whose ATP levels were already decreased (Figure R4-A, lower left panel). Furthermore, ECAR was not

altered during infection (Figure R4-A, lower right panel), indicating that the reduction in ATP levels were the result of the mitochondrial alterations caused by VACV. Consistent with defects in OXPHOS, ROS production was also decreased in VACV-infected *Isg15+/+* BMDM compared with uninfected BMDM, while it did not change in infected *Isg15-/-* BMDM (Figure R4-C).

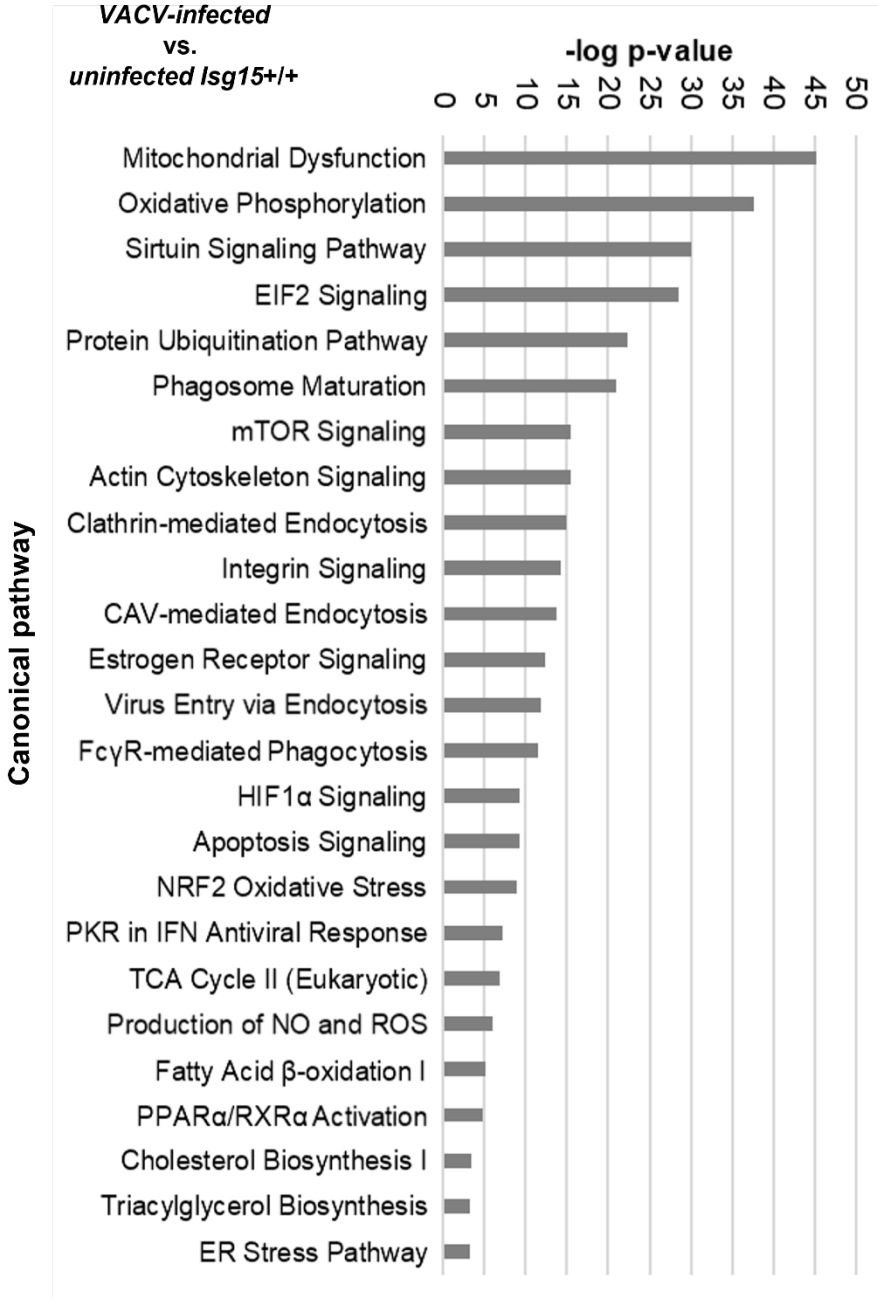

Figure R5. Differentially expressed canonical pathways between IFN-treated VACV-infected *Isg15+/+* and uninfected *Isg15+/+* BMDM. Data from the proteomic analysis of IFN-treated VACV-infected

Isg15+/+ and uninfected *Isg15+/+* BMDM were subjected to the IPA Canonical Pathway Analysis. Top differentially expressed pathways between genotypes are listed. Pathways are classified according to the *p-value* of the comparison *VACV-infected* vs. uninfected *Isg15+/+* BMDM.

The fact that the proteomic profile of uninfected *Isg15-/-* BMDM and VACV-infected *Isg15+/+* BMDM were similar prompted us to investigate the effect of VACV infection on the levels of ISG15 in BMDM. For that purpose, we analyzed the mRNA levels of *Isg15* and VACV (de Souza Trindade et al., 2008) by RT-qPCR, as well as the levels of ISG15 and ISGylated proteins by western blot. We observed a significant reduction in *Isg15* mRNA levels, as well as decreased ISGylated proteins, in response to VACV infection (Figure R6). Moreover, ISG15 was reported by the proteomic analysis of VACV-infected *Isg15+/+* BMDM as one of the most downregulated proteins, compared to uninfected cells. These results suggested that the similarities between the proteomic profiles of VACV-infected *Isg15+/+* BMDM and uninfected *Isg15-/-* BMDM, and the alterations in mitochondrial metabolism observed in these cells, might be due to decreased ISG15 levels.

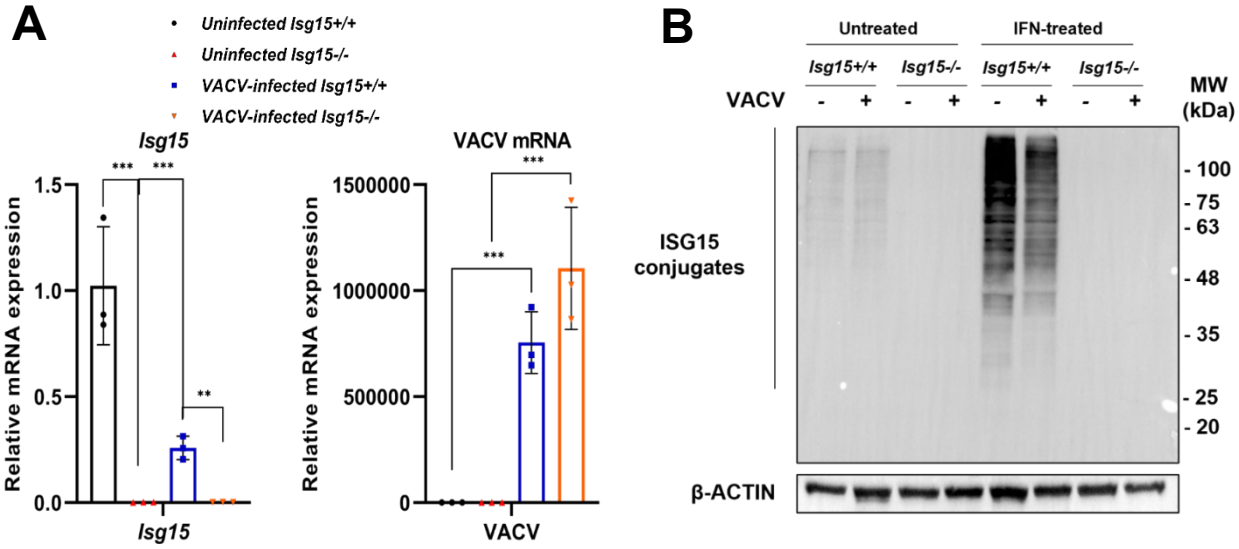

Figure R6. Analysis of the effect of VACV infection on *Isg15* expression and ISGylation. (A). VACV downregulates the expression of *Isg15*. IFN-treated *Isg15-/-* and *Isg15+/+* BMDM were infected or not with VACV (1 PFU/cell, 16 h), and *Isg15* and *VACV* mRNA levels were analyzed by RT-qPCR. Expression levels are normalized to HPRT mRNA levels. Two-way ANOVA and Tukey post-hoc analyses were performed for the comparisons. Mean ± SD of 3 biological replicates is represented. * *p-value* < *0.05; ** p-value* < *0.01: *** p-value <0.001.* **(B).** VACV reduces protein ISGylation. *Isg15-/-* and *Isg15+/+* BMDM were treated or not with type I IFN (500 U/mL, 16 h), and infected or not with VACV (1 PFU/cell, 16 h). Total protein extracts

(20 µg) were subjected to 10% SDS-PAGE and resolved by western blot. Antibodies against ISG15 and β-actin (control) were used. MW are indicated in kDa.

4.1.8. ISG15 modulates macrophage polarization

Macrophages are characterized by a highly plastic behavior, as they rapidly adapt to changing conditions to ensure an adequate immune response. These adaptation mechanisms, known as macrophage polarization, go hand in hand with metabolic changes in which mitochondria are critical players (Jones & Divakaruni, 2020; Tur et al., 2017). It is reasonable to think that the mitochondrial disturbances observed in *Isg15-/-* BMDM could have an impact on macrophage polarization. This hypothesis was reinforced by the results of the proteomic analysis, which reported alterations in the production of NO, a metabolite associated with M1 polarization (Figure R1), and upregulation of ARG1, a marker of M2 polarization, in cells lacking ISG15 (data not shown). Therefore, we sought to explore the polarization status of *Isg15-/-* and *Isg15+/+* BMDM in basal conditions and after IFN treatment. In addition, we analyzed how these cells responded to VACV infection in the context of polarization, as we showed that VACV causes metabolic alterations in macrophages, and it was demonstrated that different macrophage activation states can influence VACV replication (Byrd et al., 2014).

For that purpose, the expression levels of iNOS and ARG1 were analyzed by western blot. BMDM of both genotypes were able to polarize to M1 or M2 phenotypes when stimulated with the appropriate cytokines, as indicated by increased expression of the specific markers (Figure R7-A). Moreover, VACV infection did not have a significant impact on BMDM polarization once cells were polarized. Different results were obtained in unpolarized BMDM (Figure R7-B). In IFN-treated-, uninfected cells, ARG1 expression was detected, contrary to iNOS, what suggested polarization towards an M2 phenotype in response to type I IFN. Consistent with the proteomic analysis, *Isg15-/-* BMDM showed higher levels of ARG1, suggesting that these cells are more prone to develop an anti-inflammatory phenotype. Interestingly, ARG1 expression increased during infection in both genotypes, although it seemed to increase more rapidly in *Isg15-/-* BMDM, suggesting that these cells are more susceptible to the effect of VACV on macrophage polarization.

To assess whether the differences in enzyme levels were related to changes in enzymatic activity, we measured NO production and arginase activity. We performed a Griess assay to estimate NO production from NO_2^- levels (Bryan & Grisham, 2007) in untreated and IFN-treated *Isg15-/-* and *Isg15+/+* BMDM, infected or not with VACV WR for 24 h. As shown in Figure R7-C, NO production reached similar levels in both genotypes in all conditions, although there was a slight but

significant increase in NO levels only in *Isg15+/+* BMDM after IFN treatment, suggesting that ISG15 might be involved in NO production. ARG1 activity was determined by measuring the conversion of L-arginine to urea and L-ornithine with a specific kit. ARG1 activity was significantly higher in *Isg15-/-* BMDM compared with *Isg15+/+* cells in all conditions. Moreover, VACV infection did not have a significant effect on the activity of this enzyme (Figure R7-D).

We also measured mRNA levels of a set of cytokine genes to evaluate the cytokine expression profile of these cells. Interestingly, although our data suggested that *Isg15-/-* BMDM were prone to develop an M2 phenotype, these cells showed higher expression of proinflammatory cytokines such as IL-6 and TNFα at basal conditions (Figure R7-E). Furthermore, VACV infection significantly increased the expression of these cytokines, as well as that of IL-12, IL-1β and IFNβ, an increase that was exacerbated in *Isg15-/-* BMDM, emphasizing the differences between genotypes.

Collectively, these observations suggested that ISG15 modulates macrophage polarization, as its absence led to alterations in the production of NO, increased ARG1 levels and arginase activity, and increased expression of proinflammatory cytokines. Such metabolic features are characteristic of both M1 and M2 phenotypes, pointing to the development of a mixed activation phenotype in *Isg15-/-* BMDM.

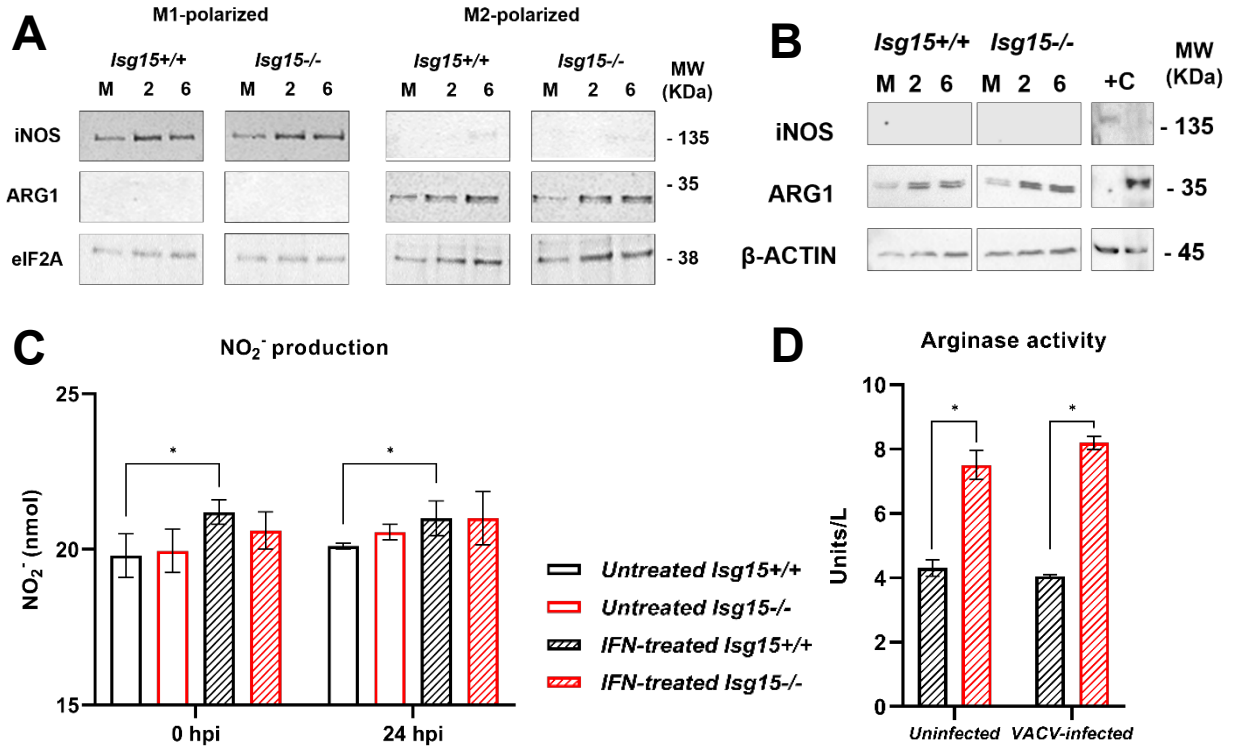

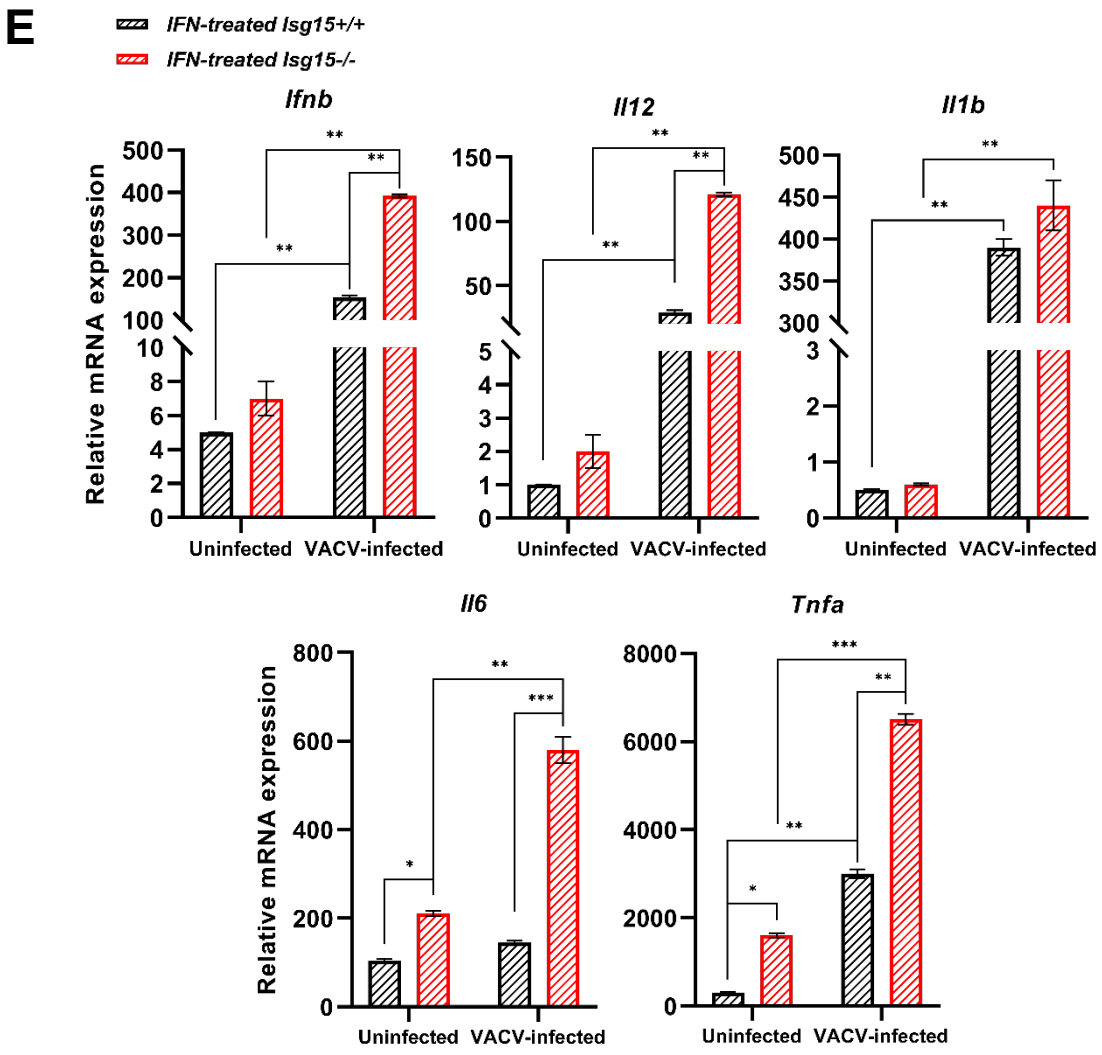

Figure R7. Analysis of macrophage polarization in uninfected and VACV-infected *Isg15-/-* and *Isg15+/+* BMDM. (A). IFN-treated-, uninfected or VACV-infected (1 PFU/cell, 2 and 6 h) *Isg15-/-* and *Isg15+/+* BMDM can polarize to either M1 or M2 phenotypes when stimulated with the appropriate cytokines. Polarization towards M1 or M2 phenotypes was induces treating BMDMs with LPS+IFNγ or IL-4, respectively. Total protein extracts were subjected to 10% SDS-PAGE and resolved by western blot. Antibodies against iNOS, ARG1 and eIF2A (control) were used. MW are indicated in kDa. **(B).** IFN-treated, unpolarized BMDM show increased ARG1 levels. Total protein extracts from IFN-treated-, uninfected or VACV-infected (1 PFU/cell, 2 and 6 h) *Isg15-/-* and *Isg15+/+* BMDM were subjected to 10% SDS-PAGE and resolved by western blot. Antibodies against iNOS, ARG1 and β-actin (control) were used. MW are indicated in kDa. **(C)**. IFN augments NO production only in *Isg15+/+* BMDM. NO production was assessed in VACV-infected- (1 PFU/cell, 0 and 24 h), untreated and IFN-treated *Isg15-/-* and *Isg15+/+* BMDM by Griess assay. Mean ± SD of 3 biological replicates is represented. **(D).** *Isg15-/-* BMDM show increased ARG1 activity. ARG1 activity was measured in IFN-treated-, uninfected and VACV-infected (1 PFU/cell, 6 h) using the Arginase Activity Assai Kit (Sigma). Mean ± SD of 3 biological replicates is represented. **(E).**

The expression of proinflammatory cytokines is increased in the absence of ISG15 and in response to VACV infection. mRNA levels of proinflammatory cytokines of IFN-treated-, uninfected and VACV-infected (1 PFU/cell, 16 h) *Isg15-/-* and *Isg15+/+* BMDM were analyzed by RT-qPCR. Expression levels are normalized to HPRT mRNA levels. Mean ± SD of 3 biological replicates is represented. Student's T-test, and Two-way ANOVA and Tukey post-hoc analyses were performed for the comparisons. * *p-value < 0.05; ** p-value < 0.01: *** p-value <0.001.*

Table R2. Differences in autophagy and intracellular trafficking protein abundances between IFN-treated *Isg15-/-* and *Isg15+/+* BMDM. Table list (from left to right): Protein ID (UniProt code) (column A); Gene name (column B); Protein description (column C); Standardized log2 fold change in protein abundance between the comparisons indicated (columns D). Targets of ISGylation are highlighted in blue.

Protein ID	Gene	Description	Std log2 FC (*Isg15-/-* vs. *Isg15+/+*)
P51150	Rab7a	Ras-related protein Rab-7a	6.05
P61021	Rab5b	Ras-related protein Rab-5B	3.15
Q9CQW1	Ykt6	Synaptobrevin homolog YKT6	-2.02
O88384	Vti1b	Vesicle transport through interaction with t-SNAREs homolog 1B	-2.05
P11438	Lamp1	Lysosome-associated membrane glycoprotein 1	-2.14
Q9D0I4	Stx17	Syntaxin-17	-2.27
Q61187	Tsg101	Tumor susceptibility gene 101 protein	-2.38
Q91W86	Vps11	Vacuolar protein sorting-associated protein 11 homolog	-2.75
Q9CPX6	Atg3	Ubiquitin-like-conjugating enzyme ATG3	-2.81
Q9D906	Atg7	Ubiquitin-like modifier-activating enzyme ATG7	-2.90
P63024	Vamp3	Vesicle-associated membrane protein 3	-3.87
O70404	Vamp8	Vesicle-associated membrane protein 8	-4.17
Q8R307	Vps18	Vacuolar protein sorting-associated protein 18 homolog	-4.55
P63044	Vamp2	Vesicle-associated membrane protein 2	-4.81
Q64337	Sqstm1	Sequestosome-1	-8.90

4.1.9. ISG15 regulates mitochondrial dynamics and mitophagy in BMDM

Mitochondria are hubs of metabolic pathways and carry out a plethora of functions to maintain cell homeostasis, what requires excellent mitochondrial quality control mechanisms. Mitochondria are highly dynamic organelles, and constantly undergo fission, fusion, and degradation events to meet the requirements of each metabolic situation (Chan, 2020). The interplay between mitochondrial dynamics and mitophagy guarantees a healthy and fully functional mitochondrial network (Onishi, Yamano, Sato, Matsuda, & Okamoto, 2021).

Our results demonstrated that mitochondria of *Isg15-/-* BMDM are defective in response to IFN stimulation; therefore, we analyzed the status of the mitochondrial network of IFN-treated *Isg15+/+* and *Isg15-/-* BMDM. For that purpose, transmission electron microscopy (TEM) and confocal microscopy analyses, using an antibody against COX4 as a mitochondrial marker, were carried out. Strikingly, *Isg15-/-* BMDM showed elongated and brighter mitochondria than *Isg15+/+* cells (Figure R8-A, B), indicating increased mitochondrial fusion and accumulation of COX4, respectively. Increased fusion was also suggested by a higher levels of the mitochondrial fusion protein OPA1 in cells lacking ISG15, as reported in the proteomic analysis (data not shown), whereas the accumulation of mitochondrial proteins was also observed by western blot analysis of COX4 and VDAC1 levels (Figure R8-C), in line with the proteomic study.

The proteomic analysis reported a differential expression of several proteins involved in endosomal trafficking and autophagy in *Isg15-/-* cells (Table R2). Interestingly, most of these proteins were downregulated, suggesting alterations in autophagic processes. Given the possibility of an impairment in mitophagy, we analyzed the levels of PARKIN, an E3 ubiquitin ligase which recruitment to mitochondria from the cytosol is critical in the first steps of the PINK1/PARKIN-mediated mitophagy pathway (Eiyama & Okamoto, 2015). As shown in Figure R8-C, PARKIN was detected in cytosolic fractions from both genotypes; however, it was not present in mitochondrial fractions from *Isg15-/-* BMDM, indicating a defective recruitment of PARKIN to mitochondria. In addition, PARKIN levels increased with IFN treatment only in *Isg15+/+* BMDM, what could be explained by an ISG15-mediated regulation of PARKIN (Im et al., 2016). Another protein involved in PINK1/PARKIN-mediated mitophagy is SQSTM1/p62, which is recruited to damaged mitochondria and promotes mitochondrial aggregation (Narendra, Kane, Hauser, Fearnley, & Youle, 2010). SQSTM1/p62 appeared strongly downregulated in *Isg15-/-* BMDM (Table R2) and, accordingly, confocal microscopy showed less p62 puncta in these cells (Figure R8-B), although there were no differences in intracellular distribution.

Altogether, our results pointed to a role of ISG15 in the regulation of mitochondrial functions, affecting essential mitochondrial processes such as OXPHOS, mitochondrial dynamics, mitochondrial protein homeostasis and mitophagy in BMDM. Being mitochondria pivotal coordinators of central metabolism, the outcome of such alterations can be profoundly detrimental to the whole spectrum of macrophage functions.

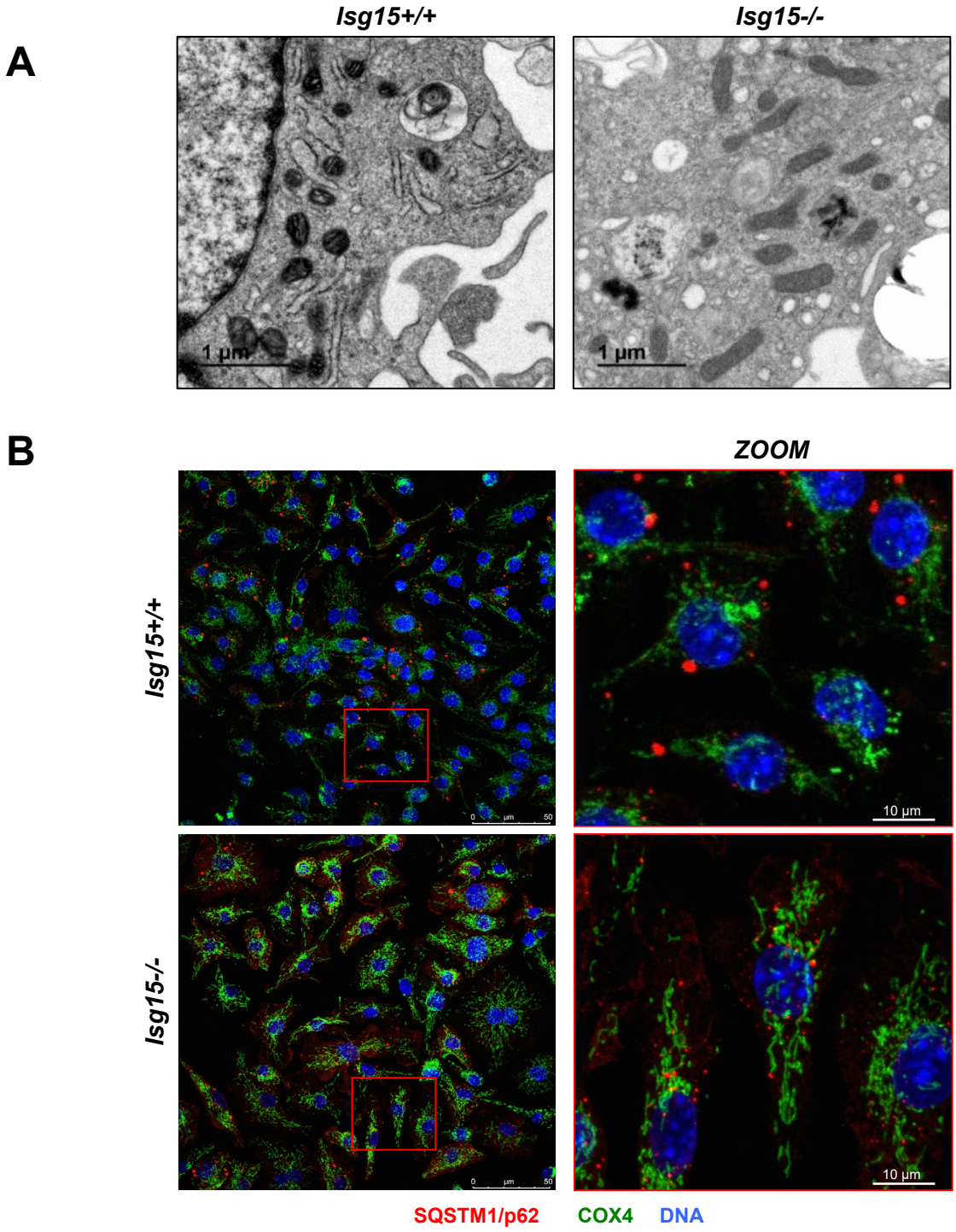

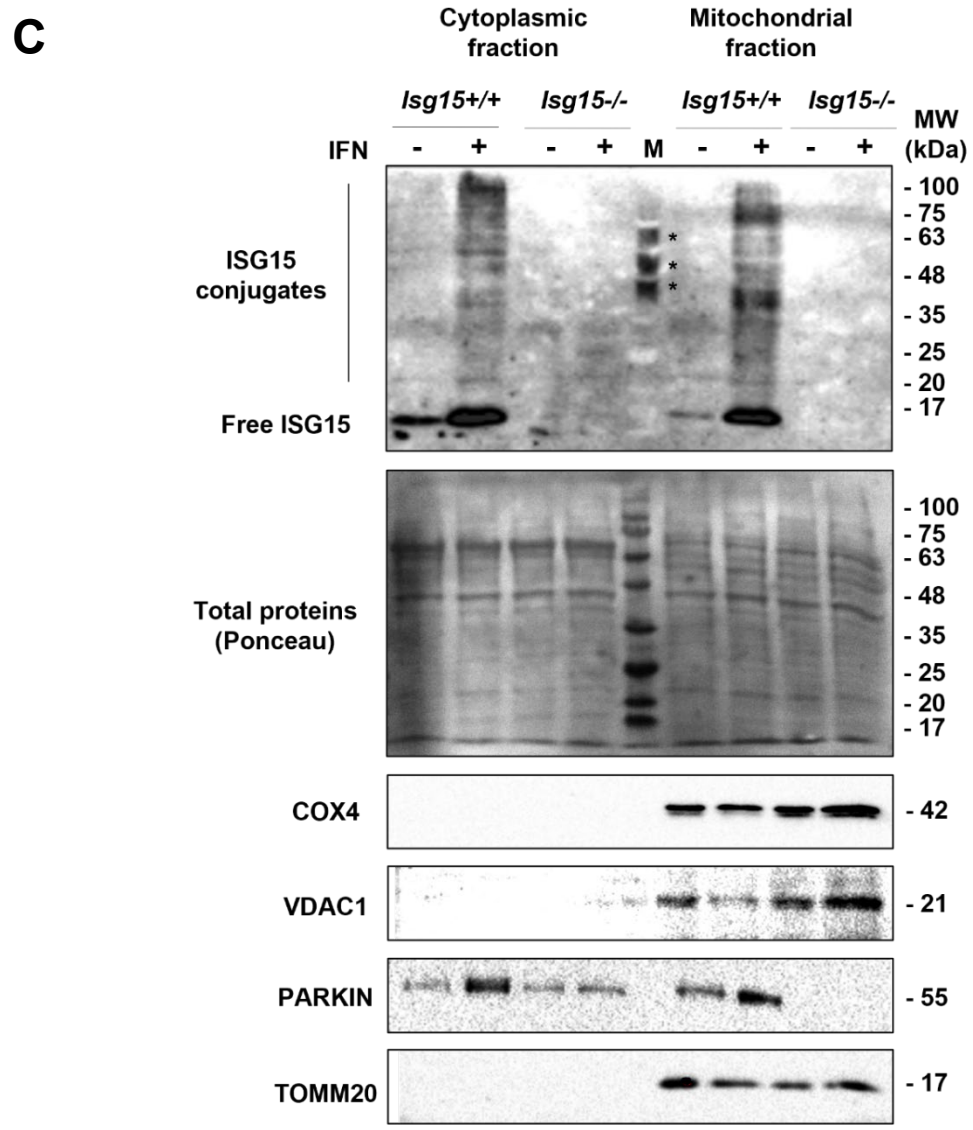

Figure R8. Evaluation of mitochondrial morphology, mitochondrial protein levels and mitophagy markers in *Isg15-/-* and *Isg15+/+* BMDM. (A). Mitochondria are elongated in *Isg15-/-* BMDM. IFN-treated *Isg15-/-* and *Isg15+/+* BMDM were subjected to TEM analysis as described in section *3.31.* of Materials and Methods. Representative images are shown. **(B).** *Isg15-/-* BMDM show elongated mitochondria and accumulation of mitochondrial proteins. IFN-treated *Isg15-/-* and *Isg15+/+* BMDM were analyzed by confocal microscopy to evaluate the status of the mitochondrial network, as well as the localization of SQSTM1/p62. Anti-COX4 plus Alexa488-labeled secondary antibodies were used to stain mitochondria. Anti-SQSTM1/p62 plus Alexa594-labeled secondary antibodies were used to stain SQSTM1/p62. DAPI was used to stain DNA. Microscopy images were obtained with a Leica SP5 confocal microscope, using a 63X objective. Images were processed with Fiji. Representative images are shown. **(C).** *Isg15-/-* BMDM show increased levels of mitochondrial proteins and fail to recruit PARKIN to mitochondria. Untreated and

IFN-treated *Isg15-/-* and *Isg15+/+* BMDM were subjected to subcellular fractionation, and the levels of mitochondrial proteins and PARKIN in the cytoplasmic and mitochondrial fractions were analyzed. 20 µg were subjected to 12% SDS-PAGE and resolved by western blot. Antibodies against ISG15, COX4, VDAC1, TOMM20 and PARKIN were used, Ponceau staining of total protein content is shown as loading control. Asterisks (*) indicate unspecific recognition of proteins of the MW marker (M). MW is indicated in kDa.

4.2. ISG15 is a novel regulator of lipid metabolism in BMDM

4.2.1. ISG15 modulates the levels of proteins involved in lipid metabolism independently of gene expression

Mitochondrial activity has a direct effect on lipid metabolism, as mitochondria participate in FAS and FAO processes (O'Neill et al., 2016). Interestingly, FAO was one of the affected pathways in *Isg15-/-* BMDM (Figure R1), suggesting that lipid metabolism could be altered in these cells. Therefore, we sought to explore the effect of ISG15 deficiency on the lipidic profile of BMDM.

Examining the data from the quantitative proteomic study, we found that several mitochondrial proteins involved in FA metabolism were differentially expressed in *Isg15-/-* BMDM (Table R3, bold). Interestingly, most of the proteins identified were upregulated, in line with our previous results in which we observed a general upregulation of mitochondrial proteins in *Isg15-/-* cells. Moreover, according to the IPA Canonical Pathway analysis, many of the proteins detected belonged to the FAO pathway. We were excited to discover that not only mitochondrial proteins involved in FA metabolism were differentially expressed between genotypes, but also non-mitochondrial enzymes that participate in diverse aspects of lipid metabolism, such as lipid synthesis, lipid hydrolysis, and lipid transport and storage (Table R3). Interestingly, proteins involved in lipid hydrolysis (e.g., NCEH1, MGLL, LIPA, LDAH) were upregulated, while critical enzymes in lipid synthesis, such as FDPS, ACACA and FASN were strongly downregulated. These results suggested that the absence of ISG15 causes a dysregulation in lipid metabolism, likely due to a shift towards lipid hydrolysis and oxidation and, therefore, an imbalance between lipid anabolic and catabolic processes.

Table R3. **Differences in lipid metabolism protein abundances between IFN-treated *Isg15-/-* and *Isg15+/+* BMDM.** Table list (from left to right): Lipid metabolism pathway (column A); Protein ID (UniProt code) (column B); Gene name (column C); Standardized log2 fold change in protein abundance between the comparisons indicated (columns D). Mitochondrial proteins are highlighted in bold. Targets of ISGylation are highlighted in blue.

Pathway	Protein ID	Gene	Std log2 FC (*Isg15-/-* vs. *Isg15+/+*)
Fatty acid oxidation	Q8BMS1	**Hadha**	11.68
	P50544	**Acadvl**	10.62
	Q9EPL9	Acox3	8.97
	Q99JY0	**Hadhb**	8.54
	P97742	**Cpt1a**	8.31
	Q8BH95	**Echs1**	7.62
	P41216	**Acsl1**	6.74
	Q07417	**Acads**	6.14
	Q9R0H0	Acox1	5.34
	P51174	**Acadl**	5.07
	Q8QZT1	**Acat1**	4.28
	P42125	**Eci1**	4.14
	Q9Z2Z6	**Slc25a20**	3.91
	P32020	Scp2	3.24
	P45952	**Acadm**	3.06
	P52825	**Cpt2**	2.32
	Q60759	**Gcdh**	2.27
	Q8CAY6	Acat2	-8.05
Lipid synthesis	Q9D517	Agpat3	4.87
	Q8BYI6	Lpcat2	2.88
	Q8CHK3	Mboat7	2.87
	Q8BHF7	Pgs1	2.73
	O35083	Agpat1	2.60
	Q91YX5	Lpgat1	2.31
	Q8K3K7	Agpat2	2.10
	Q5SWU9	Acaca	-2.20
	Q3UJQ2	Hmgcs1	-3.06
	Q920E5	Fdps	-10.60
	P19096	Fasn	-15.65
Lipid hydrolysis	Q8BLF1	Nceh1	43.15
	Q8VCI0	Plbd1	19.16
	O35678	Mgll	16.29
	Q9WV54	Asah1	14.26
	Q91WC9	Daglb	5.10
	Q9Z0M5	Lipa	4.26
	Q8VEB4	Pla2g15	4.04
	Q8BVA5	Ldah	3.51
	Q80Y98	Ddhd2	-2.27
Lipid transport and storage	P08226	Apoe	17.93
	Q91ZX7	Lrp1	12.93

	Q08857	Cd36	3.86
	P41233	Abca1	3.60
	Q00623	Apoa1	3.46
	Q61009	Scarb1	-3.38
	P11404	Fabp3	-3.47
	P48410	Abcd1	-3.61
	P43883	Plin2	-4.59
	Q9DBG5	Plin3	-9.87

To evaluate whether the differences observed at the protein level were due to variations in gene expression, mRNA levels of several lipid metabolism genes were analyzed by RT-qPCR. We selected genes involved in lipid hydrolysis (*Nceh1*), lipid synthesis (*Fasn, Hmgcr, Hmgcs*) and mitochondrial FAO (*Cpt1a*, *Acads*, *Acadm*, *Acadl*). Surprisingly, none of the genes examined showed significant differences in mRNA levels between genotypes (Figure R9-A), indicating that the differences in the levels of these proteins were independent of gene expression. It is well known that gene expression not always correlates with protein abundance, due to post-transcriptional and post-translational mechanisms involved in the regulation of protein homeostasis and turnover (Vogel & Marcotte, 2012), including ISGylation (Perez Berrocal, Witting, Ovaa, & Mulder, 2019), what might explain these results.

4.2.2. ISG15 is a potential regulator of transcription factors involved in mitochondrial and lipid metabolism

Our results suggested that the absence of ISG15 in BMDM leads to metabolic dysregulation, with strong changes in the levels of proteins involved in mitochondrial and lipid metabolism, and a noteworthy impact on mitochondrial functions. To better understand the possible origin of the observed alterations, and with the aim to elucidate a mechanism by which ISG15 could be regulating these processes, we subjected our proteomics data to the IPA Upstream Regulators Analysis. This analysis allows the identification of regulators that can explain the observed differences in protein levels, based on the number of known targets of each regulator present in the dataset. In addition, the software predicts the activation or inhibition of each regulator identified depending on the reported upregulation or downregulation of its downstream targets. Interestingly, among the regulators predicted to be significantly activated in *Isg15-/-* BMDM, we found PPARα, PPARγ, PGC-1α, ESRRA and TFAM (Figure R9-B). These factors participate in the regulation of energy metabolism by stimulating mitochondrial biogenesis and catabolic processes (Herzig & Shaw, 2018), and could be responsible for the alterations observed in *Isg15-/-* BMDM. Regarding the regulators potentially inhibited in *Isg15*-/- BMDM, we found CLPP, a

mitochondrial serine protease responsible for mitochondrial protein quality control, whose inhibition has been linked to impaired OXPHOS (Nouri, Feng, & Schimmer, 2020), and could be related with increased levels of mitochondrial proteins and defective mitochondrial respiration in *Isg15-/-* BMDM.

Once identified the potential regulators responsible for the metabolic alterations observed in our cells, we analyzed the expression of a set of transcriptional regulators by RT-qPCR. We selected PPARα (*Ppara*), PPARγ (*Pparg*), PGC-1α (*Ppargc1a*), PGC-1β (*Ppargc1b*), and TFAM (*Tfam*). In addition, we evaluated the expression of NRF1 (*Nrf1*) and ESRRA (*Esrra*), as they control pathways reported as altered in *Isg15-/-* BMDM (Figure R1) and play a relevant role in the regulation of mitochondrial biogenesis and lipid metabolism (Hock & Kralli, 2009). None of the genes evaluated showed significant differences in mRNA levels between genotypes, although our data suggested increased expression of *Pparg* and *Ppargc1a* in *Isg15-/-* BMDM (Figure R9-C). The higher expression of these regulators could explain the increase in mitochondrial proteins and the dysregulation of lipid metabolism observed in *Isg15-/-* BMDM. However, it would be reflected by an increase in the expression of their target genes, which did not occur (Figure R9-A). Hence, our data suggested that the differences in protein levels between genotypes are the result of alterations in protein homeostasis, rather than variations in gene expression.

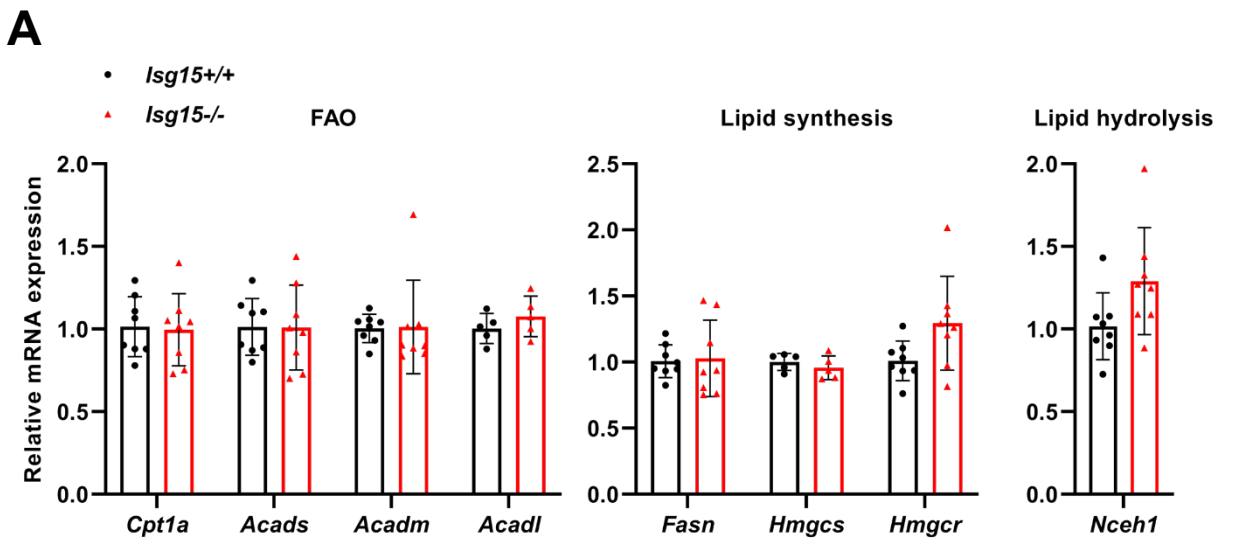

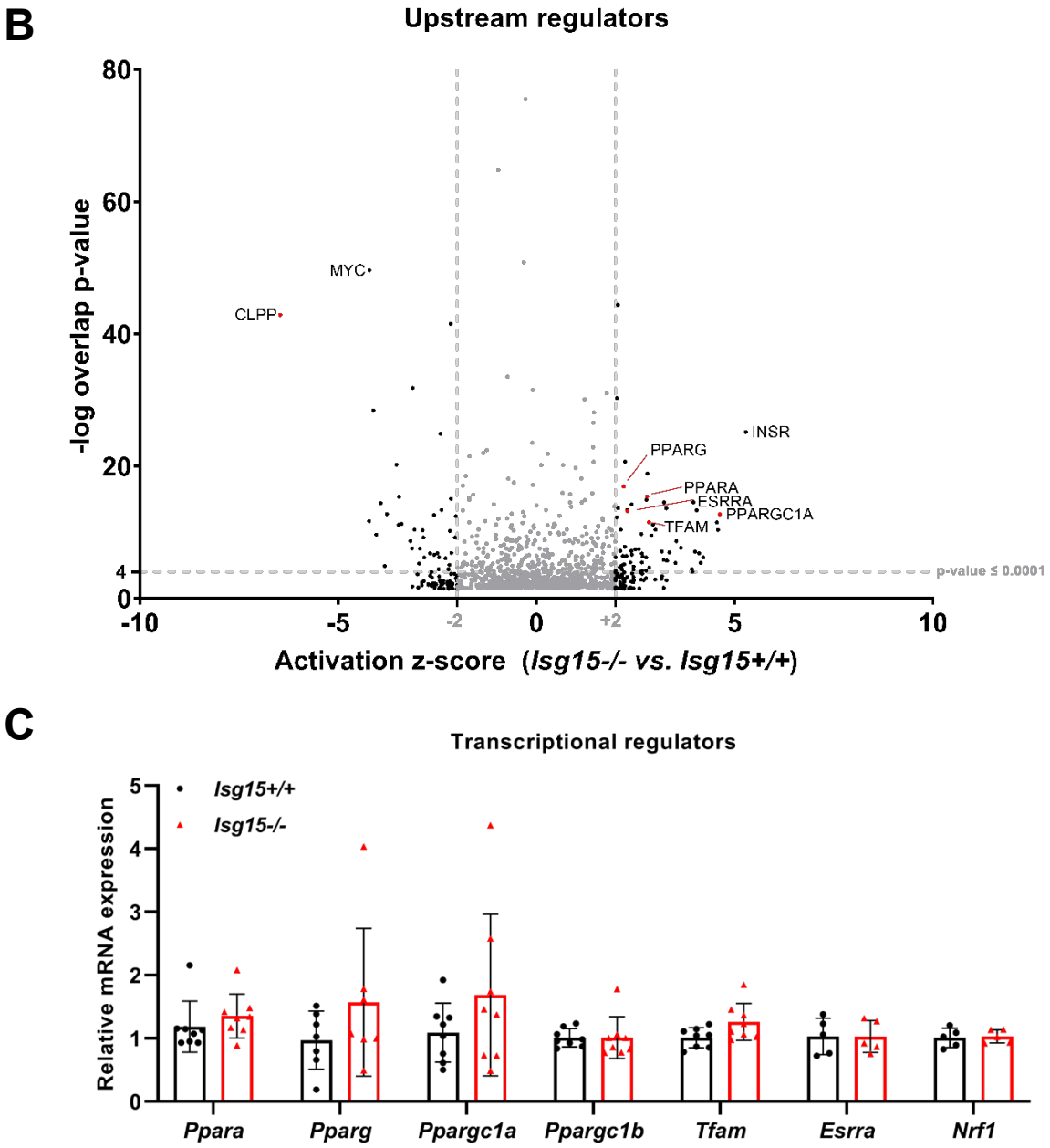

Figure R9. Analysis of the expression of lipid metabolism genes and metabolic regulators in *Isg15-/-* and *Isg15+/+* BMDM. (A). The expression levels of key genes FAO, lipid synthesis and lipid hydrolysis are similar between *Isg15-/-* and *Isg15+/+* BMDM. mRNA levels of the indicated genes were analyzed by RT-qPCR in IFN-treated *Isg15-/-* and *Isg15+/+* BMDM. Expression levels are normalized to HPRT mRNA levels. Mean ± SD of 8 biological replicates is represented. **(B)**. *Isg15-/-* BMDM show predicted activation of transcriptional regulators of mitochondrial biogenesis and lipid metabolism. Data from the proteomic analysis of IFN-treated *Isg15-/-* and *Isg15+/+* BMDM were subjected to IPA Upstream Regulators Analysis. Results of the Upstream Regulators analysis are represented as a volcano plot, according to the activation score (X axis) and the -log *p-value* of the comparison between genotypes. Relevant regulators are

highlighted in red and tagged. Thresholds for activation higher and lower than +2 and -2, respectively, and *p-value* < 0.0001 are indicated. **(C).** The expression levels of mitochondrial transcriptional regulators indicate slightly increased expression of *Pparg* and *Pparcg1a* in *Isg15-/-* BMDM. mRNA levels of the indicated genes were analyzed by RT-qPCR in IFN-treated *Isg15-/-* and *Isg15+/+* BMDM. Expression levels are normalized to HPRT mRNA levels. Mean ± SD of 8 biological replicates is represented. Student's T-test was performed for the comparisons. * *p-value < 0.05; ** p-value < 0.01: *** p-value <0.001.*

4.2.3. The macrophage lipid profile is altered in the absence of ISG15

The changes in enzymes of lipid metabolism reported by the proteomic analysis and the predicted activation of PPAR regulators and PGC-1 coactivators suggested that *Isg15-/-* BMDM might present a dysregulation in lipid metabolic pathways. Therefore, to assess the lipidic status of these cells, we performed a lipidomic analysis of type I IFN-treated *Isg15-/-* and *Isg15+/+* BMDM, in collaboration with the Center for Cooperative Research in Biosciences (CIC bioGUNE, Derio, Spain). The lipidomic analysis detected a total of 226 metabolites, which were subjected to univariate and multivariate data analyses. Multivariate data analysis with all the samples and pool samples was performed to determine the quality and reproducibility of the measurements, which were reported as high. Also, this analysis revealed a clear clustering of samples according to the genetic background, indicating substantial differences in the lipid profile between genotypes (Figure R10-B, upper panel). Metabolites responsible for this separation were TAG, SM, Cer and CE, which were decreased in *Isg15-/-* BMDM, and PE, which were increased in these cells (Figure R10-B, lower panel).

Univariate data analysis was performed, calculating percentage changes and unpaired Student's t-test p-value (or Welch's t test when necessary) for the comparisons between genotypes. A heatmap was generated to help in the visualization of the results (Figure R10-A). A detailed analysis of the comparison between genotypes showed that 112 out of 226 metabolites were significantly altered in *Isg15-/-* BMDM compared with *Isg15+/+* cells. Our attention was caught by the fact that almost the whole profile of neutral lipids (NLs: TAG, DAG, and CE) was significantly decreased in *Isg15-/-* BMDM (Figure R10-C). These lipid species play a wide range of functions in the cell, from FA storage in LDs to the generation of lipid second messengers involved in numerous signaling pathways (Gross & Han, 2009), thus being key molecules in the regulation of immune responses (Bosch et al., 2020). Considering the decrease in NLs observed in *Isg15-/-* cells and the relevance of LDs in innate immunity, we focused our study on these lipid species. However, it is also important to remark that other lipid species, mainly phospholipids (e.g., PE, PC), were also altered in *Isg15-/-* BMDM (Figure R10-A), indicating that ISG15 is necessary to maintain homeostasis of a wide variety of lipid molecules.

It was remarkable that CE were the most affected NLs in *Isg15-/-* BMDM. Interestingly, the neutral CE hydrolase 1 (NCEH1) was one of the most highly upregulated proteins in *Isg15-/-* BMDM. NCEH1 has a key role in CE hydrolysis in macrophages, and its ablation leads to accumulation of CE (Sakai et al., 2014; Sekiya et al., 2009). Therefore, we sought to analyze the levels of NCEH1 by western blot. Surprisingly, NCEH1 was only detected in *Isg15-/-* BMDM, in line with the strong upregulation observed in the proteomic analysis (Figure R10-D). It is to note that the high NCEH1 levels were independent of IFN treatment, indicating that its overexpression is the result of the absence of ISG15, even in basal conditions. However, IFN caused changes in the band pattern, shifting from an intense double band around 50 kDa, to a less intense doublet, an additional 48-kDa band and the native 46-kDa band. These observations suggested that NCEH1is processed or modified in response to type I IFN, although the cause and outcomes of these modifications are still to be determined.

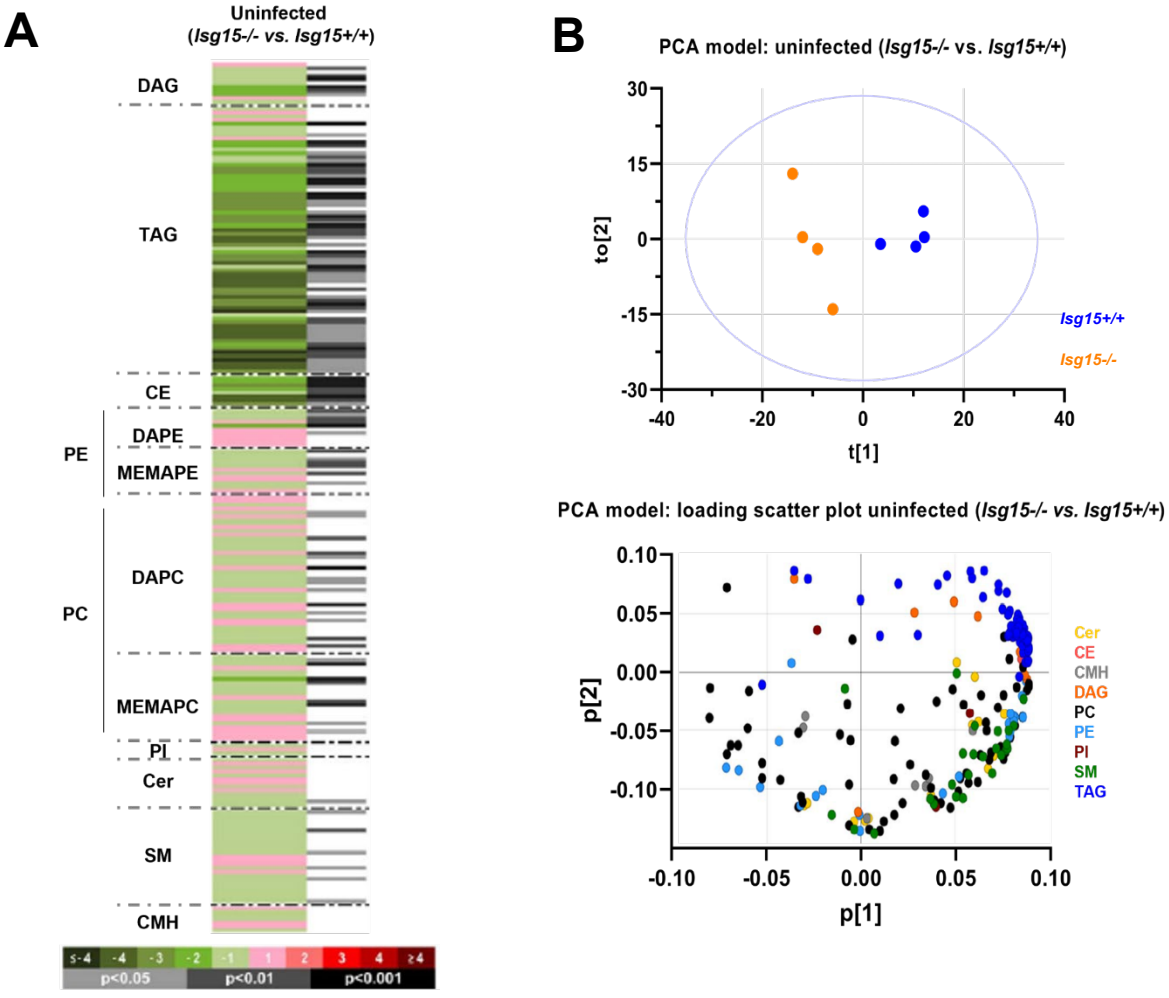

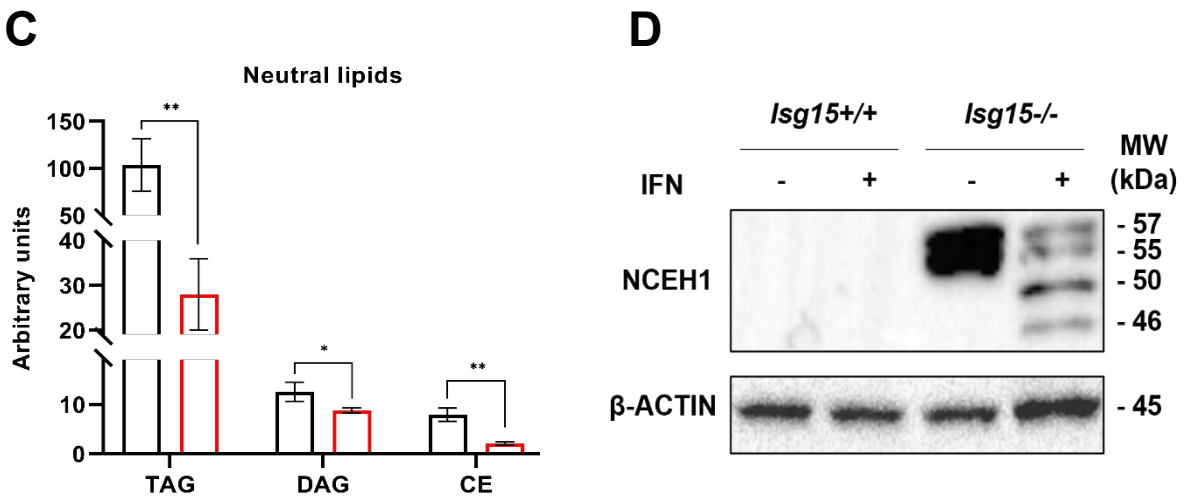

Figure R10. Analysis of the lipid profile of *Isg15-/-* and *Isg15+/+* BMDM. (A-B). Lipidomic analysis of IFN-treated *Isg15-/-* and *Isg15+/+* BMDM. BMDM from 4 mice of each genotype were subjected to UHPLC-MS-based metabolomic analysis. (A). The heatmap shows the log2 fold change (*Isg15-/-* vs. *Isg15+/+*) of the 226 metabolites analyzed, together with the *p-value* obtained in the appropriate statistical analysis. Darker green and red colors indicate higher drops or elevations of the metabolites represented, respectively. Grey lines correspond to significant fold change values of individual metabolites, being darker grey colors indicative of higher significances. Also, metabolites are represented in order according to their carbon number and unsaturation degree of acyl changes. (B). Principal component analysis (PCA) was performed to evaluate the clustering between samples. Clustering at the sample (upper panel) and metabolite (lower panel) levels is represented. **(C)**. *Isg15-/-* BMDM show lower levels of neutral lipids. The levels of TAG, DAG and CE obtained in the lipidomic analysis are shown. Mean ± SD of 4 biological replicates is represented. Statistical analyses are detailed in section *3.25.7.* of Materials and Methods. * *p-value < 0.05; ** p-value < 0.01: *** p-value <0.001.* **(D).** *Isg15-/-* BMDM show increased expression of NCEH1. Total protein extracts (25 µg) of untreated and IFN treated *Isg15-/-* and *Isg15+/+* BMDM were subjected to 7.5% SDS-PAGE and resolved by western blot. Antibodies against NCEH1 and β-actin (control) were used. MW are indicated in kDa.

4.2.4. ISG15 regulates LD homeostasis in BMDM

Given the marked decrease in NL detected in the lipidomic analysis, we evaluated the status of the LD pool in type I IFN-treated BMDM. NLs were stained with the fluorescent dye BODIPY 493/503, and LDs were analyzed by confocal microscopy. Macrophages of both genotypes showed few and small LDs, and no clear differences were detected between genotypes (Figure R11-A, upper panels). Therefore, to increase LD numbers and thus facilitate the analysis, LD synthesis was induced by treating cells with 100 µM OA for 24 h. As expected, LD content significantly increased in response to OA (Figure R11-A, lower panels). To determine whether the

LD population differed between genotypes, LDs were quantified, and the area of individual LDs was calculated. The number of LD was notably reduced in IFN-treated *Isg15-/-* BMDM compared with *Isg15+/+* cells, although these differences were not statistically significant. In lipid-loaded cells, however, we detected a significant decrease in LD number in *Isg15-/-* BMDM (Figure R11-B, left panel). Regarding the size of LDs, there were no differences in LD area between IFN-treated cells; however, lipid-loaded *Isg15-/-* BMDM showed smaller LDs than *Isg15+/+* cells, as indicated by a reduced LD area (Figure R11-B, right panel). Consistent with these results, our proteomic analysis reported a marked decrease in PLIN2 and PLIN3 in *Isg15-/-* BMDM (Table R3).

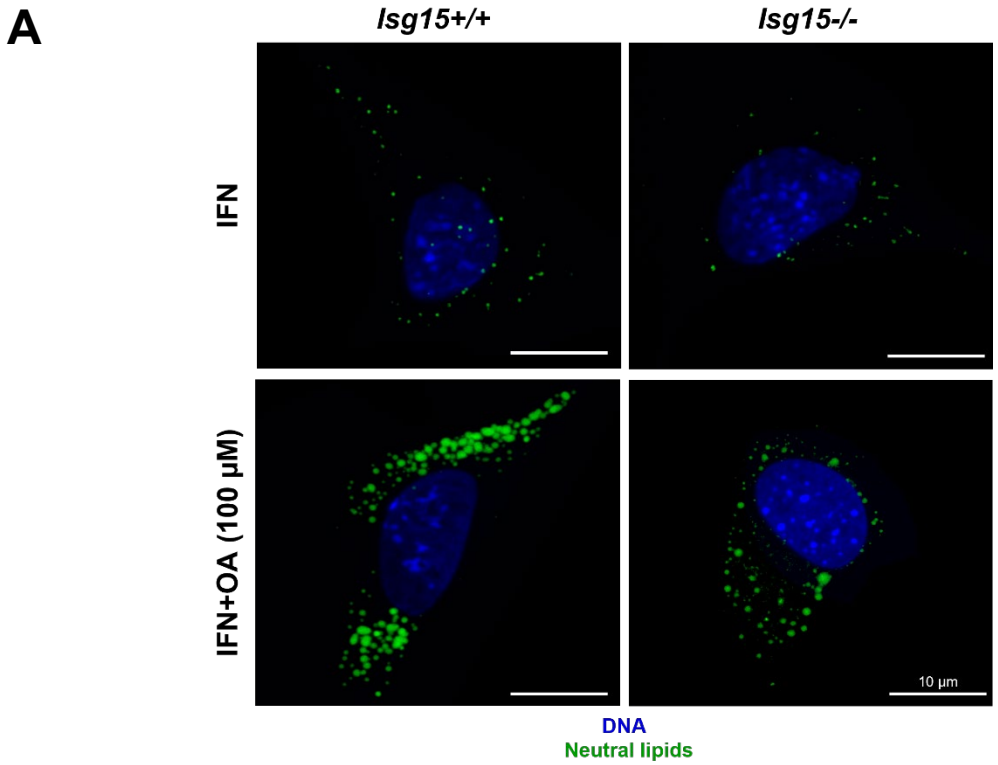

Figure R11. Analysis of the LD content of *Isg15-/-* and *Isg15+/+* BMDM. (A-B). *Isg15-/-* BMDM show less and smaller LDs than *Isg15+/+* BMDM. (A). *Isg15-/-* and *Isg15+/+* BMDM were treated with type I IFN (500 U/mlL) alone or in combination with OA (100 μM) for 24 h. LDs were stained *in vivo* for 30 min at 37°C in a humidified incubator. Cells fixed with 4% PFA and prepared for analysis by confocal microscopy. DNA was stained with DAPI. Microscopy analysis was performed in a Zeiss LSM 880 Airyscan Super-resolution microscope. Images were processed and analyzed with Aivia AI Image Analysis software. Representative images are shown. (B). LD number and area were calculated with Aivia AI Image Analysis software. 10-20 images of each condition were used to determine Mean LD numbers (left panel). 200+ individual LDs were analyzed to determine LD area (right panel). Mean ± SD is represented. Student's T-test was performed for the comparisons. * *p-value < 0.05; ** p-value < 0.01: *** p-value <0.001.*

4.2.5. The reduced LD content of Isg15-/- BMDM is linked to increased lipolysis, but not FAO

The reduction in NL levels and LDs observed in *Isg15*-/- BMDM proposed three possible scenarios: 1) increased lipid hydrolysis from LDs to fuel FAO; 2) decreased FA esterification and LD formation; or 3) a combination of the above two situations. Our proteomic analysis suggested that the first scenario was the most likely to happen, given that the levels of enzymes involved in lipid esterification were similar between genotypes (data not shown), in contrast to an increase in FAO proteins and lipid hydrolases, and a decrease in the LD proteins PLIN2 and PLIN3 (Table R3). These observations, together with the reduction in mitochondrial respiration and ATP production observed in *Isg15-/-* BMDM (Figure R4-A), led us to hypothesize that *Isg15-/-* BMDM might display increased lipolysis and FAO to counterbalance the defects in OXPHOS.

To evaluate FA dynamics in these cells, we performed a pulse-chase analysis with BODIPY 558/568 C12 (Red C12), an orange-red fluorescent FA which acts as an 18-carbon FA analog and can be incorporated into LD (Rambold, Cohen, & Lippincott-Schwartz, 2015). Cells were labeled with 1 μM Red C12 in growth medium for 16 h. Then, labeling medium was replaced with fresh medium and cells were incubated for 3 h. After incubation, red fluorescence was analyzed by confocal microscopy in live cells (Figure R12-B). Quantification of Red C12 fluorescence indicated that there were no significant differences in total Red C12 content between genotypes (Figure R12-C, left). However, the subcellular distribution of Red C12 seemed to be different between genotypes. It was noticeable that *Isg15+/+* BMDM accumulated more Red C12 in LD (Figure R12-B), further evidenced by quantification of LD numbers (Figure R12-C, right), while in *Isg15-/-* BMDM Red C12 was distributed throughout the cell. These results, together with the proteomic study, suggested that *Isg15-/-* BMDM present increased lipid hydrolysis from LDs, given that enzymes responsible for FA esterification, unlike lipases, were not altered in *Isg15-/-* BMDM. Nonetheless, we cannot rule out the possibility of a defect in lipid droplet biogenesis, and

further experiments are needed to elucidate the exact mechanism by which ISG15 controls lipid distribution.

The fact that total Red C12 levels did not significantly differ between genotypes suggested that destination of hydrolyzed lipids seemed not to be mitochondrial FAO. To assess whether there were differences in mitochondrial FAO between *Isg15-/-* and *Isg15+/+* BMDM, we measured basal and maximal OCR, and OXPHOS-linked ATP production, in the presence of etomoxir (5 μM), using a Seahorse Biosciences XF96 Extracellular Flux Analyzer platform, in collaboration with the group of Prof. Marc Liesa-Roig, at the University of California, Los Angeles (UCLA). Etomoxir is a specific inhibitor of CPT1, the enzyme responsible for the import of long chain-FAs (LCFAs) into the mitochondrion for FAO. (Schlaepfer & Joshi, 2020). The inhibition of CPT1 by etomoxir treatment reduces FAO and, hence, results in a decrease of OCR and OXPHOS-derived ATP in cells that are using FAs as a carbon source. The respirometric analysis of IFN-treated BMDM indicated that *Isg15-/-* BMDM presented reduced basal and maximal OCR, and lower levels of OXPHOS-derived ATP, independently of etomoxir treatment (Figure R12-A). Surprisingly, etomoxir did not have any effect on OCR and ATP production in any of the genotypes, as respiratory parameters were not altered comparing with untreated cells. These results indicated that, despite the increase in FAO proteins observed in *Isg15-/-* macrophages, FAO activity was not increased in these cells, and confirmed our previous results in which we observed a reduction in OXPHOS and mitochondrial ATP synthesis in *Isg15-/-* BMDM (Figure R4-A). Altogether, these results suggested that lipolysis is stimulated in *Isg15-/-* BMDM, although the generated free FAs are not oxidized in mitochondria.

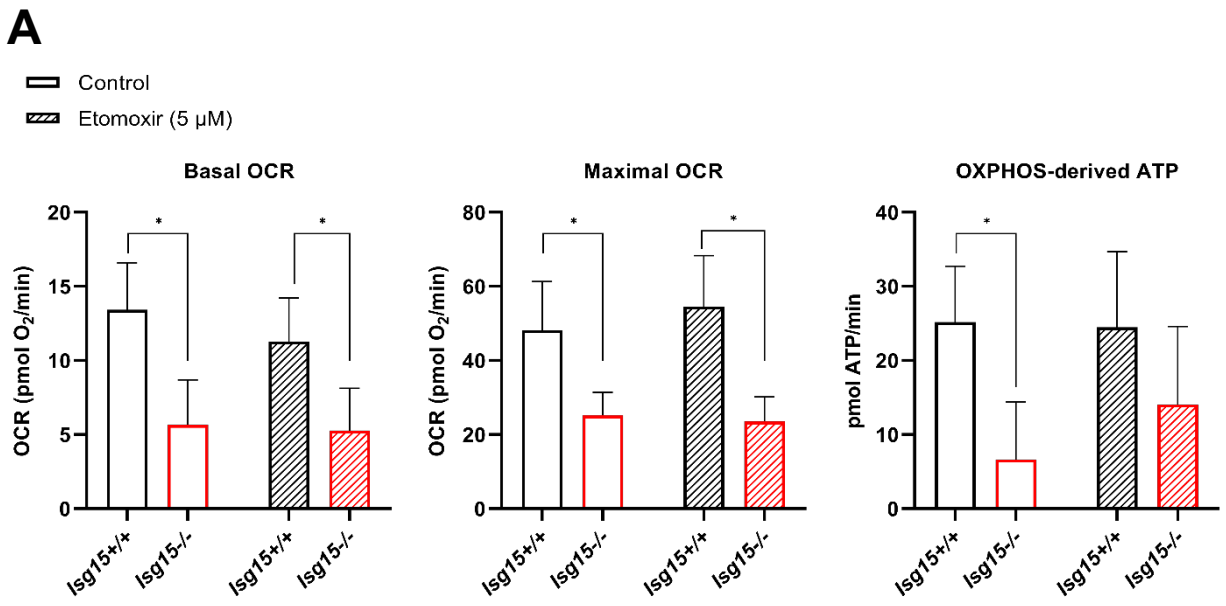

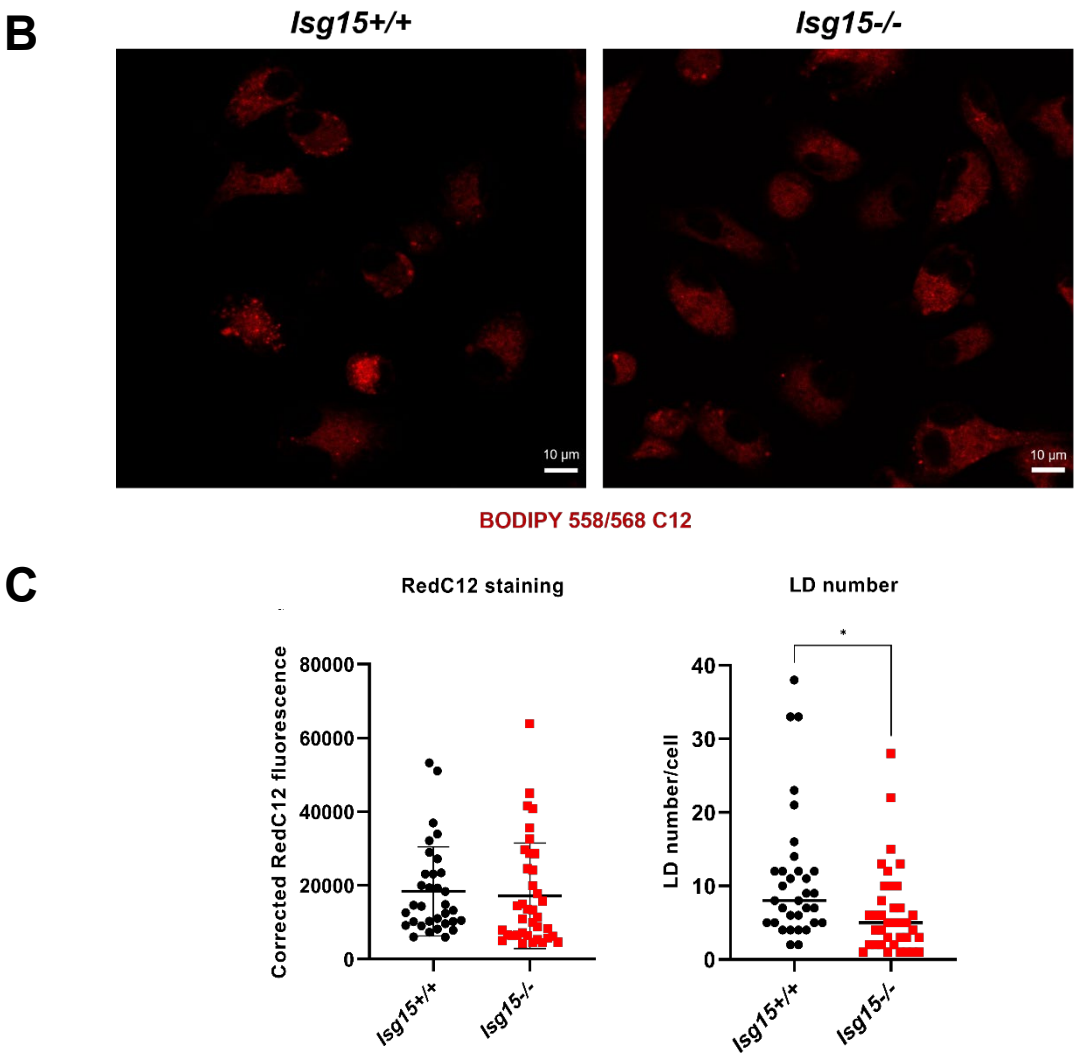

Figure R12. Analysis of mitochondrial FAO and FA dynamics in *Isg15-/-* and *Isg15+/+* BMDM. (A). Mitochondrial FAO is similar between genotypes. Mitochondrial OCR and OXPHOS-linked ATP levels of IFN-treated *Isg15-/-* and *Isg15+/+* BMDM were measured using a Seahorse Biosciences XF96 Extracellular Flux Analyzer, in the presence or not of etomoxir (5 µM). Mean ± SD of 3 biological replicates is represented. Student's T-test was performed for the comparisons. **(B-C).** FAs are differently distributed between genotypes. (B). IFN-treated *Isg15-/-* and *Isg15+/+* BMDM were treated with 1 µM Red C12 for 18 h. Red C12 was removed, cells were washed, and fresh complete medium was added. Red fluorescence was analyzed *in vivo* with a SP5 confocal microscope. Images at 3 h after medium replacement are shown. (C). Corrected Red C12 fluorescence and LD numbers of 30+ cells were measured with Fiji. Student's T-test was performed for the comparisons. * *p-value < 0.05; ** p-value < 0.01: *** p-value <0.001.*

4.2.6. VACV alters the levels of lipid metabolism proteins in BMDM

Our previous results demonstrated that ISG15 modulates mitochondrial and lipid metabolism in BMDM. Moreover, we demonstrated that VACV infection causes alterations in mitochondrial metabolism, very similar to those observed in BMDM lacking ISG15, what might be explained by reduced ISG15 levels and ISGylation during VACV infection. Given these similarities, we wondered whether VACV infection caused changes in lipid metabolism the same way the absence of ISG15 did. For that purpose, we analyzed the levels of proteins involved in lipid metabolism reported by the proteomic analysis of VACV-infected *Isg15*+/+ BMDM. Surprisingly, we found a similar profile to that observed in *Isg15*-/- BMDM, with a general increase in protein levels. However, we detected the opposite behavior for some key proteins. For example, CPT1A, the main FAO enzymes, was downregulated in infected cells (Table R4), suggesting that FAO might not be increased in VACV-infected BMDM, in contrast to what was observed for other cell types (Greseth & Traktman, 2014). In the same line, PLIN2 was upregulated, pointing to increased lipid storage in response to infection. Interestingly, proteins involved in cholesterol uptake such as CD36 and SR-B1 were upregulated, indicating increased cholesterol influx in infected cells. Furthermore, FASN was strongly downregulated in infected *Isg15*+/+ BMDM compared with uninfected cells, suggesting inhibition of FAS, contrary to what was described for BSC40 and HFF cells (Greseth & Traktman, 2014; Pant et al., 2021).

Altogether, our results indicated that VACV alters the levels of key proteins of lipid metabolism, including FAO, FAS, lipid storage and cholesterol metabolism, indicating that VACV infection impacts on the macrophage lipid homeostasis.

Table R4. Differences in lipid metabolism protein abundances between VACV-infected and uninfected *Isg15*+/+ BMDM. Table list (from left to right): Lipid metabolism pathway (column A); Protein ID (UniProt code) (column B); Gene name (column C); Standardized log2 fold change in protein abundance between the comparisons indicated (columns D). Mitochondrial proteins are highlighted in bold. Targets of ISGylation are highlighted in blue.

Pathway	Protein ID	Gene	Std log2 FC (VACV vs. uninfected *Isg15*+/+)
Fatty acid oxidation	Q99MN9	**Pccb**	10.02
	P51174	**Acadl**	8.64
	Q91ZA3	**Pcca**	8.63
	Q9EPL9	Acox3	8.62
	Q8QZT1	**Acat1**	7.71

	Q9Z2Z6	**Slc25a20**	6.67
	Q9JHI5	**Ivd**	6.39
	Q8BH95	**Echs1**	5.58
	Q8JZN5	**Acad9**	5.39
	Q99JY0	**Hadhb**	5.11
	Q9CQ62	**Decr1**	4.23
	P50544	**Acadvl**	3.55
	Q9DBL1	**Acadsb**	3.04
	Q60759	**Gcdh**	3.02
	Q8K370	**Acad10**	2.12
	Q8CAY6	**Acat2**	-2.61
	P97742	**Cpt1a**	-5.88
	Q9CZS1	**Aldh1b1**	-6.21
	P32020	Scp2	-6.86
Lipid synthesis	O35083	Agpat1	4.95
	Q9D517	Agpat3	4.62
	Q8CHK3	Mboat7	4.25
	Q8BHF7	Pgs1	4.21
	Q8K3K7	Agpat2	3.29
	Q91YX5	Lpgat1	2.47
	Q8BYI6	Lpcat2	2.44
	Q8JZK9	Hmgcs1	-2.34
	Q920E5	Fdps	-7.31
	P19096	Fasn	-8.10
Lipid hydrolysis	Q8VCI0	Plbd1	10.62
	Q99LR1	Abhd12	9.89
	Q3TCN2	Plbd2	7.85
	Q9Z0M5	Lipa	7.12
	Q91WC9	Daglb	5.27
	Q8BLF1	Nceh1	4.72
	Q9WV54	Asah1	4.12
	Q8VEB4	Pla2g15	3.61
	Q80YA3	Ddhd1	2.35
	Q8BVA5	Ldah	-2.57
Lipid transport and storage	P08226	Apoe	13.09
	Q61263	Soat1	11.56
	Q08857	Cd36	10.39
	P55302	Lrpap1	9.58
	Q91ZX7	Lrp1	7.90
	P41233	Abca1	5.22

	P48410	Abcd1	2.79
	P43883	Plin2	2.65
	Q61009	Scarb1	2.68
	Q00623	Apoa1	2.23
	Q64343	Abcg1	-3.01
	Q3B7Z2	Osbp	-4.58
	P11404	Fabp3	-6.93

4.2.7. VACV alters the expression of Isg15 and genes involved in lipid metabolism in BMDM

Our proteomic analysis of infected BMDM pointed to alterations in lipid metabolism during VACV infection, as the levels of many key proteins in lipid metabolism were differentially regulated, comparing with uninfected cells. To evaluate whether the differences in protein levels were due to increased or decreased gene expression, we analyzed the expression of genes involved in lipid synthesis (*Fasn*, *Hmgcr*), FAO (*Cpt1a*, *Acads*, *Acadm*), lipid storage (*Soat1*, *Plin2*), lipid hydrolysis (*Nceh1*), and lipid uptake and efflux (*Cd36*, *Abcg1*). Many of these genes belong to cholesterol metabolism (*Nceh1*, *Hmgcr*, *Soat1*, *Cd36*, *Abcg1*), as cholesterol homeostasis is determinant during VACV infection (Chung et al., 2005).

Significant differences were found for some genes in response to infection (Figure R13-A). *Cpt1a* mRNA levels were significantly increased in infected cells, a surprising result considering the strong downregulation observed in the proteomic analysis (Table R4), suggesting that post-transcriptional and/or post-translational mechanisms might modulate the levels of CPT1A during VACV infection. The expression of *Plin2* and *Cd36* was also increased by VACV-infection, in line with the results of the proteomic analysis, pointing to increased lipid uptake and storage. It was also remarkable that the expression of several genes was notably increased in infected *Isg15-/-* BMDM, as occurred with *Acads*, *Fasn*, *Hmgcr*, *Soat1* and *Nceh1*, although the differences were not statistically significant. However, these observations suggested that ISG15 might be relevant for the regulation of the expression of some genes during viral infections.

Overall, our results indicated that VACV infection causes an increase in lipid uptake and storage, mainly cholesterol, as suggested by increased levels of proteins involved in cholesterol uptake and esterification (CD36 and SOAT1, respectively), in line with increased levels of the LD marker PLIN2.

4.2.8. VACV modulates the expression of transcription factors involved in mitochondrial and lipid metabolism

The proteomic analysis reported differences in proteins involved in mitochondrial and lipid in response to VACV infection of BMDM, showing a similar pattern to that observed in *Isg15*-/- BMDM. Therefore, we analyzed the expression of a similar set of transcriptional regulators of metabolism to that analyzed in uninfected cells, to identify potential transcription factors responsible for the alterations observed during infection. Moreover, as cholesterol metabolism seemed to be a relevant target of infection, we included *Nr1h3* (encoding LXRα), *Srebf2* and *Scap*, key regulators of cholesterol biosynthesis, among the evaluated genes. Regarding the genes involved in energy metabolism and mitochondrial biogenesis (*Ppara*, *Pparg*, *Ppargc1a*, *Ppargc1b*, and *Tfam*), we did not find significant differences in mRNA expression of *Ppara*, *Pparg*, *Ppargc1b,* and *Tfam* in the comparisons between infected vs. uninfected cells, and between the genotypes in each condition. However, we detected a striking increase in *Ppargc1a* expression in response to infection, which was significantly higher in *Isg15-/-* BMDM (Figure R13-B, upper panel), what could explain the augmented levels of mitochondrial proteins and the stimulation of lipid uptake in infected macrophages (Supruniuk, Miklosz, & Chabowski, 2017). It is also important to remark that VACV infection caused a marked increase in the expression of *Pparg*, reaching higher levels in *Isg15-/-* BMDM, although the differences were not reported as statistically significant. Attending to the expression of the regulators of cholesterol homeostasis (Figure R13-B, lower panel), we observed a clear decrease in *Nr1h3* and *Srebf2* mRNA levels in response to infection, although statistically significant differences were reported only in the expression of *Srebf2* in infected *Isg15-/-* cells compared with uninfected cells. The expression levels of *Scap*, however, did not change between any condition.

Overall, our results suggested that the increase in mitochondrial proteins and enzymes involved in lipid uptake and esterification observed in VACV-infected BMDM could be the result of the augmented expression of *Pparg* and *Ppargc1a*, known modulators of mitochondrial biogenesis and lipid metabolism. Moreover, the decreased expression of *Srebf2* and *Nr1h3* suggested that cholesterol biosynthesis was downregulated in infected cells, consistent with a scenario of increased cholesterol uptake and storage.

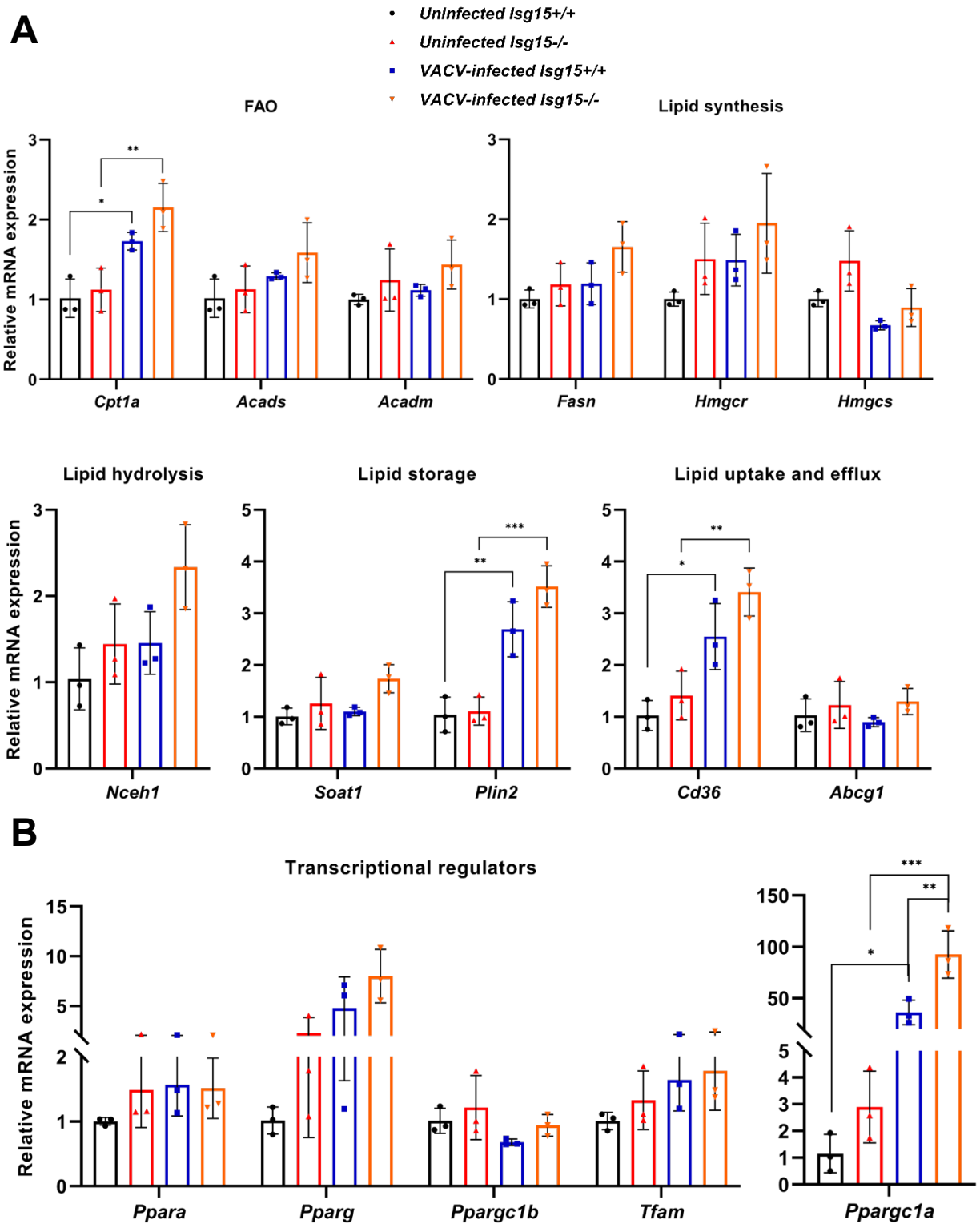
A
Uninfected Isg15+/+
Uninfected Isg15-/-
VACV-infected Isg15+/+
VACV-infected Isg15-/-
FAO
Lipid synthesis
Relative mRNA expression
Cpt1a
Acads
Acadm
Fasn
Hmgcr
Hmgcs
Lipid hydrolysis
Lipid storage
Lipid uptake and efflux
Nceh1
Soat1
Plin2
Cd36
Abcg1
B
Transcriptional regulators
Ppara
Pparg
Ppargc1b
Tfam
Ppargc1a

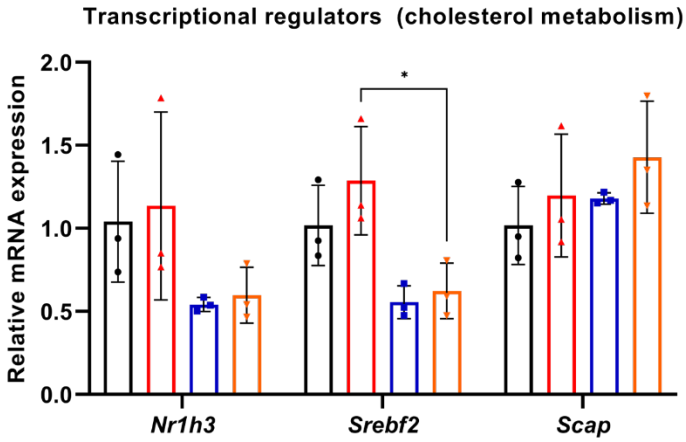

Figure R13. Analysis of the expression of lipid metabolism genes and metabolic regulators uninfected and VACV-infected *Isg15-/-* and *Isg15+/+* BMDM. (A-B). VACV enhances the expression of key genes of FAO, lipid uptake and lipid storage, as well as key regulators of mitochondrial and lipid metabolism. mRNA levels of the indicated genes were analyzed by RT-qPCR in uninfected and VACV-infected *Isg15-/-* and *Isg15+/+* BMDM treated with IFN. Expression levels are normalized to HPRT mRNA levels. Mean ± SD of 8 biological replicates is represented. Mean ± SD of 3 biological replicates is represented. Two-way ANOVA and Tukey post-hoc analyses were performed for the comparisons. * *p-value < 0.05; ** p-value < 0.01: *** p-value <0.001.*

4.2.9. VACV alters the lipid profile of BMDM

Our previous results with VACV-infected BMDM pointed to a dysregulation of lipid metabolism during VACV infection, with increased lipid uptake and accumulation, and relevant changes in cholesterol metabolism. Therefore, we sought to explore the lipid profile of VACV-infected BMDM. For that purpose, we carried out a lipidomic analysis with type I IFN-treated *Isg15*-/- and *Isg15*+/+ BMDM, infected with VACV WR (1 PFU/cell) for 16 h. Samples of infected BMDM were part of the same lipidomic analysis described for uninfected cells; therefore, cells were extracted from the same mice and subjected to the same procedures and analyses that those performed with uninfected cells (see section *3.25. Lipidomic analysis of BMDM*, in Materials and Methods).

Multivariate data analyses revealed a clear clustering of samples according to the infection, when comparing infected vs. uninfected samples of the same genotype, and according to the genetic background, when comparing infected samples of both genotypes (data not shown). In the comparison between infected vs. uninfected *Isg15+/+* cells, the metabolites responsible for the main differences were DAG, TAG, CE, Cer and PC, which were increased in samples of infected cells, and SM and PE, increased in samples of uninfected cells (Figure R14-B, upper panel). Comparing samples of infected vs. uninfected *Isg15-/-* BMDM, the main differences were found

in CE, Cer and PC, as well as several species of TAG and SM, increased in infected cells, and DAG and PE, increased in uninfected cells (Figure R14-B, middle panel). Finally, the comparison between samples of infected *Isg15-/-* vs. *Isg15+/+* BMDM reported an increase of almost all the metabolites analyzed in *Isg15+/+* cells (Figure R14-B, lower panel), consistent with the results obtained for uninfected cells.

Univariate data analyses were performed, calculating percentage changes and unpaired Student's t-test p-value (or Welch's t test when necessary) for the comparisons between infected vs. uninfected cells of the same genotype, and infected cells of the two different genotypes. As done for uninfected cells, a heatmap was generated to help in the visualization of the results (Figure R14-A). A detailed analysis of the comparison of infected vs. uninfected *Isg15+/+* BMDM reported that only 34 out of 226 metabolites were significantly altered in infected cells. It was interesting to observe that TAG and CE were increased in infected cells, with significant differences in CE (Figure R14-C, left panel), in line with our observations of upregulation of proteins involved in cholesterol uptake and flux (Table R4). The results of the comparison between infected vs. uninfected *Isg15-/-* BMDM showed that only 50 out of 226 metabolites were significantly altered. In these cells, we observed a striking increase in almost the whole CE profile of infected cells, together with a strong increase in some species of TAG and a significant decrease in DAG (Figure R14-C, middle panel). Finally, comparing infected cells of both genotypes, only 7 metabolites were significantly altered. Interestingly, the whole CE profile was significantly increased in infected *Isg15-/-* BMDM, and there was a marked but not significant decrease in DAG levels in these cells, compared with their *Isg15+/+* counterparts (Figure R14C, right panel).

Overall, our lipidomic analysis of VACV-infected BMDM indicated that VACV alters the macrophage lipid profile during infection, causing variations in several lipid species. Concerning NLs, VACV had different effects on the DAG profile comparing the two genotypes, with a slight increase in *Isg15+/+* BMDM and a significant decrease in *Isg15-/-* cells. Furthermore, VACV caused a strong increase in the levels of TAG and CE, which was exacerbated in *Isg15-/-* BMDM, suggesting that ISG15 might have a role restraining the effect of VACV on lipid metabolism.

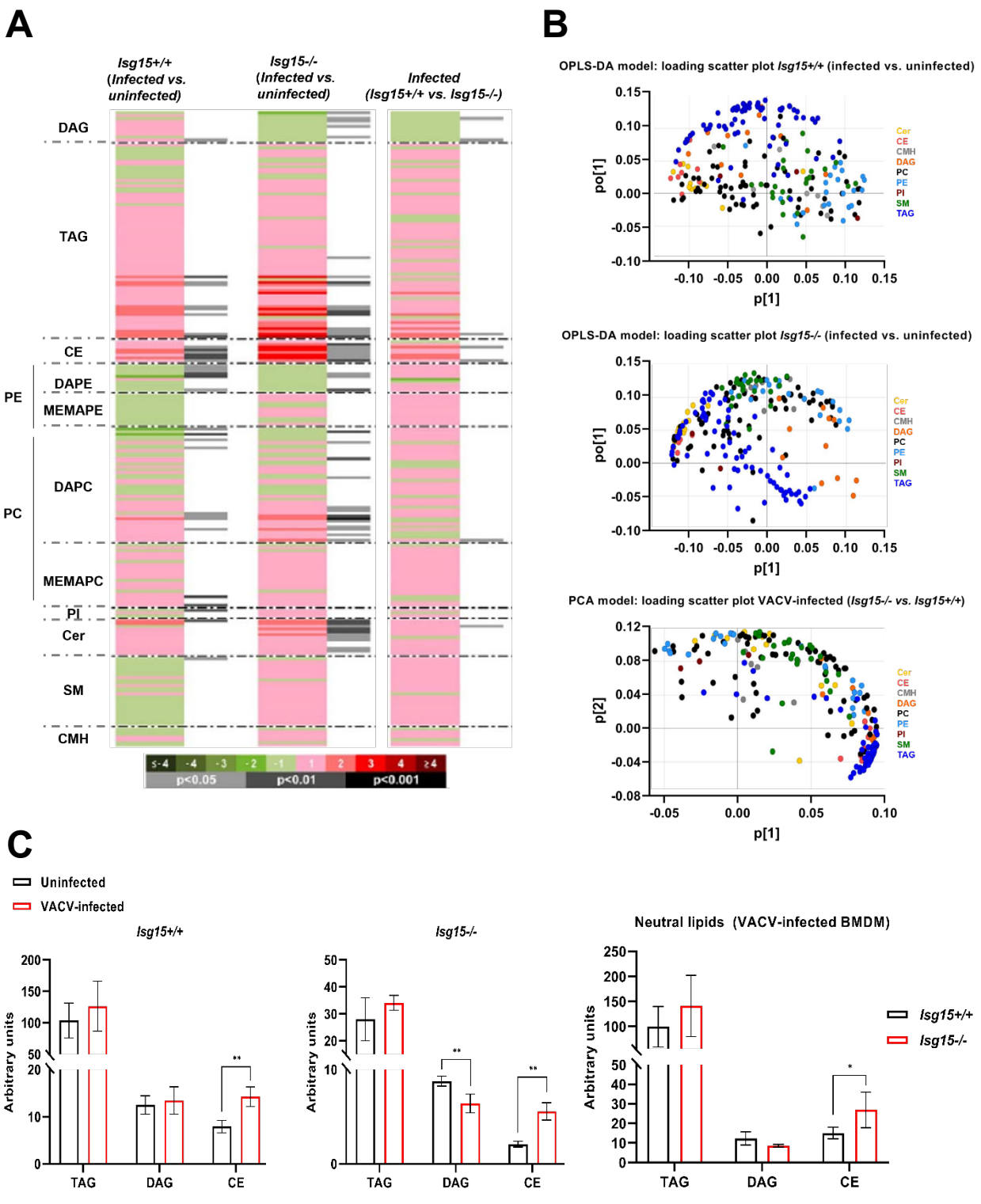

Figure R14. Analysis of the lipid profile of IFN-treated-, VACV-infected *Isg15-/-* and *Isg15+/+* BMDM. (A-B). Lipidomic analysis of IFN-treated-, VACV-infected *Isg15-/-* and *Isg15+/+* BMDM. BMDM from 4 mice of each genotype were subjected to UHPLC-MS-based metabolomic analysis. (A). The heatmap shows the

log2 fold change of the 226 metabolites analyzed for the comparisons indicated, together with the *p-value* obtained in the appropriate statistical analysis. Darker green and red colors indicate higher drops or elevations of the metabolites represented, respectively. Grey lines correspond to significant fold change values of individual metabolites, being darker grey colors indicative of higher significances. Also, metabolites are represented in order according to their carbon number and unsaturation degree of acyl changes. (B). Principal component analysis and orthogonal partial least-squares to latent structures (OPLS) analysis were performed to evaluate the clustering between samples. Clustering at the metabolite level is represented. **(C)**. VACV alters the NL content of BMDM. The levels of TAG, DAG and CE obtained in the lipidomic analysis are shown. Mean ± SD of 4 biological replicates is represented. Statistical analyses are detailed in section *3.25.7*. of Materials and Methods. * *p-value < 0.05; ** p-value < 0.01: *** p-value <0.001.*

4.2.10. Lipid loading does not affect VACV titers in BMDM

We observed that, after infection with VACV for 16 h, there was an increase in NLs that abolished the differences between genotypes almost completely (Figure R14). The increase in NLs in infected cells suggested that VACV stimulates lipid uptake and storage, in line with increased levels of proteins such as CD36, SOAT1 and PLIN2 (Table R4). LDs, far from being simple lipid storage organelles, are metabolic hubs that play pivotal roles in innate immune responses (Bosch & Pol, 2022), and play different roles during viral infections (Dias et al., 2020; Monson, Crosse, Das, & Helbig, 2018; Saka & Valdivia, 2012). The link between VACV and LD has not been established yet; therefore, we sought to explore the effect of LD content on VACV infection. *Isg15+/+* and *Isg15-/-* BMDM were treated or not with type I IFN and 100 μM OA, alone or combined, for 24 h and subsequently infected with VACV WR (1 PFU/cell) for 16 h. Then, the production of intracellular and extracellular infectious virus was analyzed by plaque assay. Regarding intracellular virus, titers were almost identical between genotypes in every condition. Attending to the treatments, OA caused a subtle and non-statistically significant increase in intracellular virus titers in both genotypes, suggesting that the addition of OA might stimulate virus replication. By contrast, IFN, alone or in combination with OA, significantly reduced virus titers in both genotypes (Figure R15-A, left panel). Similar results were obtained in the analysis of extracellular virus, with no differences between genotypes in any condition, a strong decrease in viral titers in response to IFN treatment, and a slight increase in virus titers in response to OA treatment, which was reported as significant in *Isg15+/+* BMDM (Figure R15-A, right panel). Furthermore, the antiviral effect of IFN was evidenced by a decrease in the levels of virus proteins (Figure R15-B). Collectively, these results indicated that lipid loading and, therefore, increasing LD in BMDM does not affect VACV replication and virus production, and that the mechanisms by which IFN counteracts VACV infection are independent of ISG15 in these cells.

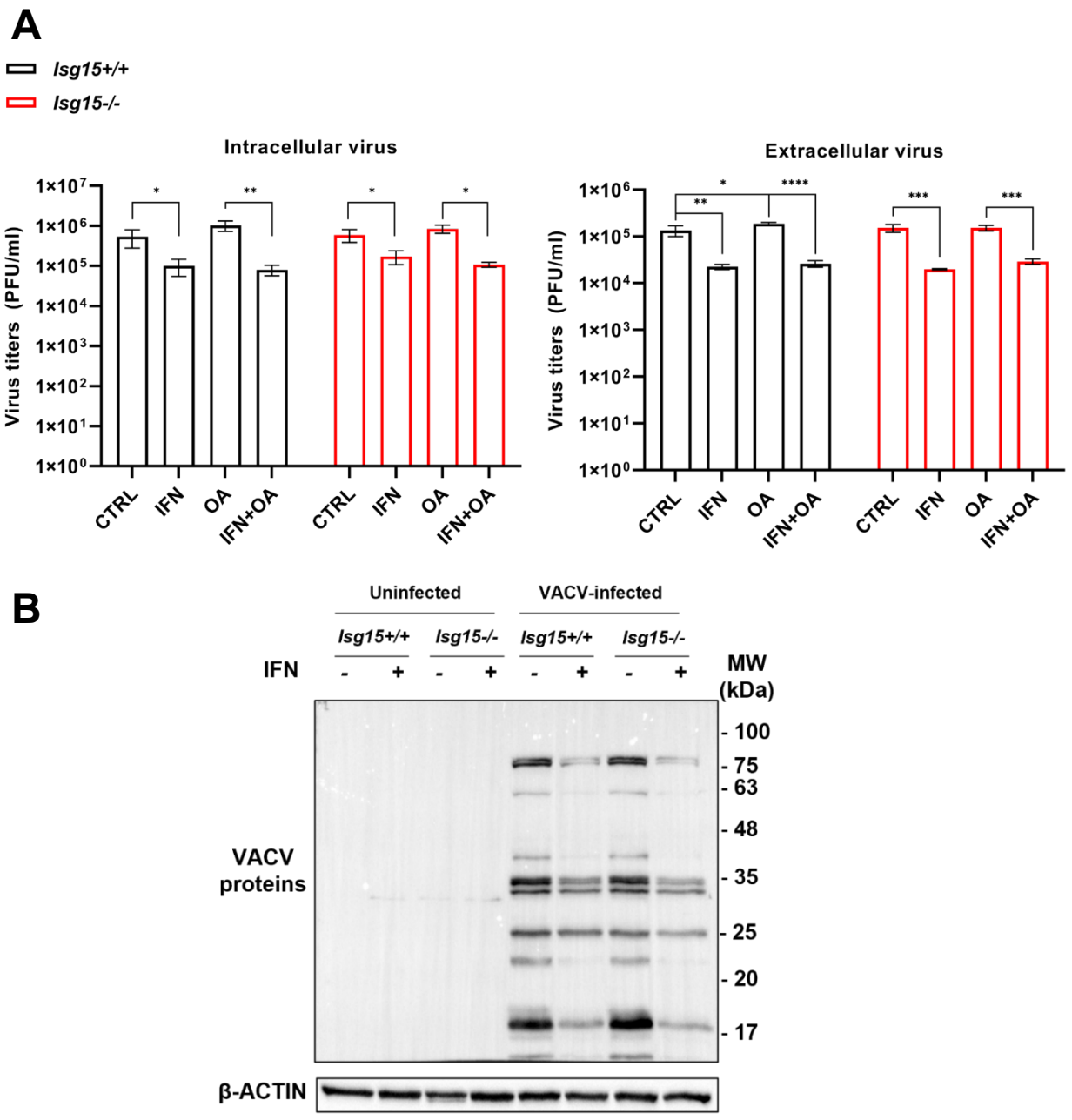

Figure R15. Analysis of the effect of OA and type I IFN on VACV replication in *Isg15-/-* and *Isg15+/+* BMDM. (A). Type I IFN, but not OA, reduces VACV titers in BMDM. *Isg15-/- and Isg15+/+ BMDM* were treated or not with type I IFN (500 U/mL), OA (100 μM), or a combination of IFN and OA, for 24 h. BMDM were infected with VACV WR (1 PFU/cell, 16 h) and titers of intracellular and extracellular virus were analyzed by plaque assay. Mean ± SD of 3 biological replicates is represented. Statistical analyses are detailed in section *3.26*. of Materials and Methods. * *p-value < 0.05; ** p-value < 0.01: *** p-value <0.001.* **(B).** VACV protein synthesis is reduced by IFN treatment. *Isg15-/- and Isg15+/+ BMDM* were treated or not with type I IFN (500 U/mL) for 24 h and infected or not with VACV WR (1 PFU/cell, 16 h). Total protein

extracts (20 µg) were subjected to 12% SDS-PAGE and resolved by western blot. An antiserum against VACV WR and an antibody against β-actin were used to detect viral proteins and actin (control), respectively. MW in kDa is indicated.

4.3. ISG15 is necessary for the efficient dissemination of VACV

As we and others have demonstrated, VACV modulates lipid metabolism during infection. Previous studies showed that VACV promotes FAS to generate FA that subsequently undergo mitochondrial FAO to fuel replication and morphogenesis (Greseth & Traktman, 2014; Pant et al., 2021; Punjabi & Traktman, 2005). VACV also depends on lipids to form membranes, and to penetrate and egress cells (Chung et al., 2005; Krijnse Locker et al., 2013; Moss, 2015). Moreover, several authors argue that EV might be formed via an exosome-like pathway (Bidgood & Mercer, 2015), in which membrane formation and composition are critical (Arumugam & Kaur, 2017). Given the role of ISG15 in the maintenance of lipid homeostasis and in the control of intracellular trafficking and exosome secretion (Villarroya-Beltri et al., 2016), we wondered whether VACV morphogenesis and spread were affected by the absence of ISG15. In macrophages, the production of viral progeny is relatively low compared with fibroblasts (Yanguez et al., 2013), what becomes more evident when macrophages are infected at an MOI of 1 PFU/cell or higher (observations from our laboratory). Many of the experiments performed to study VACV morphogenesis and dissemination require infecting at 1 or more PFU/cell, as well as the production of high amounts of virions, and the formation of cell monolayers. These conditions are difficult to achieve in macrophages, making this cell type unsuitable for our study. Therefore, we chose immortalized *Isg15-/-* and *Isg15+/+* mouse embryonic fibroblasts (MEF) to perform our experiments.

We first inspected the results of a previous proteomic analysis of untreated and type I IFN-treated *Isg15-/-* and *Isg15+/+* MEF, in search of proteins involved in lipid metabolism and membrane trafficking which were reported as altered in both BMDM and MEF. Interestingly, most of the proteins related to lipid metabolism were involved in mitochondrial FAO, supporting the role of ISG15 as a modulator of mitochondrial functions in different cell types. Regarding proteins involved in intracellular trafficking, we were curious about the fact that TSG101 was downregulated in *Isg15-/-* cells, what could have detrimental effects on the morphogenetic process of VACV, as TSG101 is required for the efficient production of EVs (Honeychurch, Yang, Jordan, & Hruby, 2007). Given that some of these proteins were altered independently of IFN treatment (Table R5), we performed our experiments in untreated cells, so that the differences in VACV morphogenesis and spread, if any, could be attributed only to the absence of ISG15.

Table R5. Quantitative proteomic analysis of untreated and IFN-treated *Isg15-/-* and *Isg15+/+* MEF. Proteins involved in lipid metabolism and autophagy/endosomal trafficking. Table list: Cellular pathway (column A); Protein ID (UniProt code) (column B); Gene name (column C), Standardized log2 fold change between the comparisons indicated (columns D and E). Targets of ISGylation are highlighted in blue.

			Std log2 FC (*Isg15-/-* vs. *Isg15+/+*)	
Pathway	**Protein ID**	**Gene**	**Untreated**	**IFN-treated**
Lipid metabolism	Q60759	Gcdh	3.000	1.000
	O35083	Agpat1	2.000	3.000
	P41216	Acsl1	2.000	1.000
	Q9D517	Agpat3	1.500	2.000
	O35459	Ech1	1.333	3.000
	P51174	Acadl	1.231	1.071
	Q07417	Acads	1.222	1.500
	P52825	Cpt2	1.200	1.143
	Q8JZN5	Acad9	-1.333	-1.571
	Q9WUR2	Eci2	-1.333	-1.333
	Q99MN9	Pccb	-1.400	-1.500
	Q9JHI5	Ivd	-1.500	-2.000
	Q91ZA3	Pcca	-1.500	-1.571
	Q9WV54	Asah1	-2.000	-1.200
	Q8R3F5	Mcat	-2.500	-5.000
	P97742	Cpt1a	-3.000	-2.000
Autophagy/Endosome trafficking	Q9CQW1	Ykt6	3.000	1.000
	P11438	Lamp1	1.500	1.000
	P51150	Rab7a	1.000	1.071
	P63024	Vamp3	1.000	1.500
	O88384	Vti1b	1.000	1.000
	Q61187	Tsg101	-2.000	-3.000

4.3.1. EV release and actin tail formation are reduced in the absence of ISG15

First, we analyzed the release of EVs from infected *Isg15+/+* and *Isg15-/-* MEF. In cell monolayers, EVs are released and infect adjacent cells or spread to distal cells by convection, forming comet-shaped plaques (comets) consisting of a central lysis plaque and a 'tail' of secondary plaques (Roberts & Smith, 2008). To analyze EV formation and release, we infected MEF monolayers with 0.0001 PFU/cell of VACV Western Reserve (WR) and VACV International Health Department-J (IHD-J) strains, and the presence of comets was analyzed by plaque assay

at 48 hours post-infection (hpi) (for IHD-J) or 72 hpi (for WR). IHD-J presents a point mutation in the protein A34, causing a significant increase in the production and release of EVs compared with WR (Figure R16-A, left panel) (Blasco, Sisler, & Moss, 1993; McIntosh & Smith, 1996), what makes this strain a good model to study the biology of EVs. As represented in Figure R16-A, comets were detected in *Isg15+/+* MEF infected with WR or IHD-J and, as expected, comets formed by IHD-J were notably larger. Surprisingly, the formation of comets was impaired in *Isg15-/-* MEF infected with either WR or IHD-J, and round plaques alone or followed by a small tail of secondary plaques were detected in these cells. These results indicated that the release and spread of EVs and, therefore, the formation of comets, were impaired in the absence of ISG15. This phenotype was much more evident infecting with IHD-J, given the high production of EV characteristic of this strain. Hence, primarily focused on this strain.

Next, we evaluated the formation of actin tails in infected *Isg15+/+* and *Isg15-/-* MEF. To assess whether ISG15 also influenced actin tail formation, we infected *Isg15+/+* and *Isg15-/-* MEF with IHD-J (2 PFU/cell) for 9 h and analyzed actin tails by confocal microscopy. Actin tails were detected in both genotypes (Figure R16-B); however, the number of actin tails was significantly lower in *Isg15-/-* MEF, as evidenced by microscopy images and quantification analysis (Figure R16-C, D). Similar results were obtained with WR (data not shown). These observations indicated that ISG15 is necessary for actin tail formation and that the absence of ISG15 impairs the mechanisms involved in virus egress and dissemination.

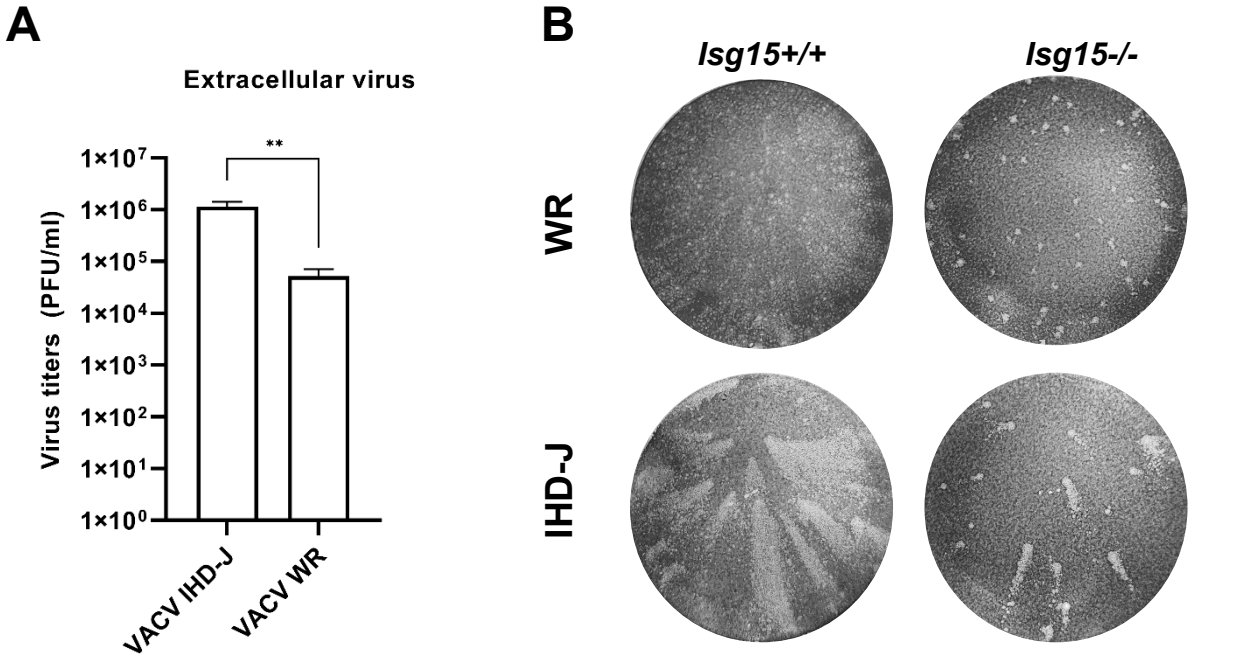

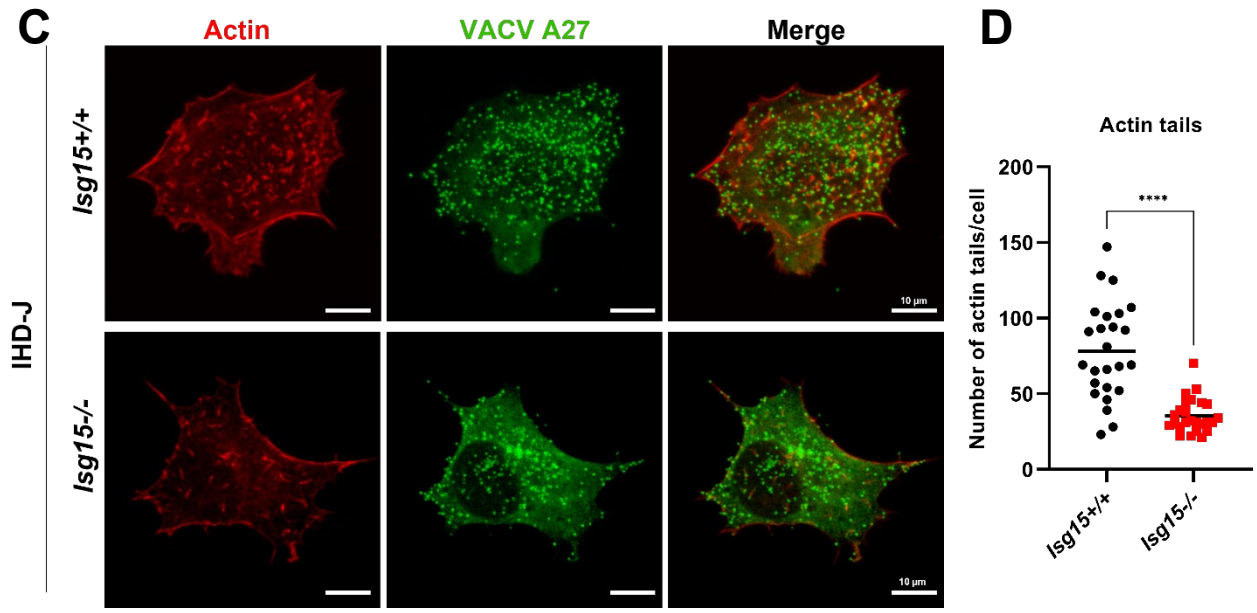

Figure R16. Analysis of EV release and actin tail production in *Isg15-/-* and *Isg15+/+* MEF. (A). VACV IHD-J strain releases more EV than VACV WR. Immortalized *Isg15-/-* and *Isg15+/+* MEF were infected with IHD-J or WR (0.01 PFU/cell) and virus secreted to the supernatant at 48 hpi was analyzed by plaque assay. Mean ± SD of 3 biological replicates is represented. **(B).** Comet production is dramatically reduced in *Isg15-/-* MEF. Monolayers of immortalized *Isg15-/-* and *Isg15+/+* MEF were infected with IHD-J or WR (0.0001 PFU/cell, 48 h), and the formation of comets was analyzed by staining with 0.2% crystal violet in 10% formaldehyde. **(C-D).** Actin tail formation is impaired in *Isg15-/-* MEF. (C). Immortalized *Isg15-/-* and *Isg15+/+* MEF growing in 12-mm coverslips were infected with IHD-J (2 PFU/cell, 9 hpi), fixed with 4% PFA, processed for immunofluorescence and analyzed by confocal microscopy using a Leica SP8 confocal microscope using a 63X objective. Actin was stained with Alexa594-phalloidin; virus particles were labeled with an antibody against VACV A27 protein, and an Alexa488-labeled secondary antibody. (D). Microscopy images were analyzed with Fiji, and actin tails were quantified in 25 cells of each condition. Student's T-test was performed for the comparisons. * *p-value < 0.05; ** p-value < 0.01: *** p-value <0.001*.

4.3.2. The absence of ISG15 does not alter viral protein synthesis and virus production

The differences in EV release and actin tail formation observed between *Isg15-/-* and *Isg15+/+* MEF could be attributed to an impairment in viral replication and viral protein translation that resulted in a decrease in virus production. To test this hypothesis, we analyzed the expression of several viral proteins by western blot and confocal microscopy in cells infected with IHD-J (2 PFU/cell) at 9 and 16 hpi. The expression of the proteins A27 (specific of MV), E3 and F13 (specific of EV) did not significantly differ between genotypes (Figure R17-A). Also, the localization and subcellular distribution of the proteins A27 and F13 was similar in *Isg15-/-* and

Isg15+/+ MEF (Figure R17-B). These results indicated that the synthesis of viral proteins was not altered in the absence of ISG15.

To analyze virus production, we infected MEF with IHD-J (2 PFU/cell) and analyzed intracellular and extracellular infectious viral particles at 16 hpi by plaque assay. The production of intracellular infectious virus did not differ between genotypes (Figure R17-C, left panel); however, there was a significant reduction in extracellular virus titers in *Isg15-/-* MEF (Figure R17-C, right panel). These results were consistent with our previous observations of impaired EV release and suggested that the absence of ISG15 does not affect the formation of intracellular virions, but the mechanisms involved in WV release and EV formation.

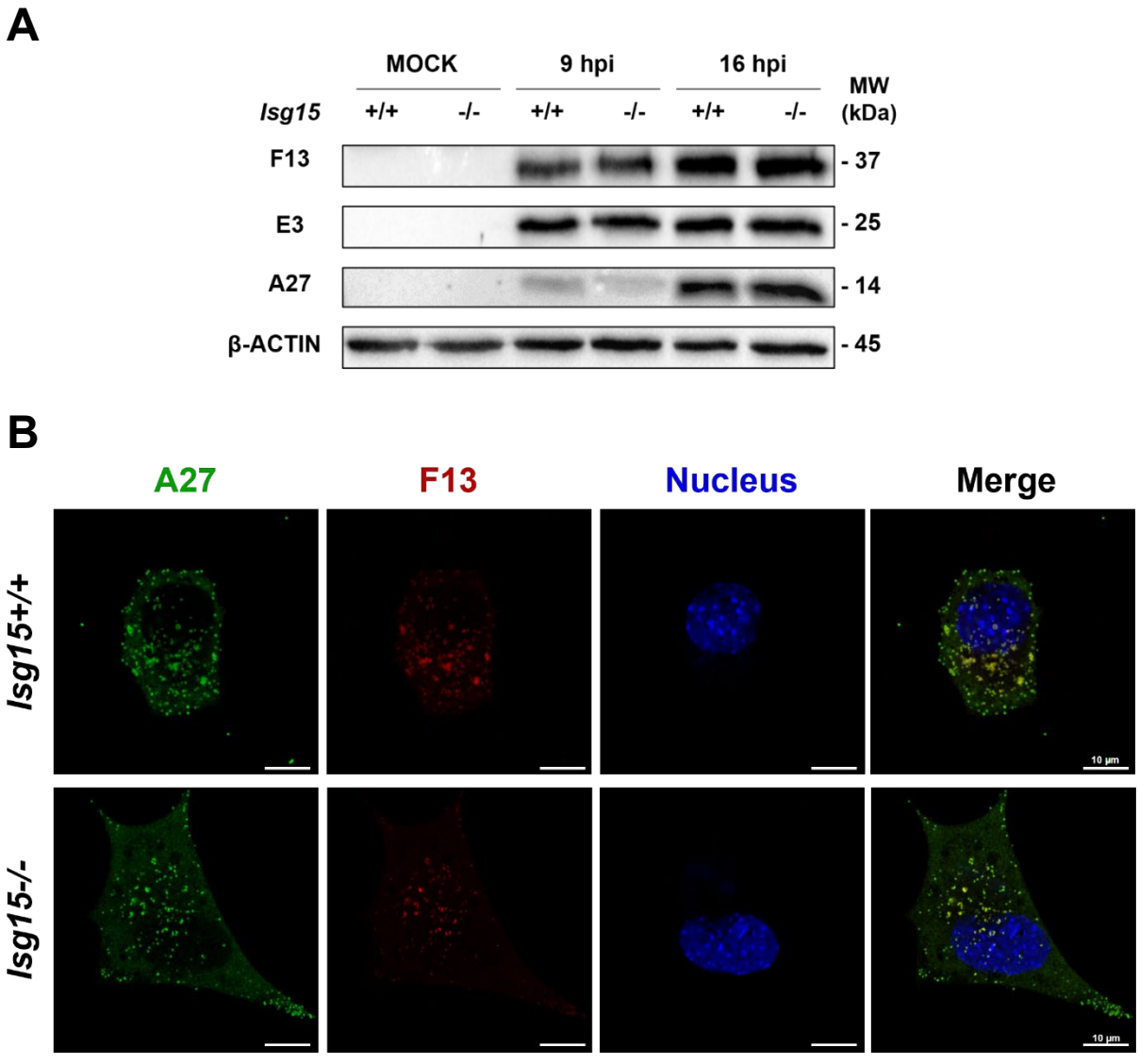

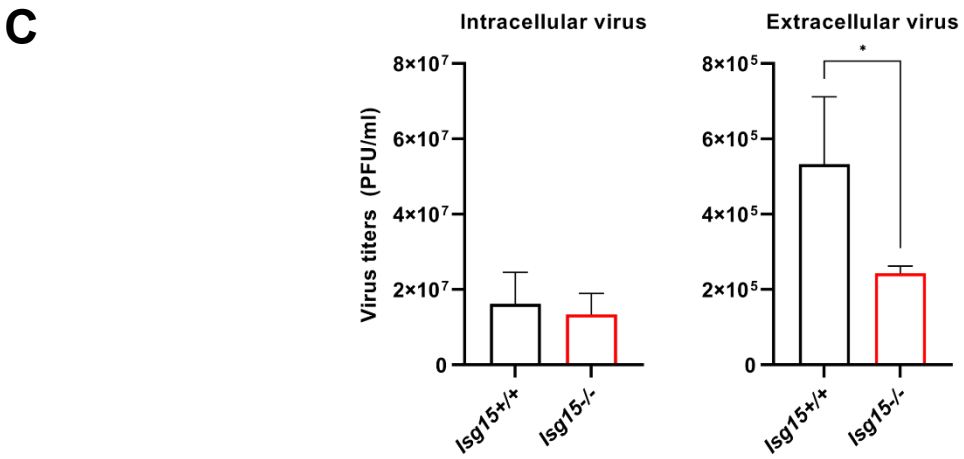

Figure R17. Analysis of viral protein production and EV release in *Isg15-/-* and *Isg15+/+* MEF. (A). Production of early, intermediate, and late proteins does not vary between genotypes. Immortalized *Isg15-/-* and *Isg15+/+* MEF were infected with IHD-J (2 PFU/cell, 9 and 16 h), and total protein extracts (20 µg) were subjected to 12% SDS-PAGE and resolved by western blot. Antibodies against viral proteins E3 (early), F13 (intermediate) and A27 (late) were used. β-actin was used as control. MW in kDa is indicated. **(B).** The localization of early, intermediate, and late proteins does not vary between genotypes. Immortalized *Isg15-/-* and *Isg15+/+* MEF were infected with IHD-J (2 PFU/cell, 9 h). Cells were fixed with 4% PFA and processed for immunofluorescence. VACV A27 and F13 proteins were labeled with specific antibodies, followed by labeling with Alexa488-labeled and Alexa594-labeled antibodies, respectively. DNA was stained with DAPI. Images were analyzed and processed with Fiji. Microscopy images were obtained with a Leica SP8 confocal microscope, using a 63X objective. **(C).** EV release is reduced in *Isg15-/-* MEF. Immortalized *Isg15-/-* and *Isg15+/+* MEF were infected with IHD-J (2 PFU/cell, 16 h), and titers of intracellular and extracellular virus were determined by plaque assay. Mean ± SD of 2 biological replicates is represented Student's T-test was performed for the comparisons. * *p-value < 0.05; ** p-value < 0.01: *** p-value <0.001*.

4.3.3. Intracellular virus particles accumulate in the absence of ISG15

Our previous results indicated that virus production did not differ between *Isg15-/-* and *Isg15+/+* MEF, albeit a clear decrease in virus release was observed in cells lacking ISG15, suggesting that virions might be accumulated in the cytoplasm of *Isg15-/-* MEF due to defective virus egress. Therefore, we infected MEF with IHD-J (2 PFU/cell) and analyzed intracellular viral particles at 9 hpi by transmission electron microscopy (TEM). Intracellular virions were present in both genotypes (Figure R18-A), although the number of intracellular virus particles was significantly higher in *Isg15-/-* MEF, as demonstrated by quantification (Figure R18-B). These results supported our hypothesis of accumulation of viral particles in the cytoplasm of *Isg15-/-* MEF.

Moreover, this observation indicated that some of these virions might be defective, as we did not detect differences in intracellular infectious virus between genotypes (Figure R17-C, left).

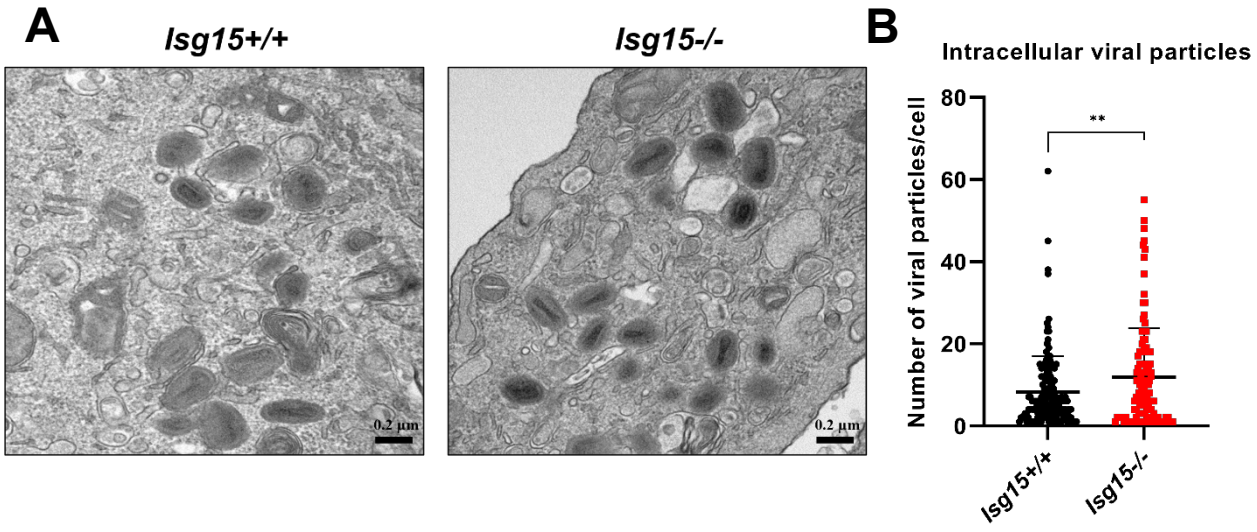

Figure R18. Analysis of intracellular viral particles in *Isg15-/-* and *Isg15+/+* MEF. (A-B). *Isg15-/-* BMDM accumulate viral particles in the cytoplasm. Immortalized *Isg15-/-* and *Isg15+/+* MEF were infected with IHD-J (2 PFU/cell, 9 h) and processed for TEM analysis. Representative images are shown. (B). Intracellular particles were quantified with Fiji (N = 145, *Isg15+/+*; N = 116, *Isg15-/-*). Mean ± SD of 2 biological replicates is represented Student's T-test was performed for the comparisons. * *p-value < 0.05; ** p-value < 0.01: *** p-value <0.001*.

One would expect a highly heterogeneous virion content in cells with defective virus egress mechanisms, as a result of the accumulation of wrapped virus forms that cannot be transported out of the cell. As described earlier, the wrapped forms of VACV contain specific proteins that are not found in unwrapped virions, and vice versa. For example, the proteins B5 and F13 are found only in wrapped virions, while the protein A26 is exclusive of unwrapped virions (Bidgood & Mercer, 2015). Considering these aspects, we analyzed and compared the proteomes of virions grown in *Isg15+/+* and *Isg15-/-* MEF. For that purpose, we infected cells with IHD-J (0.01 PFU/cell) and, at 48 hpi, cells were harvested, and virions were purified by ultracentrifugation through a 20% sucrose cushion followed by ultracentrifugation through a 20-45% sucrose gradient. Purified virions were then subjected to quantitative proteomic analysis. The proteomic analysis reported significant differences between the proteomes of virions purified from different genotypes, and a general enrichment in viral proteins was observed in samples of virions purified from *Isg15-/-* cells (Figure R19). Viral proteins that showed the most significant differences between virions from *Isg15+/+* and *Isg15-/-* MEF are collected in Table R6 and highlighted in red in Figure R19.

Interestingly, the most significantly enriched protein in virions from *Isg15-/-* MEF was B5, suggesting that the content of wrapped virions was higher in the absence of ISG15. In the same line, F13 was also significantly upregulated in virions from *Isg15-/-* cells. As well, the protein A26, exclusive of unwrapped virions, was increased in these virions. Altogether, these observations supported our hypothesis of accumulation of different virus forms in *Isg15-/-* cells, likely due to defective virus egress. Consistent with defective virus dissemination in *Isg15-/-* cells, the protein F11, involved in viral spread by modulating the actin cytoskeleton (Handa, Durkin, Dodding, & Way, 2013), was the most significantly reduced protein in virions purified from *Isg15-/-* MEF.

Overall, our results indicated that the absence of ISG15 causes alterations in virus spread mechanisms that impair EV release, reduce viral dissemination through actin tail formation, and lead to accumulation of different virus forms in the cytoplasm (and likely the surface) of the cells. However, the mechanism by which ISG15 modulates VACV dissemination is still to be determined, and further analyses will be carried out to elucidate the role of ISG15 in the control of VACV infective cycle.

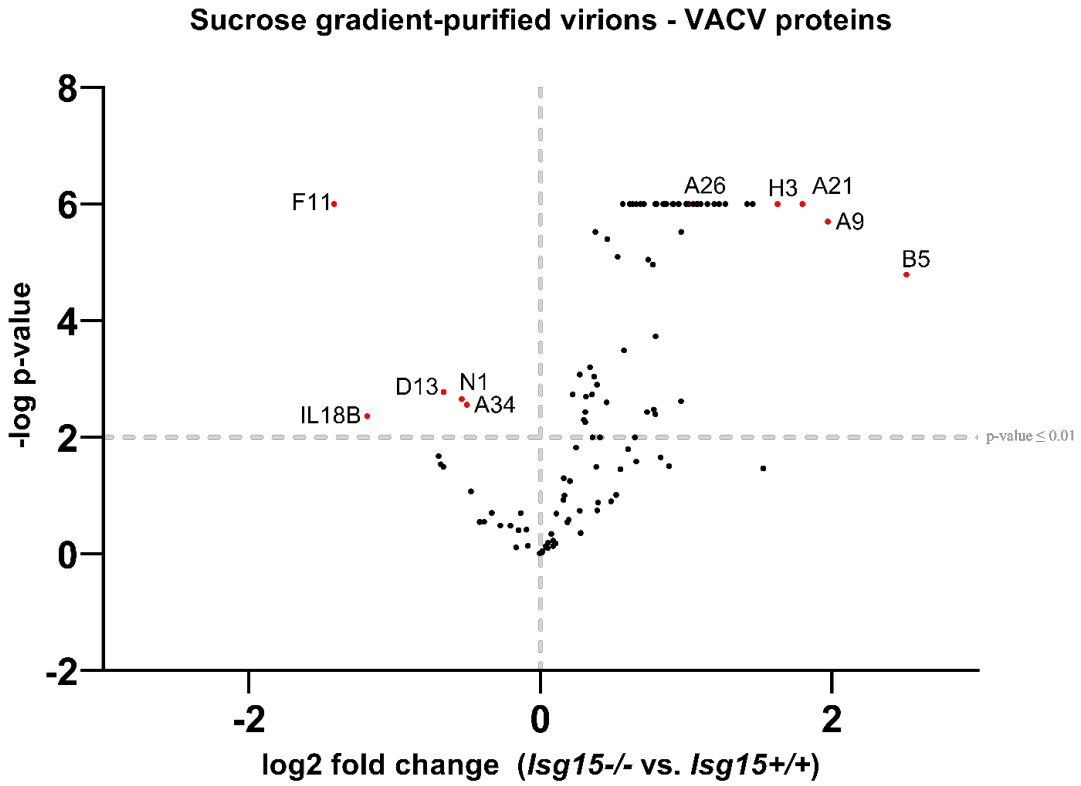

Figure R19. Quantitative proteomic analysis of sucrose gradient-purified virions grown in *Isg15-/-* and *Isg15+/+* BMDM. Immortalized *Isg15-/-* and *Isg15+/+* BMDM were infected with IHD-J (0.01 PFU/cell, 48 h), and intracellular virus was isolated and purified through a 20% sucrose cushion followed by a 20-

45% sucrose gradient. Virus pellets were then subjected to quantitative proteomic analysis. Viral proteins detected in the proteomic analysis are represented in the volcano plot, according to the fold change (*Isg15-/-* vs. *Isg15+/+*) (X axis) and the *p-value* of the comparison between genotypes (Y axis). Relevant proteins are highlighted in red and tagged. A *p-value* ≤ 0.01 threshold is indicated.

Table R6. Viral proteins detected in the quantitative proteomic analysis of highly purified virions from *Isg15+/+* and *Isg15-/-* MEF. Comparison of viral proteins present in virions purified from ISG15-/- vs. ISG15+/+ MEF, identified and quantified by LC-ESI-MS/MS. To identify proteins significantly enriched in each sample, a Student's T-test was performed (FDR = 0.05 and S0 =1). Table list: Protein ID (UniProt code) (column A); Protein/ORF name (column B); log2 fold change (FC) (*Isg15-/-* vs. *Isg15+/+*) of the levels of each protein (column D); Statistical significance (−log *p-value*) (column E). Proteins are ordered from most enriched (top) to less enriched (bottom) in *Isg15-/-* samples.

Protein ID	Protein/ORF	Std log2 FC (*Isg15-/-* vs. *Isg15+/+*)	*-log p-value*
Q01227	B5R	2.51	4.79
Q85320	A9L	1.97	5.70
P68712	A21L	1.80	6.00
P07240	H3L	1.63	6.00
Q89121	F10L (VPK2)	1.46	6.00
P07612	L1R	1.42	6.00
P12926	I7L	1.27	6.00
Q76ZP7	A24R (RP132)	1.23	6.00
P07614	F4 (L3)	1.19	6.00
P08583	H2R	1.15	6.00
P04195	D8L (CAHH)	1.10	6.00
P07392	J6R (RP147)	1.08	6.00
P16710	A16L	1.07	6.00
P12927	I8R (NPH2)	1.05	6.00
P68438	H4L (RAP94)	1.02	6.00
P24758	A26L	1.00	6.00
P07618	J5L	1.00	6.00
P24361	F9L	0.97	5.52
P68698	H6R (TOP1)	0.97	2.62
P05807	D11L (NTP1)	0.95	6.00
P21607	E6R	0.95	6.00
P24759	A25 (ATI)	0.91	6.00
P07616	J1R	0.91	6.00
P20636	A7L (VETFL)	0.86	6.00
P16712	A18R	0.86	6.00
P04300	D2L	0.85	6.00

P04298	D1R (MCEL)	0.84	6.00
P04308	D6R (VETFS)	0.80	6.00
P68623	L5R	0.79	3.73
P24765	A40R	0.79	2.40
P04302	D3R	0.79	6.00
P68593	A17L	0.78	2.48
Q80HV7	A12L	0.77	4.96
P06856	E9L (DPOL)	0.74	5.05
P68458	G3L	0.73	2.44
P07611	G9R	0.71	6.00
P06440	A3L (P4B)	0.71	6.00
P07617	J3R (MCE)	0.69	6.00
P23372	E8R	0.66	6.00
P07239	H1L (DUSP)	0.63	6.00
P23371	E1L (PAP1)	0.62	6.00
P04318	D12L (MCES)	0.61	6.00
P68633	A28L	0.57	3.49
P68716	G7L	0.57	6.00
P21603	E4L (RP30)	0.53	5.10
P16713	G1L	0.46	5.40
P68611	A5R (RP19)	0.45	2.60
P04310	D7R (RP18)	0.39	2.90
P16715	A10L (P4A)	0.38	5.52
P11258	A27L	0.37	3.04
P29192	A6L	0.35	2.74
P07242	H5R	0.34	3.20
P03295	L4R (VP8)	0.31	2.70
P68317	G5.5R (RP07)	0.31	2.44
P68638	C3L (VCP)	0.31	2.26
P21605	E3L	0.30	2.30
P04021	F13L	0.27	3.08
P16714	I1L	0.22	2.74
P24761	A34R	-0.51	2.56
P17361	N1L	-0.54	2.66
P68440	D13L	-0.67	2.78
P17357	IL18B	-1.19	2.36
Q80HX7	F11L	-1.42	6.00

DISCUSSION

5. DISCUSSION

5.1. ISG15 is a relevant modulator of the proteome

Controlling the proteome essentially means controlling cell's fate. This explains the great impact that the ISG15/ISGylation system has on cell functions. ISG15 participates in virtually every cellular process, and ISGylated proteins have been detected throughout the cell (Albert et al., 2018). The identification of ISGylated proteins has been and still is an arduous task. Proteomics-based methods sometimes are not sensitive enough to detect ISGylated peptides which, in fact, are indistinguishable from ubiquitylated peptides. Nevertheless, the development of state-of-the-art techniques in protein research has provided an extensive list of ISGylated proteins, significantly contributing to the knowledge of the cell "ISGylome" (Thery, Eggermont, & Impens, 2021; Y. Zhang et al., 2019). Apart from ISGylation, the roles of ISG15 as a free molecule, inside and outside the cell, have substantially broadened the spectrum of action of this protein, opening the door to new and exciting discoveries about the ISG15/ISGylation system.

Most of the work presented here has been focused on the study of ISG15 in macrophages. Macrophages are essential immune cells which have been used in numerous studies to assess the immune functions of ISG15. The strong induction of ISG15 in macrophages in response to type I IFNs, LPS, and viral or bacterial infections, and the suppression of the ISG15-specific protease USP18, helped to illustrate the mechanisms of ISG15-mediated responses, from the identification of ISGylated proteins to the definition of previously unknown host defense processes (J. Dai, Pan, & Wang, 2011; Hamerman et al., 2002; O. Malakhova et al., 2002; Munnur et al., 2021; Ritchie et al., 2004; Zou et al., 2007). Previous work from our group significantly contributed to the elucidation of how ISG15 modulates macrophage functions. Peritoneal macrophages from *Isg15-/-* mice showed impaired activation, reduced phagocytic capacity, and altered induction of apoptosis in response to VACV infection (Yanguez et al., 2013). Furthermore, research from our group showed that ISG15 secreted from tumor-associated macrophages is an essential factor for the progression of pancreatic ductal adenocarcinoma (Sainz, Martin, Tatari, Heeschen, & Guerra, 2014), and that in BMDM, ISG15 participates in the control of exosome secretion (Villarroya-Beltri et al., 2016). These observations evidenced that ISG15 modulates macrophage activity at many different levels. Therefore, we sought to explore which cellular pathways and functions were the most affected by the absence of ISG15 in BMDM. Given that the ISG15/ISGylation system acts at the protein level, we performed a quantitative proteomic analysis with type I IFN-treated *Isg15-/-* and *Isg15+/+* BMDM, which helped us not only to identify the major pathways in which ISG15 has a meaningful impact, but also to pinpoint the most affected proteins of each pathway and to

gauge their degree of variation. Unfortunately, this analysis did not provide any information about ISGylated proteins. It was not surprising that the proteomic analysis reported significant changes in a wide variety of cellular pathways, reinforcing the idea that ISG15 is essential for the correct function of macrophages. However, in our proteomic study, the most significant alterations derived from the absence of ISG15 were reported for one organelle: the mitochondrion.

5.2. ISG15 controls mitochondrial respiration and dynamics

The link between ISG15 and mitochondria was established with the identification of several mitochondrial proteins as direct targets of ISGylation (Giannakopoulos et al., 2005). Later, a proteomic analysis of A549 cells infected with Influenza A virus reported a significant enrichment of ISG15 in mitochondrial extracts (H. Zhao et al., 2013), suggesting a role of ISG15 in the regulation of mitochondria in response to viral infection. Consistent with previous observations, we were able to detect both free ISG15 and ISGylated proteins in mitochondria of BMDM, which were located throughout the mitochondrial structure, albeit enriched in the IMS and the IMM (Figure R2). Two main questions arise from these results. How are mitochondrial proteins ISGylated? And how does ISG15/ISGylation, or its absence, affect mitochondrial functions?

Attending to the first question, the existence of an intramitochondrial ISGylation system is an exciting and not preposterous hypothesis, considering that components of the ubiquitin conjugation machinery, which is highly similar to the ISGylation system, have been identified inside the mitochondrion (Lehmann, Udasin, & Ciechanover, 2016; Lehmann, Ziv, et al., 2016). However, this idea is easily ruled out by the fact that ISGylation occurs in a co-translational manner and none of the 13 proteins encoded by the mitochondrial genome have been identified as ISGylation targets (Thery et al., 2021). That being the case, ISGylation of mitochondrial proteins is likely the result of their conjugation to ISG15 in the cytoplasm and their subsequent translocation into the mitochondrion.

Regarding the second question, it would be difficult to offer a single answer, considering the ample variety of mitochondrial alterations detected in *Isg15-/-* BMDM. Nonetheless, our data reported OXPHOS among the most affected pathways by the absence of ISG15, indicating that mitochondrial respiration is a relevant target of the ISG15/ISGylation system (Figure R1). This hypothesis was supported by the localization of ISG15 and ISGylated proteins predominantly in the IMS and the IMM, where the OXPHOS machinery resides, and a striking increase in the levels of components of all OXPHOS complexes in the absence of ISG15 (Figures R2 and R3, and Table R1). Its central role in cellular metabolism makes OXPHOS a tightly regulated process that requires the coordination of two different gene expression systems (nuclear and mitochondrial),

an orchestrated assembly of numerous proteins, and an excellent protein quality control mechanism (Signes & Fernandez-Vizarra, 2018; Szczepanowska & Trifunovic, 2021). Hence, a dysregulation in the quantity of OXPHOS components is expected to derive in alterations in the ETC structure and function. Our evaluation of the OXPHOS system revealed altered organization and levels of ETC complexes and supercomplexes in *Isg15-/-* BMDM (Figure R3), as well as defects in OCR, ATP production and ROS levels in response to IFN (Figure R4). On one hand, the alterations in the ETC organization do not seem to be the reason of impaired OXPHOS and ROS production, considering that the differences in OXPHOS and ROS levels between genotypes were only detected in IFN-treated cells, whereas changes in the ETC were also observed in untreated cells. However, IFN treatment induced a clear increase in mitochondrial protein levels only in *Isg15-/-* BMDM, indicating that it might be the abundance of ETC components, instead of their organization, the cause of defects in respiration and ROS production. On the other hand, decreased ROS production could be explained by increased association between CI and CIII to form supercomplexes in *Isg15-/-* BMDM, as a result of the accumulation of subunits of these ETC complexes in response to IFN treatment. These complexes are the main source of ROS and their association in supercomplexes has been shown to reduce electron leakage and ROS production (Letts et al., 2016; Scialo et al., 2017). This is a double-edged sword, given that low levels of ROS prevent oxidative stress and damage of cell components, but also reduce the capacity to fight against pathogens.

An interesting observation is that ISGylation has no effect on the ETC structure, as no changes were detected in the organization of the ETC complexes comparing untreated and IFN-treated *Isg15+/+* BMDM. This points to free ISG15 as a regulator of the ETC organization. Intracellular unconjugated ISG15 has been shown to modulate protein activity through non-covalent interactions (Dos Santos & Mansur, 2017), what might contribute to coordinate the assembly of the ETC. Moreover, the fact that changes in the ETC organization are observed independently of IFN treatment indicates that even basal ISG15 levels impact on the ETC structure. It was demonstrated that in BMDM the ETC reorganizes upon bacterial detection and activation of TLR- and NLRP3-mediated signaling, modulating cell metabolism to build and effective immune response (Garaude et al., 2016). Given that PAMP recognition and TLR activation stimulate ISG15 expression (Swaim et al., 2020), our results suggest that ISG15 might participate in the control of the ETC in macrophages during infection.

Although ISGylation seems not to play a relevant role in the regulation of the ETC structure, it might be relevant for its function. Proteins belonging to all five OXPHOS complexes have been

identified as ISGylation targets (Thery et al., 2021). Not only OXPHOS proteins are bound to ISG15, but also a wide variety of mitochondrial proteins, including enzymes of the TCA cycle and FAO, and key proteins such as SLC25 carriers, which mediate the transport of molecules across the IMM (Palmieri, 2013). This broadens the spectrum of mitochondrial functions that could be impaired in the absence of ISG15. Here, we present ISG15 as a modulator of the OXPHOS machinery in BMDM, what has been also confirmed for other cell types. Recent research showed that *Coxsackievirus* infection stimulated OXPHOS in liver tissue from *Isg15+/+* mice, but not in tissue from *Isg15-/-* mice, indicating that ISG15 is necessary for metabolic reprogramming during infection (Kespohl et al., 2020). As well, the absence of ISG15 has been related to dysfunctional OXPHOS in pancreatic cancer stem cells (PaCSCs) (Alcala et al., 2020), reinforcing the role of ISG15 as a regulator of mitochondrial respiratory metabolism.

The mitochondrial dysfunction observed in *Isg15-/-* BMDM, together with the predicted alteration of autophagic processes in these cells (Figure R1), prompted us to examine the status of the mitochondrial network of *Isg15+/+* and *Isg15-/-* BMDM. The maintenance of a functional mitochondrial network is fundamental, given the central role of mitochondria in the control of cell functions, and mitochondrial dynamics and mitophagy are responsible for it. We observed an accumulation of mitochondrial proteins and elongated mitochondria in *Isg15-/-* BMDM (Figure R8), consistent with increased levels of OPA1. Mitochondrial fusion is a mechanism to complement dysfunctional mitochondria and to maximize OXPHOS under stressful conditions (Youle & van der Bliek, 2012). Therefore, increasing mitochondrial fusion could help to counterbalance the impaired OXPHOS of *Isg15-/-* BMDM. Mitochondrial fusion is also determinant for mitophagy because fused mitochondria are not targeted for autophagic degradation (Twig et al., 2008). These findings, together with our observation of decreased levels of several autophagy-related proteins (Table R2), suggested that mitophagy could be altered in the absence of ISG15. To assess the status of mitophagy in our cells, we analyzed the levels of PARKIN, as the PINK1/PARKIN pathway is the main mitophagic process in mammalian cells (Youle & Narendra, 2011), and ISG15 has been shown to modulate the activity of PARKIN (Im et al., 2016). Two interesting discoveries resulted from our analysis. First, PARKIN was not recruited to mitochondria in *Isg15-/-* BMDM and, second, IFN increased the levels of PARKIN only in *Isg15+/+* BMDM (Figure R8). The recruitment of PARKIN to mitochondria is an essential step for PINK1/PARKIN-mediated mitophagy (Narendra, Tanaka, Suen, & Youle, 2008), and it has been shown to be dependent on mitochondrial depolarization and the mitochondrial localization of PINK1 (Geisler et al., 2010). As mentioned earlier, mitochondrial fusion is a rescue mechanism for dysfunctional mitochondria, and it has been proposed to avoid damage-induced mitochondrial

depolarization (Twig et al., 2008; Youle & van der Bliek, 2012), what could explain why PARKIN is not recruited to mitochondria in *Isg15-/-* BMDM. In line with our results, recent research confirmed the importance of ISG15 in the control of mitophagy in other cell types, as ISG15-deficient PaCSCs failed to recruit PARKIN to mitochondria upon mitophagy induction (Alcala et al., 2020). The IFN-induced increase of PARKIN only in *Isg15+/+* cells suggested that type I IFN stimulates mitophagy in an ISG15-dependent manner. This result is consistent with recent observations from Dr. David Sancho's laboratory (CNIC; unpublished results), where they observed a decrease in mitochondrial membrane potential and increased mitochondrial fission in response to type I IFN only in *Isg15+/+* BMDM. Moreover, ISGylation of PARKIN has been shown to sustain its E3 ubiquitin ligase activity (Im et al., 2016), what supports a model of IFN-induced, PINK1/PARKIN-mediated mitophagy via ISG15. Increased mitochondrial fragmentation and mitophagy in response to type I IFN might be a regulatory mechanism to avoid overamplification of IFN signaling. Mitochondrial fusion is required for the formation of the MAVS signalosome, which interacts with RIG-I and enhances NF-κB and IRF signaling, resulting in the production of type I IFN (Castanier, Garcin, Vazquez, & Arnoult, 2010). Thus, defects in mitochondrial fission and turnover because of the absence of ISG15 would cause an exacerbated IFN response. Collectively, we propose that the alterations in the mitochondrial network observed in *Isg15-/-* BMDM are the combination of two phenomena: 1) increased mitochondrial fusion to alleviate IFN-induced mitochondrial dysfunction; and 2) defective mitochondrial fission and mitophagy in response to IFN due to the absence of ISG15.

5.3. ISG15 is necessary for lipid homeostasis

The role of mitochondria as hubs of central metabolism implies that mitochondrial alterations impact on numerous cellular pathways. Further exploring the results of our proteomic analysis, we were intrigued by the fact that FAO was one of the altered pathways in *Isg15-/-* BMDM, suggesting a link between mitochondrial dysfunction and lipid metabolism (Figure R1). ISG15-deficient BMDM showed high levels of FAO enzymes, pointing to increased FAO in these cells. However, FAO was not the only pathway of lipid metabolism affected by the absence of ISG15, as we also observed increased levels of lipid hydrolases, and a reduction in key enzymes of lipid synthesis (Table R3). Surprisingly, the levels of most of these proteins did not correlate with gene expression, even though our analysis of metabolic regulators pointed to the activation of PGC-1α and PPARγ (Figure R9), which link lipid metabolism with mitochondrial biogenesis and activity, and whose activation would explain the alterations observed in *Isg15-/-* BMDM (Coppi et al., 2021;

Qi et al., 2000). Therefore, different mechanisms other than transcriptional regulation may control the levels of these lipid metabolism enzymes.

The proteomic analysis suggested that *Isg15-/-* BMDM suffered a dysregulation in lipid metabolism at different levels, showing a trend towards increased lipid consumption over lipid synthesis. This was confirmed with a lipidomic analysis, which reported alterations in the lipid profile of these cells. Almost all lipid species showed differences between genotypes (Figure R10). However, NLs were the most altered lipids, being strongly reduced in *Isg15-/-* BMDM, consistent with reduced LD number and size and lower levels of PLIN2 and PLIN3 (Figure R11 and Table R3). We focused our study on NLs because they are a major source of FAs under unfavorable energetic conditions, have relevant immune functions, and are involved in diverse metabolic diseases (Welte & Gould, 2017; S. Xu et al., 2018). What is the cause of the decrease in NL content observed in *Isg15-/-* BMDM? Our results pointed to increased lipolysis from LDs. When necessary, NLs are hydrolyzed by the action of cytoplasmic neutral lipases and/or lysosomal acid lipases, generating free FAs and glycerol to be used for different purposes (Grabner, Xie, Schweiger, & Zechner, 2021). Our proteomic analysis reported an increase in both neutral lipases (e.g., NCEH1, MGLL, LDAH) and acid lipases (DAGLB, LIPA) in *Isg15-/-* BMDM (Table R3). Among these, NCEH1 was dramatically increased in the absence of ISG15, so we aimed our attention at this protein.

NCEH1, also known as KIAA1363 or ADAACL1, is a neutral CE hydrolase that resides in the ER and was shown to be determinant in macrophage cholesterol homeostasis (Igarashi et al., 2010; Okazaki et al., 2008). Although its contribution to the total neutral CE hydrolase activity in macrophages has been a matter of debate (Buchebner et al., 2010), several studies have demonstrated its relevance in the control of cholesterol storage, the attenuation of lipid-induced ER stress, and the restriction of atherosclerosis development (Sakai et al., 2014; Sekiya, Osuga, Igarashi, Okazaki, & Ishibashi, 2011; Sekiya et al., 2009; Sekiya et al., 2014; Yamazaki et al., 2019). NCEH1 expression is stimulated by the retinoic acid receptor-related orphan receptor α (RORα) (Matsuoka et al., 2020), a nuclear receptor responsible for the regulation of cholesterol metabolism, whose expression has been shown to correlate with PGC-1α levels (Lucas et al., 2014). This would explain the upregulation of NCEH1 in a scenario of PGC-1α activation, as suggested for *Isg15-/-* BMDM. However, the expression of RORα did not significantly differ between genotypes (data not shown) and neither did NCEH1 expression, suggesting that additional mechanisms are responsible for the elevated NCEH1 levels. The fact that increased NCEH1 levels were detected in *Isg15-/-* BMDM independently of IFN treatment (Figure R10)

indicated that merely the absence of ISG15 affects this protein, although the nature of the interaction between ISG15 and NCEH1 is still to be elucidated. Interestingly, IFN treatment caused a shift in the western blot band pattern of NCEH1, suggesting that this protein is targeted by an IFN-responsive post-translational modification (PTM). Phosphorylation, ubiquitylation and N-glycosylation are the reported PTMs for NCEH1, as indicated in the PhosphoSite database (Hornbeck et al., 2015). Changes in any of these PTMs would explain the molecular weight variations in a 10-kDa range detected for NCEH1. As well, IFN signaling is known to alter the action of these PTMs (Giron et al., 2020; Pilz et al., 2003). Nonetheless, further investigations are needed to unveil the exact mechanisms by which IFN impacts on NCEH1.

Our assessment of FA dynamics, consisting of a pulse-chase analysis with Red C12 (Figure R12), provided useful information about the differences in NLs between genotypes. This approach allowed us to exclude the possibility of reduced NL content due to impaired FAS. FASN, the major FAS enzyme, is a target of ISGylation (Thery et al., 2021) and appeared strongly reduced in *Isg15-/-* BMDM (Table R3), suggesting that ISG15 might regulate its levels and that decreased FASN could be the cause of reduced LD content. However, FAS was bypassed by the addition of exogenous FAs, and the differences in LDs were still detected, indicating that impaired FAS was not the cause of these alterations. The detection of Red C12-containing LDs indicated that the exogenous fluorescent FA was esterified into TAG and CE. Given that the levels of enzymes responsible for FA esterification did not differ between genotypes, defects in FA esterification might not be the reason of decreased NL content. Among the enzymes responsible for FA esterification, to date, only SOAT2 has been reported to be ISGylated (Y. Zhang et al., 2019). Defects in SOAT2 activity due to the absence of ISG15 would explain the reduction in CE levels observed in *Isg15-/-* BMDM. However, not only CEs, but also TAGs were reduced in these cells. Considering the increase in levels of both CE and TAG hydrolases, a reduction in these lipid species due to augmented lipolysis is a more plausible explanation. Nevertheless, further research is needed to elucidate the exact cause of reduced NL content in the absence of ISG15.

Interestingly, red fluorescence in the cytoplasm of *Isg15+/+* BMDM appeared to be dimmer, suggesting that Red C12 was distributed differently between genotypes. The presence of Red C12 in the cytoplasm of *Isg15-/-* BMDM could be explained by redistribution to different organelles, such as the ER or mitochondria (Quinlivan, Wilson, Ruzicka, & Farber, 2017; Rambold et al., 2015). The mitochondrial distribution of FAs for FAO was a highly probable scenario considering our previous results. We reasoned that, in *Isg15-/-* BMDM, energetic stress due to mitochondrial dysfunction could trigger the activation of lipolysis from LDs to fuel mitochondrial

FAO and ATP synthesis (Herzig & Shaw, 2018). In addition, mitochondrial fusion, another feature of *Isg15-/-* BMDM, has been shown to be required for efficient FAO (Rambold et al., 2015), supporting our hypothesis. However, when we measured mitochondrial respiration under etomoxir treatment (that is, under FAO inhibition) neither OCR nor ATP levels were reduced, indicating that neither *Isg15+/+* nor *Isg15-/-* BMDM were oxidizing FAs to produce ATP (Figure R12). These results were unexpected and suggested that, despite the high levels of FAO proteins in the absence of ISG15, the activity of these proteins was not increased. Different studies have identified FAO proteins as targets of ISGylation, including CPT1, which catalyzed the rate-limiting step of the process (S. Yan et al., 2021; Y. Zhang et al., 2019). Although the outcome of the interaction between ISG15 and these proteins is still to be determined, our results suggest that ISG15 is important for the modulation of their activity.

5.4. IFN-induced protein accumulation as the origin of the metabolic alterations observed in the absence of ISG15

It is noticeable that the most substantial differences between genotypes were detected after IFN treatment, pointing to IFN as the cause of the reported metabolic alterations. Type I IFNs have been shown to impact on cell metabolism at different levels. For example, type I IFN stimulation was demonstrated to cause a PPARα-dependent increase in OXPHOS and FAO in both hematopoietic and non-hematopoietic cells (Wu et al., 2016). As well, type I IFNs are also known to activate lipolysis (Doerrler, Feingold, & Grunfeld, 1994; Feingold, Doerrler, Dinarello, Fiers, & Grunfeld, 1992), providing FAs for FAO and for the synthesis of lipid-derived immunomodulators (Hannigan & Williams, 1991). This implies an increase in the levels of proteins involved in these pathways in response to type I IFN. Unfortunately, we lack information about the levels of OXPHOS, FAO and lipolysis proteins (except for NCEH1) in our cells in the absence of IFN treatment, and we cannot confirm an increase of these proteins after IFN treatment. Even so, *Isg15-/-* BMDM showed higher levels of these proteins compared with *Isg15+/+* BMDM, which did not correlate with gene expression and, in the case of OXPHOS proteins, neither did with protein activity. Considering our results, we hypothesize that the metabolic alterations observed in *Isg15-/-* BMDM are the result of defects in the mechanisms of protein turnover, leading to the accumulation of metabolic enzymes induced by IFN treatment.

The role of ISG15 in the modulation of protein turnover is conflicting and still not well understood. Attending to proteasome-mediated protein turnover, ISG15 has been shown to both dampen and stimulate protein degradation through this pathway (Fan et al., 2015; Huang et al., 2014). Of note, it was recently demonstrated that ISG15 conjugation does not induce proteasome-mediated

degradation of ISGylated proteins (Held, Basler, Knobeloch, & Groettrup, 2020). However, ISG15 has been shown to increase protein degradation through autophagy (Desai et al., 2013; Nakashima et al., 2015; Villarroya-Beltri et al., 2016). Our proteomic analysis predicted alterations in autophagy in *Isg15-/-* BMDM, which were reflected by decreased levels of several autophagy mediators (Table R2), what could lead to impaired protein turnover in these cells.

Alterations in proteostasis trigger the unfolded protein response (UPR), a stress response that integrates different signaling pathways with the common aim of restoring protein homeostasis. The UPR is usually associated with accumulation of misfolded proteins in the ER (ER stress), although it is also activated when proteins accumulate into mitochondria, namely, the mitochondrial UPR (mtUPR) (Moehle, Shen, & Dillin, 2019; Ron & Walter, 2007). Furthermore, the UPR/mtUPR can be induced by lipotoxicity due to excess free FAs and cholesterol (Sukhorukov et al., 2020), a probable situation in *Isg15-/-* BMDM due to increased lipolysis. In line with our hypothesis, signaling pathways such as sirtuin signaling, NRF2 oxidative stress response and eIF2 signaling, which are involved in the UPR/mtUPR (Koga et al., 2015; Ron & Walter, 2007; Sarcinelli et al., 2020; Zhu, Luo, Fu, & Chen, 2021), were reported as altered *Isg15-/-* BMDM (Figure R1). As well, these cells showed increased levels of GRP78 (*Zq = +4.32*), a key sensor of ER stress (A. S. Lee, 2005), suggesting the activation of this pathway. Moreover, the IPA Upstream Regulators Analysis predicted the inhibition of the mitochondrial protease CLPP (Figure R9), which plays an essential role in mitochondrial proteostasis and the modulation of the mtUPR (Haynes, Petrova, Benedetti, Yang, & Ron, 2007). Last, the heterogeneous polarization phenotype of *Isg15-/-* BMDM could also point to activated ER stress. *Isg15-/-* BMDM showed increased expression of the cytokines IL-6 and TNFα, which have been shown to be produced by macrophages under ER stress (Y. Li et al., 2005). In addition, an increase in ARG1 expression was observed in macrophages with activated UPR after exposure to exogenous ER-stress factors (Mahadevan et al., 2011). Considering these findings, we cannot rule out the possibility that the origin of the metabolic alterations observed in *Isg15-/-* BMDM are caused by disturbances in cell proteostasis.

5.5. ISG15 in the VACV-host interaction

Macrophage functions are closely linked to their metabolic features, which are reprogrammed by viruses to maximize replication. We wondered how VACV infection impacts on BMDM metabolism, given that a metabolic characterization of VACV-infected BMDM was missing. In addition, given the metabolic dysregulation observed in the absence of ISG15, we explored how the absence of ISG15 affects VACV-BMDM interactions from a metabolic point of view.

The proteomic analysis of infected BMDM showed that mitochondria were the most affected organelles during VACV infection (Figure R5). It is well known that VACV stimulates mitochondrial metabolism during infection. VACV depends on metabolite flux through the TCA cycle to synthesize FAs that subsequently undergo FAO to generate ATP through OXPHOS (Fontaine et al., 2014; Greseth & Traktman, 2014; Pant et al., 2021). This requires the upregulation of OXPHOS genes during infection (A. Dai et al., 2017). Our proteomics data were consistent with these observations, showing increased levels of proteins involved in OXPHOS (Table R1), the TCA cycle (data not shown) and FAO (Table R4) in response to VACV infection. It was demonstrated that VACV uses its viral growth factor (VGF; C11 protein) to stimulate mitochondrial biogenesis and metabolism through EGFR/MAPK and MAPK/ERK signaling pathways (Bonjardim, 2017; Pant et al., 2021). We reported a striking upregulation of PGC-1α expression and a remarkable, yet non-statistically significant upregulation of PPARγ in infected BMDM (Figure R13). PGC-1α is a major regulator of mitochondrial biogenesis, whereas PPARγ is mainly involved in the regulation of lipid metabolism (Hock & Kralli, 2009). Interestingly, PPARγ has been shown to stimulate PGC-1α expression, thus enhancing mitochondrial biogenesis (Hondares et al., 2006). These transcriptional regulators act downstream EGFR/MAPK and MAPK/ERK signaling pathways (Fernandez-Marcos & Auwerx, 2011; Mansure et al., 2013), suggesting that the upregulation of PGC-1α in infected BMDM may be caused by VGF expression. Moreover, the higher PGC-1α expression in *Isg15-/-* BMDM pointed to increased susceptibility of these cells to the effects of VACV on metabolism.

Consistent with increased PGC-1α and PPARγ expression, VACV-infected BMDM showed increased lipid uptake and storage, as indicated by the upregulation of CD36, SOAT1 and PLIN2 (Table R4). This was reflected in the lipidomic analysis of infected BMDM, showing an increase in NL levels. The increase in NL was intensified in *Isg15-/-* BMDM, supporting our idea of higher susceptibility of these cells to the effects of VACV. (Figure R14). Also, several lipases (e.g., NCEH1, LIPA) were increased in response to infection, suggesting that VACV might stimulate lipid uptake and storage followed by lipolysis to generate FAs to fuel FAO. VACV has been shown to use FAS-derived palmitate to sustain FAO and OXPHOS in BSC40 cells (Greseth & Traktman, 2014). However, FAS was not predicted to be increased in infected BMDM, as suggested by unaltered *Fasn* expression and a strong reduction of FASN in response to infection (Figure R13 and Table R4). This suggests that lipid uptake, instead of FAS, might be the main lipid source in VACV-infected BMDM. Macrophages are efficient lipid scavengers, and express many different proteins involved in lipid uptake (Remmerie & Scott, 2018). In addition, it was demonstrated that type I IFN shifts lipid obtention mechanisms towards lipid uptake over *de novo* biosynthesis in

macrophages (York et al., 2015), supporting this hypothesis. In this sense, experiments with IFNAR-deficient BMDM would help to elucidate whether VACV enhances lipid uptake through the modulation of IFN signaling.

Given the favorable situation for increased FAO in infected BMDM, we were surprised to observe a notable reduction in CPT1A levels in these cells (Table R4), even though *Cpt1a* expression was significantly increased in response to infection (Figure R13). CPT1A is the rate-limiting enzyme of FAO, and it is subjected to multi-level regulation (Schlaepfer & Joshi, 2020). Interestingly, CPT1 isoforms A and C have been identified as targets of ISGylation (S. Yan et al., 2021; Y. Zhang et al., 2019), although the effect of ISGylation on this protein remains unknown. A reduction of CPT1A levels during VACV infection would cause a drop in mitochondrial respiration. Accordingly, VACV-infected *Isg15+/+* BMDM showed a significant decrease in OCR and ATP levels compared with uninfected cells. However, VACV did not alter the levels of this parameters in *Isg15-/-* BMDM, which were already reduced to similar levels to those observed in uninfected *Isg15-/-* cells (Figure R4). Considering that altered OXPHOS is uninfected *Isg15-/-* BMDM was independent of etomoxir treatment (Figure R12), these observations suggest that different mechanisms other than alterations in CPT1A might be the cause of decreased OXPHOS. Moreover, the fact that VACV reduced mitochondrial respiration only in IFN-treated *Isg15+/+* BMDM suggests that ISG15 is involved in such alteration.

Intriguingly, VACV-infected *Isg15+/+* BMDM and uninfected *Isg15-/-* BMDM share diverse phenotypic features under IFN treatment. Both present increased levels of mitochondrial proteins and impaired OXPHOS and ROS production (Figure R4 and Table R1), a heterogeneous activation phenotype with high levels of ARG1 and proinflammatory cytokines (Figure R7), and characteristics pointing to altered proteostasis, such as a striking upregulation of GRP78 (*Zq = +19.93* for infected *Isg15+/+* BMDM) and predicted alterations in sirtuin-, eIF2- and NRF2 oxidative stress signaling pathways (Figures R1 and R5). Based on these observations, we hypothesize that decreased ISG15/ISGylation in the context of IFN stimulation might be the cause of these alterations, which seem to be linked to mitochondrial dysfunction. We propose a model in which the absence of ISG15, or reduced ISG15/ISGylation due to VACV infection (Eduardo-Correia et al., 2014; S. Guerra et al., 2008) (Figure R6), dampens the ability of BMDM to modulate the IFN-induced reprogramming of mitochondrial metabolism, leading to mitochondrial dysfunction. This would explain why VACV reduces OXPHOS in *Isg15+/+* BMDM and not in *Isg15-/-* BMDM, and why alterations in proteostasis, likely caused by accumulation of mitochondrial proteins, are predicted for both conditions. Interestingly, IFN-treated *Usp18*$^{C61A/C61A}$

BMDM, which present enhanced ISGylation due to a mutation in the catalytic domain of USP18 (Ketscher et al., 2015), also exhibit increased levels of OXPHOS proteins (data not shown). Although we do not know whether these cells suffer mitochondrial alterations, these observations suggest that, in BMDM, ISG15 levels must be tightly regulated to guarantee mitochondrial functionality in response to type I IFN.

The absence of ISG15 determines the magnitude of the alterations in lipid metabolism caused by VACV. As mentioned earlier, we argue that *Isg15-/-* BMDM are more susceptible to VACV-induced dysregulation of lipid metabolism. In accordance, NL storage in response to VACV infection was higher in these cells (Figure R14). The accumulation of NLs and the activation of LD biogenesis is a common feature during infection by viral and non-viral pathogens (Monson, Trenerry, Laws, Mackenzie, & Helbig, 2021). Though, the effect of LD content on viral infection can be either beneficial or detrimental. On one hand, LD have been shown to favor replication of many viruses. For example, viruses of the *Flaviviridae* family, such as HCV, *Dengue virus* and *Zika virus*, use LDs as scaffolds for viral replication and assembly, as well as an energy reserve (J. Zhang, Lan, & Sanyal, 2017). Similar functions were attributed to LDs during SARS-CoV-2 and *Rotavirus* infection (Criglar, Estes, & Crawford, 2022; Dias et al., 2020). On the other hand, the role of LDs as key modulators of the innate immune response has gained strength. It was recently demonstrated that LD content modulates type I and III IFN signaling, and that cells with reduced LD density showed decreased expression of ISGs and responded inefficiently to viral infection (Monson et al., 2018). As well, Bosch and coworkers (Bosch et al., 2020) showed that LDs exert antimicrobial activity at two levels: 1) direct contact with pathogens, which are eliminated by LD-associated antimicrobial proteins (e.g., viperin); and 2) metabolic reprogramming of infected cells to enhance immune responses.

The relationship between VACV and LDs has not been explored. Our lipidomic analysis suggests that VACV might promote the accumulation of CE-enriched LDs (Figure R14). In this line, the downregulation of *Nr3h1* and *Srebf2* pointed to decreased cholesterol efflux and biosynthesis, respectively, suggesting a scenario of high cholesterol availability (Remmerie & Scott, 2018). Increased cholesterol availability is expected to be beneficial for VACV, as it has been shown that VACV depends on the cholesterol content of membrane lipid rafts to penetrate and egress host cells (Chung et al., 2005; Orynbayeva et al., 2007). This would favor VACV replication in *Isg15-/-* BMDM, as these cells contained higher CE levels; however, VACV titers did not differ between genotypes. VACV titers neither changed after the induction of LD accumulation by OA treatment, suggesting that LD content neither benefits nor impairs VACV replication in BMDM. As well, IFN

treatment decreased viral titers independently of OA treatment, indicating that LD density did not enhance the antiviral effects of IFN in these conditions. The induction of LDs upon viral infection has been shown to follow a similar time course to the expression of IFN (Monson, Crosse, et al., 2021), what suggests that the LD-mediated enhancement of IFN requires the two phenomena to occur simultaneously. In our approach, BMDM were treated with IFN and OA 16 h before infection, perhaps not the best conditions to observe an effect on viral replication. Then, different results might be obtained by treating cells with IFN and OA at the same time or right after infection. The fact that VACV titers do not vary between genotypes does not mean that ISG15 does not exert antiviral activity against VACV. The antiviral activity of ISG15 is well established, although it is not always reflected in a decrease of viral titers *in vitro*, as it has been demonstrated for IBV, HSV-1, *Murine gammaherpesvirus 68*, *Sindbis virus*, and VACV (Lenschow et al., 2007; Yanguez et al., 2013). Nevertheless, ISG15 is determinant for the control of viral and bacterial infections *in vivo* (Ketscher et al., 2015; Lenschow et al., 2007; Radoshevich et al., 2015). In the case of VACV, *Isg15+/+* and *Isg15-/-* mice infected with the WR strain did not show differences in survival (S. Guerra et al., 2008). However, $Usp18^{C61A/C61A}$ mice were more resistant to infection with VACV WR (Ketscher et al., 2015), suggesting that the levels of ISGylation are important for the restriction of VACV infection *in vivo*. Furthermore, macrophages have been shown to serve as vehicles for VACV dissemination, significantly contributing to viral load and viral spread *in vivo* (Byrd et al., 2014), what suggests that alterations in macrophage functions might affect how VACV disseminates throughout the organism.

Lipids are also involved in VACV morphogenesis and dissemination. Several VACV proteins, such as F13 and B5, require FA acylation (e.g., palmitoylation, myristoylation) to exert their functions. These proteins are essential for VACV morphogenesis and spread, and it has been shown that impaired FA acylation blunts these processes (Grosenbach, Hansen, & Hruby, 2000; Grosenbach & Hruby, 1998). As well, several lines of evidence defend that the formation of WVs and EVs may follow an exosome-like pathway, which is highly dependent on the lipidic status of cells (Arumugam & Kaur, 2017). This hypothesis is based on the demonstrated interaction of F13 with the endosomal sorting complex required for transport (ESCRT) protein ALIX (Honeychurch et al., 2007), a key mediator in exosome biogenesis and secretion (Baietti et al., 2012). Moreover, ALIX interacts with TSG101, another ESCRT component, and the absence of either of these proteins impairs EV production (Honeychurch et al., 2007). In view of these observations, we explored whether the absence of ISG15 alters the release and spread of wrapped forms of VACV. As mentioned in the Results section, we used MEF instead of BMDM for this approach, as the latter present several features that make them unsuitable for our study. Despite our lack of a complete

metabolic characterization of *Isg15+/+* and *Isg15-/-* MEF, data from a previous proteomic analysis reported differences in the levels of proteins involved in lipid metabolism and intracellular trafficking in these cells (Table R5), suggesting that these pathways might be altered. In addition, the fact that several of these proteins showed the same trend independently of IFN treatment highlights the relevance of basal ISG15 levels in the control of cellular functions.

Our study revealed that VACV dissemination is impaired in the absence of ISG15. This was indicated by reduced EV release and actin tail formation, a dramatic reduction in comet-shaped plaques, and the accumulation of viral particles in the cytoplasm of *Isg15-/-* MEF (Figures R16-18). The latter was further supported by a quantitative proteomic analysis of virions purified from *Isg15-/-* MEF, which showed an enrichment in viral proteins specific of both unwrapped (e.g., A26) and wrapped (e.g., B5, F13) VACV forms (Table R6). The reduction in comet and actin tail formation was observed infecting with two different VACV strains, indicating that the cause of these alterations is not inherent to the virus. Furthermore, lentivirus-mediated knockdown of *Isg15* in NIH-3T3 cells also abolished comet formation (data not shown), confirming that the absence of ISG15, and not cell type-specific features, is the cause of impaired VACV dissemination.

Isg15-/- MEF present defects in EV release and actin tail formation, two processes that, despite contributing to VACV spread, are dependent on different mechanisms. Increasing evidence supports that EVs are released through an exosome-like pathway. In this line, a recent study has demonstrated that VACV hijacks the ESCRT machinery to package virions into multivesicular bodies that aid virus spread (Huttunen et al., 2021). As mentioned above, this intracellular trafficking process depends on proteins such as ALIX and TSG101 (Honeychurch et al., 2007), directly linking VACV egress with ISG15, since it was demonstrated that the ISGylation of TSG101 promotes its degradation and abrogates the secretion of multivesicular bodies (Villarroya-Beltri et al., 2016). Accordingly, IFN treatment has been demonstrated to abolish comet formation in RK13 cells (Alcami et al., 2000), as well as in *Isg15+/+* MEF (data not shown). Although this mechanism would imply a reduction in EV release in *Isg15+/+* and not in *Isg15-/-* MEF, our proteomic analysis showed that TSG101 was reduced in cells lacking ISG15 independently of IFN treatment (Table R5), what could explain the defects in virus egress. As well, the process of EV release involves an initial step of transport of WV on microtubules to the plasma membrane, which has been shown to be dependent on kinesin and the VACV A36 and F12 proteins (Rietdorf et al., 2001; van Eijl, Hollinshead, Rodger, Zhang, & Smith, 2002). Recent experiments in our laboratory identified A36 as a potential target of ISGylation, suggesting that ISG15 might be relevant for the correct function and/or localization of the protein, resulting in a reduction in EV release when ISG15 is absent.

Several experiments are underway to confirm the ISGylation of A36 and to identify additional ISGylated VACV proteins, what will significantly help in the comprehension of the ISG15-VACV interaction.

Actin tail formation consists of the polymerization of actin filaments beneath CEVs at the cell surface, which project CEVs to neighboring cells (Cudmore et al., 1995). This process has been shown to be initiated by the presence of A36 in the cell membrane after fusion of WVs (Frischknecht et al., 1999). Hence, the suggested defects in the function and/or localization of A36 due to the absence of ISG15 could result in impaired actin tail formation. Moreover, the VACV F11 protein is also relevant for actin tail formation, as it promotes virus spread by interacting with myosin-9A and RhoA GTPase, a key regulator of actin cytoskeleton dynamics (Cordeiro et al., 2009; Handa et al., 2013; Zhou & Zheng, 2013). Interestingly, the levels of F11 were significantly reduced in virions purified from *Isg15-/-* MEF (Table R6), what is expected to result in impaired remodeling of actin cytoskeleton and, consequently, in a defective actin tail formation. Whether ISG15 interacts with F11 is still unknown; however, myosin and actin are targets of ISGylation (Thery et al., 2021). Studies carried out in breast cancer cells have shown that conjugation of ISG15 with actin and myosin promotes cell motility and the progression of cancer (Cruz-Ramos, Macias-Silva, Sandoval-Hernandez, & Tecalco-Cruz, 2019; Desai et al., 2012). In this sense, the absence of ISG15 could result in alterations in the cytoskeleton that impede the formation of actin tails, reducing VACV spread.

5.6. Concluding remarks

The functions of ISG15 are continuously expanding, and growing evidence supports its role as a relevant modulator of cell metabolism. This work has contributed to enlighten how the absence of ISG15 impacts on mitochondrial and lipid metabolism in macrophages in the context of viral infections. Our results open the door to new advances in the comprehension of macrophage immunometabolism and the interaction between VACV and the host. Our next steps are directed towards the elucidation of the molecular mechanisms that underlie the metabolic alterations observed in the absence of ISG15, what will help to better understand the complex and multifunctional ISG15/ISGylation system.

CONCLUSIONS

CONCLUSIONES

6a. CONCLUSIONS

1. The absence of ISG15 alters the macrophage proteome, significantly impacting on mitochondrial functions.
2. ISG15 and ISGylated proteins are found in mitochondria, and mainly localize in the intermembrane space and the inner mitochondria membrane.
3. ISG15 controls the levels and organization of ETC components, and its absence results in impaired OXPHOS and ROS production.
4. VACV reduces ISG15 levels and causes mitochondrial alterations similar to those observed in the absence of ISG15.
5. The absence of ISG15 leads to the accumulation of mitochondrial proteins and defective mitophagy, in line with impaired recruitment of PARKIN to mitochondria.
6. Both the absence of ISG15 and VACV infection induce macrophage polarization towards a mixed M1/M2 phenotype, in line with increased ARG1 levels and activity, and increased production of proinflammatory cyokines.
7. The absence of ISG15 alters the macrophage lipid profile, causing a reduction in neutral lipids (TAG, DAG, CE), consistent with reduced lipid droplet number and size, and increased levels of lipases.
8. VACV infection alters the macrophage lipid profile, enhancing lipid uptake and storage, and increasing the levels of TAG and CE. These alterations are intensified in *Isg15-/-* BMDM.
9. The absence of ISG15 negatively impacts on VACV dissemination, reducing comet and actin tail formation, causing accumulation of intracellular virus particles, and decreasing EV release.
10. The absence of ISG15 alters the VACV virion proteome, as a result of an impaired virus morphogenetic program.

6b. CONCLUSIONES

1. La ausencia de ISG15 altera el proteoma del macrófago, impactando significativamente en las funciones mitocondriales.
2. Las mitocondrias contienen ISG15 y proteínas ISGiladas, localizadas principalmente en el espacio intermembrana y la membrana mitocondrial interna.
3. ISG15 controla los niveles y la organización de los componentes de la cadena de transporte electrónico mitocondrial, y su ausencia causa defectos en la fosforilación oxidativa y la producción de especies reactivas de oxígeno.
4. VACV disminuye los niveles de ISG15 y causa alteraciones mitocondriales similares a las observadas en ausencia de ISG15.
5. La ausencia de ISG15 provoca acumulación de proteínas mitocondriales y defectos en la mitofagia, de acuerdo con un defecto en el reclutamiento de PARKIN a las mitocondrias.
6. Tanto la ausencia de ISG15 como la infección por VACV inducen la polarización de macrófagos hacia un fenotipo mixto M1/M2, de acuerdo con un aumento en los niveles y la actividad de la enzima arginasa-1, así como un aumento de la producción de citoquinas proinflamatorias.
7. La ausencia de ISG15 altera el perfil lipídico del macrófago, causando una reducción en los niveles de lípidos neutros (triacilgliceroles, diacilgliceroles y ésteres de colesterol), de acuerdo con una disminución en el número de *lipid droplets* y un aumento de lipasas.
8. La infección por VACV altera el perfil lipídico del macrófago, aumentando la captación y almacenamiento de lípidos, y causando un aumento en los niveles de triacilgliceroles y ésteres de colesterol. Estas alteraciones son más intensas en macrófagos *Isg15-/-*.
9. La ausencia de ISG15 tiene un impacto negativo en la diseminación de VACV, causando una reducción en la formación de cometas y colas de actina, provocando la acumulación de partículas virales intracelulares, y disminuyendo la liberación de virus extracelular.
10. La ausencia de ISG15 altera el proteoma del virión de VACV, como resultado de un defecto en el proceso morfogenético del virus.

REFERENCES

REFERENCES

Adeva-Andany, M. M., Carneiro-Freire, N., Seco-Filgueira, M., Fernandez-Fernandez, C., & Mourino-Bayolo, D. (2019). Mitochondrial beta-oxidation of saturated fatty acids in humans. *Mitochondrion, 46*, 73-90. doi:10.1016/j.mito.2018.02.009

Al Ghouleh, I., Khoo, N. K., Knaus, U. G., Griendling, K. K., Touyz, R. M., Thannickal, V. J., . . . Pagano, P. J. (2011). Oxidases and peroxidases in cardiovascular and lung disease: new concepts in reactive oxygen species signaling. *Free Radic Biol Med, 51*(7), 1271-1288. doi:10.1016/j.freeradbiomed.2011.06.011

Albert, M., Becares, M., Falqui, M., Fernandez-Lozano, C., & Guerra, S. (2018). ISG15, a Small Molecule with Huge Implications: Regulation of Mitochondrial Homeostasis. *Viruses, 10*(11). doi:10.3390/v10110629

Alcala, S., Sancho, P., Martinelli, P., Navarro, D., Pedrero, C., Martin-Hijano, L., . . . Sainz, B., Jr. (2020). ISG15 and ISGylation is required for pancreatic cancer stem cell mitophagy and metabolic plasticity. *Nat Commun, 11*(1), 2682. doi:10.1038/s41467-020-16395-2

Alcami, A., Symons, J. A., & Smith, G. L. (2000). The vaccinia virus soluble alpha/beta interferon (IFN) receptor binds to the cell surface and protects cells from the antiviral effects of IFN. *J Virol, 74*(23), 11230-11239. doi:10.1128/jvi.74.23.11230-11239.2000

Arumugam, S., & Kaur, A. (2017). The Lipids of the Early Endosomes: Making Multimodality Work. *Chembiochem, 18*(12), 1053-1060. doi:10.1002/cbic.201700046

Assarsson, E., Greenbaum, J. A., Sundstrom, M., Schaffer, L., Hammond, J. A., Pasquetto, V., . . . Sette, A. (2008). Kinetic analysis of a complete poxvirus transcriptome reveals an immediate-early class of genes. *Proc Natl Acad Sci U S A, 105*(6), 2140-2145. doi:10.1073/pnas.0711573105

Bahar, M. W., Graham, S. C., Chen, R. A., Cooray, S., Smith, G. L., Stuart, D. I., & Grimes, J. M. (2011). How vaccinia virus has evolved to subvert the host immune response. *J Struct Biol, 175*(2), 127-134. doi:10.1016/j.jsb.2011.03.010

Baietti, M. F., Zhang, Z., Mortier, E., Melchior, A., Degeest, G., Geeraerts, A., . . . David, G. (2012). Syndecan-syntenin-ALIX regulates the biogenesis of exosomes. *Nat Cell Biol, 14*(7), 677-685. doi:10.1038/ncb2502

Baldanta, S., Fernandez-Escobar, M., Acin-Perez, R., Albert, M., Camafeita, E., Jorge, I., . . . Guerra, S. (2017). ISG15 governs mitochondrial function in macrophages following vaccinia virus infection. *PLoS Pathog, 13*(10), e1006651. doi:10.1371/journal.ppat.1006651

Balsinde, J., Winstead, M. V., & Dennis, E. A. (2002). Phospholipase A(2) regulation of arachidonic acid mobilization. *FEBS Lett, 531*(1), 2-6. doi:10.1016/s0014-5793(02)03413-0

Bersuker, K., & Olzmann, J. A. (2017). Establishing the lipid droplet proteome: Mechanisms of lipid droplet protein targeting and degradation. *Biochim Biophys Acta Mol Cell Biol Lipids, 1862*(10 Pt B), 1166-1177. doi:10.1016/j.bbalip.2017.06.006

Bhushan, J., Radke, J. B., Perng, Y. C., McAllaster, M., Lenschow, D. J., Virgin, H. W., & Sibley, L. D. (2020). ISG15 Connects Autophagy and IFN-gamma-Dependent Control of Toxoplasma gondii Infection in Human Cells. *mBio, 11*(5). doi:10.1128/mBio.00852-20

Bidgood, S. R., & Mercer, J. (2015). Cloak and Dagger: Alternative Immune Evasion and Modulation Strategies of Poxviruses. *Viruses, 7*(8), 4800-4825. doi:10.3390/v7082844

Blanc, M., Hsieh, W. Y., Robertson, K. A., Kropp, K. A., Forster, T., Shui, G., . . . Ghazal, P. (2013). The transcription factor STAT-1 couples macrophage synthesis of 25-hydroxycholesterol to the interferon antiviral response. *Immunity, 38*(1), 106-118. doi:10.1016/j.immuni.2012.11.004

Blasco, R., Sisler, J. R., & Moss, B. (1993). Dissociation of progeny vaccinia virus from the cell membrane is regulated by a viral envelope glycoprotein: effect of a point mutation in the lectin homology domain of the A34R gene. *J Virol, 67*(6), 3319-3325. doi:10.1128/JVI.67.6.3319-3325.1993

Bogunovic, D., Byun, M., Durfee, L. A., Abhyankar, A., Sanal, O., Mansouri, D., . . . Casanova, J. L. (2012). Mycobacterial disease and impaired IFN-gamma immunity in humans with inherited ISG15 deficiency. *Science, 337*(6102), 1684-1688. doi:10.1126/science.1224026

Bonjardim, C. A. (2017). Viral exploitation of the MEK/ERK pathway - A tale of vaccinia virus and other viruses. *Virology, 507*, 267-275. doi:10.1016/j.virol.2016.12.011

Bonzon-Kulichenko, E., Garcia-Marques, F., Trevisan-Herraz, M., & Vazquez, J. (2015). Revisiting peptide identification by high-accuracy mass spectrometry: problems associated with the use of narrow mass precursor windows. *J Proteome Res, 14*(2), 700-710. doi:10.1021/pr5007284

Bosch, M., & Pol, A. (2022). Eukaryotic lipid droplets: metabolic hubs, and immune first responders. *Trends Endocrinol Metab*. doi:10.1016/j.tem.2021.12.006

Bosch, M., Sanchez-Alvarez, M., Fajardo, A., Kapetanovic, R., Steiner, B., Dutra, F., . . . Pol, A. (2020). Mammalian lipid droplets are innate immune hubs integrating cell metabolism and host defense. *Science, 370*(6514). doi:10.1126/science.aay8085

Boudewijns, R., Perez, P., Lazaro-Frias, A., Van Looveren, D., Vercruysse, T., Thibaut, H. J., . . . Garcia-Arriaza, J. (2022). MVA-CoV2-S Vaccine Candidate Neutralizes Distinct Variants of Concern and Protects Against SARS-CoV-2 Infection in Hamsters. *Front Immunol, 13*, 845969. doi:10.3389/fimmu.2022.845969

Broering, R., Zhang, X., Kottilil, S., Trippler, M., Jiang, M., Lu, M., . . . Schlaak, J. F. (2010). The interferon stimulated gene 15 functions as a proviral factor for the hepatitis C virus and as a regulator of the IFN response. *Gut, 59*(8), 1111-1119. doi:10.1136/gut.2009.195545

Broyles, S. S. (2003). Vaccinia virus transcription. *J Gen Virol, 84*(Pt 9), 2293-2303. doi:10.1099/vir.0.18942-0

Brubaker, S. W., Bonham, K. S., Zanoni, I., & Kagan, J. C. (2015). Innate immune pattern recognition: a cell biological perspective. *Annu Rev Immunol, 33*, 257-290. doi:10.1146/annurev-immunol-032414-112240

Bryan, N. S., & Grisham, M. B. (2007). Methods to detect nitric oxide and its metabolites in biological samples. *Free Radic Biol Med, 43*(5), 645-657. doi:10.1016/j.freeradbiomed.2007.04.026

Buchebner, M., Pfeifer, T., Rathke, N., Chandak, P. G., Lass, A., Schreiber, R., . . . Kratky, D. (2010). Cholesteryl ester hydrolase activity is abolished in HSL-/- macrophages but unchanged in macrophages lacking KIAA1363. *J Lipid Res, 51*(10), 2896-2908. doi:10.1194/jlr.M004259

Buhman, K. K., Chen, H. C., & Farese, R. V., Jr. (2001). The enzymes of neutral lipid synthesis. *J Biol Chem, 276*(44), 40369-40372. doi:10.1074/jbc.R100050200

Byrd, D., Shepherd, N., Lan, J., Hu, N., Amet, T., Yang, K., . . . Yu, Q. (2014). Primary human macrophages serve as vehicles for vaccinia virus replication and dissemination. *J Virol, 88*(12), 6819-6831. doi:10.1128/JVI.03726-13

Cai, B., Bai, Q., Chi, X., Goraya, M. U., Wang, L., Wang, S., . . . Chen, J. L. (2017). Infection with Classical Swine Fever Virus Induces Expression of Type III Interferons and Activates Innate Immune Signaling. *Front Microbiol, 8*, 2558. doi:10.3389/fmicb.2017.02558

Calvano, S. E., Xiao, W., Richards, D. R., Felciano, R. M., Baker, H. V., Cho, R. J., . . . Host Response to Injury Large Scale Collab. Res, P. (2005). A network-based analysis of systemic inflammation in humans. *Nature, 437*(7061), 1032-1037. doi:10.1038/nature03985

Carter, G. C., Law, M., Hollinshead, M., & Smith, G. L. (2005). Entry of the vaccinia virus intracellular mature virion and its interactions with glycosaminoglycans. *J Gen Virol, 86*(Pt 5), 1279-1290. doi:10.1099/vir.0.80831-0

Carter, G. C., Rodger, G., Murphy, B. J., Law, M., Krauss, O., Hollinshead, M., & Smith, G. L. (2003). Vaccinia virus cores are transported on microtubules. *J Gen Virol, 84*(Pt 9), 2443-2458. doi:10.1099/vir.0.19271-0

Cassetta, L., Cassol, E., & Poli, G. (2011). Macrophage polarization in health and disease. *ScientificWorldJournal, 11*, 2391-2402. doi:10.1100/2011/213962

Castanier, C., Garcin, D., Vazquez, A., & Arnoult, D. (2010). Mitochondrial dynamics regulate the RIG-I-like receptor antiviral pathway. *EMBO Rep, 11*(2), 133-138. doi:10.1038/embor.2009.258

Chan, D. C. (2020). Mitochondrial Dynamics and Its Involvement in Disease. *Annu Rev Pathol, 15*, 235-259. doi:10.1146/annurev-pathmechdis-012419-032711

Chang, H. W., Watson, J. C., & Jacobs, B. L. (1992). The E3L gene of vaccinia virus encodes an inhibitor of the interferon-induced, double-stranded RNA-dependent protein kinase. *Proc Natl Acad Sci U S A, 89*(11), 4825-4829. doi:10.1073/pnas.89.11.4825

Checa, A., Bedia, C., & Jaumot, J. (2015). Lipidomic data analysis: tutorial, practical guidelines and applications. *Anal Chim Acta, 885*, 1-16. doi:10.1016/j.aca.2015.02.068

Chouchani, E. T., Pell, V. R., Gaude, E., Aksentijevic, D., Sundier, S. Y., Robb, E. L., . . . Murphy, M. P. (2014). Ischaemic accumulation of succinate controls reperfusion injury through mitochondrial ROS. *Nature, 515*(7527), 431-435. doi:10.1038/nature13909

Christofides, A., Konstantinidou, E., Jani, C., & Boussiotis, V. A. (2021). The role of peroxisome proliferator-activated receptors (PPAR) in immune responses. *Metabolism, 114*, 154338. doi:10.1016/j.metabol.2020.154338

Chua, P. K., McCown, M. F., Rajyaguru, S., Kular, S., Varma, R., Symons, J., . . . Najera, I. (2009). Modulation of alpha interferon anti-hepatitis C virus activity by ISG15. *J Gen Virol, 90*(Pt 12), 2929-2939. doi:10.1099/vir.0.013128-0

Chung, C. S., Huang, C. Y., & Chang, W. (2005). Vaccinia virus penetration requires cholesterol and results in specific viral envelope proteins associated with lipid rafts. *J Virol, 79*(3), 1623-1634. doi:10.1128/JVI.79.3.1623-1634.2005

Cockcroft, S. (2021). Mammalian lipids: structure, synthesis and function. *Essays Biochem, 65*(5), 813-845. doi:10.1042/EBC20200067

Codrea, M. C., & Nahnsen, S. (2016). Platforms and Pipelines for Proteomics Data Analysis and Management. *Adv Exp Med Biol, 919*, 203-215. doi:10.1007/978-3-319-41448-5_9

Coppi, L., Ligorio, S., Mitro, N., Caruso, D., De Fabiani, E., & Crestani, M. (2021). PGC1s and Beyond: Disentangling the Complex Regulation of Mitochondrial and Cellular Metabolism. *Int J Mol Sci, 22*(13). doi:10.3390/ijms22136913

Cordeiro, J. V., Guerra, S., Arakawa, Y., Dodding, M. P., Esteban, M., & Way, M. (2009). F11-mediated inhibition of RhoA signalling enhances the spread of vaccinia virus in vitro and in vivo in an intranasal mouse model of infection. *PLoS One, 4*(12), e8506. doi:10.1371/journal.pone.0008506

Criglar, J. M., Estes, M. K., & Crawford, S. E. (2022). Rotavirus-Induced Lipid Droplet Biogenesis Is Critical for Virus Replication. *Front Physiol, 13*, 836870. doi:10.3389/fphys.2022.836870

Cruz-Ramos, E., Macias-Silva, M., Sandoval-Hernandez, A., & Tecalco-Cruz, A. C. (2019). Non-muscle myosin IIA is post-translationally modified by interferon-stimulated gene 15 in breast cancer cells. *Int J Biochem Cell Biol, 107*, 14-26. doi:10.1016/j.biocel.2018.12.002

Cudmore, S., Cossart, P., Griffiths, G., & Way, M. (1995). Actin-based motility of vaccinia virus. *Nature, 378*(6557), 636-638. doi:10.1038/378636a0

D'Cunha, J., Knight, E., Jr., Haas, A. L., Truitt, R. L., & Borden, E. C. (1996). Immunoregulatory properties of ISG15, an interferon-induced cytokine. *Proc Natl Acad Sci U S A, 93*(1), 211-215. doi:10.1073/pnas.93.1.211

Dai, A., Cao, S., Dhungel, P., Luan, Y., Liu, Y., Xie, Z., & Yang, Z. (2017). Ribosome Profiling Reveals Translational Upregulation of Cellular Oxidative Phosphorylation mRNAs during Vaccinia Virus-Induced Host Shutoff. *J Virol, 91*(5). doi:10.1128/JVI.01858-16

Dai, J., Pan, W., & Wang, P. (2011). ISG15 facilitates cellular antiviral response to dengue and west nile virus infection in vitro. *Virol J, 8*, 468. doi:10.1186/1743-422X-8-468

Dan Dunn, J., Alvarez, L. A., Zhang, X., & Soldati, T. (2015). Reactive oxygen species and mitochondria: A nexus of cellular homeostasis. *Redox Biol, 6*, 472-485. doi:10.1016/j.redox.2015.09.005

Dang, E. V., Madhani, H. D., & Vance, R. E. (2020). Cholesterol in quarantine. *Nat Immunol, 21*(7), 716-717. doi:10.1038/s41590-020-0712-7

Darnell, J. E., Jr., Kerr, I. M., & Stark, G. R. (1994). Jak-STAT pathways and transcriptional activation in response to IFNs and other extracellular signaling proteins. *Science, 264*(5164), 1415-1421. doi:10.1126/science.8197455

de Souza Trindade, G., Li, Y., Olson, V. A., Emerson, G., Regnery, R. L., da Fonseca, F. G., . . . Damon, I. (2008). Real-time PCR assay to identify variants of Vaccinia virus: implications for the diagnosis of bovine vaccinia in Brazil. *J Virol Methods, 152*(1-2), 63-71. doi:10.1016/j.jviromet.2008.05.028

Der, S. D., Zhou, A., Williams, B. R., & Silverman, R. H. (1998). Identification of genes differentially regulated by interferon alpha, beta, or gamma using oligonucleotide arrays. *Proc Natl Acad Sci U S A, 95*(26), 15623-15628. doi:10.1073/pnas.95.26.15623

Desai, S. D., Reed, R. E., Babu, S., & Lorio, E. A. (2013). ISG15 deregulates autophagy in genotoxin-treated ataxia telangiectasia cells. *J Biol Chem, 288*(4), 2388-2402. doi:10.1074/jbc.M112.403832

Desai, S. D., Reed, R. E., Burks, J., Wood, L. M., Pullikuth, A. K., Haas, A. L., . . . Sankar, S. (2012). ISG15 disrupts cytoskeletal architecture and promotes motility in human breast cancer cells. *Exp Biol Med (Maywood), 237*(1), 38-49. doi:10.1258/ebm.2011.011236

Dias, S. S. G., Soares, V. C., Ferreira, A. C., Sacramento, C. Q., Fintelman-Rodrigues, N., Temerozo, J. R., . . . Bozza, P. T. (2020). Lipid droplets fuel SARS-CoV-2 replication and production of inflammatory mediators. *PLoS Pathog, 16*(12), e1009127. doi:10.1371/journal.ppat.1009127

Dinkova-Kostova, A. T., & Abramov, A. Y. (2015). The emerging role of Nrf2 in mitochondrial function. *Free Radic Biol Med, 88*(Pt B), 179-188. doi:10.1016/j.freeradbiomed.2015.04.036

Divakaruni, A. S., Paradyse, A., Ferrick, D. A., Murphy, A. N., & Jastroch, M. (2014). Analysis and interpretation of microplate-based oxygen consumption and pH data. *Methods Enzymol, 547*, 309-354. doi:10.1016/B978-0-12-801415-8.00016-3

Doceul, V., Hollinshead, M., Breiman, A., Laval, K., & Smith, G. L. (2012). Protein B5 is required on extracellular enveloped vaccinia virus for repulsion of superinfecting virions. *J Gen Virol, 93*(Pt 9), 1876-1886. doi:10.1099/vir.0.043943-0

Doceul, V., Hollinshead, M., van der Linden, L., & Smith, G. L. (2010). Repulsion of superinfecting virions: a mechanism for rapid virus spread. *Science, 327*(5967), 873-876. doi:10.1126/science.1183173

Doerrler, W., Feingold, K. R., & Grunfeld, C. (1994). Cytokines induce catabolic effects in cultured adipocytes by multiple mechanisms. *Cytokine, 6*(5), 478-484. doi:10.1016/1043-4666(94)90074-4

Dos Santos, P. F., & Mansur, D. S. (2017). Beyond ISGlylation: Functions of Free Intracellular and Extracellular ISG15. *J Interferon Cytokine Res, 37*(6), 246-253. doi:10.1089/jir.2016.0103

Durfee, L. A., & Huibregtse, J. M. (2012). The ISG15 conjugation system. *Methods Mol Biol, 832*, 141-149. doi:10.1007/978-1-61779-474-2_9

Durfee, L. A., Lyon, N., Seo, K., & Huibregtse, J. M. (2010). The ISG15 conjugation system broadly targets newly synthesized proteins: implications for the antiviral function of ISG15. *Mol Cell, 38*(5), 722-732. doi:10.1016/j.molcel.2010.05.002

Dzimianski, J. V., Scholte, F. E. M., Bergeron, E., & Pegan, S. D. (2019). ISG15: It's Complicated. *J Mol Biol, 431*(21), 4203-4216. doi:10.1016/j.jmb.2019.03.013

Eduardo-Correia, B., Martinez-Romero, C., Garcia-Sastre, A., & Guerra, S. (2014). ISG15 is counteracted by vaccinia virus E3 protein and controls the proinflammatory response against viral infection. *J Virol, 88*(4), 2312-2318. doi:10.1128/JVI.03293-13

Eichmann, T. O., & Lass, A. (2015). DAG tales: the multiple faces of diacylglycerol--stereochemistry, metabolism, and signaling. *Cell Mol Life Sci, 72*(20), 3931-3952. doi:10.1007/s00018-015-1982-3

Eiyama, A., & Okamoto, K. (2015). PINK1/Parkin-mediated mitophagy in mammalian cells. *Curr Opin Cell Biol, 33*, 95-101. doi:10.1016/j.ceb.2015.01.002

Epelman, S., Lavine, K. J., & Randolph, G. J. (2014). Origin and functions of tissue macrophages. *Immunity, 41*(1), 21-35. doi:10.1016/j.immuni.2014.06.013

Falvey, C. M., O'Donovan, T. R., El-Mashed, S., Nyhan, M. J., O'Reilly, S., & McKenna, S. L. (2017). UBE2L6/UBCH8 and ISG15 attenuate autophagy in esophageal cancer cells. *Oncotarget, 8*(14), 23479-23491. doi:10.18632/oncotarget.15182

Fan, J. B., Arimoto, K., Motamedchaboki, K., Yan, M., Wolf, D. A., & Zhang, D. E. (2015). Identification and characterization of a novel ISG15-ubiquitin mixed chain and its role in regulating protein homeostasis. *Sci Rep, 5*, 12704. doi:10.1038/srep12704

Feingold, K. R., Doerrler, W., Dinarello, C. A., Fiers, W., & Grunfeld, C. (1992). Stimulation of lipolysis in cultured fat cells by tumor necrosis factor, interleukin-1, and the interferons is blocked by inhibition of prostaglandin synthesis. *Endocrinology, 130*(1), 10-16. doi:10.1210/endo.130.1.1370149

Fernandez-Marcos, P. J., & Auwerx, J. (2011). Regulation of PGC-1alpha, a nodal regulator of mitochondrial biogenesis. *Am J Clin Nutr, 93*(4), 884S-890. doi:10.3945/ajcn.110.001917

Ficenec, D., Osborne, M., Pradines, J., Richards, D., Felciano, R., Cho, R. J., . . . Clark, T. (2003). Computational knowledge integration in biopharmaceutical research. *Brief Bioinform, 4*(3), 260-278. doi:10.1093/bib/4.3.260

Filipe, A., & McLauchlan, J. (2015). Hepatitis C virus and lipid droplets: finding a niche. *Trends Mol Med, 21*(1), 34-42. doi:10.1016/j.molmed.2014.11.003

Fontaine, K. A., Camarda, R., & Lagunoff, M. (2014). Vaccinia virus requires glutamine but not glucose for efficient replication. *J Virol, 88*(8), 4366-4374. doi:10.1128/JVI.03134-13

Foster, D. W. (2012). Malonyl-CoA: the regulator of fatty acid synthesis and oxidation. *J Clin Invest, 122*(6), 1958-1959. doi:10.1172/jci63967

Foy, E., Li, K., Sumpter, R., Jr., Loo, Y. M., Johnson, C. L., Wang, C., . . . Gale, M., Jr. (2005). Control of antiviral defenses through hepatitis C virus disruption of retinoic acid-inducible gene-I signaling. *Proc Natl Acad Sci U S A, 102*(8), 2986-2991. doi:10.1073/pnas.0408707102

Frias-Staheli, N., Giannakopoulos, N. V., Kikkert, M., Taylor, S. L., Bridgen, A., Paragas, J., . . . Virgin, H. W. t. (2007). Ovarian tumor domain-containing viral proteases evade ubiquitin- and ISG15-dependent innate immune responses. *Cell Host Microbe, 2*(6), 404-416. doi:10.1016/j.chom.2007.09.014

Friedman, J. R., & Nunnari, J. (2014). Mitochondrial form and function. *Nature, 505*(7483), 335-343. doi:10.1038/nature12985

Frischknecht, F., Moreau, V., Rottger, S., Gonfloni, S., Reckmann, I., Superti-Furga, G., & Way, M. (1999). Actin-based motility of vaccinia virus mimics receptor tyrosine kinase signalling. *Nature, 401*(6756), 926-929. doi:10.1038/44860

Gadina, M., Chisolm, D. A., Philips, R. L., McInness, I. B., Changelian, P. S., & O'Shea, J. J. (2020). Translating JAKs to Jakinibs. *J Immunol, 204*(8), 2011-2020. doi:10.4049/jimmunol.1901477

Ganesan, M., Poluektova, L. Y., Tuma, D. J., Kharbanda, K. K., & Osna, N. A. (2016). Acetaldehyde Disrupts Interferon Alpha Signaling in Hepatitis C Virus-Infected Liver Cells by Up-Regulating USP18. *Alcohol Clin Exp Res, 40*(11), 2329-2338. doi:10.1111/acer.13226

Garaude, J., Acin-Perez, R., Martinez-Cano, S., Enamorado, M., Ugolini, M., Nistal-Villan, E., . . . Sancho, D. (2016). Mitochondrial respiratory-chain adaptations in macrophages contribute to antibacterial host defense. *Nat Immunol, 17*(9), 1037-1045. doi:10.1038/ni.3509

Garcia-Marques, F., Trevisan-Herraz, M., Martinez-Martinez, S., Camafeita, E., Jorge, I., Lopez, J. A., . . . Vazquez, J. (2016). A Novel Systems-Biology Algorithm for the Analysis of Coordinated Protein

Responses Using Quantitative Proteomics. *Mol Cell Proteomics, 15*(5), 1740-1760. doi:10.1074/mcp.M115.055905

Gearing, K. L., Gottlicher, M., Teboul, M., Widmark, E., & Gustafsson, J. A. (1993). Interaction of the peroxisome-proliferator-activated receptor and retinoid X receptor. *Proc Natl Acad Sci U S A, 90*(4), 1440-1444. doi:10.1073/pnas.90.4.1440

Geijtenbeek, T. B., & Gringhuis, S. I. (2009). Signalling through C-type lectin receptors: shaping immune responses. *Nat Rev Immunol, 9*(7), 465-479. doi:10.1038/nri2569

Geisler, S., Holmstrom, K. M., Skujat, D., Fiesel, F. C., Rothfuss, O. C., Kahle, P. J., & Springer, W. (2010). PINK1/Parkin-mediated mitophagy is dependent on VDAC1 and p62/SQSTM1. *Nat Cell Biol, 12*(2), 119-131. doi:10.1038/ncb2012

Ghosh, S. (2012). Early steps in reverse cholesterol transport: cholesteryl ester hydrolase and other hydrolases. *Curr Opin Endocrinol Diabetes Obes, 19*(2), 136-141. doi:10.1097/MED.0b013e3283507836

Giannakopoulos, N. V., Luo, J. K., Papov, V., Zou, W., Lenschow, D. J., Jacobs, B. S., . . . Zhang, D. E. (2005). Proteomic identification of proteins conjugated to ISG15 in mouse and human cells. *Biochem Biophys Res Commun, 336*(2), 496-506. doi:10.1016/j.bbrc.2005.08.132

Giron, L. B., Colomb, F., Papasavvas, E., Azzoni, L., Yin, X., Fair, M., . . . Abdel-Mohsen, M. (2020). Interferon-alpha alters host glycosylation machinery during treated HIV infection. *EBioMedicine, 59*, 102945. doi:10.1016/j.ebiom.2020.102945

Gonzalez-Amor, M., Garcia-Redondo, A. B., Jorge, I., Zalba, G., Becares, M., Ruiz-Rodriguez, M. J., . . . Briones, A. M. (2021). Interferon stimulated gene 15 pathway is a novel mediator of endothelial dysfunction and aneurysms development in angiotensin II infused mice through increased oxidative stress. *Cardiovasc Res*. doi:10.1093/cvr/cvab321

Gordon, S., & Taylor, P. R. (2005). Monocyte and macrophage heterogeneity. *Nat Rev Immunol, 5*(12), 953-964. doi:10.1038/nri1733

Grabner, G. F., Xie, H., Schweiger, M., & Zechner, R. (2021). Lipolysis: cellular mechanisms for lipid mobilization from fat stores. *Nat Metab, 3*(11), 1445-1465. doi:10.1038/s42255-021-00493-6

Greseth, M. D., & Traktman, P. (2014). De novo fatty acid biosynthesis contributes significantly to establishment of a bioenergetically favorable environment for vaccinia virus infection. *PLoS Pathog, 10*(3), e1004021. doi:10.1371/journal.ppat.1004021

Grosenbach, D. W., Hansen, S. G., & Hruby, D. E. (2000). Identification and analysis of vaccinia virus palmitylproteins. *Virology, 275*(1), 193-206. doi:10.1006/viro.2000.0522

Grosenbach, D. W., & Hruby, D. E. (1998). Biology of vaccinia virus acylproteins. *Front Biosci, 3*, d354-364. doi:10.2741/a280

Grosenbach, D. W., Ulaeto, D. O., & Hruby, D. E. (1997). Palmitylation of the vaccinia virus 37-kDa major envelope antigen. Identification of a conserved acceptor motif and biological relevance. *J Biol Chem, 272*(3), 1956-1964. doi:10.1074/jbc.272.3.1956

Gross, R. W., & Han, X. (2009). Shotgun lipidomics of neutral lipids as an enabling technology for elucidation of lipid-related diseases. *Am J Physiol Endocrinol Metab, 297*(2), E297-303. doi:10.1152/ajpendo.90970.2008

Guerra, B., Recio, C., Aranda-Tavio, H., Guerra-Rodriguez, M., Garcia-Castellano, J. M., & Fernandez-Perez, L. (2021). The Mevalonate Pathway, a Metabolic Target in Cancer Therapy. *Front Oncol, 11*, 626971. doi:10.3389/fonc.2021.626971

Guerra, S., Caceres, A., Knobeloch, K. P., Horak, I., & Esteban, M. (2008). Vaccinia virus E3 protein prevents the antiviral action of ISG15. *PLoS Pathog, 4*(7), e1000096. doi:10.1371/journal.ppat.1000096

Haan, C., Kreis, S., Margue, C., & Behrmann, I. (2006). Jaks and cytokine receptors--an intimate relationship. *Biochem Pharmacol, 72*(11), 1538-1546. doi:10.1016/j.bcp.2006.04.013

Hamerman, J. A., Hayashi, F., Schroeder, L. A., Gygi, S. P., Haas, A. L., Hampson, L., . . . Aderem, A. (2002). Serpin 2a is induced in activated macrophages and conjugates to a ubiquitin homolog. *J Immunol, 168*(5), 2415-2423. doi:10.4049/jimmunol.168.5.2415

Han, H. G., Moon, H. W., & Jeon, Y. J. (2018). ISG15 in cancer: Beyond ubiquitin-like protein. *Cancer Lett, 438*, 52-62. doi:10.1016/j.canlet.2018.09.007

Handa, Y., Durkin, C. H., Dodding, M. P., & Way, M. (2013). Vaccinia virus F11 promotes viral spread by acting as a PDZ-containing scaffolding protein to bind myosin-9A and inhibit RhoA signaling. *Cell Host Microbe, 14*(1), 51-62. doi:10.1016/j.chom.2013.06.006

Hannigan, G. E., & Williams, B. R. (1991). Signal transduction by interferon-alpha through arachidonic acid metabolism. *Science, 251*(4990), 204-207. doi:10.1126/science.1898993

Hare, N. J., Chan, B., Chan, E., Kaufman, K. L., Britton, W. J., & Saunders, B. M. (2015). Microparticles released from Mycobacterium tuberculosis-infected human macrophages contain increased levels of the type I interferon inducible proteins including ISG15. *Proteomics, 15*(17), 3020-3029. doi:10.1002/pmic.201400610

Haynes, C. M., Petrova, K., Benedetti, C., Yang, Y., & Ron, D. (2007). ClpP mediates activation of a mitochondrial unfolded protein response in C. elegans. *Dev Cell, 13*(4), 467-480. doi:10.1016/j.devcel.2007.07.016

Held, T., Basler, M., Knobeloch, K. P., & Groettrup, M. (2020). Evidence for an involvement of the ubiquitin-like modifier ISG15 in MHC class I antigen presentation. *Eur J Immunol*. doi:10.1002/eji.202048646

Henle, W. (1950). Interference phenomena between animal viruses; a review. *J Immunol, 64*(3), 203-236.

Hernaez, B., Alonso-Lobo, J. M., Montanuy, I., Fischer, C., Sauer, S., Sigal, L., . . . Alcami, A. (2018). A virus-encoded type I interferon decoy receptor enables evasion of host immunity through cell-surface binding. *Nat Commun, 9*(1), 5440. doi:10.1038/s41467-018-07772-z

Herzig, S., & Shaw, R. J. (2018). AMPK: guardian of metabolism and mitochondrial homeostasis. *Nat Rev Mol Cell Biol, 19*(2), 121-135. doi:10.1038/nrm.2017.95

Hock, M. B., & Kralli, A. (2009). Transcriptional control of mitochondrial biogenesis and function. *Annu Rev Physiol, 71*, 177-203. doi:10.1146/annurev.physiol.010908.163119

Hondares, E., Mora, O., Yubero, P., Rodriguez de la Concepcion, M., Iglesias, R., Giralt, M., & Villarroya, F. (2006). Thiazolidinediones and rexinoids induce peroxisome proliferator-activated receptor-coactivator (PGC)-1alpha gene transcription: an autoregulatory loop controls PGC-1alpha expression in adipocytes via peroxisome proliferator-activated receptor-gamma coactivation. *Endocrinology, 147*(6), 2829-2838. doi:10.1210/en.2006-0070

Honeychurch, K. M., Yang, G., Jordan, R., & Hruby, D. E. (2007). The vaccinia virus F13L YPPL motif is required for efficient release of extracellular enveloped virus. *J Virol, 81*(13), 7310-7315. doi:10.1128/JVI.00034-07

Honke, N., Shaabani, N., Zhang, D. E., Hardt, C., & Lang, K. S. (2016). Multiple functions of USP18. *Cell Death Dis, 7*(11), e2444. doi:10.1038/cddis.2016.326

Hornbeck, P. V., Zhang, B., Murray, B., Kornhauser, J. M., Latham, V., & Skrzypek, E. (2015). PhosphoSitePlus, 2014: mutations, PTMs and recalibrations. *Nucleic Acids Res, 43*(Database issue), D512-520. doi:10.1093/nar/gku1267

Houten, S. M., Violante, S., Ventura, F. V., & Wanders, R. J. (2016). The Biochemistry and Physiology of Mitochondrial Fatty Acid beta-Oxidation and Its Genetic Disorders. *Annu Rev Physiol, 78*, 23-44. doi:10.1146/annurev-physiol-021115-105045

Huang da, W., Sherman, B. T., Zheng, X., Yang, J., Imamichi, T., Stephens, R., & Lempicki, R. A. (2009). Extracting biological meaning from large gene lists with DAVID. *Curr Protoc Bioinformatics, Chapter 13*, Unit 13 11. doi:10.1002/0471250953.bi1311s27

Huang, Y. F., Wee, S., Gunaratne, J., Lane, D. P., & Bulavin, D. V. (2014). Isg15 controls p53 stability and functions. *Cell Cycle, 13*(14), 2200-2210. doi:10.4161/cc.29209

Huttunen, M., Samolej, J., Evans, R. J., Yakimovich, A., White, I. J., Kriston-Vizi, J., . . . Mercer, J. (2021). Vaccinia virus hijacks ESCRT-mediated multivesicular body formation for virus egress. *Life Sci Alliance, 4*(8). doi:10.26508/lsa.202000910

Icard, P., Lincet, H., Wu, Z., Coquerel, A., Forgez, P., Alifano, M., & Fournel, L. (2021). The key role of Warburg effect in SARS-CoV-2 replication and associated inflammatory response. *Biochimie, 180*, 169-177. doi:10.1016/j.biochi.2020.11.010

Igarashi, M., Osuga, J., Isshiki, M., Sekiya, M., Okazaki, H., Takase, S., . . . Ishibashi, S. (2010). Targeting of neutral cholesterol ester hydrolase to the endoplasmic reticulum via its N-terminal sequence. *J Lipid Res, 51*(2), 274-285. doi:10.1194/jlr.M900201-JLR200

Im, E., Yoo, L., Hyun, M., Shin, W. H., & Chung, K. C. (2016). Covalent ISG15 conjugation positively regulates the ubiquitin E3 ligase activity of parkin. *Open Biol, 6*(8). doi:10.1098/rsob.160193

Incardona, J. P., & Eaton, S. (2000). Cholesterol in signal transduction. *Curr Opin Cell Biol, 12*(2), 193-203. doi:10.1016/s0955-0674(99)00076-9

Infantino, V., Iacobazzi, V., Palmieri, F., & Menga, A. (2013). ATP-citrate lyase is essential for macrophage inflammatory response. *Biochem Biophys Res Commun, 440*(1), 105-111. doi:10.1016/j.bbrc.2013.09.037

Isaacs, A., & Lindenmann, J. (1957). Virus interference. I. The interferon. *Proc R Soc Lond B Biol Sci, 147*(927), 258-267. doi:10.1098/rspb.1957.0048

Isaacs, A., Lindenmann, J., & Valentine, R. C. (1957). Virus interference. II. Some properties of interferon. *Proc R Soc Lond B Biol Sci, 147*(927), 268-273. doi:10.1098/rspb.1957.0049

Jarc, E., & Petan, T. (2020). A twist of FATe: Lipid droplets and inflammatory lipid mediators. *Biochimie, 169*, 69-87. doi:10.1016/j.biochi.2019.11.016

Jeon, Y. J., Choi, J. S., Lee, J. Y., Yu, K. R., Kim, S. M., Ka, S. H., . . . Chung, C. H. (2009). ISG15 modification of filamin B negatively regulates the type I interferon-induced JNK signalling pathway. *EMBO Rep, 10*(4), 374-380. doi:10.1038/embor.2009.23

Jeon, Y. J., Park, J. H., & Chung, C. H. (2017). Interferon-Stimulated Gene 15 in the Control of Cellular Responses to Genotoxic Stress. *Mol Cells, 40*(2), 83-89. doi:10.14348/molcells.2017.0027

Jin, S. M., & Youle, R. J. (2012). PINK1- and Parkin-mediated mitophagy at a glance. *J Cell Sci, 125*(Pt 4), 795-799. doi:10.1242/jcs.093849

Jones, A. E., & Divakaruni, A. S. (2020). Macrophage activation as an archetype of mitochondrial repurposing. *Mol Aspects Med, 71*, 100838. doi:10.1016/j.mam.2019.100838

Kang, Z., & Fan, R. (2020). PPARalpha and NCOR/SMRT corepressor network in liver metabolic regulation. *FASEB J, 34*(7), 8796-8809. doi:10.1096/fj.202000055RR

Kawai, T., Takahashi, K., Sato, S., Coban, C., Kumar, H., Kato, H., . . . Akira, S. (2005). IPS-1, an adaptor triggering RIG-I- and Mda5-mediated type I interferon induction. *Nat Immunol, 6*(10), 981-988. doi:10.1038/ni1243

Kawasaki, T., & Kawai, T. (2014). Toll-like receptor signaling pathways. *Front Immunol, 5*, 461. doi:10.3389/fimmu.2014.00461

Kerr, J. S., Adriaanse, B. A., Greig, N. H., Mattson, M. P., Cader, M. Z., Bohr, V. A., & Fang, E. F. (2017). Mitophagy and Alzheimer's Disease: Cellular and Molecular Mechanisms. *Trends Neurosci, 40*(3), 151-166. doi:10.1016/j.tins.2017.01.002

Kespohl, M., Bredow, C., Klingel, K., Voss, M., Paeschke, A., Zickler, M., . . . Beling, A. (2020). Protein modification with ISG15 blocks coxsackievirus pathology by antiviral and metabolic reprogramming. *Sci Adv, 6*(11), eaay1109. doi:10.1126/sciadv.aay1109

Ketscher, L., Hannss, R., Morales, D. J., Basters, A., Guerra, S., Goldmann, T., . . . Knobeloch, K. P. (2015). Selective inactivation of USP18 isopeptidase activity in vivo enhances ISG15 conjugation and viral resistance. *Proc Natl Acad Sci U S A, 112*(5), 1577-1582. doi:10.1073/pnas.1412881112

Kim, J. W., Tchernyshyov, I., Semenza, G. L., & Dang, C. V. (2006). HIF-1-mediated expression of pyruvate dehydrogenase kinase: a metabolic switch required for cellular adaptation to hypoxia. *Cell Metab, 3*(3), 177-185. doi:10.1016/j.cmet.2006.02.002

Kim, K. I., Giannakopoulos, N. V., Virgin, H. W., & Zhang, D. E. (2004). Interferon-inducible ubiquitin E2, Ubc8, is a conjugating enzyme for protein ISGylation. *Mol Cell Biol, 24*(21), 9592-9600. doi:10.1128/MCB.24.21.9592-9600.2004

Kim, M. J., Hwang, S. Y., Imaizumi, T., & Yoo, J. Y. (2008). Negative feedback regulation of RIG-I-mediated antiviral signaling by interferon-induced ISG15 conjugation. *J Virol, 82*(3), 1474-1483. doi:10.1128/JVI.01650-07

Kim, Y. J., Kim, E. T., Kim, Y. E., Lee, M. K., Kwon, K. M., Kim, K. I., . . . Ahn, J. H. (2016). Consecutive Inhibition of ISG15 Expression and ISGylation by Cytomegalovirus Regulators. *PLoS Pathog, 12*(8), e1005850. doi:10.1371/journal.ppat.1005850

Kimmel, A. R., & Sztalryd, C. (2016). The Perilipins: Major Cytosolic Lipid Droplet-Associated Proteins and Their Roles in Cellular Lipid Storage, Mobilization, and Systemic Homeostasis. *Annu Rev Nutr, 36*, 471-509. doi:10.1146/annurev-nutr-071813-105410

Kisseleva, T., Bhattacharya, S., Braunstein, J., & Schindler, C. W. (2002). Signaling through the JAK/STAT pathway, recent advances and future challenges. *Gene, 285*(1-2), 1-24. doi:10.1016/s0378-1119(02)00398-0

Koga, T., Suico, M. A., Shimasaki, S., Watanabe, E., Kai, Y., Koyama, K., . . . Kai, H. (2015). Endoplasmic Reticulum (ER) Stress Induces Sirtuin 1 (SIRT1) Expression via the PI3K-Akt-GSK3beta Signaling Pathway and Promotes Hepatocellular Injury. *J Biol Chem, 290*(51), 30366-30374. doi:10.1074/jbc.M115.664169

Korber, M., Klein, I., & Daum, G. (2017). Steryl ester synthesis, storage and hydrolysis: A contribution to sterol homeostasis. *Biochim Biophys Acta Mol Cell Biol Lipids, 1862*(12), 1534-1545. doi:10.1016/j.bbalip.2017.09.002

Kotenko, S. V., Gallagher, G., Baurin, V. V., Lewis-Antes, A., Shen, M., Shah, N. K., . . . Donnelly, R. P. (2003). IFN-lambdas mediate antiviral protection through a distinct class II cytokine receptor complex. *Nat Immunol, 4*(1), 69-77. doi:10.1038/ni875

Krijnse Locker, J., Chlanda, P., Sachsenheimer, T., & Brugger, B. (2013). Poxvirus membrane biogenesis: rupture not disruption. *Cell Microbiol, 15*(2), 190-199. doi:10.1111/cmi.12072

Kumar, H., Kawai, T., & Akira, S. (2011). Pathogen recognition by the innate immune system. *Int Rev Immunol, 30*(1), 16-34. doi:10.3109/08830185.2010.529976

Kusnadi, A., Park, S. H., Yuan, R., Pannellini, T., Giannopoulou, E., Oliver, D., . . . Ivashkiv, L. B. (2019). The Cytokine TNF Promotes Transcription Factor SREBP Activity and Binding to Inflammatory Genes to Activate Macrophages and Limit Tissue Repair. *Immunity, 51*(2), 241-257 e249. doi:10.1016/j.immuni.2019.06.005

Langland, J. O., & Jacobs, B. L. (2002). The role of the PKR-inhibitory genes, E3L and K3L, in determining vaccinia virus host range. *Virology, 299*(1), 133-141. doi:10.1006/viro.2002.1479

Larsen, S., Nielsen, J., Hansen, C. N., Nielsen, L. B., Wibrand, F., Stride, N., . . . Hey-Mogensen, M. (2012). Biomarkers of mitochondrial content in skeletal muscle of healthy young human subjects. *J Physiol, 590*(14), 3349-3360. doi:10.1113/jphysiol.2012.230185

Law, M., & Smith, G. L. (2001). Antibody neutralization of the extracellular enveloped form of vaccinia virus. *Virology, 280*(1), 132-142. doi:10.1006/viro.2000.0750

Leduc-Gaudet, J. P., Hussain, S. N. A., Barreiro, E., & Gouspillou, G. (2021). Mitochondrial Dynamics and Mitophagy in Skeletal Muscle Health and Aging. *Int J Mol Sci, 22*(15). doi:10.3390/ijms22158179

Lee, A. J., & Ashkar, A. A. (2018). The Dual Nature of Type I and Type II Interferons. *Front Immunol, 9*, 2061. doi:10.3389/fimmu.2018.02061

Lee, A. S. (2005). The ER chaperone and signaling regulator GRP78/BiP as a monitor of endoplasmic reticulum stress. *Methods, 35*(4), 373-381. doi:10.1016/j.ymeth.2004.10.010

Lee, H., & Yoon, Y. (2016). Mitochondrial fission and fusion. *Biochem Soc Trans, 44*(6), 1725-1735. doi:10.1042/BST20160129

Lee, J. H., Bae, J. A., Lee, J. H., Seo, Y. W., Kho, D. H., Sun, E. G., . . . Kim, K. K. (2010). Glycoprotein 90K, downregulated in advanced colorectal cancer tissues, interacts with CD9/CD82 and suppresses the Wnt/beta-catenin signal via ISGylation of beta-catenin. *Gut, 59*(7), 907-917. doi:10.1136/gut.2009.194068

Lefkowitz, E. J., Wang, C., & Upton, C. (2006). Poxviruses: past, present and future. *Virus Res, 117*(1), 105-118. doi:10.1016/j.virusres.2006.01.016

Lehmann, G., Udasin, R. G., & Ciechanover, A. (2016). On the linkage between the ubiquitin-proteasome system and the mitochondria. *Biochem Biophys Res Commun, 473*(1), 80-86. doi:10.1016/j.bbrc.2016.03.055

Lehmann, G., Ziv, T., Braten, O., Admon, A., Udasin, R. G., & Ciechanover, A. (2016). Ubiquitination of specific mitochondrial matrix proteins. *Biochem Biophys Res Commun, 475*(1), 13-18. doi:10.1016/j.bbrc.2016.04.150

Lengyel, P. (1982). Biochemistry of interferons and their actions. *Annu Rev Biochem, 51*, 251-282. doi:10.1146/annurev.bi.51.070182.001343

Lenschow, D. J., Lai, C., Frias-Staheli, N., Giannakopoulos, N. V., Lutz, A., Wolff, T., . . . Virgin, H. W. t. (2007). IFN-stimulated gene 15 functions as a critical antiviral molecule against influenza, herpes, and Sindbis viruses. *Proc Natl Acad Sci U S A, 104*(4), 1371-1376. doi:10.1073/pnas.0607038104

Letts, J. A., Fiedorczuk, K., & Sazanov, L. A. (2016). The architecture of respiratory supercomplexes. *Nature, 537*(7622), 644-648. doi:10.1038/nature19774

Levine, B., & Kroemer, G. (2019). Biological Functions of Autophagy Genes: A Disease Perspective. *Cell, 176*(1-2), 11-42. doi:10.1016/j.cell.2018.09.048

Levy, D. E., & Darnell, J. E., Jr. (2002). Stats: transcriptional control and biological impact. *Nat Rev Mol Cell Biol, 3*(9), 651-662. doi:10.1038/nrm909

Li, S. F., Gong, M. J., Zhao, F. R., Shao, J. J., Xie, Y. L., Zhang, Y. G., & Chang, H. Y. (2018). Type I Interferons: Distinct Biological Activities and Current Applications for Viral Infection. *Cell Physiol Biochem, 51*(5), 2377-2396. doi:10.1159/000495897

Li, Y., Li, S., Duan, X., Chen, Y., Jiao, B., Ye, H., . . . Chen, L. (2016). Interferon-Stimulated Gene 15 Conjugation Stimulates Hepatitis B Virus Production Independent of Type I Interferon Signaling Pathway In Vitro. *Mediators Inflamm, 2016*, 7417648. doi:10.1155/2016/7417648

Li, Y., Schwabe, R. F., DeVries-Seimon, T., Yao, P. M., Gerbod-Giannone, M. C., Tall, A. R., . . . Tabas, I. (2005). Free cholesterol-loaded macrophages are an abundant source of tumor necrosis factor-alpha and interleukin-6: model of NF-kappaB- and map kinase-dependent inflammation in advanced atherosclerosis. *J Biol Chem, 280*(23), 21763-21772. doi:10.1074/jbc.M501759200

Liesa, M., & Shirihai, O. S. (2013). Mitochondrial dynamics in the regulation of nutrient utilization and energy expenditure. *Cell Metab, 17*(4), 491-506. doi:10.1016/j.cmet.2013.03.002

Listenberger, L. L., Han, X., Lewis, S. E., Cases, S., Farese, R. V., Jr., Ory, D. S., & Schaffer, J. E. (2003). Triglyceride accumulation protects against fatty acid-induced lipotoxicity. *Proc Natl Acad Sci U S A, 100*(6), 3077-3082. doi:10.1073/pnas.0630588100

Liu, P. S., & Ho, P. C. (2018). Mitochondria: A master regulator in macrophage and T cell immunity. *Mitochondrion, 41*, 45-50. doi:10.1016/j.mito.2017.11.002

Liu, S. Y., Aliyari, R., Chikere, K., Li, G., Marsden, M. D., Smith, J. K., . . . Cheng, G. (2013). Interferon-inducible cholesterol-25-hydroxylase broadly inhibits viral entry by production of 25-hydroxycholesterol. *Immunity, 38*(1), 92-105. doi:10.1016/j.immuni.2012.11.005

Lombard, D. B., Tishkoff, D. X., & Bao, J. (2011). Mitochondrial sirtuins in the regulation of mitochondrial activity and metabolic adaptation. *Handb Exp Pharmacol, 206*, 163-188. doi:10.1007/978-3-642-21631-2_8

Lorenzo, M. M., Sanchez-Puig, J. M., & Blasco, R. (2012). Mutagenesis of the palmitoylation site in vaccinia virus envelope glycoprotein B5. *J Gen Virol, 93*(Pt 4), 733-743. doi:10.1099/vir.0.039016-0

Loson, O. C., Song, Z., Chen, H., & Chan, D. C. (2013). Fis1, Mff, MiD49, and MiD51 mediate Drp1 recruitment in mitochondrial fission. *Mol Biol Cell, 24*(5), 659-667. doi:10.1091/mbc.E12-10-0721

Lou, Z., Wei, J., Riethman, H., Baur, J. A., Voglauer, R., Shay, J. W., & Wright, W. E. (2009). Telomere length regulates ISG15 expression in human cells. *Aging (Albany NY), 1*(7), 608-621. doi:10.18632/aging.100066

Lucas, E. K., Dougherty, S. E., McMeekin, L. J., Reid, C. S., Dobrunz, L. E., West, A. B., . . . Cowell, R. M. (2014). PGC-1alpha provides a transcriptional framework for synchronous neurotransmitter release from parvalbumin-positive interneurons. *J Neurosci, 34*(43), 14375-14387. doi:10.1523/JNEUROSCI.1222-14.2014

Luo, C., Widlund, H. R., & Puigserver, P. (2016). PGC-1 Coactivators: Shepherding the Mitochondrial Biogenesis of Tumors. *Trends Cancer, 2*(10), 619-631. doi:10.1016/j.trecan.2016.09.006

Luo, J., Yang, H., & Song, B. L. (2020). Mechanisms and regulation of cholesterol homeostasis. *Nat Rev Mol Cell Biol, 21*(4), 225-245. doi:10.1038/s41580-019-0190-7

Mahadevan, N. R., Rodvold, J., Sepulveda, H., Rossi, S., Drew, A. F., & Zanetti, M. (2011). Transmission of endoplasmic reticulum stress and pro-inflammation from tumor cells to myeloid cells. *Proc Natl Acad Sci U S A, 108*(16), 6561-6566. doi:10.1073/pnas.1008942108

Malakhov, M. P., Malakhova, O. A., Kim, K. I., Ritchie, K. J., & Zhang, D. E. (2002). UBP43 (USP18) specifically removes ISG15 from conjugated proteins. *J Biol Chem, 277*(12), 9976-9981. doi:10.1074/jbc.M109078200

Malakhova, O., Malakhov, M., Hetherington, C., & Zhang, D. E. (2002). Lipopolysaccharide activates the expression of ISG15-specific protease UBP43 via interferon regulatory factor 3. *J Biol Chem, 277*(17), 14703-14711. doi:10.1074/jbc.M111527200

Malakhova, O. A., Kim, K. I., Luo, J. K., Zou, W., Kumar, K. G., Fuchs, S. Y., . . . Zhang, D. E. (2006). UBP43 is a novel regulator of interferon signaling independent of its ISG15 isopeptidase activity. *EMBO J, 25*(11), 2358-2367. doi:10.1038/sj.emboj.7601149

Malik, A. N., Czajka, A., & Cunningham, P. (2016). Accurate quantification of mouse mitochondrial DNA without co-amplification of nuclear mitochondrial insertion sequences. *Mitochondrion, 29*, 59-64. doi:10.1016/j.mito.2016.05.003

Malpartida, A. B., Williamson, M., Narendra, D. P., Wade-Martins, R., & Ryan, B. J. (2021). Mitochondrial Dysfunction and Mitophagy in Parkinson's Disease: From Mechanism to Therapy. *Trends Biochem Sci, 46*(4), 329-343. doi:10.1016/j.tibs.2020.11.007

Mann, B. A., Huang, J. H., Li, P., Chang, H. C., Slee, R. B., O'Sullivan, A., . . . Kaplan, M. H. (2008). Vaccinia virus blocks Stat1-dependent and Stat1-independent gene expression induced by type I and type II interferons. *J Interferon Cytokine Res, 28*(6), 367-380. doi:10.1089/jir.2007.0113

Mansure, J. J., Nassim, R., Chevalier, S., Szymanski, K., Rocha, J., Aldousari, S., & Kassouf, W. (2013). A novel mechanism of PPAR gamma induction via EGFR signalling constitutes rational for combination therapy in bladder cancer. *PLoS One, 8*(2), e55997. doi:10.1371/journal.pone.0055997

Martinez-Arranz, I., Mayo, R., Perez-Cormenzana, M., Minchole, I., Salazar, L., Alonso, C., & Mato, J. M. (2015). Enhancing metabolomics research through data mining. *J Proteomics, 127*(Pt B), 275-288. doi:10.1016/j.jprot.2015.01.019

Martinez-Bartolome, S., Navarro, P., Martin-Maroto, F., Lopez-Ferrer, D., Ramos-Fernandez, A., Villar, M., . . . Vazquez, J. (2008). Properties of average score distributions of SEQUEST: the probability ratio method. *Mol Cell Proteomics, 7*(6), 1135-1145. doi:10.1074/mcp.M700239-MCP200

Martinez-Reyes, I., & Chandel, N. S. (2020). Mitochondrial TCA cycle metabolites control physiology and disease. *Nat Commun, 11*(1), 102. doi:10.1038/s41467-019-13668-3

Matsuoka, H., Tokunaga, R., Katayama, M., Hosoda, Y., Miya, K., Sumi, K., . . . Michihara, A. (2020). Retinoic acid receptor-related orphan receptor alpha reduces lipid droplets by upregulating neutral cholesterol ester hydrolase 1 in macrophages. *BMC Mol Cell Biol, 21*(1), 32. doi:10.1186/s12860-020-00276-z

Mazewski, C., Perez, R. E., Fish, E. N., & Platanias, L. C. (2020). Type I Interferon (IFN)-Regulated Activation of Canonical and Non-Canonical Signaling Pathways. *Front Immunol, 11*, 606456. doi:10.3389/fimmu.2020.606456

Mazzon, M., Peters, N. E., Loenarz, C., Krysztofinska, E. M., Ember, S. W., Ferguson, B. J., & Smith, G. L. (2013). A mechanism for induction of a hypoxic response by vaccinia virus. *Proc Natl Acad Sci U S A, 110*(30), 12444-12449. doi:10.1073/pnas.1302140110

McCarthy, M. (2014). Smallpox samples are found in FDA storage room in Maryland. *BMJ, 349*, g4545. doi:10.1136/bmj.g4545

McIntosh, A. A., & Smith, G. L. (1996). Vaccinia virus glycoprotein A34R is required for infectivity of extracellular enveloped virus. *J Virol, 70*(1), 272-281. doi:10.1128/JVI.70.1.272-281.1996

McNab, F., Mayer-Barber, K., Sher, A., Wack, A., & O'Garra, A. (2015). Type I interferons in infectious disease. *Nat Rev Immunol, 15*(2), 87-103. doi:10.1038/nri3787

Meade, N., Furey, C., Li, H., Verma, R., Chai, Q., Rollins, M. G., . . . Walsh, D. (2018). Poxviruses Evade Cytosolic Sensing through Disruption of an mTORC1-mTORC2 Regulatory Circuit. *Cell, 174*(5), 1143-1157 e1117. doi:10.1016/j.cell.2018.06.053

Meeusen, S., DeVay, R., Block, J., Cassidy-Stone, A., Wayson, S., McCaffery, J. M., & Nunnari, J. (2006). Mitochondrial inner-membrane fusion and crista maintenance requires the dynamin-related GTPase Mgm1. *Cell, 127*(2), 383-395. doi:10.1016/j.cell.2006.09.021

Meiser, A., Sancho, C., & Krijnse Locker, J. (2003). Plasma membrane budding as an alternative release mechanism of the extracellular enveloped form of vaccinia virus from HeLa cells. *J Virol, 77*(18), 9931-9942. doi:10.1128/jvi.77.18.9931-9942.2003

Mercer, J., & Helenius, A. (2008). Vaccinia virus uses macropinocytosis and apoptotic mimicry to enter host cells. *Science, 320*(5875), 531-535. doi:10.1126/science.1155164

Meyer, H., Ehmann, R., & Smith, G. L. (2020). Smallpox in the Post-Eradication Era. *Viruses, 12*(2). doi:10.3390/v12020138

Moehle, E. A., Shen, K., & Dillin, A. (2019). Mitochondrial proteostasis in the context of cellular and organismal health and aging. *J Biol Chem, 294*(14), 5396-5407. doi:10.1074/jbc.TM117.000893

Monson, E. A., Crosse, K. M., Das, M., & Helbig, K. J. (2018). Lipid droplet density alters the early innate immune response to viral infection. *PLoS One, 13*(1), e0190597. doi:10.1371/journal.pone.0190597

Monson, E. A., Crosse, K. M., Duan, M., Chen, W., O'Shea, R. D., Wakim, L. M., . . . Helbig, K. J. (2021). Intracellular lipid droplet accumulation occurs early following viral infection and is required for an efficient interferon response. *Nat Commun, 12*(1), 4303. doi:10.1038/s41467-021-24632-5

Monson, E. A., Trenerry, A. M., Laws, J. L., Mackenzie, J. M., & Helbig, K. J. (2021). Lipid droplets and lipid mediators in viral infection and immunity. *FEMS Microbiol Rev, 45*(4). doi:10.1093/femsre/fuaa066

Moon, J. S., Nakahira, K., Chung, K. P., DeNicola, G. M., Koo, M. J., Pabon, M. A., . . . Choi, A. M. (2016). NOX4-dependent fatty acid oxidation promotes NLRP3 inflammasome activation in macrophages. *Nat Med, 22*(9), 1002-1012. doi:10.1038/nm.4153

Morales, D. J., & Lenschow, D. J. (2013). The antiviral activities of ISG15. *J Mol Biol, 425*(24), 4995-5008. doi:10.1016/j.jmb.2013.09.041

Morris, R., Kershaw, N. J., & Babon, J. J. (2018). The molecular details of cytokine signaling via the JAK/STAT pathway. *Protein Sci, 27*(12), 1984-2009. doi:10.1002/pro.3519

Moss, B. (2013). Poxvirus DNA replication. *Cold Spring Harb Perspect Biol, 5*(9). doi:10.1101/cshperspect.a010199

Moss, B. (2015). Poxvirus membrane biogenesis. *Virology, 479-480*, 619-626. doi:10.1016/j.virol.2015.02.003

Munnur, D., Teo, Q., Eggermont, D., Lee, H. H. Y., Thery, F., Ho, J., . . . Sanyal, S. (2021). Altered ISGylation drives aberrant macrophage-dependent immune responses during SARS-CoV-2 infection. *Nat Immunol, 22*(11), 1416-1427. doi:10.1038/s41590-021-01035-8

Murray, P. J., & Wynn, T. A. (2011). Protective and pathogenic functions of macrophage subsets. *Nat Rev Immunol, 11*(11), 723-737. doi:10.1038/nri3073

Najarro, P., Traktman, P., & Lewis, J. A. (2001). Vaccinia virus blocks gamma interferon signal transduction: viral VH1 phosphatase reverses Stat1 activation. *J Virol, 75*(7), 3185-3196. doi:10.1128/JVI.75.7.3185-3196.2001

Nakahira, K., Hisata, S., & Choi, A. M. (2015). The Roles of Mitochondrial Damage-Associated Molecular Patterns in Diseases. *Antioxid Redox Signal, 23*(17), 1329-1350. doi:10.1089/ars.2015.6407

Nakashima, H., Nguyen, T., Goins, W. F., & Chiocca, E. A. (2015). Interferon-stimulated gene 15 (ISG15) and ISG15-linked proteins can associate with members of the selective autophagic process, histone deacetylase 6 (HDAC6) and SQSTM1/p62. *J Biol Chem, 290*(3), 1485-1495. doi:10.1074/jbc.M114.593871

Napolitano, A., van der Veen, A. G., Bunyan, M., Borg, A., Frith, D., Howell, S., . . . Frickel, E. M. (2018). Cysteine-Reactive Free ISG15 Generates IL-1beta-Producing CD8alpha(+) Dendritic Cells at the Site of Infection. *J Immunol, 201*(2), 604-614. doi:10.4049/jimmunol.1701322

Narasimhan, J., Wang, M., Fu, Z., Klein, J. M., Haas, A. L., & Kim, J. J. (2005). Crystal structure of the interferon-induced ubiquitin-like protein ISG15. *J Biol Chem, 280*(29), 27356-27365. doi:10.1074/jbc.M502814200

Narendra, D., Kane, L. A., Hauser, D. N., Fearnley, I. M., & Youle, R. J. (2010). p62/SQSTM1 is required for Parkin-induced mitochondrial clustering but not mitophagy; VDAC1 is dispensable for both. *Autophagy, 6*(8), 1090-1106. doi:10.4161/auto.6.8.13426

Narendra, D., Tanaka, A., Suen, D. F., & Youle, R. J. (2008). Parkin is recruited selectively to impaired mitochondria and promotes their autophagy. *J Cell Biol, 183*(5), 795-803. doi:10.1083/jcb.200809125

Navarro, P., Trevisan-Herraz, M., Bonzon-Kulichenko, E., Nunez, E., Martinez-Acedo, P., Perez-Hernandez, D., . . . Vazquez, J. (2014). General statistical framework for quantitative proteomics by stable isotope labeling. *J Proteome Res, 13*(3), 1234-1247. doi:10.1021/pr4006958

Navarro, P., & Vazquez, J. (2009). A refined method to calculate false discovery rates for peptide identification using decoy databases. *J Proteome Res, 8*(4), 1792-1796. doi:10.1021/pr800362h

Nes, W. D. (2011). Biosynthesis of cholesterol and other sterols. *Chem Rev, 111*(10), 6423-6451. doi:10.1021/cr200021m

Neupert, W., & Herrmann, J. M. (2007). Translocation of proteins into mitochondria. *Annu Rev Biochem, 76*, 723-749. doi:10.1146/annurev.biochem.76.052705.163409

Nouri, K., Feng, Y., & Schimmer, A. D. (2020). Mitochondrial ClpP serine protease-biological function and emerging target for cancer therapy. *Cell Death Dis, 11*(10), 841. doi:10.1038/s41419-020-03062-z

O'Donnell, V. B., Rossjohn, J., & Wakelam, M. J. (2018). Phospholipid signaling in innate immune cells. *J Clin Invest, 128*(7), 2670-2679. doi:10.1172/JCI97944

O'Neill, L. A., Kishton, R. J., & Rathmell, J. (2016). A guide to immunometabolism for immunologists. *Nat Rev Immunol, 16*(9), 553-565. doi:10.1038/nri.2016.70

Okazaki, H., Igarashi, M., Nishi, M., Sekiya, M., Tajima, M., Takase, S., . . . Ishibashi, S. (2008). Identification of neutral cholesterol ester hydrolase, a key enzyme removing cholesterol from macrophages. *J Biol Chem, 283*(48), 33357-33364. doi:10.1074/jbc.M802686200

Okumura, A., Pitha, P. M., & Harty, R. N. (2008). ISG15 inhibits Ebola VP40 VLP budding in an L-domain-dependent manner by blocking Nedd4 ligase activity. *Proc Natl Acad Sci U S A, 105*(10), 3974-3979. doi:10.1073/pnas.0710629105

Okumura, F., Lenschow, D. J., & Zhang, D. E. (2008). Nitrosylation of ISG15 prevents the disulfide bond-mediated dimerization of ISG15 and contributes to effective ISGylation. *J Biol Chem, 283*(36), 24484-24488. doi:10.1074/jbc.M803795200

Okumura, F., Okumura, A. J., Uematsu, K., Hatakeyama, S., Zhang, D. E., & Kamura, T. (2013). Activation of double-stranded RNA-activated protein kinase (PKR) by interferon-stimulated gene 15 (ISG15) modification down-regulates protein translation. *J Biol Chem, 288*(4), 2839-2847. doi:10.1074/jbc.M112.401851

Onishi, M., Yamano, K., Sato, M., Matsuda, N., & Okamoto, K. (2021). Molecular mechanisms and physiological functions of mitophagy. *EMBO J, 40*(3), e104705. doi:10.15252/embj.2020104705

Orynbayeva, Z., Kolusheva, S., Groysman, N., Gavrielov, N., Lobel, L., & Jelinek, R. (2007). Vaccinia virus interactions with the cell membrane studied by new chromatic vesicle and cell sensor assays. *J Virol, 81*(3), 1140-1147. doi:10.1128/JVI.01345-06

Owen, O. E., Kalhan, S. C., & Hanson, R. W. (2002). The key role of anaplerosis and cataplerosis for citric acid cycle function. *J Biol Chem, 277*(34), 30409-30412. doi:10.1074/jbc.R200006200

Owhashi, M., Taoka, Y., Ishii, K., Nakazawa, S., Uemura, H., & Kambara, H. (2003). Identification of a ubiquitin family protein as a novel neutrophil chemotactic factor. *Biochem Biophys Res Commun, 309*(3), 533-539. doi:10.1016/j.bbrc.2003.08.038

Padovan, E., Terracciano, L., Certa, U., Jacobs, B., Reschner, A., Bolli, M., . . . Heberer, M. (2002). Interferon stimulated gene 15 constitutively produced by melanoma cells induces e-cadherin expression on human dendritic cells. *Cancer Res, 62*(12), 3453-3458.

Palmieri, F. (2013). The mitochondrial transporter family SLC25: identification, properties and physiopathology. *Mol Aspects Med, 34*(2-3), 465-484. doi:10.1016/j.mam.2012.05.005

Pant, A., Dsouza, L., Cao, S., Peng, C., & Yang, Z. (2021). Viral growth factor- and STAT3 signaling-dependent elevation of the TCA cycle intermediate levels during vaccinia virus infection. *PLoS Pathog, 17*(2), e1009303. doi:10.1371/journal.ppat.1009303

Papa, S., Martino, P. L., Capitanio, G., Gaballo, A., De Rasmo, D., Signorile, A., & Petruzzella, V. (2012). The oxidative phosphorylation system in mammalian mitochondria. *Adv Exp Med Biol, 942*, 3-37. doi:10.1007/978-94-007-2869-1_1

Paradies, G., Paradies, V., Ruggiero, F. M., & Petrosillo, G. (2019). Role of Cardiolipin in Mitochondrial Function and Dynamics in Health and Disease: Molecular and Pharmacological Aspects. *Cells, 8*(7). doi:10.3390/cells8070728

Park, J. H., Yang, S. W., Park, J. M., Ka, S. H., Kim, J. H., Kong, Y. Y., . . . Chung, C. H. (2016). Positive feedback regulation of p53 transactivity by DNA damage-induced ISG15 modification. *Nat Commun, 7*, 12513. doi:10.1038/ncomms12513

Park, J. M., Yang, S. W., Yu, K. R., Ka, S. H., Lee, S. W., Seol, J. H., . . . Chung, C. H. (2014). Modification of PCNA by ISG15 plays a crucial role in termination of error-prone translesion DNA synthesis. *Mol Cell, 54*(4), 626-638. doi:10.1016/j.molcel.2014.03.031

Park, Y. M. (2014). CD36, a scavenger receptor implicated in atherosclerosis. *Exp Mol Med, 46*, e99. doi:10.1038/emm.2014.38

Payne, A. H., & Hales, D. B. (2004). Overview of steroidogenic enzymes in the pathway from cholesterol to active steroid hormones. *Endocr Rev, 25*(6), 947-970. doi:10.1210/er.2003-0030

Payne, L. G. (1980). Significance of extracellular enveloped virus in the in vitro and in vivo dissemination of vaccinia. *J Gen Virol, 50*(1), 89-100. doi:10.1099/0022-1317-50-1-89

Peace, C. G., & O'Neill, L. A. (2022). The role of itaconate in host defense and inflammation. *J Clin Invest, 132*(2). doi:10.1172/JCI148548

Pearce, S. F., Rebelo-Guiomar, P., D'Souza, A. R., Powell, C. A., Van Haute, L., & Minczuk, M. (2017). Regulation of Mammalian Mitochondrial Gene Expression: Recent Advances. *Trends Biochem Sci, 42*(8), 625-639. doi:10.1016/j.tibs.2017.02.003

Peng, M., Yin, N., Chhangawala, S., Xu, K., Leslie, C. S., & Li, M. O. (2016). Aerobic glycolysis promotes T helper 1 cell differentiation through an epigenetic mechanism. *Science, 354*(6311), 481-484. doi:10.1126/science.aaf6284

Perdiguero, B., Sanchez-Corzo, C., Sorzano, C. O. S., Saiz, L., Mediavilla, P., Esteban, M., & Gomez, C. E. (2019). A Novel MVA-Based HIV Vaccine Candidate (MVA-gp145-GPN) Co-Expressing Clade C Membrane-Bound Trimeric gp145 Env and Gag-Induced Virus-Like Particles (VLPs) Triggered Broad and Multifunctional HIV-1-Specific T Cell and Antibody Responses. *Viruses, 11*(2). doi:10.3390/v11020160

Perez Berrocal, D. A., Witting, K. F., Ovaa, H., & Mulder, M. P. C. (2019). Hybrid Chains: A Collaboration of Ubiquitin and Ubiquitin-Like Modifiers Introducing Cross-Functionality to the Ubiquitin Code. *Front Chem, 7*, 931. doi:10.3389/fchem.2019.00931

Perng, Y. C., & Lenschow, D. J. (2018). ISG15 in antiviral immunity and beyond. *Nat Rev Microbiol, 16*(7), 423-439. doi:10.1038/s41579-018-0020-5

Petersen, E., Kantele, A., Koopmans, M., Asogun, D., Yinka-Ogunleye, A., Ihekweazu, C., & Zumla, A. (2019). Human Monkeypox: Epidemiologic and Clinical Characteristics, Diagnosis, and Prevention. *Infect Dis Clin North Am, 33*(4), 1027-1043. doi:10.1016/j.idc.2019.03.001

Phillips, M. C. (2014). Molecular mechanisms of cellular cholesterol efflux. *J Biol Chem, 289*(35), 24020-24029. doi:10.1074/jbc.R114.583658

Pilz, A., Ramsauer, K., Heidari, H., Leitges, M., Kovarik, P., & Decker, T. (2003). Phosphorylation of the Stat1 transactivating domain is required for the response to type I interferons. *EMBO Rep, 4*(4), 368-373. doi:10.1038/sj.embor.embor802

Pitha-Rowe, I., Hassel, B. A., & Dmitrovsky, E. (2004). Involvement of UBE1L in ISG15 conjugation during retinoid-induced differentiation of acute promyelocytic leukemia. *J Biol Chem, 279*(18), 18178-18187. doi:10.1074/jbc.M309259200

Platanias, L. C. (2005). Mechanisms of type-I- and type-II-interferon-mediated signalling. *Nat Rev Immunol, 5*(5), 375-386. doi:10.1038/nri1604

Potter, J. L., Narasimhan, J., Mende-Mueller, L., & Haas, A. L. (1999). Precursor processing of pro-ISG15/UCRP, an interferon-beta-induced ubiquitin-like protein. *J Biol Chem, 274*(35), 25061-25068. doi:10.1074/jbc.274.35.25061

Prokunina-Olsson, L., Muchmore, B., Tang, W., Pfeiffer, R. M., Park, H., Dickensheets, H., . . . O'Brien, T. R. (2013). A variant upstream of IFNL3 (IL28B) creating a new interferon gene IFNL4 is associated with impaired clearance of hepatitis C virus. *Nat Genet, 45*(2), 164-171. doi:10.1038/ng.2521

Punjabi, A., & Traktman, P. (2005). Cell biological and functional characterization of the vaccinia virus F10 kinase: implications for the mechanism of virion morphogenesis. *J Virol, 79*(4), 2171-2190. doi:10.1128/JVI.79.4.2171-2190.2005

Qi, C., Zhu, Y., & Reddy, J. K. (2000). Peroxisome proliferator-activated receptors, coactivators, and downstream targets. *Cell Biochem Biophys, 32 Spring*, 187-204. doi:10.1385/cbb:32:1-3:187

Quinlivan, V. H., Wilson, M. H., Ruzicka, J., & Farber, S. A. (2017). An HPLC-CAD/fluorescence lipidomics platform using fluorescent fatty acids as metabolic tracers. *J Lipid Res, 58*(5), 1008-1020. doi:10.1194/jlr.D072918

Radoshevich, L., Impens, F., Ribet, D., Quereda, J. J., Nam Tham, T., Nahori, M. A., . . . Cossart, P. (2015). ISG15 counteracts Listeria monocytogenes infection. *Elife, 4*. doi:10.7554/eLife.06848

Rambold, A. S., Cohen, S., & Lippincott-Schwartz, J. (2015). Fatty acid trafficking in starved cells: regulation by lipid droplet lipolysis, autophagy, and mitochondrial fusion dynamics. *Dev Cell, 32*(6), 678-692. doi:10.1016/j.devcel.2015.01.029

Remmerie, A., & Scott, C. L. (2018). Macrophages and lipid metabolism. *Cell Immunol, 330*, 27-42. doi:10.1016/j.cellimm.2018.01.020

Repa, J. J., Liang, G., Ou, J., Bashmakov, Y., Lobaccaro, J. M., Shimomura, I., . . . Mangelsdorf, D. J. (2000). Regulation of mouse sterol regulatory element-binding protein-1c gene (SREBP-1c) by oxysterol receptors, LXRalpha and LXRbeta. *Genes Dev, 14*(22), 2819-2830. doi:10.1101/gad.844900

Rietdorf, J., Ploubidou, A., Reckmann, I., Holmstrom, A., Frischknecht, F., Zettl, M., . . . Way, M. (2001). Kinesin-dependent movement on microtubules precedes actin-based motility of vaccinia virus. *Nat Cell Biol, 3*(11), 992-1000. doi:10.1038/ncb1101-992

Ritchie, K. J., Hahn, C. S., Kim, K. I., Yan, M., Rosario, D., Li, L., . . . Zhang, D. E. (2004). Role of ISG15 protease UBP43 (USP18) in innate immunity to viral infection. *Nat Med, 10*(12), 1374-1378. doi:10.1038/nm1133

Robenek, H., Robenek, M. J., & Troyer, D. (2005). PAT family proteins pervade lipid droplet cores. *J Lipid Res, 46*(6), 1331-1338. doi:10.1194/jlr.M400323-JLR200

Roberts, K. L., & Smith, G. L. (2008). Vaccinia virus morphogenesis and dissemination. *Trends Microbiol, 16*(10), 472-479. doi:10.1016/j.tim.2008.07.009

Robertson, K. A., & Ghazal, P. (2016). Interferon Control of the Sterol Metabolic Network: Bidirectional Molecular Circuitry-Mediating Host Protection. *Front Immunol, 7*, 634. doi:10.3389/fimmu.2016.00634

Rodríguez, D., Esteban, M., & Rodríguez, J. R. (1995). Vaccinia virus A17L gene product is essential for an early step in virion morphogenesis. *J Virol, 69*(8), 4640-4648. doi:10.1128/JVI.69.8.4640-4648.1995

Rohrig, F., & Schulze, A. (2016). The multifaceted roles of fatty acid synthesis in cancer. *Nat Rev Cancer, 16*(11), 732-749. doi:10.1038/nrc.2016.89

Ron, D., & Walter, P. (2007). Signal integration in the endoplasmic reticulum unfolded protein response. *Nat Rev Mol Cell Biol, 8*(7), 519-529. doi:10.1038/nrm2199

Rong, X., Albert, C. J., Hong, C., Duerr, M. A., Chamberlain, B. T., Tarling, E. J., . . . Tontonoz, P. (2013). LXRs regulate ER stress and inflammation through dynamic modulation of membrane phospholipid composition. *Cell Metab, 18*(5), 685-697. doi:10.1016/j.cmet.2013.10.002

Ruggles, K. V., Turkish, A., & Sturley, S. L. (2013). Making, baking, and breaking: the synthesis, storage, and hydrolysis of neutral lipids. *Annu Rev Nutr, 33*, 413-451. doi:10.1146/annurev-nutr-071812-161254

Rybicka, J. M., Balce, D. R., Khan, M. F., Krohn, R. M., & Yates, R. M. (2010). NADPH oxidase activity controls phagosomal proteolysis in macrophages through modulation of the lumenal redox environment of phagosomes. *Proc Natl Acad Sci U S A, 107*(23), 10496-10501. doi:10.1073/pnas.0914867107

Sainz, B., Jr., Martin, B., Tatari, M., Heeschen, C., & Guerra, S. (2014). ISG15 is a critical microenvironmental factor for pancreatic cancer stem cells. *Cancer Res, 74*(24), 7309-7320. doi:10.1158/0008-5472.CAN-14-1354

Saka, H. A., & Valdivia, R. (2012). Emerging roles for lipid droplets in immunity and host-pathogen interactions. *Annu Rev Cell Dev Biol, 28*, 411-437. doi:10.1146/annurev-cellbio-092910-153958

Sakai, K., Igarashi, M., Yamamuro, D., Ohshiro, T., Nagashima, S., Takahashi, M., . . . Ishibashi, S. (2014). Critical role of neutral cholesteryl ester hydrolase 1 in cholesteryl ester hydrolysis in murine macrophages. *J Lipid Res, 55*(10), 2033-2040. doi:10.1194/jlr.M047787

Sanchez, E. L., & Lagunoff, M. (2015). Viral activation of cellular metabolism. *Virology, 479-480*, 609-618. doi:10.1016/j.virol.2015.02.038

Sandy, Z., da Costa, I. C., & Schmidt, C. K. (2020). More than Meets the ISG15: Emerging Roles in the DNA Damage Response and Beyond. *Biomolecules, 10*(11). doi:10.3390/biom10111557

Sarcinelli, C., Dragic, H., Piecyk, M., Barbet, V., Duret, C., Barthelaix, A., . . . Manie, S. N. (2020). ATF4-Dependent NRF2 Transcriptional Regulation Promotes Antioxidant Protection during Endoplasmic Reticulum Stress. *Cancers (Basel), 12*(3). doi:10.3390/cancers12030569

Scarpulla, R. C. (2008). Transcriptional paradigms in mammalian mitochondrial biogenesis and function. *Physiol Rev, 88*(2), 611-638. doi:10.1152/physrev.00025.2007

Schindelin, J., Arganda-Carreras, I., Frise, E., Kaynig, V., Longair, M., Pietzsch, T., . . . Cardona, A. (2012). Fiji: an open-source platform for biological-image analysis. *Nat Methods, 9*(7), 676-682. doi:10.1038/nmeth.2019

Schlaepfer, I. R., & Joshi, M. (2020). CPT1A-mediated Fat Oxidation, Mechanisms, and Therapeutic Potential. *Endocrinology, 161*(2). doi:10.1210/endocr/bqz046

Schmelz, M., Sodeik, B., Ericsson, M., Wolffe, E. J., Shida, H., Hiller, G., & Griffiths, G. (1994). Assembly of vaccinia virus: the second wrapping cisterna is derived from the trans Golgi network. *J Virol, 68*(1), 130-147. doi:10.1128/JVI.68.1.130-147.1994

Schneider, W. M., Chevillotte, M. D., & Rice, C. M. (2014). Interferon-stimulated genes: a complex web of host defenses. *Annu Rev Immunol, 32*, 513-545. doi:10.1146/annurev-immunol-032713-120231

Schrepfer, E., & Scorrano, L. (2016). Mitofusins, from Mitochondria to Metabolism. *Mol Cell, 61*(5), 683-694. doi:10.1016/j.molcel.2016.02.022

Schultz, J. R., Tu, H., Luk, A., Repa, J. J., Medina, J. C., Li, L., . . . Shan, B. (2000). Role of LXRs in control of lipogenesis. *Genes Dev, 14*(22), 2831-2838. doi:10.1101/gad.850400

Scialo, F., Fernandez-Ayala, D. J., & Sanz, A. (2017). Role of Mitochondrial Reverse Electron Transport in ROS Signaling: Potential Roles in Health and Disease. *Front Physiol, 8*, 428. doi:10.3389/fphys.2017.00428

Scutts, S. R., Ember, S. W., Ren, H., Ye, C., Lovejoy, C. A., Mazzon, M., . . . Smith, G. L. (2018). DNA-PK Is Targeted by Multiple Vaccinia Virus Proteins to Inhibit DNA Sensing. *Cell Rep, 25*(7), 1953-1965 e1954. doi:10.1016/j.celrep.2018.10.034

Sebastian, D., Palacin, M., & Zorzano, A. (2017). Mitochondrial Dynamics: Coupling Mitochondrial Fitness with Healthy Aging. *Trends Mol Med, 23*(3), 201-215. doi:10.1016/j.molmed.2017.01.003

Sekiya, M., Osuga, J., Igarashi, M., Okazaki, H., & Ishibashi, S. (2011). The role of neutral cholesterol ester hydrolysis in macrophage foam cells. *J Atheroscler Thromb, 18*(5), 359-364. doi:10.5551/jat.7013

Sekiya, M., Osuga, J., Nagashima, S., Ohshiro, T., Igarashi, M., Okazaki, H., . . . Ishibashi, S. (2009). Ablation of neutral cholesterol ester hydrolase 1 accelerates atherosclerosis. *Cell Metab, 10*(3), 219-228. doi:10.1016/j.cmet.2009.08.004

Sekiya, M., Yamamuro, D., Ohshiro, T., Honda, A., Takahashi, M., Kumagai, M., . . . Ishibashi, S. (2014). Absence of Nceh1 augments 25-hydroxycholesterol-induced ER stress and apoptosis in macrophages. *J Lipid Res, 55*(10), 2082-2092. doi:10.1194/jlr.M050864

Seth, R. B., Sun, L., Ea, C. K., & Chen, Z. J. (2005). Identification and characterization of MAVS, a mitochondrial antiviral signaling protein that activates NF-kappaB and IRF 3. *Cell, 122*(5), 669-682. doi:10.1016/j.cell.2005.08.012

Shao, D., Liu, Y., Liu, X., Zhu, L., Cui, Y., Cui, A., . . . Chang, Y. (2010). PGC-1 beta-regulated mitochondrial biogenesis and function in myotubes is mediated by NRF-1 and ERR alpha. *Mitochondrion, 10*(5), 516-527. doi:10.1016/j.mito.2010.05.012

Shen, W. J., Azhar, S., & Kraemer, F. B. (2018). SR-B1: A Unique Multifunctional Receptor for Cholesterol Influx and Efflux. *Annu Rev Physiol, 80*, 95-116. doi:10.1146/annurev-physiol-021317-121550

Shi, H. X., Yang, K., Liu, X., Liu, X. Y., Wei, B., Shan, Y. F., . . . Wang, C. (2010). Positive regulation of interferon regulatory factor 3 activation by Herc5 via ISG15 modification. *Mol Cell Biol, 30*(10), 2424-2436. doi:10.1128/MCB.01466-09

Shimano, H., & Sato, R. (2017). SREBP-regulated lipid metabolism: convergent physiology - divergent pathophysiology. *Nat Rev Endocrinol, 13*(12), 710-730. doi:10.1038/nrendo.2017.91

Shin, D., Mukherjee, R., Grewe, D., Bojkova, D., Baek, K., Bhattacharya, A., . . . Dikic, I. (2020). Papain-like protease regulates SARS-CoV-2 viral spread and innate immunity. *Nature, 587*(7835), 657-662. doi:10.1038/s41586-020-2601-5

Shuai, K., & Liu, B. (2003). Regulation of JAK-STAT signalling in the immune system. *Nat Rev Immunol, 3*(11), 900-911. doi:10.1038/nri1226

Sica, A., & Mantovani, A. (2012). Macrophage plasticity and polarization: in vivo veritas. *J Clin Invest, 122*(3), 787-795. doi:10.1172/JCI59643

Signes, A., & Fernandez-Vizarra, E. (2018). Assembly of mammalian oxidative phosphorylation complexes I-V and supercomplexes. *Essays Biochem, 62*(3), 255-270. doi:10.1042/EBC20170098

Smith, G. L., Benfield, C. T. O., Maluquer de Motes, C., Mazzon, M., Ember, S. W. J., Ferguson, B. J., & Sumner, R. P. (2013). Vaccinia virus immune evasion: mechanisms, virulence and immunogenicity. *J Gen Virol, 94*(Pt 11), 2367-2392. doi:10.1099/vir.0.055921-0

Smith, G. L., Talbot-Cooper, C., & Lu, Y. (2018). How Does Vaccinia Virus Interfere With Interferon? *Adv Virus Res, 100*, 355-378. doi:10.1016/bs.aivir.2018.01.003

Sommereyns, C., Paul, S., Staeheli, P., & Michiels, T. (2008). IFN-lambda (IFN-lambda) is expressed in a tissue-dependent fashion and primarily acts on epithelial cells in vivo. *PLoS Pathog, 4*(3), e1000017. doi:10.1371/journal.ppat.1000017

Sonoda, J., Laganiere, J., Mehl, I. R., Barish, G. D., Chong, L. W., Li, X., . . . Evans, R. M. (2007). Nuclear receptor ERR alpha and coactivator PGC-1 beta are effectors of IFN-gamma-induced host defense. *Genes Dev, 21*(15), 1909-1920. doi:10.1101/gad.1553007

Speer, S. D., Li, Z., Buta, S., Payelle-Brogard, B., Qian, L., Vigant, F., . . . Bogunovic, D. (2016). ISG15 deficiency and increased viral resistance in humans but not mice. *Nat Commun, 7*, 11496. doi:10.1038/ncomms11496

Spinelli, J. B., & Haigis, M. C. (2018). The multifaceted contributions of mitochondria to cellular metabolism. *Nat Cell Biol, 20*(7), 745-754. doi:10.1038/s41556-018-0124-1

Stanifer, M. L., Guo, C., Doldan, P., & Boulant, S. (2020). Importance of Type I and III Interferons at Respiratory and Intestinal Barrier Surfaces. *Front Immunol, 11*, 608645. doi:10.3389/fimmu.2020.608645

Stincone, A., Prigione, A., Cramer, T., Wamelink, M. M., Campbell, K., Cheung, E., . . . Ralser, M. (2015). The return of metabolism: biochemistry and physiology of the pentose phosphate pathway. *Biol Rev Camb Philos Soc, 90*(3), 927-963. doi:10.1111/brv.12140

Strnadova, P., Ren, H., Valentine, R., Mazzon, M., Sweeney, T. R., Brierley, I., & Smith, G. L. (2015). Inhibition of Translation Initiation by Protein 169: A Vaccinia Virus Strategy to Suppress Innate and Adaptive Immunity and Alter Virus Virulence. *PLoS Pathog, 11*(9), e1005151. doi:10.1371/journal.ppat.1005151

Sukhorukov, V. N., Khotina, V. A., Bagheri Ekta, M., Ivanova, E. A., Sobenin, I. A., & Orekhov, A. N. (2020). Endoplasmic Reticulum Stress in Macrophages: The Vicious Circle of Lipid Accumulation and Pro-Inflammatory Response. *Biomedicines, 8*(7). doi:10.3390/biomedicines8070210

Sun, L., Wang, X., Zhou, Y., Zhou, R. H., Ho, W. Z., & Li, J. L. (2016). Exosomes contribute to the transmission of anti-HIV activity from TLR3-activated brain microvascular endothelial cells to macrophages. *Antiviral Res, 134*, 167-171. doi:10.1016/j.antiviral.2016.07.013

Supruniuk, E., Miklosz, A., & Chabowski, A. (2017). The Implication of PGC-1alpha on Fatty Acid Transport across Plasma and Mitochondrial Membranes in the Insulin Sensitive Tissues. *Front Physiol, 8*, 923. doi:10.3389/fphys.2017.00923

Swaim, C. D., Canadeo, L. A., Monte, K. J., Khanna, S., Lenschow, D. J., & Huibregtse, J. M. (2020). Modulation of Extracellular ISG15 Signaling by Pathogens and Viral Effector Proteins. *Cell Rep, 31*(11), 107772. doi:10.1016/j.celrep.2020.107772

Swaim, C. D., Scott, A. F., Canadeo, L. A., & Huibregtse, J. M. (2017). Extracellular ISG15 Signals Cytokine Secretion through the LFA-1 Integrin Receptor. *Mol Cell, 68*(3), 581-590 e585. doi:10.1016/j.molcel.2017.10.003

Swanson, K. V., Deng, M., & Ting, J. P. (2019). The NLRP3 inflammasome: molecular activation and regulation to therapeutics. *Nat Rev Immunol, 19*(8), 477-489. doi:10.1038/s41577-019-0165-0

Symons, J. A., Alcami, A., & Smith, G. L. (1995). Vaccinia virus encodes a soluble type I interferon receptor of novel structure and broad species specificity. *Cell, 81*(4), 551-560. doi:10.1016/0092-8674(95)90076-4

Szczepanowska, K., & Trifunovic, A. (2021). Tune instead of destroy: How proteolysis keeps OXPHOS in shape. *Biochim Biophys Acta Bioenerg, 1862*(4), 148365. doi:10.1016/j.bbabio.2020.148365

Szklarczyk, D., Gable, A. L., Nastou, K. C., Lyon, D., Kirsch, R., Pyysalo, S., . . . von Mering, C. (2021). The STRING database in 2021: customizable protein-protein networks, and functional characterization of user-uploaded gene/measurement sets. *Nucleic Acids Res, 49*(D1), D605-D612. doi:10.1093/nar/gkaa1074

Sztalryd, C., & Brasaemle, D. L. (2017). The perilipin family of lipid droplet proteins: Gatekeepers of intracellular lipolysis. *Biochim Biophys Acta Mol Cell Biol Lipids, 1862*(10 Pt B), 1221-1232. doi:10.1016/j.bbalip.2017.07.009

Takeuchi, T., Iwahara, S., Saeki, Y., Sasajima, H., & Yokosawa, H. (2005). Link between the ubiquitin conjugation system and the ISG15 conjugation system: ISG15 conjugation to the UbcH6 ubiquitin E2 enzyme. *J Biochem, 138*(6), 711-719. doi:10.1093/jb/mvi172

Takeuchi, T., & Yokosawa, H. (2005). ISG15 modification of Ubc13 suppresses its ubiquitin-conjugating activity. *Biochem Biophys Res Commun, 336*(1), 9-13. doi:10.1016/j.bbrc.2005.08.034

Tal, M. C., Sasai, M., Lee, H. K., Yordy, B., Shadel, G. S., & Iwasaki, A. (2009). Absence of autophagy results in reactive oxygen species-dependent amplification of RLR signaling. *Proc Natl Acad Sci U S A, 106*(8), 2770-2775. doi:10.1073/pnas.0807694106

Tall, A. R., & Yvan-Charvet, L. (2015). Cholesterol, inflammation and innate immunity. *Nat Rev Immunol, 15*(2), 104-116. doi:10.1038/nri3793

Tan, Z., Xie, N., Cui, H., Moellering, D. R., Abraham, E., Thannickal, V. J., & Liu, G. (2015). Pyruvate dehydrogenase kinase 1 participates in macrophage polarization via regulating glucose metabolism. *J Immunol, 194*(12), 6082-6089. doi:10.4049/jimmunol.1402469

Tang, Y., Zhong, G., Zhu, L., Liu, X., Shan, Y., Feng, H., . . . Wang, C. (2010). Herc5 attenuates influenza A virus by catalyzing ISGylation of viral NS1 protein. *J Immunol, 184*(10), 5777-5790. doi:10.4049/jimmunol.0903588

Tannahill, G. M., Curtis, A. M., Adamik, J., Palsson-McDermott, E. M., McGettrick, A. F., Goel, G., . . . O'Neill, L. A. (2013). Succinate is an inflammatory signal that induces IL-1beta through HIF-1alpha. *Nature, 496*(7444), 238-242. doi:10.1038/nature11986

Taylor, J. L., D'Cunha, J., Tom, P., O'Brien, W. J., & Borden, E. C. (1996). Production of ISG-15, an interferon-inducible protein, in human corneal cells. *J Interferon Cytokine Res, 16*(11), 937-940. doi:10.1089/jir.1996.16.937

Taylor, P. R., Martinez-Pomares, L., Stacey, M., Lin, H. H., Brown, G. D., & Gordon, S. (2005). Macrophage receptors and immune recognition. *Annu Rev Immunol, 23*, 901-944. doi:10.1146/annurev.immunol.23.021704.115816

Tecalco Cruz, A. C., & Mejia-Barreto, K. (2017). Cell type-dependent regulation of free ISG15 levels and ISGylation. *J Cell Commun Signal, 11*(2), 127-135. doi:10.1007/s12079-017-0385-7

Thaker, S. K., Ch'ng, J., & Christofk, H. R. (2019). Viral hijacking of cellular metabolism. *BMC Biol, 17*(1), 59. doi:10.1186/s12915-019-0678-9

Thery, F., Eggermont, D., & Impens, F. (2021). Proteomics Mapping of the ISGylation Landscape in Innate Immunity. *Front Immunol, 12*, 720765. doi:10.3389/fimmu.2021.720765

Toda, G., Yamauchi, T., Kadowaki, T., & Ueki, K. (2021). Preparation and culture of bone marrow-derived macrophages from mice for functional analysis. *STAR Protoc, 2*(1), 100246. doi:10.1016/j.xpro.2020.100246

Tokarz, S., Berset, C., La Rue, J., Friedman, K., Nakayama, K., Nakayama, K., . . . Lanker, S. (2004). The ISG15 isopeptidase UBP43 is regulated by proteolysis via the SCFSkp2 ubiquitin ligase. *J Biol Chem, 279*(45), 46424-46430. doi:10.1074/jbc.M403189200

Tooze, J., Hollinshead, M., Reis, B., Radsak, K., & Kern, H. (1993). Progeny vaccinia and human cytomegalovirus particles utilize early endosomal cisternae for their envelopes. *Eur J Cell Biol, 60*(1), 163-178.

Tripathi, M., Yen, P. M., & Singh, B. K. (2020). Estrogen-Related Receptor Alpha: An Under-Appreciated Potential Target for the Treatment of Metabolic Diseases. *Int J Mol Sci, 21*(5). doi:10.3390/ijms21051645

Tur, J., Vico, T., Lloberas, J., Zorzano, A., & Celada, A. (2017). Macrophages and Mitochondria: A Critical Interplay Between Metabolism, Signaling, and the Functional Activity. *Adv Immunol, 133*, 1-36. doi:10.1016/bs.ai.2016.12.001

Twig, G., Elorza, A., Molina, A. J., Mohamed, H., Wikstrom, J. D., Walzer, G., . . . Shirihai, O. S. (2008). Fission and selective fusion govern mitochondrial segregation and elimination by autophagy. *EMBO J, 27*(2), 433-446. doi:10.1038/sj.emboj.7601963

Ulaeto, D., Grosenbach, D., & Hruby, D. E. (1996). The vaccinia virus 4c and A-type inclusion proteins are specific markers for the intracellular mature virus particle. *J Virol, 70*(6), 3372-3377. doi:10.1128/JVI.70.6.3372-3377.1996

Van den Bossche, J., O'Neill, L. A., & Menon, D. (2017). Macrophage Immunometabolism: Where Are We (Going)? *Trends Immunol, 38*(6), 395-406. doi:10.1016/j.it.2017.03.001

van der Kloet, F. M., Bobeldijk, I., Verheij, E. R., & Jellema, R. H. (2009). Analytical error reduction using single point calibration for accurate and precise metabolomic phenotyping. *J Proteome Res, 8*(11), 5132-5141. doi:10.1021/pr900499r

van der Veen, J. N., Kennelly, J. P., Wan, S., Vance, J. E., Vance, D. E., & Jacobs, R. L. (2017). The critical role of phosphatidylcholine and phosphatidylethanolamine metabolism in health and disease. *Biochim Biophys Acta Biomembr, 1859*(9 Pt B), 1558-1572. doi:10.1016/j.bbamem.2017.04.006

van Eijl, H., Hollinshead, M., Rodger, G., Zhang, W. H., & Smith, G. L. (2002). The vaccinia virus F12L protein is associated with intracellular enveloped virus particles and is required for their egress to the cell surface. *J Gen Virol, 83*(Pt 1), 195-207. doi:10.1099/0022-1317-83-1-195

Vance, J. E. (2015). Phospholipid synthesis and transport in mammalian cells. *Traffic, 16*(1), 1-18. doi:10.1111/tra.12230

Vanderplasschen, A., Mathew, E., Hollinshead, M., Sim, R. B., & Smith, G. L. (1998). Extracellular enveloped vaccinia virus is resistant to complement because of incorporation of host complement control proteins into its envelope. *Proc Natl Acad Sci U S A, 95*(13), 7544-7549. doi:10.1073/pnas.95.13.7544

Vernier, M., & Giguere, V. (2021). Aging, senescence and mitochondria: the PGC-1/ERR axis. *J Mol Endocrinol, 66*(1), R1-R14. doi:10.1530/JME-20-0196

Villarino, A. V., Kanno, Y., & O'Shea, J. J. (2017). Mechanisms and consequences of Jak-STAT signaling in the immune system. *Nat Immunol, 18*(4), 374-384. doi:10.1038/ni.3691

Villarroya-Beltri, C., Baixauli, F., Mittelbrunn, M., Fernandez-Delgado, I., Torralba, D., Moreno-Gonzalo, O., . . . Sanchez-Madrid, F. (2016). ISGylation controls exosome secretion by promoting lysosomal degradation of MVB proteins. *Nat Commun, 7*, 13588. doi:10.1038/ncomms13588

Vives-Bauza, C., Yang, L., & Manfredi, G. (2007). Assay of mitochondrial ATP synthesis in animal cells and tissues. *Methods Cell Biol, 80*, 155-171. doi:10.1016/S0091-679X(06)80007-5

Vogel, C., & Marcotte, E. M. (2012). Insights into the regulation of protein abundance from proteomic and transcriptomic analyses. *Nat Rev Genet, 13*(4), 227-232. doi:10.1038/nrg3185

Walther, T. C., Chung, J., & Farese, R. V., Jr. (2017). Lipid Droplet Biogenesis. *Annu Rev Cell Dev Biol, 33*, 491-510. doi:10.1146/annurev-cellbio-100616-060608

Wang, B., & Tontonoz, P. (2018). Liver X receptors in lipid signalling and membrane homeostasis. *Nat Rev Endocrinol, 14*(8), 452-463. doi:10.1038/s41574-018-0037-x

Wang, H., Airola, M. V., & Reue, K. (2017). How lipid droplets "TAG" along: Glycerolipid synthetic enzymes and lipid storage. *Biochim Biophys Acta Mol Cell Biol Lipids, 1862*(10 Pt B), 1131-1145. doi:10.1016/j.bbalip.2017.06.010

Wculek, S. K., Dunphy, G., Heras-Murillo, I., Mastrangelo, A., & Sancho, D. (2022). Metabolism of tissue macrophages in homeostasis and pathology. *Cell Mol Immunol, 19*(3), 384-408. doi:10.1038/s41423-021-00791-9

Welte, M. A., & Gould, A. P. (2017). Lipid droplet functions beyond energy storage. *Biochim Biophys Acta Mol Cell Biol Lipids, 1862*(10 Pt B), 1260-1272. doi:10.1016/j.bbalip.2017.07.006

West, A. P., Shadel, G. S., & Ghosh, S. (2011). Mitochondria in innate immune responses. *Nat Rev Immunol, 11*(6), 389-402. doi:10.1038/nri2975

Wiedemann, N., & Pfanner, N. (2017). Mitochondrial Machineries for Protein Import and Assembly. *Annu Rev Biochem, 86*, 685-714. doi:10.1146/annurev-biochem-060815-014352

Wittig, I., Braun, H. P., & Schagger, H. (2006). Blue native PAGE. *Nat Protoc, 1*(1), 418-428. doi:10.1038/nprot.2006.62

Wong, E., Bejarano, E., Rakshit, M., Lee, K., Hanson, H. H., Zaarur, N., . . . Cuervo, A. M. (2012). Molecular determinants of selective clearance of protein inclusions by autophagy. *Nat Commun, 3*, 1240. doi:10.1038/ncomms2244

Wu, D., Sanin, D. E., Everts, B., Chen, Q., Qiu, J., Buck, M. D., . . . Pearce, E. J. (2016). Type 1 Interferons Induce Changes in Core Metabolism that Are Critical for Immune Function. *Immunity, 44*(6), 1325-1336. doi:10.1016/j.immuni.2016.06.006

Wynn, T. A., Chawla, A., & Pollard, J. W. (2013). Macrophage biology in development, homeostasis and disease. *Nature, 496*(7446), 445-455. doi:10.1038/nature12034

Xu, D., Zhang, T., Xiao, J., Zhu, K., Wei, R., Wu, Z., . . . Yuan, J. (2015). Modification of BECN1 by ISG15 plays a crucial role in autophagy regulation by type I IFN/interferon. *Autophagy, 11*(4), 617-628. doi:10.1080/15548627.2015.1023982

Xu, S., Zhang, X., & Liu, P. (2018). Lipid droplet proteins and metabolic diseases. *Biochim Biophys Acta Mol Basis Dis, 1864*(5 Pt B), 1968-1983. doi:10.1016/j.bbadis.2017.07.019

Yamazaki, H., Takahashi, M., Wakabayashi, T., Sakai, K., Yamamuro, D., Takei, A., . . . Ishibashi, S. (2019). Loss of ACAT1 Attenuates Atherosclerosis Aggravated by Loss of NCEH1 in Bone Marrow-Derived Cells. *J Atheroscler Thromb, 26*(3), 246-259. doi:10.5551/jat.44040

Yan, J., & Horng, T. (2020). Lipid Metabolism in Regulation of Macrophage Functions. *Trends Cell Biol, 30*(12), 979-989. doi:10.1016/j.tcb.2020.09.006

Yan, S., Kumari, M., Xiao, H., Jacobs, C., Kochumon, S., Jedrychowski, M., . . . Rosen, E. D. (2021). IRF3 reduces adipose thermogenesis via ISG15-mediated reprogramming of glycolysis. *J Clin Invest, 131*(7). doi:10.1172/JCI144888

Yang, Z., Gray, M., & Winter, L. (2021). Why do poxviruses still matter? *Cell Biosci, 11*(1), 96. doi:10.1186/s13578-021-00610-8

Yang, Z., & Klionsky, D. J. (2010). Eaten alive: a history of macroautophagy. *Nat Cell Biol, 12*(9), 814-822. doi:10.1038/ncb0910-814

Yanguez, E., Garcia-Culebras, A., Frau, A., Llompart, C., Knobeloch, K. P., Gutierrez-Erlandsson, S., . . . Guerra, S. (2013). ISG15 regulates peritoneal macrophages functionality against viral infection. *PLoS Pathog, 9*(10), e1003632. doi:10.1371/journal.ppat.1003632

Yeh, Y. H., Yang, Y. C., Hsieh, M. Y., Yeh, Y. C., & Li, T. K. (2013). A negative feedback of the HIF-1alpha pathway via interferon-stimulated gene 15 and ISGylation. *Clin Cancer Res, 19*(21), 5927-5939. doi:10.1158/1078-0432.CCR-13-0018

Yin, M., & O'Neill, L. A. J. (2021). The role of the electron transport chain in immunity. *FASEB J, 35*(12), e21974. doi:10.1096/fj.202101161R

York, A. G., Williams, K. J., Argus, J. P., Zhou, Q. D., Brar, G., Vergnes, L., . . . Bensinger, S. J. (2015). Limiting Cholesterol Biosynthetic Flux Spontaneously Engages Type I IFN Signaling. *Cell, 163*(7), 1716-1729. doi:10.1016/j.cell.2015.11.045

Youle, R. J., & Narendra, D. P. (2011). Mechanisms of mitophagy. *Nat Rev Mol Cell Biol, 12*(1), 9-14. doi:10.1038/nrm3028

Youle, R. J., & van der Bliek, A. M. (2012). Mitochondrial fission, fusion, and stress. *Science, 337*(6098), 1062-1065. doi:10.1126/science.1219855

Yuan, W., & Krug, R. M. (2001). Influenza B virus NS1 protein inhibits conjugation of the interferon (IFN)-induced ubiquitin-like ISG15 protein. *EMBO J, 20*(3), 362-371. doi:10.1093/emboj/20.3.362

Yvan-Charvet, L., Welch, C., Pagler, T. A., Ranalletta, M., Lamkanfi, M., Han, S., . . . Tall, A. R. (2008). Increased inflammatory gene expression in ABC transporter-deficient macrophages: free cholesterol accumulation, increased signaling via toll-like receptors, and neutrophil infiltration of atherosclerotic lesions. *Circulation, 118*(18), 1837-1847. doi:10.1161/CIRCULATIONAHA.108.793869

Zamora, M., & Villena, J. A. (2014). Targeting mitochondrial biogenesis to treat insulin resistance. *Curr Pharm Des, 20*(35), 5527-5557. doi:10.2174/1381612820666140306102514

Zangari, J., Petrelli, F., Maillot, B., & Martinou, J. C. (2020). The Multifaceted Pyruvate Metabolism: Role of the Mitochondrial Pyruvate Carrier. *Biomolecules, 10*(7). doi:10.3390/biom10071068

Zhang, D., & Zhang, D. E. (2011). Interferon-stimulated gene 15 and the protein ISGylation system. *J Interferon Cytokine Res, 31*(1), 119-130. doi:10.1089/jir.2010.0110

Zhang, J., Lan, Y., & Sanyal, S. (2017). Modulation of Lipid Droplet Metabolism-A Potential Target for Therapeutic Intervention in Flaviviridae Infections. *Front Microbiol, 8*, 2286. doi:10.3389/fmicb.2017.02286

Zhang, L., Rajbhandari, P., Priest, C., Sandhu, J., Wu, X., Temel, R., . . . Tontonoz, P. (2017). Inhibition of cholesterol biosynthesis through RNF145-dependent ubiquitination of SCAP. *Elife, 6*. doi:10.7554/eLife.28766

Zhang, X., Bogunovic, D., Payelle-Brogard, B., Francois-Newton, V., Speer, S. D., Yuan, C., . . . Pellegrini, S. (2015). Human intracellular ISG15 prevents interferon-alpha/beta over-amplification and auto-inflammation. *Nature, 517*(7532), 89-93. doi:10.1038/nature13801

Zhang, X., Goncalves, R., & Mosser, D. M. (2008). The isolation and characterization of murine macrophages. *Curr Protoc Immunol, Chapter 14*, Unit 14 11. doi:10.1002/0471142735.im1401s83

Zhang, Y., Breevoort, S. R., Angdisen, J., Fu, M., Schmidt, D. R., Holmstrom, S. R., . . . Schulman, I. G. (2012). Liver LXRalpha expression is crucial for whole body cholesterol homeostasis and reverse cholesterol transport in mice. *J Clin Invest, 122*(5), 1688-1699. doi:10.1172/JCI59817

Zhang, Y., Thery, F., Wu, N. C., Luhmann, E. K., Dussurget, O., Foecke, M., . . . Radoshevich, L. (2019). The in vivo ISGylome links ISG15 to metabolic pathways and autophagy upon Listeria monocytogenes infection. *Nat Commun, 10*(1), 5383. doi:10.1038/s41467-019-13393-x

Zhao, C., Denison, C., Huibregtse, J. M., Gygi, S., & Krug, R. M. (2005). Human ISG15 conjugation targets both IFN-induced and constitutively expressed proteins functioning in diverse cellular pathways. *Proc Natl Acad Sci U S A, 102*(29), 10200-10205. doi:10.1073/pnas.0504754102

Zhao, C., Hsiang, T. Y., Kuo, R. L., & Krug, R. M. (2010). ISG15 conjugation system targets the viral NS1 protein in influenza A virus-infected cells. *Proc Natl Acad Sci U S A, 107*(5), 2253-2258. doi:10.1073/pnas.0909144107

Zhao, C., Sridharan, H., Chen, R., Baker, D. P., Wang, S., & Krug, R. M. (2016). Influenza B virus non-structural protein 1 counteracts ISG15 antiviral activity by sequestering ISGylated viral proteins. *Nat Commun, 7*, 12754. doi:10.1038/ncomms12754

Zhao, H., Yang, J., Li, K., Ding, X., Lin, R., Ma, Y., . . . Wang, S. (2013). Proteomic analysis at the subcellular level for host targets against influenza A virus (H1N1). *Antiviral Res, 100*(3), 673-687. doi:10.1016/j.antiviral.2013.10.005

Zhao, Y. Y., Wu, S. P., Liu, S., Zhang, Y., & Lin, R. C. (2014). Ultra-performance liquid chromatography-mass spectrometry as a sensitive and powerful technology in lipidomic applications. *Chem Biol Interact, 220*, 181-192. doi:10.1016/j.cbi.2014.06.029

Zhou, X., & Zheng, Y. (2013). Cell type-specific signaling function of RhoA GTPase: lessons from mouse gene targeting. *J Biol Chem, 288*(51), 36179-36188. doi:10.1074/jbc.R113.515486

Zhu, L., Luo, X., Fu, N., & Chen, L. (2021). Mitochondrial unfolded protein response: A novel pathway in metabolism and immunity. *Pharmacol Res, 168*, 105603. doi:10.1016/j.phrs.2021.105603

Zou, W., Kim, J. H., Handidu, A., Li, X., Kim, K. I., Yan, M., . . . Zhang, D. E. (2007). Microarray analysis reveals that Type I interferon strongly increases the expression of immune-response related genes in Ubp43 (Usp18) deficient macrophages. *Biochem Biophys Res Commun, 356*(1), 193-199. doi:10.1016/j.bbrc.2007.02.101

ANNEXES

PLOS | PATHOGENS

RESEARCH ARTICLE

ISG15 governs mitochondrial function in macrophages following vaccinia virus infection

Sara Baldanta[1☯¤], Mercedes Fernández-Escobar[1☯¤], Rebeca Acín-Perez[2☯], Manuel Albert[1☯¤], Emilio Camafeita[3,4], Inmaculada Jorge[3,4], Jesús Vázquez[3,4], José Antonio Enríquez[2], Susana Guerra[1¤]*

1 Department of Preventive Medicine, Public Health and Microbiology, Universidad Autónoma, Madrid, Spain, **2** Functional Genetics of the Oxidative Phosphorylation System, Centro Nacional de Investigaciones Cardiovasculares Carlos III; Madrid (SPAIN), **3** Laboratory of Cardiovascular Proteomics, Centro Nacional Investigaciones Cardiovasculares Carlos III (CNIC), Madrid (SPAIN), **4** Laboratory of Cardiovascular Proteomics, Centro Nacional de Investigaciones Cardiovasculares Carlos III (CNIC) and CIBER de Enfermedades Cardiovasculares (CIBER-CV), Madrid (SPAIN)

☯ These authors contributed equally to this work.
¤ Current address: Department of Preventive Medicine and Public Health, Universidad Autónoma, Madrid, Spain
* susana.guerra@uam.es

Citation: Baldanta S, Fernández-Escobar M, Acín-Perez R, Albert M, Camafeita E, Jorge I, et al. (2017) ISG15 governs mitochondrial function in macrophages following vaccinia virus infection. PLoS Pathog 13(10): e1006651. https://doi.org/10.1371/journal.ppat.1006651

Editor: Deborah J. Lenschow, Washington University School of Medicine, UNITED STATES

Received: March 2, 2017

Accepted: September 17, 2017

Published: October 27, 2017

Data Availability Statement: All relevant data are within the paper and its Supporting Information files.

Funding: This research is supported by a grant from Spanish Ministry of Economy and Competitiveness (MINECO) to SG (SAF2014-54623-R), and to JV from MINECO (BIO2015-67580-P) and from the Carlos III Institute of Health-Fondo de Investigación Sanitaria (PRB2, IPT13/0001—ISCIII-SGEFI/FEDER, ProteoRed). The funders had no role in study design, data

Abstract

The interferon (IFN)-stimulated gene 15 (*ISG15*) encodes one of the most abundant proteins induced by interferon, and its expression is associated with antiviral immunity. To identify protein components implicated in IFN and ISG15 signaling, we compared the proteomes of *ISG15*$^{-/-}$ and *ISG15*$^{+/+}$ bone marrow derived macrophages (BMDM) after vaccinia virus (VACV) infection. The results of this analysis revealed that mitochondrial dysfunction and oxidative phosphorylation (OXPHOS) were pathways altered in *ISG15*$^{-/-}$ BMDM treated with IFN. Mitochondrial respiration, Adenosine triphosphate (ATP) and reactive oxygen species (ROS) production was higher in *ISG15*$^{+/+}$ BMDM than in *ISG15*$^{-/-}$ BMDM following IFN treatment, indicating the involvement of ISG15-dependent mechanisms. An additional consequence of *ISG15* depletion was a significant change in macrophage polarization. Although infected *ISG15*$^{-/-}$ macrophages showed a robust proinflammatory cytokine expression pattern typical of an M1 phenotype, a clear blockade of nitric oxide (NO) production and arginase-1 activation was detected. Accordingly, following IFN treatment, NO release was higher in *ISG15*$^{+/+}$ macrophages than in *ISG15*$^{-/-}$ macrophages concomitant with a decrease in viral titer. Thus, *ISG15*$^{-/-}$ macrophages were permissive for VACV replication following IFN treatment. In conclusion, our results demonstrate that ISG15 governs the dynamic functionality of mitochondria, specifically, OXPHOS and mitophagy, broadening its physiological role as an antiviral agent.

collection and analysis, decision to publish, or preparation of the manuscript.

Competing interests: The authors have declared that no competing interests exist.

Author summary

Protein modification by ubiquitin and ubiquitin-like proteins is a key regulatory process of the innate and adaptive immune response. Interferon-stimulated gene 15 product (ISG15) is an ubiquitin-like protein modifier that can reversibly attach to different viral and cellular proteins, mediating potent antiviral responses. In turn, many viruses, including poxviruses, have evolved strategies to antagonize the antiviral and inflammatory effects of the innate immune response in order to keep infected cells alive until virus replication is complete. Here, we describe a novel role for ISG15 in the control of mitochondrial function. Post-translational modifications such as ISGylation regulate essential mitochondrial processes including respiration and mitophagy, and influence macrophage innate immunity signaling. These findings are clinically relevant since mitochondrial dysfunction is seen in many pathologies, such as infectious disease, cancer, and cardiovascular or neurological disorders, among others, underscoring the importance of the relationship between cellular metabolism and immune response.

Introduction

The type I interferon (IFN) signaling system is activated following viral infection, resulting in upregulation of interferon-stimulated genes (ISGs) that have diverse functions in the antiviral innate immune response. ISG15 is an IFN α/β-induced ubiquitin-like protein that exists in two distinct states: as a free molecule (intracellular and extracellular), or conjugated to lysine residues of target proteins (ISGylation). Biochemically, ISGylation occurs in a manner similar to ubiquitin conjugation, and is carried out in three main steps, activation, conjugation, and ligation, which are performed by ISG15-activating enzymes, ISG15-conjugating enzymes, and ISG15 E3 ligases, respectively [1]. As a reversible modification, ISG15 is removed from conjugated proteins by the ISG15-specific protease USP18 [2]. ISGylation has been shown to occur in a cotranslational process favoring modification of viral proteins in infected cells, which in turn obstructs virus assembly or function [3–5]. Furthermore, cellular proteins involved in antiviral defense or trafficking of viral particles have been shown to be ISGylated, supporting the antiviral function of ISG15 [5, 6]. Several viral proteins can be conjugated to ISG15, such as the non-structural NS1 protein from influenza A/B virus and the human immunodeficiency virus (HIV) Gag protein [7], which inhibits specific viral functions or virion assembly and blocks viral progression [8, 9]. The non-structural protein of influenza B virus 1 (NS1B) has been recently shown to antagonize ISGylation-mediated antiviral activity by binding and sequestering ISGylated viral proteins, primarily ISGylated viral nucleoproteins, to facilitate viral replication [10]. Moreover, ISG15 expression has been shown to disrupt the process of virus-budding *via* different mechanisms such as by blocking the endosomal sorting complexes required for transport (ESCRT machinery in HIV-infected cells) [11], or by inhibiting Nedd4 E3 ubiquitin ligase activity in the case of Ebola and other enveloped viruses [12].

Studies in mice have demonstrated a credible role for ISG15 in antiviral immunity. Accordingly, mice lacking ISG15 have enhanced susceptibility to several pathogens including viruses [13] and bacteria [14, 15], and this phenotype is rescued in USP18-mutant mice in which high levels of ISG15 conjugates are observed [16]. By contrast, human ISG15 has essential immune functions, but not in antiviral immunity. Specifically, free extracellular human ISG15 is crucial for IFN-γ-dependent antimycobacterial immunity [17], while free intracellular ISG15 is important for USP18-mediated downregulation of IFN-α/β signaling [18]. A recent

publication has demonstrated that ISG15 deficiency is related to increased viral resistance in humans, but not in mice [19].

Our previous work demonstrated that ISG15 plays an important role in vaccinia virus (VACV) infection [20, 21], and in the regulation of macrophage responses. Accordingly, *ISG15*$^{-/-}$ macrophages display reduced activation, phagocytic capacity and programmed cell death in response to VACV infection [22]. In addition to the antiviral role associated with ISGylation, we also showed that ISG15 secreted by tumor-associated macrophages plays a critical support role for pancreatic cancer stem cells [23]. Macrophages are specialized antigen presenting cells that have important functions in innate defense against infection, in clearance of host infected cells and molecules, and in viral antigen presentation [24]. Macrophages are characterized by high phenotypic plasticity including the ability to polarize to an "activated or M1" or an "alternatively-activated or M2" form in response to environmental signals (reviewed in [25, 26]). M1 macrophages are defined by their strong inflammatory cytokine secretion and production of NO, resulting in an effective pathogen killing mechanism [27, 28]. By contrast, M2 macrophages have high phagocytic capacity and promote tissue repair/remodeling during wound healing.

Mitochondria have recently been shown to have essential roles in the immune system, particularly in regulating macrophage responses to pathogen infections [29], tissue damage and inflammation. Consequently, defects in macrophages functionality can lead to chronic inflammation in different animal models [30]. Polarization of macrophages to pro-inflammatory (M1) or anti-inflammatory (M2) phenotypes results in distinct metabolic reprogramming, which corresponds to the progression or resolution of inflammation, respectively. Moreover, mitochondria regulate other mechanisms that are important for the response to viral infection, such as apoptosis, and there is evidence that the regulation of cell death in the mitochondrial-mediated antiviral immunity depends on their metabolism.

In the present study, we observed that several proteins from mitochondria are ISGylated, and that ISG15 regulates multiple mitochondrial processes including metabolism and mitophagy, a specialized form of autophagy involving the selective degradation and recycling of mitochondria. We also found that ISG15 modulates macrophage polarization, which has been shown to be dependent on cellular metabolism [31], suggesting that the antiviral effect of ISG15 may also be due to the fine regulation of its polarization. In summary, we demonstrate that ISG15 regulates the functionality and stability of mitochondria, which are essential for cellular homeostasis. Given the large number of pathologies associated with mitochondrial dysfunction, including infectious diseases, heart damage, mental disorders and cancer, among others, the elucidation of the mechanisms by which ISG15 controls this organelle is an important future challenge.

Results

ISG15 controls cellular metabolism and mitochondrial activity

It has been previously shown that several macrophage mitochondrial proteins are specific targets of ISGylation [14, 32], suggesting an important role for ISG15 in mitochondria of these cells. We therefore sought to explore the involvement of ISG15 in mitochondrial metabolism in macrophages. To gain a comprehensive overview of cellular protein dynamics regulated by ISG15, we analyzed total proteomes of murine IFN-treated bone marrow-derived macrophages (BMDM) from *ISG15*$^{+/+}$ and *ISG15*$^{-/-}$ mice. As illustrated in Fig 1, the absence of ISG15 led to a change in the expression of specific molecules involved in several functions including OXPHOS, mitochondrial dysfunction, phagocytosis, integrin signaling, cellular trafficking and ubiquitin modifications. Of particular interest was the observation that expression

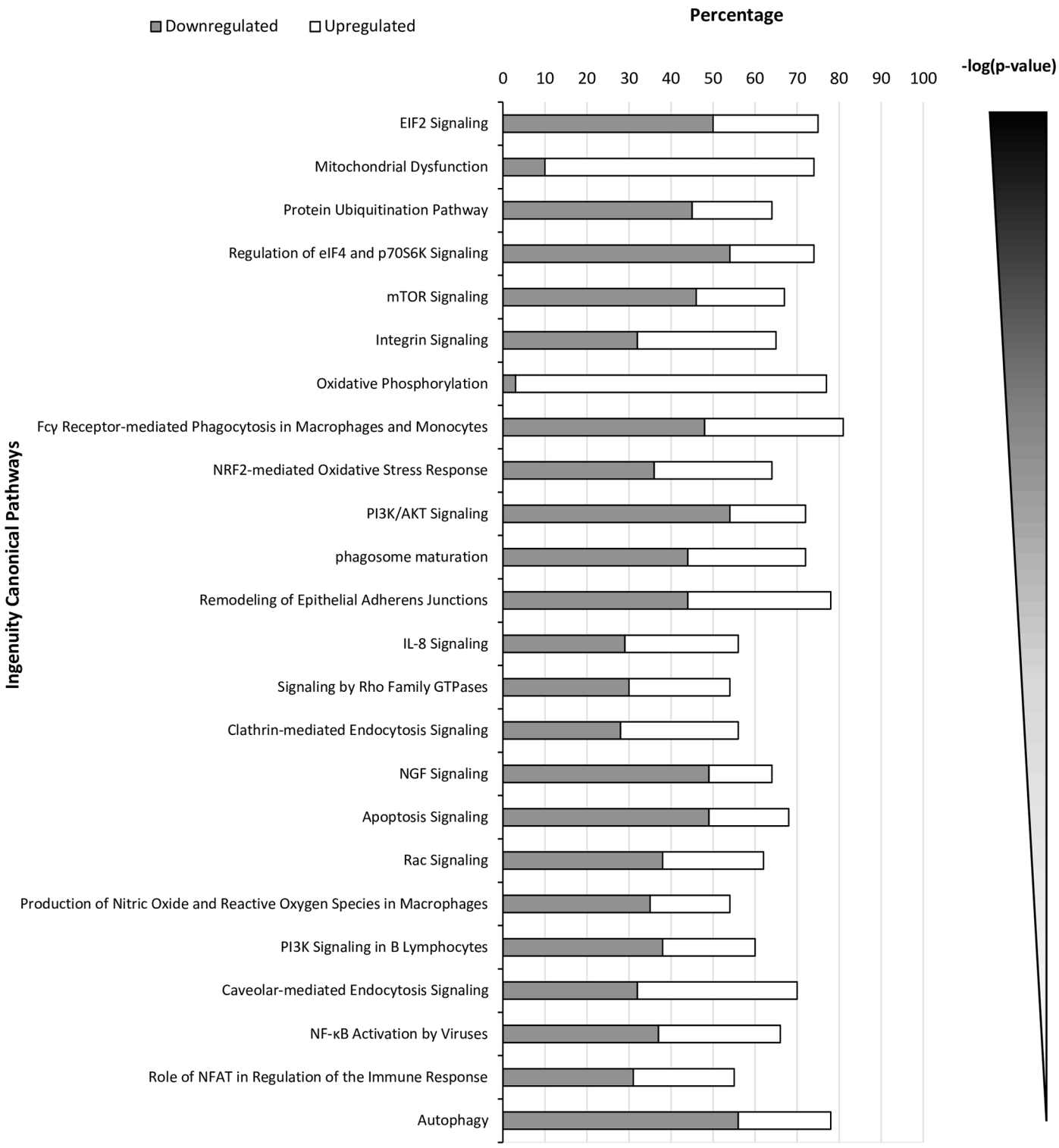

Fig 1. Comparative proteomics analysis of *ISG15*$^{-/-}$ *versus ISG15*$^{+/+}$ IFN-treated BMDM. Ingenuity pathway analysis showing selected canonical pathways differently modulated in *ISG15*$^{-/-}$ *versus ISG15*$^{+/+}$ positives values IFN-treated BMDM ($p < 0.05$). Percentage of proteins down- or up-regulated in selected canonical pathways differently modulated in *ISG15*$^{-/-}$ *versus ISG15*$^{+/+}$ BMDM after pretreatment with IFN (500 units/ml, 16 hours) ($p < 0.05$).

https://doi.org/10.1371/journal.ppat.1006651.g001

levels of several proteins related to OXPHOS and oxidative stress response differed between *ISG15*$^{+/+}$ and *ISG15*$^{-/-}$ BMDM, pointing to the involvement of ISG15 in these mitochondrial processes (Table 1).

To investigate the role of ISG15 and ISGylation in macrophages, we evaluated the presence of ISGylated proteins in total extracts from *ISG15*$^{+/+}$ and *ISG15*$^{-/-}$ BMDM infected or not with VACV, or pre-treated or not with IFN. A clear increase in ISGylation levels was observed in IFN-treated *ISG15*$^{+/+}$ BMDM but not in equivalent non-treated VACV-infected cells (Fig 2A). To characterize further the subcellular localization of these proteins, we evaluated in uninfected BMDM ISGylation in total, or cytoplasmic or mitochondrial proteins extracts. We observed ISGylated proteins in all fractions and their levels increased following IFN pre-treatment (Fig 2B). As the proteomic study indicated that several mitochondrial processes were regulated by ISG15 (Table 1), we focused our attention on this organelle. In concordance with our data, a clear activation of ISG15 in the mitochondrial proteome of cells infected with influenza virus has been previously reported [33], demonstrating a causal link between mitochondria and ISG15. To study the intra-mitochondrial localization of the ISGylated proteins, we performed proteinase K assays using isolated mitochondria, and thus only proteins localized in the outer membrane are sensitive to proteolytic cleavage. The majority of the ISGylated proteins were resistant to proteinase K (PK) (Fig 2C), indicating a possible localization in the intermembrane compartment (IC), inner membrane (IM) or in the matrix. The same result was found for mitochondria isolated from IFN-treated cells, albeit with an elevated expression of ISGylated proteins (Fig 2C). To examine deeper if ISG15 and ISGylated proteins localized, we performed a PK digestion combined with digitonin permeabilization in isolated mitochondria as previously described [34]. In addition, we performed a PK assay with osmotic shock (OS) with or without Triton X-100 as was described [35]. We used TOMM20 as an OM, TIMM23 as an IM and SOD2 as a matrix protein as controls of the indicated mitochondrial compartments. The experiments depicted in Fig 2D showed that ISG15 and ISGylated proteins displayed resistance to PK treatment in isolated mitochondria, but became accessible to protease digestion at elevated digitonin concentration and also when the OM was disrupted by OS. The integrity of the mitochondria was lost when we incubated it with OS and TritonX-100, this was the unique condition in which SOD2 localized in the matrix was accessible to PK [36]. Consequently, we concluded that the localization of monomeric ISG15 is localized in the IC, and ISGyated proteins can be localized mostly in the IC or IM but also in the matrix (Fig 2D).

To assess the role of ISG15 in mitochondria in more detail, we first analyzed the metabolic consequences of *ISG15* deletion in BMDM by measuring respiratory parameters with the Seahorse Biosciences Flux Analyzer platform. We measured the oxygen consumption rate (OCR) in non-infected or infected *ISG15*$^{+/+}$ and *ISG15*$^{-/-}$ BDBM treated or not with IFN to gauge mitochondrial OXPHOS. Basal OCR is an indicator of the normal respiration rate of cells in physiological conditions, whereas maximal OCR is reached following stimulation of the mitochondrial electron transport chain (ETC) with a potent protonophore such as carbonyl cyanide-4-(trifluoromethoxy)phenylhydrazone (FCCP). In non IFN-treated cells, similar respiration levels were observed in *ISG15*$^{+/+}$ and *ISG15*$^{-/-}$ BMDM uninfected or at early times post-infection. However, following IFN treatment, both basal and maximal OCR levels in non-infected *ISG15*$^{+/+}$ cells were significantly higher than those in non-infected *ISG15*$^{-/-}$ BMDM (Fig 3A and 3B). At 2 hours post-infection (hpi), respiratory levels were slightly reduced in *ISG15*$^{-/-}$ BMDM (Fig 3A and 3B), but at later stages there was a similar decrease in the OCR (both basal and FCCP-induced) in both populations, indicating that viral infection reduces OXPHOS (S1 Fig).

In agreement with the reduction in OXPHOS, a clear decrease in mitochondrial ATP production was observed in IFN-treated *ISG15*$^{-/-}$ BMDM when compared with *ISG15*$^{+/+}$ BMDM

Table 1. Representative protein abundance changes in the *ISG15*$^{-/-}$ vs *ISG15*$^{+/+}$ comparison in BMDM. Positive/negative values indicate increased/decreased abundance in *ISG15*$^{-/-}$ as compared to *ISG15*$^{+/+}$.

Ingenuity Canonical Pathways	Symbol	Description	Standardized log2 (Fold change)
	ISG15	Ubiquitin-like protein ISG15	-18,42
Apoptosis signaling	FSCN1	Fascin	4,68
	BAK	Bcl-2 homologous antagonist/killer	4,50
	CYC	Cytochrome c, somatic	4,20
	SPTN1	Spectrin alpha chain, non-erythrocytic 1	3,53
	KPCA	Protein kinase C alpha type	3,15
	CAN1	Calpain-1 catalytic subunit	2,10
	MK01	Mitogen-activated protein kinase 1	-2,40
	B2L11	Bcl-2-like protein 11	-2,69
	ACINU	Apoptotic chromatin condensation inducer in the nucleus	-2,80
	MK03	Mitogen-activated protein kinase 3	-3,02
	BIR1A	Baculoviral IAP repeat-containing protein 1a	-3,04
	MCL1	Induced myeloid leukemia cell differentiation protein Mcl-1 homolog	-3,31
	BAX	Apoptosis regulator BAX	-3,56
	IKBB	NF-kappa-B inhibitor beta	-3,57
	PLCG2	1-phosphatidylinositol 4,5-bisphosphate phosphodiesterase gamma-2	-3,98
	BID	BH3-interacting domain death agonist	-4,06
	NFKB2	Nuclear factor NF-kappa-B p100 subunit	-4,27
	KS6A1	Ribosomal protein S6 kinase alpha-1	-4,55
	CAN2	Calpain-2 catalytic subunit	-5,50
	MP2K2	Dual specificity mitogen-activated protein kinase kinase 2	-5,58
	MP2K1	Dual specificity mitogen-activated protein kinase kinase 1	-12,29
Autophagy	LAMP1	Lysosome-associated membrane glycoprotein 1	-2,14
	STX17	Syntaxin-17	-2,27
	VPS11	Vacuolar protein sorting-associated protein 11 homolog	-2,75
	ATG3	Ubiquitin-like-conjugating enzyme ATG3	-2,81
	ATG7	Ubiquitin-like modifier-activating enzyme ATG7	-2,90
	VPS18	Vacuolar protein sorting-associated protein 18 homolog	-4,55
	SQSTM	Sequestosome-1	-8,90
Mitochondrial Dysfunction	AOFA	Amine oxidase [flavin-containing] A	16,29
	ACON	Aconitate hydratase, mitochondrial	10,94
	ODO1	2-oxoglutarate dehydrogenase, mitochondrial	10,07
	CPT1A	Carnitine O-palmitoyltransferase 1, liver isoform	8,31
	GSHR	Glutathione reductase, mitochondrial	8,25
	PRDX5	Peroxiredoxin-5, mitochondrial	7,56
	GPDM	Glycerol-3-phosphate dehydrogenase, mitochondrial	7,24
	VDAC1	Voltage-dependent anion-selective channel protein 1	7,05
	SODM	Superoxide dismutase [Mn], mitochondrial	6,76
	VDAC3	Voltage-dependent anion-selective channel protein 3	4,79
	FIS1	Mitochondrial fission 1 protein	4,20
	VDAC2	Voltage-dependent anion-selective channel protein 2	3,79
	ODPA	Pyruvate dehydrogenase E1 component subunit alpha, somatic form, mitochondrial	3,70
	HCD2	3-hydroxyacyl-CoA dehydrogenase type-2	3,51
	MK09	Mitogen-activated protein kinase 9	-2,95
	PARK7	Protein deglycase DJ-1	-4,58
	PSN2	Presenilin-2	-5,58
	LRRK2	Leucine-rich repeat serine/threonine-protein kinase 2	-8,69
Mitochondrial Dysfunction and apoptosis signaling	AIFM1	Apoptosis-inducing factor 1, mitochondrial	5,48
	CASP8	Caspase-8	-3,74
	CASP3	Caspase-3	-3,77
Oxidative Phosphorylation	CYC2	Cytochrome c, testis-specific	2,49
Ingenuity Canonical Pathways	**Symbol**	**Description**	**Standardized log2 (Fold change)**

(*Continued*)

Table 1. (*Continued*)

Mitochondrial Dysfunction and Oxidative Phosphorylation	NDUB2	NADH dehydrogenase [ubiquinone] 1 beta subcomplex subunit 2, mitochondrial	40,54
	SDHB	Succinate dehydrogenase [ubiquinone] iron-sulfur subunit, mitochondrial	9,34
	SDHA	Succinate dehydrogenase [ubiquinone] flavoprotein subunit, mitochondrial	8,30
	ATPA	ATP synthase subunit alpha, mitochondrial	8,15
	ATPB	ATP synthase subunit beta, mitochondrial	7,48
	ATPG	ATP synthase subunit gamma, mitochondrial	6,74
	QCR1	Cytochrome b-c1 complex subunit 1, mitochondrial	5,74
	QCR7	Cytochrome b-c1 complex subunit 7	5,73
	NDUAA	NADH dehydrogenase [ubiquinone] 1 alpha subcomplex subunit 10, mitochondrial	5,38
	QCR2	Cytochrome b-c1 complex subunit 2, mitochondrial	5,15
	ATP5J	ATP synthase-coupling factor 6, mitochondrial	4,90
	NDUS1	NADH-ubiquinone oxidoreductase 75 kDa subunit, mitochondrial	4,80
	NDUS3	NADH dehydrogenase [ubiquinone] iron-sulfur protein 3, mitochondrial	4,76
	NDUV3	NADH dehydrogenase [ubiquinone] flavoprotein 3, mitochondrial	4,71
	QCR9	Cytochrome b-c1 complex subunit 9	4,69
	NDUS8	NADH dehydrogenase [ubiquinone] iron-sulfur protein 8, mitochondrial	4,61
	AT5F1	ATP synthase F(0) complex subunit B1, mitochondrial	4,59
	ACPM	Acyl carrier protein, mitochondrial	4,53
	NDUA4	Cytochrome c oxidase subunit NDUFA4	4,52
	ATPO	ATP synthase subunit O, mitochondrial	4,51
	ATP5H	ATP synthase subunit d, mitochondrial	4,24
	CYC	Cytochrome c, somatic	4,20
	COX2	Cytochrome c oxidase subunit 2	4,16
	C560	Succinate dehydrogenase cytochrome b560 subunit, mitochondrial	3,97
	NDUV1	NADH dehydrogenase [ubiquinone] flavoprotein 1, mitochondrial	3,81
	NDUA5	NADH dehydrogenase [ubiquinone] 1 alpha subcomplex subunit 5	3,65
	QCR8	Cytochrome b-c1 complex subunit 8	3,50
	NDUS6	NADH dehydrogenase [ubiquinone] iron-sulfur protein 6, mitochondrial	3,41
	CY1	Cytochrome c1, heme protein, mitochondrial	3,40
	NDUAD	NADH dehydrogenase [ubiquinone] 1 alpha subcomplex subunit 13	3,38
	NDUS2	NADH dehydrogenase [ubiquinone] iron-sulfur protein 2, mitochondrial	3,29
	CYB	Cytochrome b	3,10
	NDUS7	NADH dehydrogenase [ubiquinone] iron-sulfur protein 7, mitochondrial	3,01
	NDUS4	NADH dehydrogenase [ubiquinone] iron-sulfur protein 4, mitochondrial	2,96
	NDUBA	NADH dehydrogenase [ubiquinone] 1 beta subcomplex subunit 10	2,92
	ATP5L	ATP synthase subunit g, mitochondrial	2,89
	NU4M	NADH-ubiquinone oxidoreductase chain 4	2,89
	COX5A	Cytochrome c oxidase subunit 5A, mitochondrial	2,83
	NDUA6	NADH dehydrogenase [ubiquinone] 1 alpha subcomplex subunit 6	2,61
	COX1	Cytochrome c oxidase subunit 1	2,60
	NDUB5	NADH dehydrogenase [ubiquinone] 1 beta subcomplex subunit 5, mitochondrial	2,58
	NDUA7	NADH dehydrogenase [ubiquinone] 1 alpha subcomplex subunit 7	2,57
	NDUA3	NADH dehydrogenase [ubiquinone] 1 alpha subcomplex subunit 3	2,40
	NDUB8	NADH dehydrogenase [ubiquinone] 1 beta subcomplex subunit 8, mitochondrial	2,38
	ATPK	ATP synthase subunit f, mitochondrial	2,28
	NDUA8	NADH dehydrogenase [ubiquinone] 1 alpha subcomplex subunit 8	2,16
	COX41	Cytochrome c oxidase subunit 4 isoform 1, mitochondrial	2,13
	NDUA9	NADH dehydrogenase [ubiquinone] 1 alpha subcomplex subunit 9, mitochondrial	2,10
	AT5G1	ATP synthase F(0) complex subunit C1, mitochondrial	2,09
	ATP5E	ATP synthase subunit epsilon, mitochondrial	2,07
	ATPD	ATP synthase subunit delta, mitochondrial	2,06

https://doi.org/10.1371/journal.ppat.1006651.t001

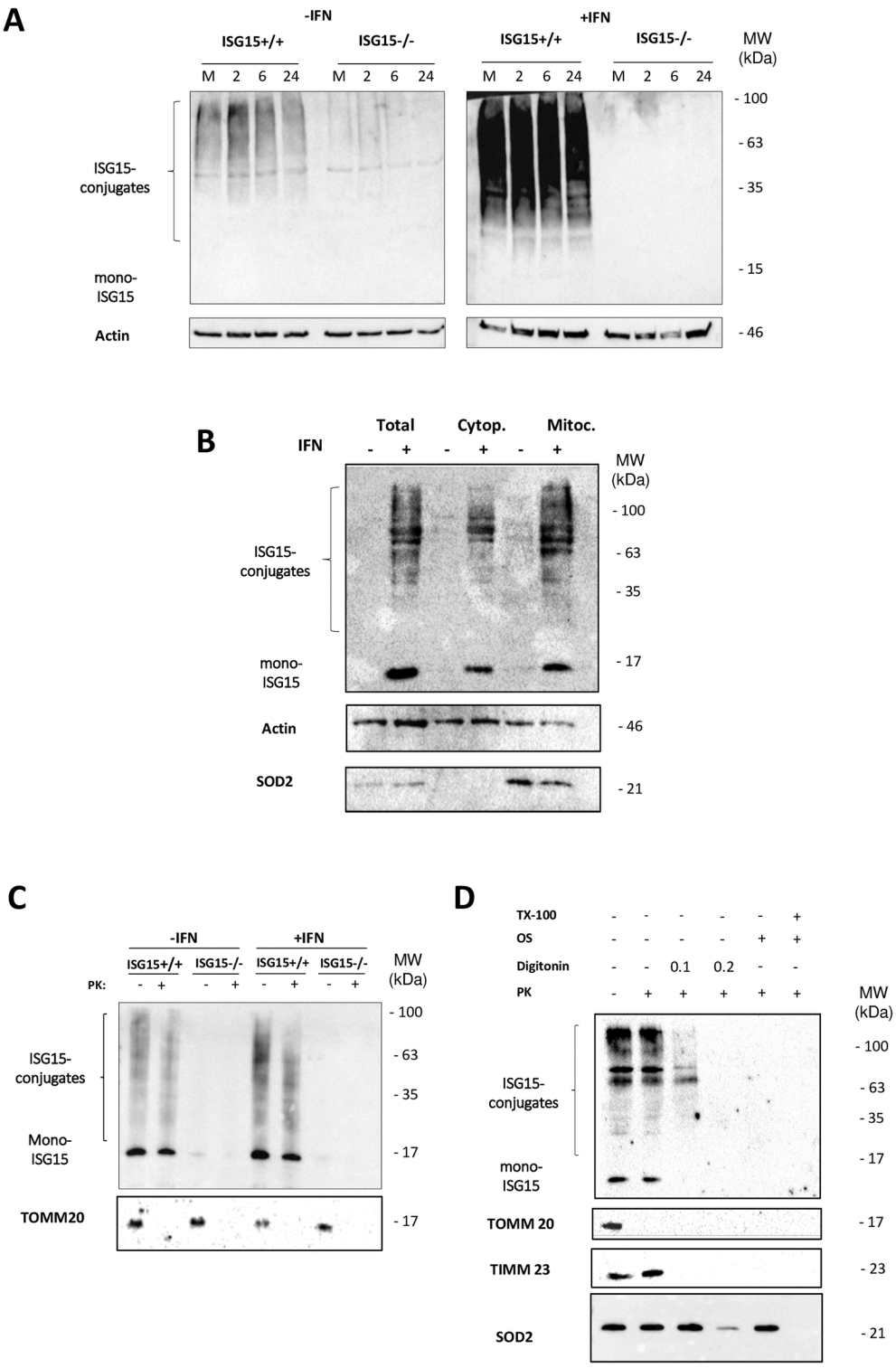

Fig 2. ISGylation in non-treated or IFN-treated *ISG15*$^{+/+}$ or *ISG15*$^{-/-}$ BMDM infected or not with VACV. **(A)** *ISG15*$^{+/+}$ and *ISG15*$^{-/-}$ BMDM pretreated or not with IFN (500 units/ml, 16 hours) were infected (1 PFU/cell) with VACV and total protein extracts collected at mock, 2, 6 and 24 hpi and were fractionated by 12% SDS-PAGE, transferred to nitrocellulose membranes, and incubated with anti-ISG15 antibody. Molecular weights (MWs) are indicated. **(B)**. Total or cytoplasmic or mitochondria protein extracts from *ISG15*$^{+/+}$ and *ISG15*$^{-/-}$ BMDM pretreated or not with IFN (500 units/ml, 16 hours) were obtained (20 μg) and were

fractionated by 12% SDS-PAGE, transferred to nitrocellulose membranes, and incubated with anti-ISG15, anti-SOD2 (specific mitochondrial control) or anti-actin (specific cytoplamatic control) antibodies. MWs are indicated. **(C)** Validation of the localization of ISGylated proteins by proteinase K treatment of intact mitochondria. A total of 15 μg of hypotonically isolated mitochondria from *ISG15*$^{+/+}$ or *ISG15*$^{-/-}$ BMDM, IFN treated or not, were analyzed by western blotting (as above) using an ISG15 antibody. As a control of protease activity, TOMM20 levels were measured. Molecular weights are indicated. **(D)** Isolated mitochondria from *ISG15*$^{+/+}$ BMDM were subjected to proteinase K (50 μg/ml) combined with digitonin permeabilization, osmotic shock and 1% Triton X-100 incubation. After treatments as indicated, proteinase K activity was blocked with PMSF (2 mM) and proteins extracts were subjected to SDS-PAGE and western blotting analysis using antibodies against TOMM20, TIMM23, SOD2 and ISG15. MWs are indicated.

https://doi.org/10.1371/journal.ppat.1006651.g002

(Fig 3C). When we measured the extracellular acidification rate (ECAR) as an index of glycolysis and lactate production, we observed no differences between *ISG15*$^{+/+}$ and *ISG15*$^{-/-}$ BMDM (Fig 3D). Consistent with this finding, acidification rates of the culture medium for a period of up to 48 h were similar irrespective of the carbon source (glucose *vs* galactose) or the infection status, as assessed by color shift of the culture medium (S2 Fig). Furthermore, no major differences in the amount of mitochondrial deoxyribonucleic acid (DNA) (Fig 3E) or in the citrate synthase activity (Fig 3F), were observed between *ISG15*$^{+/+}$ and *ISG15*$^{-/-}$ BMDM when we compared the ratio changes compared the IFN- to non IFN-treated, suggesting that the amount of mitochondrial genome was unaltered after IFN treatment.

The mitochondrion is a major source of ROS. Superoxide (O2•−) is generated under specific bioenergetic conditions at several sites within the ETC [37]. When we evaluated whether ISG15 could have an effect on ROS production, we observed that ROS levels (assessed by MitoSOX) were increased after IFN treatment by an ISG15-dependent mechanism. Accordingly, ROS levels in non-infected IFN-treated *ISG15*$^{-/-}$ BMDM were significantly lower than in equivalent *ISG15*$^{+/+}$ BMDM (Fig 3G). When we measured ROS levels after infection, we found an increase only in *ISG15*$^{-/-}$ BMDM (Fig 3G), indicating that following VACV infection ROS accumulation occurs in *ISG15*$^{-/-}$ cells. These discrepancies in the ROS production in *ISG15*$^{+/+}$ *vs ISG15*$^{-/-}$ BMDM production may be due to a disturbance in the ETC, generating a different source of oxidative stress. To determine whether ISG15 or ISGylation impacts the mitochondria respiratory chain, we analyzed the ETC organization of *ISG15*$^{+/+}$ or *ISG15*$^{-/-}$ BMDM treated or not with IFN. For that, we performed blue-native (BN)-PAGE analysis of mitochondrial extract (100 μg) and we observed several differences in the ETC components from *ISG15*$^{-/-}$ mice in comparison to the WT (Fig 3H): (i) an absence of free complex I (CI); (ii) the presence of an upper band close to the supercomplex (SC) (I+III2) and (iii) the presence of a clear upper band close to the complex II (CII). This result indicated that the absence of ISG15 has an effect on mitochondrial complexes and supercomplexes rearrangements.

Mitochondria are dynamic organelles that continuously remodel to regulate their activity and to maintain integrity. These events include fission (mitochondrial fragmentation) and fusion (mitochondrial elongation), which control processes such as OXPHOS and apoptosis. Moreover, mitochondrial dynamics regulates mitophagy, as the number of mitochondria within cells is regulated by the equilibrium between biogenesis [38] and the removal of damaged mitochondria. Given that the proteomic study revealed autophagy as a cellular category significantly activated by ISG15 (Fig 1 and Table 1), we chose to analyze several autophagy/mitophagy markers by western blotting. After IFN treatment, a clear decrease in the steady-state levels of autophagy- related gene (ATG) 3, ATG5, ATG7 and light chain 3B protein (LC3B) was observed in *ISG15*$^{-/-}$ cells irrespective of VACV infection compare to those in ISG15$^{+/+}$ (Fig 4A and S3 Fig), indicating that ISG15 affects mitophagy in addition to mitochondrial respiration. Collectively, these data allow us to speculate that the mitophagy impairment in *ISG15*$^{-/-}$ BMDM might be linked to the increase in ROS levels observed after

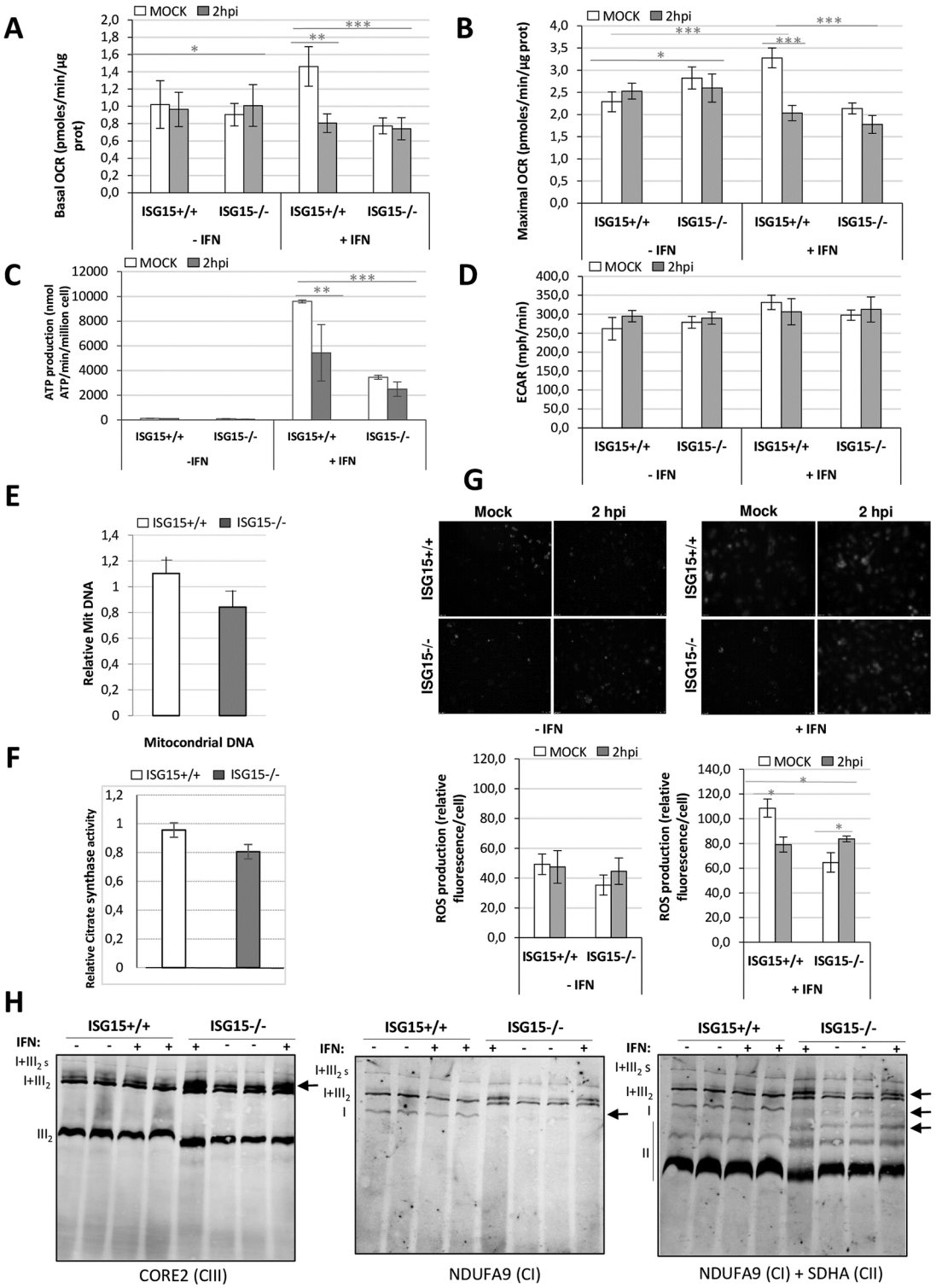

Fig 3. Characterization of the energy metabolism of VACV-infected *ISG15*$^{+/+}$ or *ISG15*$^{-/-}$ BMDM. *ISG15*$^{+/+}$ or *ISG15*$^{-/-}$ BMDM pretreated or not with IFN (500 units/ml, 16 hours) were infected (1 PFU/cell) with VACV at the times indicated. **(A-B)** Basal and maximal OCR rates were monitored using the Seahorse Biosciences extracellular flux analyzer. Results represent the mean ± the standard deviation of 4 biological replicates. **(C)** Mitochondrial ATP production was measured as indicated in materials and methods. **(D)** ECAR rates were monitored using the Seahorse Biosciences extracellular flux analyzer. **(E)** Variation of the mtDNA levels (MitoF) relative to nuclear DNA (B2) after IFN

treatment in *ISG15*$^{+/+}$ or *ISG15*$^{-/-}$ BMDM was quantified by real time PCR. For each condition, the data represent the ratio of mitochondrial DNA in untreated *vs* those after IFN treatment. Each point represents 3 independent samples measured in duplicate **(F)** Citrate synthase activity after IFN treatment in *ISG15*$^{+/+}$ or *ISG15*$^{-/-}$. In total cell extracts from *ISG15*$^{+/+}$ or *ISG15*$^{-/-}$ the citrate synthase activity was measured by spectrophotometric procedure. Each point represents 3 independent samples measured in duplicate. **(G)** ROS production was analyzed by fluorescence microscopy using MitoSOX Red in Mock or VACV-infected *ISG15*$^{+/+}$ or *ISG15*$^{-/-}$ IFN-treated or not BMDM. At the indicated times post-infection, relative ROS production was quantified using ImageJ software and represented as the relative fluorescence value in relation to that in non-infected cells. Significance was tested using a two-tailed t test assuming non-equal variance. In all cases $p < 0.01$. **(H)** Analysis of the electronic transport chain (ETC) complex. Isolated mitochondria from *ISG15*$^{+/+}$ or *ISG15*$^{-/-}$ BMDM pretreated or not with IFN (500 units/ml, 16 hours) were subjected to a blue native gel and the presence of the chain complex were analyzed using the following specific antibodies: anti-CORE2 for the complex III, anti- NDUFA9, for complex I and ant-SDHA for complex II.

https://doi.org/10.1371/journal.ppat.1006651.g003

VACV infection. Optic atrophy protein 1 (OPA1) is a major regulator of both mitochondrial dynamics and bioenergetics [39], and its level was elevated in IFN-treated *ISG15*$^{-/-}$ regarding to those in ISG15$^{+/+}$ macrophages, as detected by proteomics or western blotting (Fig 4B and S3 Fig). This finding suggests that ISG15 also controls mitochondrial fragmentation.

Mitophagy entails the formation of a double-membrane autophagosome and subsequent degradation of mitochondria by specific autophagy-lysosome pathways [40]. To study the mechanism by which ISG15 controls mitophagy, we first assessed the subcellular localization of the aggresome marker p62 because of its importance for the integration of mitochondrial and lysosomal biogenesis [41]. In the absence or presence of IFN treatment, no differences in p62 localization were observed between *ISG15*$^{+/+}$ and *ISG15*$^{-/-}$ non-infected BMDM. However, using a specific antibody that recognized the oxidative phosphorylation complex IV (COX4), an elongated mitochondrial morphology and an increase in the signal was observed in IFN-treated *ISG15*$^{-/-}$ in comparison to those in *ISG15*$^{+/+}$ cells (Fig 4C). These results were in line with the increased OPA1 levels and the reduced autophagy/mitophagy makers' levels in *ISG15*$^{-/-}$ observed in Fig 4A and 4B, and also with the increase in the supercomplexes detected by BN-PAGE (Fig 3F). Also we studied the oxidative phosphorylation complex IV protein levels by western blot in cytoplasmic or mitochondrial subcellular fractions from *ISG15*$^{+/+}$ or *ISG15*$^{-/-}$ BMDM treated or not with IFN. As is illustrated in Fig 4D, taking into account that the total protein levels loaded into the gel were similar in all the lines, a clear increase in COX4 and VDAC protein was observed in *ISG15*$^{-/-}$ BMDM, validating the result observed by microscopy (Fig 4C) and the proteomic analysis (Table 1). We next questioned whether ISGylation has a role in mitophagy mediated by Parkin, an E3 ubiquitin ligase that promotes degradation of dysfunctional mitochondria [42]. We first analyzed the protein levels of Parkin in cytoplasmic and mitochondrial fractions of BMDM from *ISG15*$^{+/+}$ and *ISG15*$^{-/-}$ mice treated or not with IFN. A clear increase of Parkin protein levels was observed after IFN treatment exclusively in *ISG15*$^{+/+}$ cytoplasmic and mitochondrial extracts. Surprisingly, in mitochondrial fraction from *ISG15*$^{-/-}$ BMDM (with or without IFN treatment) Parkin levels were dramatically reduced (Fig 4D).

ISG15 controls macrophages polarization and NO production. Cellular metabolism is implicated in macrophage polarization [31]. Particularly, classic (M1) *versus* M2 macrophage activation involves the expression of specific networks of metabolic enzymes intended to meet the energy demands of the activated cells [31]. M1 activation is associated with higher aerobic glycolysis and extracellular acidification rates, whereas M2-regulated gene transcription is implicated in mitochondrial metabolism and oxidative glucose metabolism [43, 44]. To study whether mitochondrial dysfunction correlated with changes in macrophage polarization after VACV infection, we analyzed BMDM phenotypes following exogenous polarization using specific treatments. After triggering specific M1 or M2 polarization, we observed that both *ISG15*$^{+/+}$ and *ISG15*$^{-/-}$ BMDM presented the same levels of inducible nitric oxide synthase

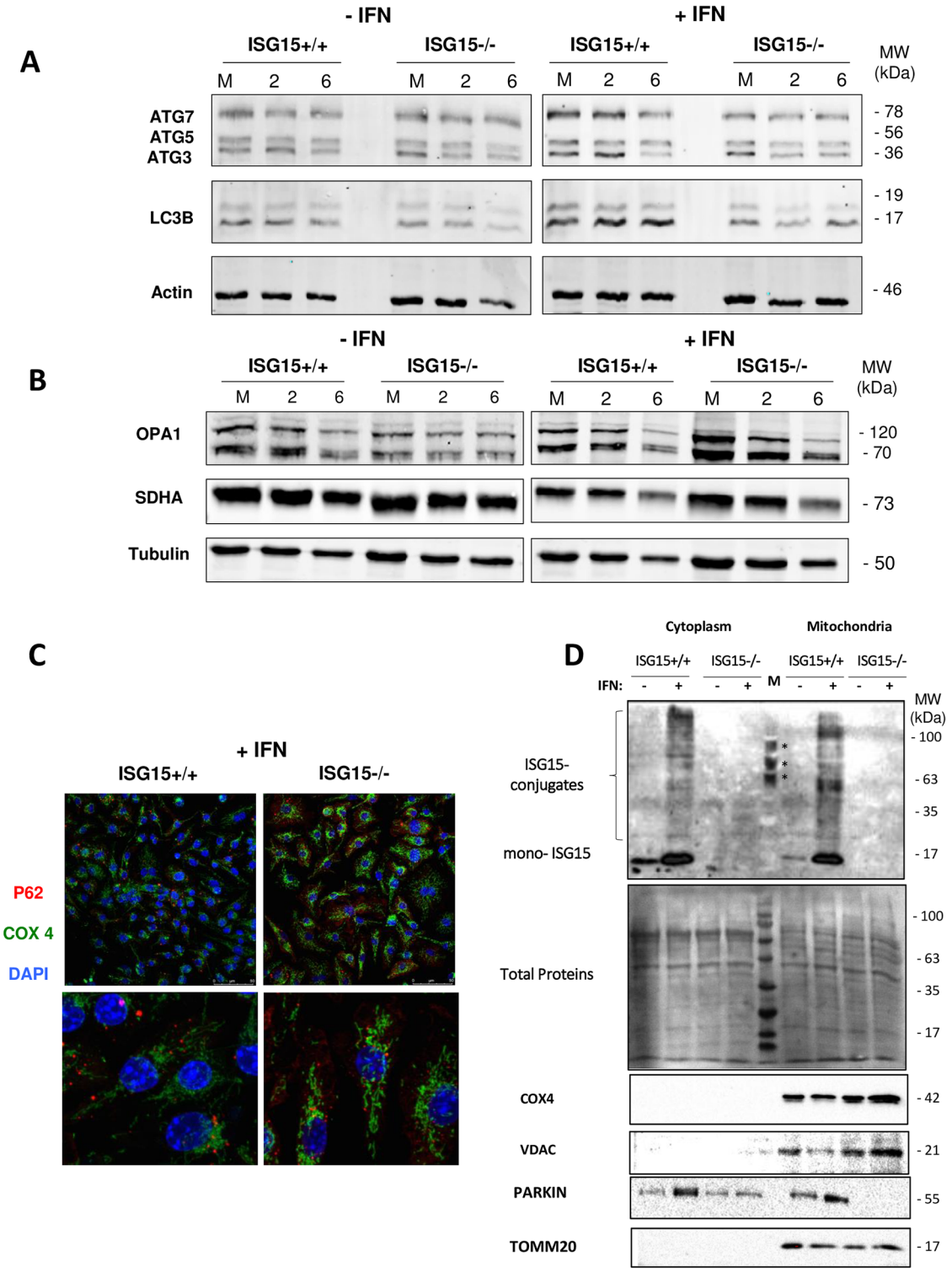

Fig 4. Mitophagy activity of *ISG15*$^{+/+}$ and *ISG15*$^{-/-}$ BMDM. (A) *ISG15*$^{+/+}$ or *ISG15*$^{-/-}$BMDMs treated or not with IFN (500 units/ml, 16 hours) were infected (1 PFU/cell) with VACV at the times indicated. Cellular lysates were analyzed by 12 or 7.5% SDS-PAGE followed by transfer to nitrocellulose membranes. The expression of ATG3, ATG5, ATG7, LC3B and β-actin (protein loading control) was detected by western blotting using specific antibodies. Molecular weights are indicated. **(B)** Altered levels of mitochondrial dynamism in ISG15$^{-/-}$ BMDM. *ISG15*$^{+/+}$ or *ISG15*$^{-/-}$ BMDMs treated or not with IFN (500 units/ml, 16 hours) were infected (1 PFU/cell) with VACV at the times indicated. Cellular lysates were analyzed by 12 or

7,5% SDS-PAGE, transferred to nitrocellulose membranes and the expression of OPA1, SDHA and tubulin (protein loading control) were detected by Western blot using specific antibodies. MWs are indicated. **(C)** Subcellular COX4 and p62 localization. Uninfected *ISG15*$^{+/+}$ or *ISG15*$^{-/-}$ BMDMs treated or not with IFN (500 units/ml, 16 hours) were fixed and stained using a specific COX4 and p62 antibodies post-infection. 4 ',6-diamino-2-fenilindol (DAPI) was used to stain DNA (blue). Cells were visualized by confocal immunofluorescence microscopy. The images show representative fields (×73 magnification). **(D)** Validation of mitochondrial protein in cytoplasmic or mitochondrial protein extracts from BMDM from IFN-treated or not *ISG15*$^{+/+}$ or *ISG15*$^{-/-}$ mice (20 μg). Proteins were fractionated by 12% SDS-PAGE, transferred to nitrocellulose membranes, and incubated with anti-TOMM20, anti-COX4, anti-Parkin or anti-VDAC proteins. Total protein loaded into the gel is visualized after Ponceau staining. The asterisks are signal specific for the protein molecular weight marker used. Molecular weights are indicated.

https://doi.org/10.1371/journal.ppat.1006651.g004

(iNOS) (M1 marker) and arginase-1 (Arg-1; M2 marker) protein by western blotting, independently of infection and of the presence of ISG15 (S4 Fig). By contrast, in VACV-infected non-polarized macrophages, iNOS expression was undetectable in both cell types and Arg-1 levels were considerably increased, especially in IFN-treated *ISG15*$^{-/-}$ BMDM (Fig 5A). The differences detected in Arg-1 protein levels were validated by measuring enzymatic Arg-1 activity (the hydrolysis of L-arginine to urea), showing that the absence of ISG15 was accompanied by an increase in Arg-1 activity (Fig 5B). In relation to the increased levels of Arg-1 protein in *ISG15*$^{-/-}$ BMDM, microarray analysis of IFN-treated and VACV-infected (6 h) *ISG15*$^{+/+}$ and *ISG15*$^{-/-}$ peritoneal macrophages revealed an increase in Arg-1 messenger ribonucleic acid (mRNA) levels in *ISG15*$^{-/-}$ cells, confirming the finding in BMDM (S1 Table). In addition, VACV-infected *ISG15*$^{-/-}$ BMDM presented an increase in the mRNA levels of the inflammatory cytokines tumor necrosis factor alpha (TNF-α), interferon beta (IFN-β), interleukin-6 (IL-6), interleukin-1 beta (IL-1β) and interleukin-12 (IL-12) (Fig 5C) and as measured by ELISA (Fig 5D), which was more marked following IFN treatment, (Fig 5C and 5D). The literature suggests that these cytokines are produced primarily by M1 macrophages and are commonly accompanied by an increase in NO production (4).

To explore whether the alterations in macrophage polarization impacted on VACV replication, we measured viral production by the plaque assay in *ISG15*$^{+/+}$ and *ISG15*$^{-/-}$ BMDM treated or not with IFN. In the absence of IFN treatment, VACV was able to grow in *ISG15*$^{+/+}$ and *ISG15*$^{-/-}$ BMDM at similar levels; however, viral production was slightly but significantly reduced following IFN treatment of *ISG15*$^{+/+}$ BMDM (Fig 6A). By contrast, viral replication was unaltered in *ISG15*$^{-/-}$ cells after IFN treatment. These results suggest that IFN-induced upregulation of ISG15 has a potential antiviral role by diminishing viral titers. A possible explanation for the relatively small decrease in viral titer could be that BMDM are resistant to VACV infection. As shown in Fig 6A, with a virus input of 10^5 plaque-forming units (PFU)/cell (MOI 1), viral load reached only 10^7 PFU/ml at 24 hpi. Considering that the VACV infection efficiency in BMDM is low, we believe that the decrease in titer after IFN treatment is relevant. Nevertheless, as a complementary approach to measure VAVC replication in BMDM, we used VACV labeled with YFP, which allowed us to follow viral progression confirmed our previous results. (S5 Fig). Collectively, these experiments confirm that whereas VACV is able to grow in BMDM, it is sensitive to IFN *via* a mechanism that is dependent on ISG15.

Finally, we asked whether the differences observed in proinflammatory cytokine production impacted on the production of NO. We thus measured NO levels in supernatants from *ISG15*$^{+/+}$ and *ISG15*$^{-/-}$ BMDM treated or not with IFN, before and after infection. A clear increase in NO production was observed following IFN treatment in *ISG15*$^{+/+}$ BMDM, which was maintained after infection (Fig 6B). By contrast, IFN treatment failed to increase NO levels in *ISG15*$^{-/-}$ macrophages (Fig 6B), suggesting that IFN treatment provokes an increase in NO production *via* an ISG15-dependent mechanism. To question whether the differences in viral titer between IFN-treated *ISG15*$^{+/+}$ and *ISG15*$^{-/-}$ BMDM were due to differences in NO levels,

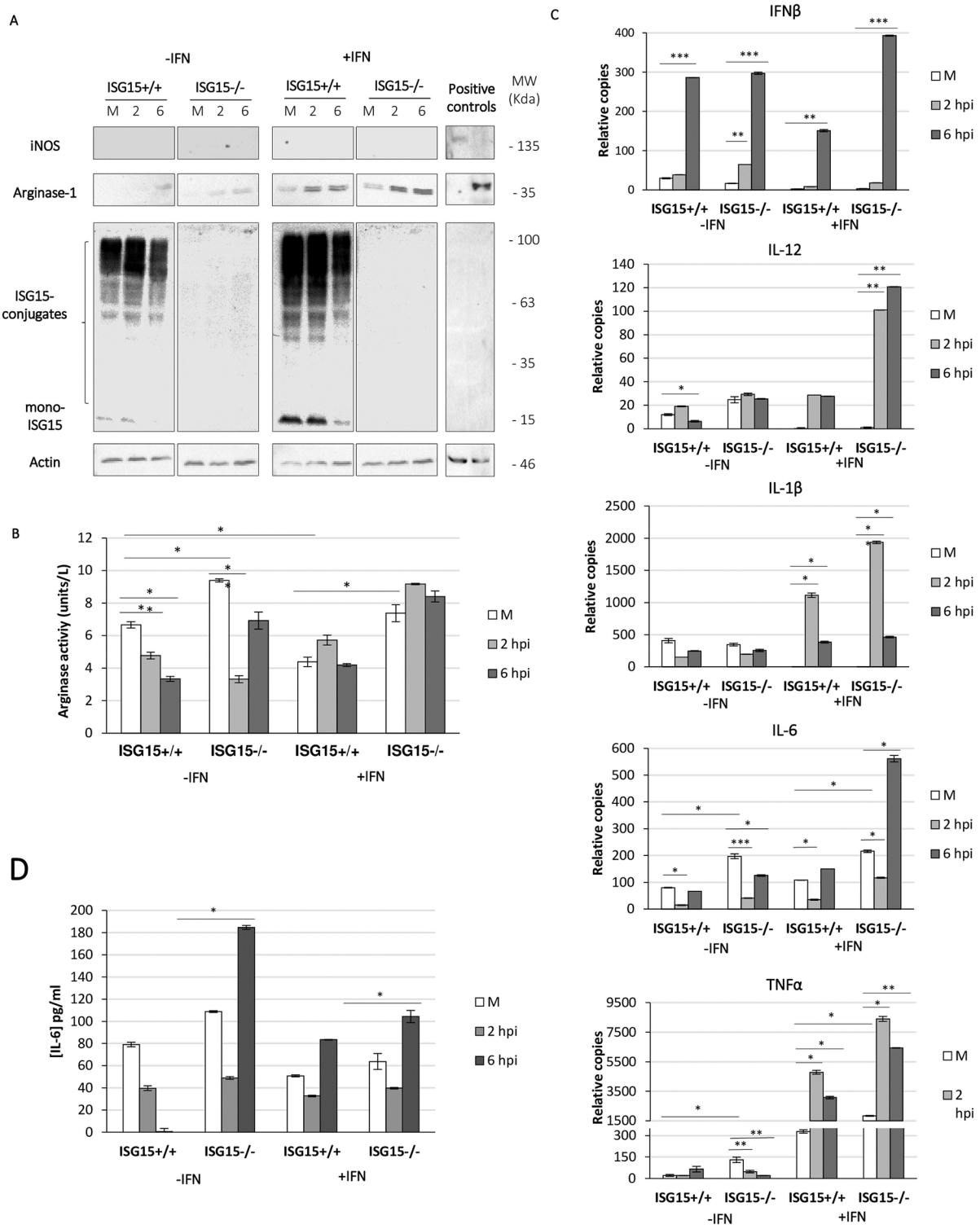

Fig 5. IFN and VACV infection increases proinflammatory cytokine levels in *ISG15*$^{-/-}$ BMDM and increases arginase-1 activity. (A) *ISG15*$^{+/+}$ or *ISG15*$^{-/-}$ BMDM were infected with VACV (1 PFU/cell). Cellular lysates collected at 2 and 6 hpi, or from mock-infected cultures, were analyzed by 12% SDS-PAGE, transferred to nitrocellulose membranes, and the expression of iNOS, Arg-1, ISG15 or β-actin (protein loading control) was examined by western blotting using specific antibodies. Uninfected M1 or M2 polarized *ISG15*$^{-/-}$ BMDM were used as iNOS or Arg-1 controls. **(B)** Under the same conditions as above, the production of urea was measured as a marker of Arg-1 activity. The reaction was performed following the indications of the manufacturer. Results

represent the mean ± the standard deviation of five biological replicates. **(C)** The expression level of TNF-α, IFN-β, IL-6, IL-1β and IL-12 genes was measured by quantitative RT-PCR. Triplicate samples were measured in three independent experiments; data shown is representative of one experiment. **(D)** IL-6 levels in the medium of *ISG15*$^{+/+}$ and *ISG15*$^{-/-}$ BMDM were quantified by ELISA. Aliquots (100 μl) of supernatant from *ISG15*$^{+/+}$ or *ISG15*$^{-/-}$ BMDM uninfected or at 2, 6, hpi were used for ELISA according to the manufacturer's instructions. Triplicate samples were measured in two independent experiments.

https://doi.org/10.1371/journal.ppat.1006651.g005

we added L-arginine (an iNOS substrate) to the culture medium and followed the viral progression and NO production. In IFN-treated *ISG15*$^{+/+}$ macrophages, addition of L-arginine increased NO levels (compare Fig 6B and 6D), which correlated with a reduction in the viral titer (compare Fig 6C and 6D), indicating that ISG15 is an essential requirement in BMDM for proper NO production, with functional consequences for VACV proliferation.

Discussion

Viruses exploit host cell metabolic resources to obtain energy and components required for replication. Changes in cellular metabolism correlate with viral infection efficacy, and a link has been established between the innate immune response and the host metabolic status [45]. Macrophages have a major role in the immune system as antimicrobial effectors that can regulate the adaptive immune response. Macrophages are polarized by microenvironmental signals to distinct functional programs, and L-arginine metabolism is a key aspect in this process as it acts as a substrate for two competing enzymes, iNOS and Arg-1. Macrophage M1 polarization and L-arginine metabolism by iNOS is characterized by an increase in glycolysis and a decrease in OXPHOS. By contrast, L-arginine metabolism by Arg-1 (M2 phenotype) is characterized by high levels of mitochondrial OXPHOS, fatty acid oxidation and augmented ATP synthesis [46, 47]. In this context, levels of OXPHOS in macrophages could also be used as an indicator of differential polarization and a determinant factor for viral progression. Mitochondria are multifunctional organelles with diverse roles including energy production and distribution, apoptosis and host immune response induction. It is increasingly evident that mitochondria have key roles in innate immune response against viral infections, and an association exists between mitochondrial metabolism and viral growth [48, 49]. Moreover, viruses manipulate mitochondrial processes to promote replication and produce progeny [50].

ISG15 is one of the most abundantly upregulated ISGs, and induces a post-translational modification termed ISGylation that conjugates ISG15 molecules to lysine residues of *de novo* synthesized viral or cellular proteins [1]. ISGylation can exert an antiviral pressure against some infections as has been described *in vitro* and/or *in vivo* for both DNA and RNA viruses [51, 52].

Here, we show that IFN and ISG15 have an essential role in regulating mitochondria functionally and specifically IFN increases mitochondrial proteins ISGylation (Fig 2). The mechanism by how the mitochondrial proteins are modified needs to be elucidated, because it can occur directly in the mitochondrial interior or in the cytoplasm. Although, we cannot rule out that ISGylation occurs in the mitochondria, for which all machinery should enter into the organelle considering that ISGylation is a cotranslational process, our hypothesis is that ISGylation occurs in the cytoplasm and once the mitochondrial proteins are modified, enter the mitochondria.

A proteomic analysis revealed that several mitochondrial pathways as mitochondrial dysfunction and OXPHOS were regulated by ISG15 (Fig 1). When we analyzed several mitochondrial related functions we observed that specifically, OXPHOS (Fig 3A) and mitophagy (Fig 4) were decrease in macrophages deficient in ISG15 and mitochondrial ROS production (Fig 3G) and macrophage polarization after VACV infection differs between *ISG15*$^{-/-}$ and

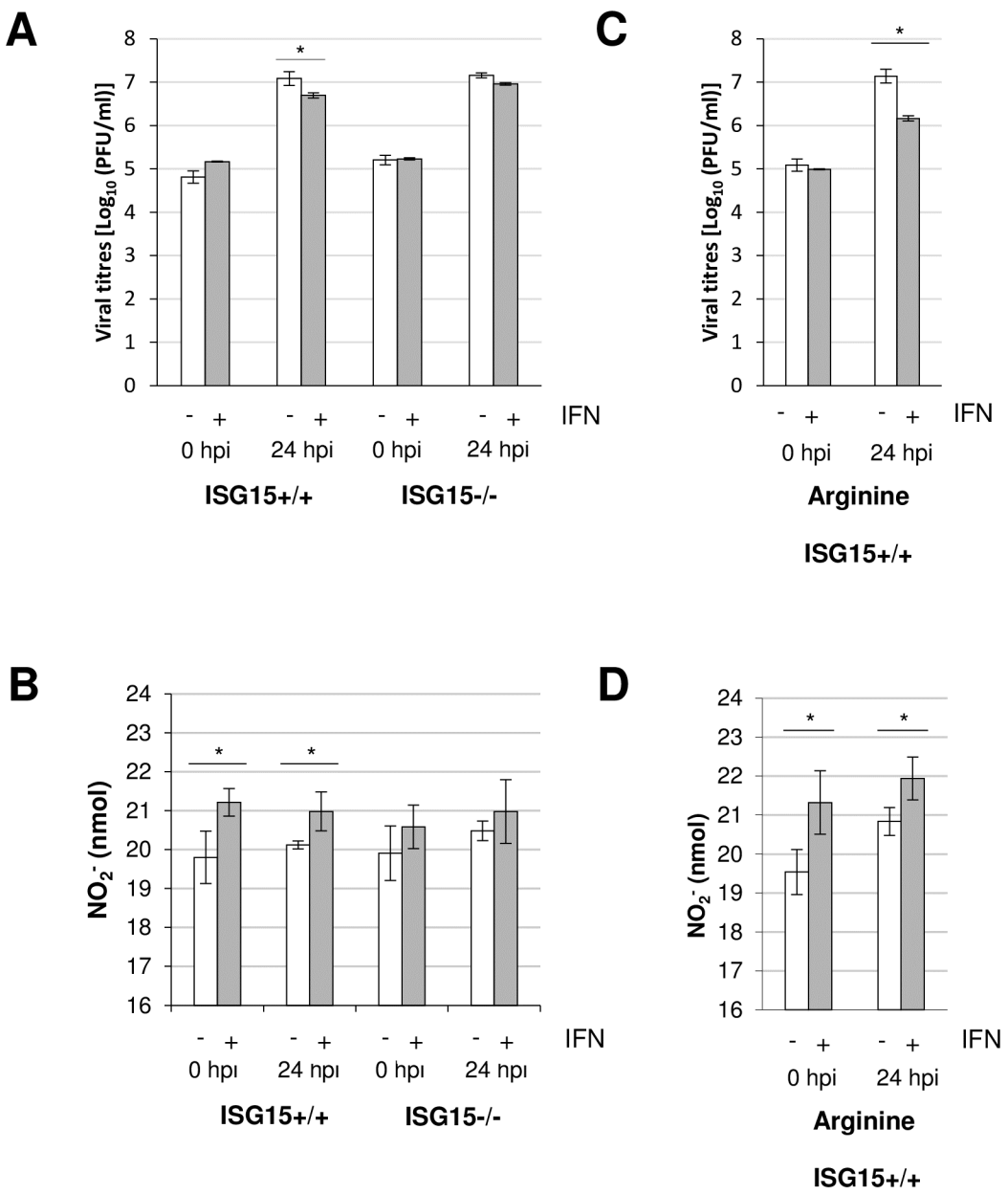

Fig 6. Effect of IFN on virus replication and NO production in VACV-infected *ISG15*$^{+/+}$ and *ISG15*$^{-/-}$ BMDM. **(A)** One-step VACV growth on infected (1 PFU/cell) *ISG15*$^{+/+}$ or *ISG15*$^{-/-}$ BMDM treated or not treated with IFN (500 units/ml, 16 hours). Cells were infected and at the times indicated cells were harvested and virus progression was determined by plaque assay. Results represent the mean ± the standard deviation of three independent experiments. Significance was tested using a two-tailed t test assuming non-equal variance. In all cases $p < 0.01$. **(B)** IFN treatment increases NO production in *ISG15*$^{+/+}$ BMDM. NO production was quantified using the Griess assay in the supernatant of *ISG15*$^{+/+}$ or *ISG15*$^{-/-}$ BMDM detailed above. Results represent the mean ± the standard deviation of three independent experiments. Significance was tested using a two-tailed t test assuming non-equal variance. In all cases $p < 0.01$. **(C)** Viral production in infected *ISG15*$^{+/+}$ BMDM in the presence of L-arginine (0.5 mM). Results represent the mean ± the standard deviation of three independent experiments. Significance was tested using a two-tailed t test assuming non-equal variance. In all cases $p < 0.01$. **(D)** NO release in infected *ISG15*$^{+/+}$ BMDM in the presence of L-arginine (0.5 mM). Results represent the mean ± the standard deviation of three independent experiments. Significance was tested a two-tailed t test assuming non-equal variance. In all cases $p < 0.01$.

https://doi.org/10.1371/journal.ppat.1006651.g006

ISG15$^{+/+}$ BMDM (Fig 5). Surprisingly, the collapse of mitochondrial stability and macrophage polarization in *ISG15*$^{-/-}$ BMDM corresponded with an advantage for viral replication because an increase in viral titers was observed. Regarding the mitochondrial parameters OXPHOS, ATP and ROS production, we found that IFN treatment produces an induction in OXPHOS exclusively in *ISG15*$^{+/+}$ BMDM (Fig 3). Given the demonstration that IFN triggers an increase in OXPHOS [53] and in mitochondrial ROS production [54], our data clearly indicate that IFN promotes these events *via* an ISG15-dependent mechanism, and thus *ISG15*$^{-/-}$ BMDM could be desensitized to the actions of IFN. Moreover, we observed several differences in the ETC organization from *ISG15*$^{+/+}$ or *ISG15*$^{-/-}$ BMDM. Particularly, in response to IFN treatment in *ISG15*$^{-/-}$ BMDM the ETC architecture was altered with a decrease in the abundance of free CI and the presence of supercomplexes rearrangements (Fig 3H). Although it is not known whether the ETC complexes can contribute to immune function, recently it has been reported a critical role for mitochondrial ETC in innate immune responses to bacterial infection [29]. Despite the massive mitochondrial ISGylation observed after IFN treatment, no changes in ETC complexes in ISG15$^{+/+}$ cells were observed (Fig 3H), suggesting that changes in ETC complexes are not due to ISGylation of mitochondrial proteins. The mechanism by which ISG15 deficiency causes this ETC alteration will be studied in the future.

Autophagic processes play a crucial role in cell-to-virus interaction [55] and are also critical for cellular homeostasis by supporting cell survival and regulating inflammation [56]. Several studies show that type I IFN induces autophagy by sequestering pathogens in autophagosome vesicles that fuse with lysosomes, leading to their degradation [57]. In collaboration, we have previously shown that ISG15 controls endosomal trafficking [58]. Specifically, ISGylation blocks exosome secretion and this deficiency was rescued upon inhibition of autophagy, supporting an important role for ISG15 in autophagy as recently described [59]. During mitophagy, damaged mitochondria are degraded by specific autophagy-lysosome pathways in the autophagosome [40]. By confocal microscopy staining with an antibody specific anti-COX4 we observed remarkable differences in mitochondrial morphology in IFN-treated *ISG15*$^{-/-}$ *vs* ISG15$^{+/+}$ BMDM. In the absence of ISG15 and ISGylation the removal of damaged and dysfunctional mitochondria through mitophagy was clearly reduced (Fig 4C), which is dependent on the fission/fusion cycle and is in line with the reduction in OXPHOS. Moreover, is described that in damaged mitochondria, Parkin translocates from the cytoplasm to the outer mitochondrial membrane to trigger mitophagy [42]. We also show that ISG15 controls Parkin protein levels (Fig 4E), which is required for correct mitophagy initiation. Despite the low levels of OXPHOS, the increased expression of mitochondrial proteins (Table 1 and Fig 4D) and the mitophagy blockade in *ISG15*$^{-/-}$ BMDM (Fig 4C), may be a specific mechanism to compensate for the loss of mitochondrial functionality, due perhaps to the lack of the proper ISGylation of mitochondrial components.

An additional activity of autophagy is to regulate apoptosis since it acts to clear dysfunctional materials that are signals for cell death processes [60]. We previously showed that VACV-infected *ISG15*$^{-/-}$ peritoneal macrophages are deficient in apoptosis as a clear reduction was found in poly-(ADP-ribose) polymerase-1 (PARP-1) fragmentation and caspase activity when compared to wild-type cells [22]. Along this line, our proteomic analysis revealed a decrease in the expression of apoptosis-related proteins in *ISG15*$^{-/-}$ BMDM (Table 1), indicating that the loss of mitochondrial functionality provoked by the absence of ISG15 might be the reason for the impairment in cell death.

Under normal conditions, mitophagy eliminates dysfunctional mitochondria, thereby controlling levels of toxic ROS [37]. Poxvirus infection leads to an increase in ROS levels in the host cell due to mitochondrial β-oxidation of palmitates, which are the main source of

intermediates for the tricarboxylic acid cycle in the virus [61]. The effects of ROS during poxvirus infection correlate with a decrease in translation fidelity [62]. Under physiological conditions, ROS are produced as a normal byproduct of metabolism; however, exacerbated ROS accumulation can cause vascular damage and inflammation by inducing the production of proinflammatory cytokines [63, 64]. Thus, ROS levels act as a sensor for macrophage polarization, promoting an M1 phenotype [65]. Our data demonstrate the novel function of ISG15 in controlling cellular metabolism and macrophage polarization. An imbalance in Arg-1 activation over iNOS activity, with a resultant depletion of intracellular L-arginine, could be responsible for variations in infectious disease pathogenesis, as has been described for parasitic infections [66–68]. While the role of Arg-1 in viral infections is not well understood, it has been shown that Arg-1 overexpression blocks Chikungunya virus (CHIKV) clearance and tissue pathology, suggesting a pathogenic role for Arg-1 after infection [69, 70]. Interestingly, CHIKV-infected *ISG15*$^{-/-}$ mice present a dramatic increase in proinflammatory cytokines, which contributes to their lethality [71]. This finding is in line with our results pointing to a role for ISG15 in macrophage polarization by modulating L-arginine metabolism and proinflammatory cytokine induction.

Regarding the antiviral role of ISG15 against VACV, between one third and one half of the 200 genes that form the VACV genome encode proteins with immunomodulatory roles [72]. Some of these proteins have the ability to block IFN in a dual way as recently described for the VACV C6 protein, which inhibits IFN signaling as well as type I IFN production [73]. In addition, we previously described that the viral E3 protein blocks protein ISGylation *in vitro* [21]. The existence of these mechanisms is quite possibly the reason why the antiviral role of ISG15 against VACV is limited, as several viral proteins can block IFN action. However, in the murine system when the ISGylation machinery is overexpressed prior to infection (S6 Fig) or when USP18-mutant cells are infected, where high levels of ISG15 conjugation are observed [16], viral titers decrease by more than one log (S6 Fig). This points to a clear antiviral role for ISG15 after VACV infection [16]. We demonstrate here the novel role of ISG15 in the fine-tuning of mitochondrial processes, which is associated with its antiviral capacities.

A proposed model for the role of ISG15 in the regulation of BMDM metabolism is depicted in Fig 7. Briefly, IFN stimulates ISG15 production with a subsequent increase in ISGylated proteins (Fig 2A). Following IFN treatment, ISGylated proteins are detected in BMDM cytoplasm, nucleus and mitochondria (Fig 2B): **1**. Proteomics indicate that several mitochondrial processes are regulated by ISG15 (Table 1). Although we have not yet detected which mitochondrial proteins are ISGylated, most of them appear not to be located in the outer membrane (Fig 2C). IFN treatment produces an increase in OXPHOS (Fig 3A and 3B), ATP production (Fig 3C) and ROS production (Fig 3E). **2**. IFN treatment increases the presence of ATG and LC3B proteins, which are involved in autophagic processes (Fig 4A and Table 1). **3**. ISG15 controls Parkin protein levels required for correct mitophagy initiation (Fig 4C). **4**. Mitochondrial function is linked to polarization and *vice versa*. ISG15 blocks Arg-1 at the mRNA (microarray data) and protein (Fig 5A and Table 1) level, and also blocks its activity (Fig 5B), promoting NO production (Fig 6A) with a reduction in viral titer (Fig 6B).

These novel findings further underline the importance of ISG15 in the control of cellular metabolism and the immune response. Nevertheless, a better understanding of how these different processes regulated by ISG15 may affect downstream immune functions *in vivo* will be required to elucidate the complete role of ISG15 in the generation of protective responses during infection with different pathogens.

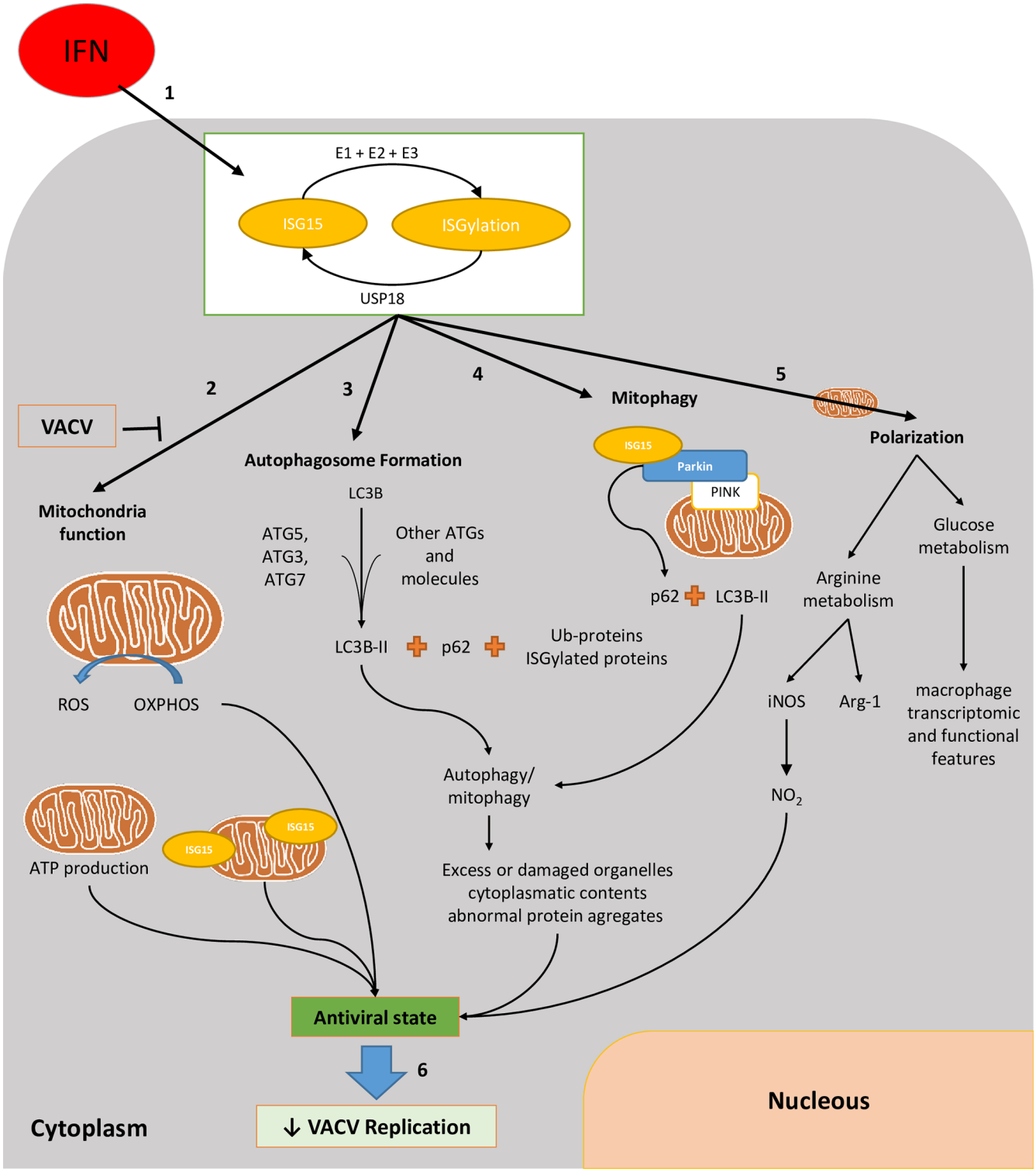

Fig 7. Model.

https://doi.org/10.1371/journal.ppat.1006651.g007

Materials and methods

Virus infections

VACV wild-type Western Reserve strain (WR) was grown on monkey BSC-40 cells (African green monkey kidney cells, American Type Culture Collection (ATCC) number CRL-2761), purified by sucrose gradient banding and titrated on BSC-40 cells as described [74]. VAC-V-YFP, a generous gift of Michael Way, was grown as described [75].

Interferon treatment

Universal type I IFN (200 Units/ml) provided by PBL-Interferon Source was added to BMDM cultures for 16 hours. Mice were treated intraperitoneally with 2000 Units/ g of IFN.

BMDM isolation

The origin of *ISG15*$^{-/-}$ mice has been described elsewhere [76]. Mice were sacrificed and both tibias and femurs were collected. Bone marrow was flushed out using a syringe filled with growth medium. Bone marrow cells were cultured in Dulbecco's modified Eagle's medium (DMEM) medium (Sigma), containing 10% fetal bovine serum (FBS; Sigma) and supplemented with macrophage colony-stimulating factor (M-CSF, PeproTech). Cultures were incubated at 37˚C in a 5% CO_2 atmosphere. After 5 days, non-adherent cells were removed and adherent cells were used for experiments. To determine the purity of murine macrophages, BMDM were incubated with antigen presenting cells-conjugated rat anti-mouse F4/80 antibodies (eBioscience) prior to analysis by flow cytometry. The purity of isolated macrophages varied between 90% and 95% in six separate experiments (S7 Fig).

Ethics statement

All animals were handled in strict accordance with good animal practice as defined by the relevant national, international, and/or local animal welfare bodies, and with the Spanish Royal Decree (RD 1201/2005). The Ethics Committee of Animal Experimentation of the UAM approved all animal work. Animals were bred and housed under conventional conditions, the project license number assigned by the ethics committee is PROEX 041/15.

Western blotting

BMDM were infected (10^6 cells/time post-infection; 1 PFU/cell) with VACV and collected at the indicated times post-infection. Cell extracts were obtained using lysis buffer (50 mM Tris-HCl, 0.5 M NaCl, 10% NP-40, 1% SDS) and protein extraction was performed for 5 min on ice. Protein lysates (100 μg) were fractionated by 12% or 7.5% SDS-PAGE, transferred to nitrocellulose membranes, and incubated with the following primary antibodies: anti-ISG15, anti-Arg-1 and anti-iNOS (Santa Cruz Biotechnology), anti-actin and anti-tubulin (Cell Signaling Technology), anti-ATG3, anti-ATG5, anti-ATG7, anti-LC3B and anti-SDHA (Novus Biologicals), anti-OPA-1, anti-CORE2 and anti-NDUFA9 (Abcam). Secondary antibodies were goat peroxidase conjugates (Santa Cruz Biotechnology) and mouse and rabbit peroxidase conjugates (Sigma). Protein expression was detected using enhanced chemiluminescence (ECL) reagents (Amersham). For the quantification Image J software was used and density of the specific band related to actin was represented.

Mitochondria isolation

Mitochondria were isolated from BMDM as described elsewhere [29]. 1x10^8 BMDMs were collected in phosphate buffered saline (PBS) supplemented with 5 mM EDTA and washed with PBS. Cell pellets were frozen at −80˚C to increase cell breakage and were homogenized in a tightly fitting glass-teflon homogenizer with 10 volumes of buffer A (83mM sucrose, 10 mM MOPS, pH 7.2). An equal volume of buffer B (250 mM sucrose, 30 mM MOPS, pH 7.2) was added and nuclei and unbroken cells were removed by centrifugation at 1000 *g* for 5 minutes. Supernatants were collected and centrifuged at 12 000 g for 2 min. Mitochondria pellets were washed once with buffer C (320 mM sucrose, EDTA 1 mM, 10 mM Tris-HCl, pH 7.4). Mitochondria were then suspended in an appropriate volume of PBS for storage at −80˚C.

Assessment of oxygen consumption and glycolytic flux

Real time oxygen consumption and extracellular acidification was conducted on BMDM (10^5 cells per well) using a XF-96 Extracellular Flux Analyzer (Seahorse Bioscience) as described [29].

ATP synthesis assay

ATP synthesis was measured in permeabilized BMDM (10^6) by kinetic luminescence assay as described [77]. Briefly, cells (2x10^6) were suspended in 160 μl of buffer A (150mM KCl, 25mM Tris-HCl, 2mM EDTA, 0.1% BSA FA, 10mM K-phosphate, 0.1mM MgCl2, pH 7.4) at room temperature (RT) and 50 μg/ml digitonin was added. Samples were mixed gently for 1 min, and the reaction was stopped by addition of 1ml of buffer A. Cells were centrifuged at 3000 rpm for 2 min at RT, and pellets were suspended in 160 μl of buffer A and dispensed into the wells of a 96-well luminescence reading plate (Costar). Substrate cocktail (50 μl) and 20 μl of buffer B (0.5M Tris-acetate, pH 7.75, 0.8mM luciferine, 20 μg/ml luciferase) were added, and luminescence was measured over 1 min. Substrate cocktails were composed of 6 mM diadenosin pentaphosphate and 6 mM ADP supplemented with 1 M glutamate + 1 M malate for determination of CI activity or with 1 M succinate for CII activity. ATP production rate is expressed as 'nmol of ATP/min/mg of protein.' All measurements were performed in triplicate.

Blue native gel

Mitochondrial isolated from *ISG15*$^{+/+}$ or *ISG15*$^{-/-}$ BMDM treated or not with IFN(500 Units/ml, 16 h), were harvested and 10 μl of sample buffer (5% Blue G-250, 5% glycerol in AA Buffer (500 mM 6-aminohexanoic acid, 50 mM immidazole, 1 mM EDTA, pH 7)) was added. Samples were separated according to their indicated masses on a linear 3.5 → 16% acrylamide gradient gel for BN-PAGE, as was described [78], transferred to nitrocellulose membranes, and incubated with the following primary antibodies anti-CORE2 for the complex III, anti-NDUFA9, for complex I and ant-SDHA for complex II.

Citrate synthase activity

The activity of citrate synthase in total extract from *ISG15*$^{+/+}$ or *ISG15*$^{-/-}$ BMDM treated or not with IFN (500Units/ml, 16 h) were measured spectrophotometrically in a Beckman DU-650 spectrophotometer (Beckman Instruments) by monitoring the SH-CoA production. Protein concentration was measured by the Lowry's method. Specific activities were expressed as nmol × min^{-1} × mg $protein^{-1}$. All measurements were performed in triplicate.

Quantification of mitochondrial DNA using real time PCR

mtDNA content was assessed by absolute quantification using real time PCR as described [79]. Primers for mouse mtDNA (mMitoF CTAGAAACCCCGAAACCAAA and mMitoR CCAGCTATCACCAAGCTCGT) and mouse B2M (mB2MF ATGGGAAGCCGAACA TACTG, mB2MR CAGTCTCAGTGGGGGTGAAT) were used to amplify the respective products from mouse genomic DNA. mtDNA copy number per cell were determined from template DNA by carrying out qPCR in a total volume of 10 μl, containing 5 μl of Quantifast SYBR Master Mix (Qiagen), 0.5 μl of forward and reverse primer (400 nM final concentration each), 2 μl template DNA and 2 μl of DNase free water. The reactions were performed in Roche LightCycler (LC) 480 instrument using the following protocol: pre-incubation at 95˚C for 5 min (1 cycle); denaturation at 95˚C for 10 s, annealing and extension at 60˚C for 30 s (repeat denaturation and extension steps for 40 cycles), melting at 95˚C for 5 s, 65˚C for 60 s, and 95˚C continues (melt curve analysis: 1 cycle) and the last step, cooling at 40˚C for 30 s.

MitoSOX imaging

BMDM were plated on 8-well chamber slides (ibidi) at a density of 200,000 cells/well. The culture medium was replaced with medium supplemented with MitoSOX Red mitochondrial superoxide indicator (Life Technologies) at 10 μM during 1 hour in the dark. In some experiments, 1 PFU/cell was also added to the medium. Culture dishes were washed with PBS, replenished with culture medium and then imaged with an inverted confocal microscope, taking photographs each hour until 6 hpi. Image analysis was done with ImageJ. The fluorescence was measured in several points of the well and was expressed as relative fluorescence per cell.

Proteinase K digestion

Isolated mitochondria from ISG15$^{+/+}$ or ISG15$^{-/-}$ BMDM treated or not with IFN (25 μg each) were resuspended in 20 mM Tris, pH 7.2, 15 mM KH_2PO_4, 20 mM $MgSO_4$ and 0.6 M sorbitol in a volume of 50 μl. Proteinase K was applied (final concentration of 50 or 250 μg/ml; Roche Applied Science) for 15 min on ice. Alternatively ISG15+/+ isolated mitochondria were subjected to proteinase K (50 μg/ml) proteolysis to digest in combination with increased digitonin concentration. Osmotic shock (25 mM sucrose, 10 mM MOPS-KOH, pH 7.2) in the presence of not of 1% TritonX-100 was used to disrupt the outer mitochondrial membrane. Addition of PMSF to a final concentration of 5 mM was used to stop the reaction. Subsequently, mitochondrial vesicles were centrifuged at 6800×*g* for 3 min at 4˚C in a tabletop centrifuge and the pellet was resuspended in SDS sample buffer containing 60 mM β-mercaptoethanol and boiled for 3 min at 95˚C.

Griess assay for NO

NO was determined by measuring nitrites in cell supernatants. Supernatants were combined with an equal volume of sulphanilamide (10 mM; Sigma) and N-1 naphthyletliylenediamine dihydrochloride (10 mM; Sigma) and incubated at room temperature for 5–10 min, and the absorbance was measured at 490 nm in a microplate reader. Nitrite levels were determined based on a standard curve of known concentrations of sodium nitrite.

Arginase assay

Arginase activity was assessed by measuring urea production with the Arginase Activity Assay Kit (Sigma). Arginase activity was expressed in arbitrary units, where 1 unit equals the amount

of enzyme needed to convert 1 micromole of L-arginine to ornithine and urea per minute at pH 9.5 and 37˚C.

Fluorescence confocal microscopy

Cells were fixed and processed for immunofluorescence analysis. Briefly, cells were washed with PBS, fixed with 4% PFA, and permeabilized with 0.1% Triton X-100 in PBS (room temperature, 10 min). Localization of p62 and COX4 was performed using specifics antibodies (Sigma and Abcam) and DNA was stained with ToPro 3 (Life Technologies). Images were obtained using a Bio-Rad Radiance 2100 confocal laser microscope.

ELISA

Secreted IL-6 in the medium of BMDM was measured with the quantitative murine IL-6 kit (BD Biosciences). Aliquots (100 μl) of supernatant from uninfected or BMDM at 2, 6, hpi were used for ELISA according to the manufacturer's instructions. Captured IL-6 was quantified at 450 nm with a spectrophotometer. Triplicate samples were measured in two independent experiments.

Quantitative real-time PCR

Total RNA was extracted from macrophages and reverse-transcribed to cDNA using the Transcriptor First Strand cDNA Synthesis Kit (Roche). The mRNA expression of mouse TNF-α, IFN-β, IL-6, IL-12β and IL-1β was detected by quantitative RT-PCR, which was performed in a StepOnePlus Real-Time PCR System (Applied Biosystems) using iTaq Universal SYBR Green Supermix (Bio-Rad). PCR cycling conditions were as follows: 1 cycle of 95˚C for 20 s followed by 40 cycles of 95˚C for 3 s, and 60˚C for 30 s. Relative mRNA expression of target genes was obtained by normalizing to 36B4 gene expression.

Proteomics analysis

Protein extracts from BMDM treated with IFN (500 Units/ml, 16 h), were obtained from cells lysed in extraction buffer (50mM Tris-HCl, 1mM EDTA, 1.5% SDS, pH 8.5). Samples were subjected to tryptic digestion and the resulting peptides were subjected to 4-plex isobaric labeling (iTRAQ) and separated into 8 fractions by cation exchange chromatography using Waters Oasis MCX cartridges (Waters Corp, Milford, MA, USA) and graded concentrations of ammonium formate, pH 3.0 (AF3) in acetonitrile (ACN). The tryptic peptide fractions were subjected to nanoLC-MS/MS. High-resolution analysis was performed on a nano-HPLC Easy nLC 1000 liquid chromatograph (Thermo Scientific, San Jose, CA, USA) coupled to an Orbitrap Fusion mass spectrometer (Thermo Scientific). Protein identification was performed using the SEQUEST HT algorithm integrated in Proteome Discoverer 1.4 (Thermo Scientific). MS/MS scans were matched against a mouse database (UniProtKB/Swiss-Prot 2015_11 Release). Peptides were identified from MS/MS data using the probability ratio method [80]. False discovery rate of peptide identifications was calculated by the refined method [81, 82] Quantitative information was extracted from the MS/MS spectra of iTRAQ-labeled peptides. For comparative analysis of protein abundance changes, we applied the Weighted Scan-Peptide-Protein (WSPP) statistical workflow [83, 84] The quantified proteins were functionally annotated using the Ingenuity Knowledge Database [85, 86] and DAVID [87]. The DAVID repository includes 13 functional databases, including Gene Ontology, KEGG, and Panther.

Ingenuity pathway analysis

To explore the differences in cellular protein dynamics regulated by ISG15, we used ingenuity pathway analysis (IPA) (http://www.ingenuity.com/), which is a software platform that identifies biological pathways and functions relevant to biomolecules of interest [88]. We uploaded the proteins identified in the proteomic analysis and the ratio fold-change between *ISG15*$^{-/-}$ and *ISG15*$^{+/+}$ BMDM. Canonical pathway analysis identified the canonical pathways from the IPA library that were most significant to our data set. The statistical significance of the association between the data set and the canonical pathway was determined by Fisher´s exact test, for which the p-value cutoff was set at 0.05 [89].

Supporting information

S1 Fig. Characterization of the energy metabolism of VACV-infected *ISG15*$^{+/+}$ or *ISG15*$^{-/-}$ BMDM. *ISG15*$^{+/+}$ or *ISG15*$^{-/-}$ BMDM pretreated with IFN (500 units/ml, 16 hours) were infected (1 PFU/cell) with VACV at the times indicated. OCR rates were monitored using the Seahorse Biosciences extracellular flux analyzer. Four different biological replicates were measured and the value represents the mean.
(TIF)

S2 Fig. Glucose or galactose consumption is independent of ISG15. *ISG15*$^{+/+}$ or *ISG15*$^{-/-}$ BMDM treated with IFN (500 units/ml, 16 hours) were infected (1 PFU/cell) with VACV. After infection, the medium was exchanged for a glucose- or galactose-enriched culture medium. Analysis of the color change of the medium was quantified using a colorimetric assay and represented as arbitrary units.
(TIF)

S3 Fig. Altered levels of autophagic and mitochondrial dynamism markers in ISG15$^{-/-}$ BMDM. ISG15$^{+/+}$ or ISG15$^{-/-}$ BMDMs treated or not with IFN (500 units/ml, 16 hours) were infected (1 PFU/cell) with VACV at the times indicated. **(A)** Cellular lysates were analyzed by 12 or 7.5% SDS-PAGE followed by transfer to nitrocellulose membranes. The expression of ATG-3, ATG-5, ATG-7, LC3-B and β-actin (protein loading control) was detected by western blotting using specific antibodies and graphs represents quantification of each protein normalized with actin levels obtained from IFN-I-treated and untreated cells in two independent experiments. **(B)** Cellular lysates were analyzed by 12 or 7,5% SDS-PAGE, transferred to nitrocellulose membranes and the expression of OPA-1, SDHA and tubulin (protein loading control) were detected by Western blot using specific antibodies, graphs in the bottom represents quantification of each protein normalized with actin levels obtained from IFN-I-treated and untreated cells in two independent experiments.
(TIF)

S4 Fig. Exogenous polarization is independent of ISG15. *ISG15*$^{+/+}$ and *ISG15*$^{-/-}$ BMDM were polarized to M1 using 10 ng/ml IFN-γ (PeproTech) and LPS (Sigma) or to M2 with 10 ng/ml IL-4 (PeproTech) for 8 hours. After this, cells were infected with VACV (1 PFU/cell) for the times indicated. Cellular lysates were analyzed by 12% SDS-PAGE, transferred to nitrocellulose membranes and the expression of iNOS, Arg-1, ISG15 or actin (protein loading control) was detected by western blotting using specific antibodies.
(TIF)

S5 Fig. VACV replication assessment in *ISG15*$^{+/+}$ and *ISG15*$^{-/-}$ BMDM and in HeLa cells. **(A, B)** One-step VACV-YFP growth in infected (1 PFU/cell) *ISG15*$^{+/+}$ and *ISG15*$^{-/-}$ BMDM and HeLa cells treated or not with IFN (500 units/ml, 16 hours). Cells were infected and

fluorescence due to viral replication was visualized by fluorescent microscopy at the times indicated (A); cells were harvested and virus yields were determined by plaque assay (B). Results represent the mean ± standard deviation of three independent experiments. Significance was tested using a two-tailed t test assuming non-equal variance. In all the cases $p < 0.01$. HeLa cells were used as a control of viral growth and IFN resistance. **(C)** Viral growth was also detected by immunofluorescence in BMDM treated or not with IFN (500 units/ml, 16 hours) and infected for 24 hours with VACV (1 PFU/cell). Cells were grown in coverslips, fixed with 4% PFA and processed for microscopy. Actin filaments were stained with phalloidin (red), DNA was stained with Topro (blue), and viral protein A27 was visualized using a specific antibody. Images show representative fields (×73 magnification).
(TIF)

S6 Fig. Overexpression of murine ISGylation machinery reduces VACV replication. 293T cells were cotransfected with the murine E1, E2, E3, and GG-ISG15 and at 24 hours post transfection infected with VACV (1 PFU/cell). At 24 h post infection viral titter was analysed by plaque assay. Results represent the mean ± standard deviation of three independent experiments. Significance was tested using a two-tailed t test assuming non-equal variance. In all the cases $p < 0.01$
(TIF)

S7 Fig. Control of VACV infection and BMDM purity using a specific anti-F4/80 macrophage marker antibody and VACV-YFP. *ISG15*$^{+/+}$ and *ISG15*$^{-/-}$ BMDM were infected with VACV-YFP (1PFU/cell) and at 24 hpi cells were collected and processed for flow cytometry. **(A, B)** Uninfected *ISG15*$^{+/+}$ (A) or *ISG15*$^{-/-}$ (B) BMDM were 97% positive for F4/80 antibody. No signal for YFP was detected. **(C, D)** *ISG15*$^{+/+}$ (C) or *ISG15*$^{-/-}$ (D) BMDM infected for 24 hours with VACV-YFP (1 PFU/cell) were 80 or 88%, respectively, double positive for F4/80 and YFP, indicating that the majority of BMDM were infected with VACV-YFP.
(TIF)

S1 Table. Genes regulated by ISG15 in infected macrophages. Comparison of gene expression profile (microarray analysis) of *ISG15*$^{+/+}$ and *ISG15*$^{-/-}$ peritoneal macrophages pre-treated with IFN (500 units/ml, 16 hours) and infected with VACV (1PFU/cell) for 6 hours. Gene symbol, description and *x*-fold change in expression are indicated.
(TIF)

Acknowledgments

We thank the expert technical assistance of Beatriz Martín and Kenneth McCreath for excellent editorial help. We are grateful to our colleagues who have kindly provided reagents indicated in the methods section.

Author Contributions

Conceptualization: Susana Guerra.

Data curation: Susana Guerra.

Formal analysis: Rebeca Acín-Perez, Manuel Albert, Susana Guerra.

Funding acquisition: Susana Guerra.

Investigation: Sara Baldanta, Mercedes Fernández-Escobar, Rebeca Acín-Perez, Manuel Albert, Emilio Camafeita, Inmaculada Jorge, Jesús Vázquez, José Antonio Enríquez, Susana Guerra.

Methodology: Rebeca Acín-Perez, Manuel Albert, Emilio Camafeita, Inmaculada Jorge, Jesús Vázquez, José Antonio Enríquez, Susana Guerra.

Project administration: Susana Guerra.

Resources: Susana Guerra.

Validation: Susana Guerra.

Visualization: Susana Guerra.

Writing – original draft: Susana Guerra.

Writing – review & editing: Susana Guerra.

References

1. Durfee LA, Huibregtse JM. The ISG15 conjugation system. Methods Mol Biol. 2012; 832:141–9. https://doi.org/10.1007/978-1-61779-474-2_9 PMID: 22350882.
2. Ketscher L, Knobeloch KP. ISG15 uncut: Dissecting enzymatic and non-enzymatic functions of USP18 in vivo. Cytokine. 2015; 76(2):569–71. https://doi.org/10.1016/j.cyto.2015.03.006 PMID: 25805508.
3. Rahnefeld A, Klingel K, Schuermann A, Diny NL, Althof N, Lindner A, et al. Ubiquitin-like protein ISG15 (interferon-stimulated gene of 15 kDa) in host defense against heart failure in a mouse model of virus-induced cardiomyopathy. Circulation. 2014; 130(18):1589–600. https://doi.org/10.1161/CIRCULATIONAHA.114.009847 PMID: 25165091.
4. Zhao C, Hsiang TY, Kuo RL, Krug RM. ISG15 conjugation system targets the viral NS1 protein in influenza A virus-infected cells. Proceedings of the National Academy of Sciences of the United States of America. 2010; 107(5):2253–8. https://doi.org/10.1073/pnas.0909144107 PMID: 20133869
5. Durfee LA, Lyon N, Seo K, Huibregtse JM. The ISG15 conjugation system broadly targets newly synthesized proteins: implications for the antiviral function of ISG15. Mol Cell. 2010; 38(5):722–32. https://doi.org/10.1016/j.molcel.2010.05.002 PMID: 20542004.
6. Villarroya-Beltri C, Guerra S, Sanchez-Madrid F. ISGylation—a key to lock the cell gates for preventing the spread of threats. J Cell Sci. 2017. https://doi.org/10.1242/jcs.205468 PMID: 28842471.
7. Pincetic A, Kuang Z, Seo EJ, Leis J. The interferon-induced gene ISG15 blocks retrovirus release from cells late in the budding process. J Virol. 2010; 84(9):4725–36. https://doi.org/10.1128/JVI.02478-09 PMID: 20164219.
8. Tang Y, Zhong G, Zhu L, Liu X, Shan Y, Feng H, et al. Herc5 attenuates influenza A virus by catalyzing ISGylation of viral NS1 protein. J Immunol. 2010; 184(10):5777–90. Epub 2010/04/14. https://doi.org/10.4049/jimmunol.0903588 PMID: 20385878.
9. Zhao C, Hsiang TY, Kuo RL, Krug RM. ISG15 conjugation system targets the viral NS1 protein in influenza A virus-infected cells. Proc Natl Acad Sci U S A. 2010; 107(5):2253–8. https://doi.org/10.1073/pnas.0909144107 PMID: 20133869.
10. Zhao C, Sridharan H, Chen R, Baker DP, Wang S, Krug RM. Influenza B virus non-structural protein 1 counteracts ISG15 antiviral activity by sequestering ISGylated viral proteins. Nat Commun. 2016; 7:12754. https://doi.org/10.1038/ncomms12754 PMID: 27587337.
11. Okumura A, Lu G, Pitha-Rowe I, Pitha PM. Innate antiviral response targets HIV-1 release by the induction of ubiquitin-like protein ISG15. Proc Natl Acad Sci U S A. 2006; 103(5):1440–5. https://doi.org/10.1073/pnas.0510518103 PMID: 16434471.
12. Malakhova OA, Zhang DE. ISG15 inhibits Nedd4 ubiquitin E3 activity and enhances the innate antiviral response. J Biol Chem. 2008; 283(14):8783–7. https://doi.org/10.1074/jbc.C800030200 PMID: 18287095.
13. Lenschow DJ. Antiviral Properties of ISG15. Viruses. 2010; 2(10):2154–68. https://doi.org/10.3390/v2102154 PMID: 21994614.
14. Radoshevich L, Impens F, Ribet D, Quereda JJ, Nam Tham T, Nahori MA, et al. ISG15 counteracts Listeria monocytogenes infection. Elife. 2015; 4. https://doi.org/10.7554/eLife.06848 PMID: 26259872.
15. Kimmey JM, Campbell JA, Weiss LA, Monte KJ, Lenschow DJ, Stallings CL. The impact of ISGylation during Mycobacterium tuberculosis infection in mice. Microbes Infect. 2017. https://doi.org/10.1016/j.micinf.2016.12.006 PMID: 28087453.
16. Ketscher L, Hannss R, Morales DJ, Basters A, Guerra S, Goldmann T, et al. Selective inactivation of USP18 isopeptidase activity in vivo enhances ISG15 conjugation and viral resistance. Proc Natl Acad Sci U S A. 2015; 112(5):1577–82. https://doi.org/10.1073/pnas.1412881112 PMID: 25605921.

17. Bogunovic D, Byun M, Durfee LA, Abhyankar A, Sanal O, Mansouri D, et al. Mycobacterial disease and impaired IFN-gamma immunity in humans with inherited ISG15 deficiency. Science. 2012; 337 (6102):1684–8. https://doi.org/10.1126/science.1224026 PMID: 22859821.

18. Zhang X, Bogunovic D, Payelle-Brogard B, Francois-Newton V, Speer SD, Yuan C, et al. Human intracellular ISG15 prevents interferon-alpha/beta over-amplification and auto-inflammation. Nature. 2015; 517(7532):89–93. https://doi.org/10.1038/nature13801 PMID: 25307056.

19. Speer SD, Li Z, Buta S, Payelle-Brogard B, Qian L, Vigant F, et al. ISG15 deficiency and increased viral resistance in humans but not mice. Nat Commun. 2016; 7:11496. https://doi.org/10.1038/ncomms11496 PMID: 27193971.

20. Guerra S, Caceres A, Knobeloch KP, Horak I, Esteban M. Vaccinia virus E3 protein prevents the antiviral action of ISG15. PLoS Pathog. 2008; 4(7):e1000096. https://doi.org/10.1371/journal.ppat.1000096 PMID: 18604270.

21. Eduardo-Correia B, Martinez-Romero C, Garcia-Sastre A, Guerra S. ISG15 is counteracted by vaccinia virus E3 protein and controls the proinflammatory response against viral infection. J Virol. 2014; 88 (4):2312–8. https://doi.org/10.1128/JVI.03293-13 PMID: 24257616.

22. Yanguez E, Garcia-Culebras A, Frau A, Llompart C, Knobeloch KP, Gutierrez-Erlandsson S, et al. ISG15 regulates peritoneal macrophages functionality against viral infection. PLoS Pathog. 2013; 9 (10):e1003632. https://doi.org/10.1371/journal.ppat.1003632 PMID: 24137104.

23. Sainz B Jr., Martin B, Tatari M, Heeschen C, Guerra S. ISG15 is a critical microenvironmental factor for pancreatic cancer stem cells. Cancer Res. 2014; 74(24):7309–20. https://doi.org/10.1158/0008-5472.CAN-14-1354 PMID: 25368022.

24. Murray PJ, Allen JE, Biswas SK, Fisher EA, Gilroy DW, Goerdt S, et al. Macrophage activation and polarization: nomenclature and experimental guidelines. Immunity. 2014; 41(1):14–20. https://doi.org/10.1016/j.immuni.2014.06.008 PMID: 25035950.

25. Biswas SK, Mantovani A. Macrophage plasticity and interaction with lymphocyte subsets: cancer as a paradigm. Nat Immunol. 2010; 11(10):889–96. https://doi.org/10.1038/ni.1937 PMID: 20856220.

26. Gordon S, Taylor PR. Monocyte and macrophage heterogeneity. Nature reviews Immunology. 2005; 5 (12):953–64. https://doi.org/10.1038/nri1733 PMID: 16322748.

27. Sica A, Mantovani A. Macrophage plasticity and polarization: in vivo veritas. J Clin Invest. 2012; 122 (3):787–95. https://doi.org/10.1172/JCI59643 PMID: 22378047.

28. Benoit M, Desnues B, Mege JL. Macrophage polarization in bacterial infections. J Immunol. 2008; 181 (6):3733–9. PMID: 18768823.

29. Garaude J, Acin-Perez R, Martinez-Cano S, Enamorado M, Ugolini M, Nistal-Villan E, et al. Mitochondrial respiratory-chain adaptations in macrophages contribute to antibacterial host defense. Nat Immunol. 2016; 17(9):1037–45. https://doi.org/10.1038/ni.3509 PMID: 27348412.

30. Mills EL, O'Neill LA. Reprogramming mitochondrial metabolism in macrophages as an anti-inflammatory signal. Eur J Immunol. 2016; 46(1):13–21. https://doi.org/10.1002/eji.201445427 PMID: 26643360.

31. Rodriguez-Prados JC, Traves PG, Cuenca J, Rico D, Aragones J, Martin-Sanz P, et al. Substrate fate in activated macrophages: a comparison between innate, classic, and alternative activation. Journal of immunology. 2010; 185(1):605–14. https://doi.org/10.4049/jimmunol.0901698 PMID: 20498354.

32. Giannakopoulos NV, Luo JK, Papov V, Zou W, Lenschow DJ, Jacobs BS, et al. Proteomic identification of proteins conjugated to ISG15 in mouse and human cells. Biochem Biophys Res Commun. 2005; 336 (2):496–506. https://doi.org/10.1016/j.bbrc.2005.08.132 PMID: 16139798.

33. Zhao H, Yang J, Li K, Ding X, Lin R, Ma Y, et al. Proteomic analysis at the subcellular level for host targets against influenza A virus (H1N1). Antiviral Res. 2013; 100(3):673–87. https://doi.org/10.1016/j.antiviral.2013.10.005 PMID: 24161511.

34. Sancak Y, Markhard AL, Kitami T, Kovacs-Bogdan E, Kamer KJ, Udeshi ND, et al. EMRE is an essential component of the mitochondrial calcium uniporter complex. Science. 2013; 342(6164):1379–82. https://doi.org/10.1126/science.1242993 PMID: 24231807.

35. Harner M, Korner C, Walther D, Mokranjac D, Kaesmacher J, Welsch U, et al. The mitochondrial contact site complex, a determinant of mitochondrial architecture. EMBO J. 2011; 30(21):4356–70. https://doi.org/10.1038/emboj.2011.379 PMID: 22009199.

36. Guarani V, McNeill EM, Paulo JA, Huttlin EL, Frohlich F, Gygi SP, et al. QIL1 is a novel mitochondrial protein required for MICOS complex stability and cristae morphology. Elife. 2015; 4. https://doi.org/10.7554/eLife.06265 PMID: 25997101.

37. Kurihara Y, Kanki T, Aoki Y, Hirota Y, Saigusa T, Uchiumi T, et al. Mitophagy plays an essential role in reducing mitochondrial production of reactive oxygen species and mutation of mitochondrial DNA by maintaining mitochondrial quantity and quality in yeast. J Biol Chem. 2012; 287(5):3265–72. https://doi.org/10.1074/jbc.M111.280156 PMID: 22157017.

38. Pourcelot M, Arnoult D. Mitochondrial dynamics and the innate antiviral immune response. FEBS J. 2014; 281(17):3791–802. https://doi.org/10.1111/febs.12940 PMID: 25051991.

39. Cogliati S, Frezza C, Soriano ME, Varanita T, Quintana-Cabrera R, Corrado M, et al. Mitochondrial cristae shape determines respiratory chain supercomplexes assembly and respiratory efficiency. Cell. 2013; 155(1):160–71. https://doi.org/10.1016/j.cell.2013.08.032 PMID: 24055366.

40. Mishra P, Chan DC. Metabolic regulation of mitochondrial dynamics. J Cell Biol. 2016; 212(4):379–87. https://doi.org/10.1083/jcb.201511036 PMID: 26858267.

41. Nakashima H, Nguyen T, Goins WF, Chiocca EA. Interferon-stimulated gene 15 (ISG15) and ISG15-linked proteins can associate with members of the selective autophagic process, histone deacetylase 6 (HDAC6) and SQSTM1/p62. J Biol Chem. 2015; 290(3):1485–95. https://doi.org/10.1074/jbc.M114.593871 PMID: 25429107.

42. Ivankovic D, Chau KY, Schapira AH, Gegg ME. Mitochondrial and lysosomal biogenesis are activated following PINK1/parkin-mediated mitophagy. J Neurochem. 2016; 136(2):388–402. https://doi.org/10.1111/jnc.13412 PMID: 26509433.

43. Izquierdo E, Cuevas VD, Fernandez-Arroyo S, Riera-Borrull M, Orta-Zavalza E, Joven J, et al. Reshaping of Human Macrophage Polarization through Modulation of Glucose Catabolic Pathways. J Immunol. 2015; 195(5):2442–51. https://doi.org/10.4049/jimmunol.1403045 PMID: 26209622.

44. Biswas SK, Mantovani A. Orchestration of metabolism by macrophages. Cell Metab. 2012; 15(4):432–7. https://doi.org/10.1016/j.cmet.2011.11.013 PMID: 22482726.

45. Odegaard JI, Chawla A. The immune system as a sensor of the metabolic state. Immunity. 2013; 38(4):644–54. https://doi.org/10.1016/j.immuni.2013.04.001 PMID: 23601683.

46. Galvan-Pena S, O'Neill LA. Metabolic reprograming in macrophage polarization. Front Immunol. 2014; 5:420. https://doi.org/10.3389/fimmu.2014.00420 PMID: 25228902.

47. Malyshev I, Malyshev Y. Current Concept and Update of the Macrophage Plasticity Concept: Intracellular Mechanisms of Reprogramming and M3 Macrophage "Switch" Phenotype. Biomed Res Int. 2015; 2015:341308. https://doi.org/10.1155/2015/341308 PMID: 26366410.

48. Vrbacky M, Krijt J, Drahota Z, Melkova Z. Inhibitory effects of Bcl-2 on mitochondrial respiration. Physiol Res. 2003; 52(5):545–54. PMID: 14535829.

49. Gregorczyk KP, Szulc-Dabrowska L, Wyzewski Z, Struzik J, Niemialtowski M. Changes in the mitochondrial network during ectromelia virus infection of permissive L929 cells. Acta Biochim Pol. 2014; 61(1):171–7. PMID: 24660173.

50. Anand SK, Tikoo SK. Viruses as modulators of mitochondrial functions. Adv Virol. 2013; 2013:738794. https://doi.org/10.1155/2013/738794 PMID: 24260034.

51. Morales DJ, Lenschow DJ. The antiviral activities of ISG15. J Mol Biol. 2013; 425(24):4995–5008. https://doi.org/10.1016/j.jmb.2013.09.041 PMID: 24095857.

52. Harty RN, Pitha PM, Okumura A. Antiviral activity of innate immune protein ISG15. J Innate Immun. 2009; 1(5):397–404. https://doi.org/10.1159/000226245 PMID: 19680460.

53. Wu D, Sanin DE, Everts B, Chen Q, Qiu J, Buck MD, et al. Type 1 Interferons Induce Changes in Core Metabolism that Are Critical for Immune Function. Immunity. 2016; 44(6):1325–36. https://doi.org/10.1016/j.immuni.2016.06.006 PMID: 27332732.

54. Yim HY, Yang Y, Lim JS, Lee MS, Zhang DE, Kim KI. The mitochondrial pathway and reactive oxygen species are critical contributors to interferon-alpha/beta-mediated apoptosis in Ubp43-deficient hematopoietic cells. Biochem Biophys Res Commun. 2012; 423(2):436–40. PMID: 22683641.

55. Jackson WT. Viruses and the autophagy pathway. Virology. 2015; 479–480:450–6. https://doi.org/10.1016/j.virol.2015.03.042 PMID: 25858140.

56. Nakahira K, Choi AM. Autophagy: a potential therapeutic target in lung diseases. Am J Physiol Lung Cell Mol Physiol. 2013; 305(2):L93–107. https://doi.org/10.1152/ajplung.00072.2013 PMID: 23709618.

57. Schmeisser H, Bekisz J, Zoon KC. New function of type I IFN: induction of autophagy. J Interferon Cytokine Res. 2014; 34(2):71–8. https://doi.org/10.1089/jir.2013.0128 PMID: 24428799.

58. Villarroya-Beltri C, Baixauli F, Mittelbrunn M, Fernández-Delgado I, Torralba D, Moreno-Gonzalo O, et al. ISGylation controls exosome secretion by promoting lysosomal degradation of MVB proteins. Nat Commun. 2016.

59. Xu D, Zhang T, Xiao J, Zhu K, Wei R, Wu Z, et al. Modification of BECN1 by ISG15 plays a crucial role in autophagy regulation by type I IFN/interferon. Autophagy. 2015; 11(4):617–28. https://doi.org/10.1080/15548627.2015.1023982 PMID: 25906440.

60. Khan M, Syed GH, Kim SJ, Siddiqui A. Mitochondrial dynamics and viral infections: A close nexus. Biochim Biophys Acta. 2015; 1853(10 Pt B):2822–33. https://doi.org/10.1016/j.bbamcr.2014.12.040 PMID: 25595529.

61. Greseth MD, Traktman P. De novo fatty acid biosynthesis contributes significantly to establishment of a bioenergetically favorable environment for vaccinia virus infection. PLoS Pathog. 2014; 10(3): e1004021. https://doi.org/10.1371/journal.ppat.1004021 PMID: 24651651.

62. Lee JY, Kim DG, Kim BG, Yang WS, Hong J, Kang T, et al. Promiscuous methionyl-tRNA synthetase mediates adaptive mistranslation to protect cells against oxidative stress. J Cell Sci. 2014; 127(Pt 19):4234–45. https://doi.org/10.1242/jcs.152470 PMID: 25097229.

63. Mittal M, Siddiqui MR, Tran K, Reddy SP, Malik AB. Reactive oxygen species in inflammation and tissue injury. Antioxid Redox Signal. 2014; 20(7):1126–67. https://doi.org/10.1089/ars.2012.5149 PMID: 23991888.

64. Dickinson BC, Chang CJ. Chemistry and biology of reactive oxygen species in signaling or stress responses. Nat Chem Biol. 2011; 7(8):504–11. https://doi.org/10.1038/nchembio.607 PMID: 21769097.

65. Tan HY, Wang N, Li S, Hong M, Wang X, Feng Y. The Reactive Oxygen Species in Macrophage Polarization: Reflecting Its Dual Role in Progression and Treatment of Human Diseases. Oxid Med Cell Longev. 2016; 2016:2795090. https://doi.org/10.1155/2016/2795090 PMID: 27143992.

66. Das P, Lahiri A, Lahiri A, Chakravortty D. Modulation of the arginase pathway in the context of microbial pathogenesis: a metabolic enzyme moonlighting as an immune modulator. PLoS Pathog. 2010; 6(6): e1000899. https://doi.org/10.1371/journal.ppat.1000899 PMID: 20585552.

67. Pesce JT, Ramalingam TR, Mentink-Kane MM, Wilson MS, El Kasmi KC, Smith AM, et al. Arginase-1-expressing macrophages suppress Th2 cytokine-driven inflammation and fibrosis. PLoS Pathog. 2009; 5(4):e1000371. https://doi.org/10.1371/journal.ppat.1000371 PMID: 19360123.

68. Munder M. Arginase: an emerging key player in the mammalian immune system. Br J Pharmacol. 2009; 158(3):638–51. https://doi.org/10.1111/j.1476-5381.2009.00291.x PMID: 19764983.

69. Burrack KS, Tan JJ, McCarthy MK, Her Z, Berger JN, Ng LF, et al. Myeloid Cell Arg1 Inhibits Control of Arthritogenic Alphavirus Infection by Suppressing Antiviral T Cells. PLoS Pathog. 2015; 11(10): e1005191. https://doi.org/10.1371/journal.ppat.1005191 PMID: 26436766.

70. Stoermer KA, Burrack A, Oko L, Montgomery SA, Borst LB, Gill RG, et al. Genetic ablation of arginase 1 in macrophages and neutrophils enhances clearance of an arthritogenic alphavirus. J Immunol. 2012; 189(8):4047–59. https://doi.org/10.4049/jimmunol.1201240 PMID: 22972923.

71. Werneke SW, Schilte C, Rohatgi A, Monte KJ, Michault A, Arenzana-Seisdedos F, et al. ISG15 is critical in the control of Chikungunya virus infection independent of UbE1L mediated conjugation. PLoS Pathog. 2011; 7(10):e1002322. https://doi.org/10.1371/journal.ppat.1002322 PMID: 22028657.

72. Perdiguero B, Esteban M. The interferon system and vaccinia virus evasion mechanisms. J Interferon Cytokine Res. 2009; 29(9):581–98. https://doi.org/10.1089/jir.2009.0073 PMID: 19708815.

73. Stuart JH, Sumner RP, Lu Y, Snowden JS, Smith GL. Vaccinia Virus Protein C6 Inhibits Type I IFN Signalling in the Nucleus and Binds to the Transactivation Domain of STAT2. PLoS Pathog. 2016; 12(12): e1005955. https://doi.org/10.1371/journal.ppat.1005955 PMID: 27907166.

74. Guerra S, Lopez-Fernandez LA, Pascual-Montano A, Munoz M, Harshman K, Esteban M. Cellular gene expression survey of vaccinia virus infection of human HeLa cells. Journal of virology. 2003; 77 (11):6493–506. Epub 2003/05/14. https://doi.org/10.1128/JVI.77.11.6493-6506.2003 PMID: 12743306.

75. Arakawa Y, Cordeiro JV, Schleich S, Newsome TP, Way M. The release of vaccinia virus from infected cells requires RhoA-mDia modulation of cortical actin. Cell host & microbe. 2007; 1(3):227–40. Epub 2007/11/17. https://doi.org/10.1016/j.chom.2007.04.006 PMID: 18005701.

76. Osiak A, Utermohlen O, Niendorf S, Horak I, Knobeloch KP. ISG15, an interferon-stimulated ubiquitin-like protein, is not essential for STAT1 signaling and responses against vesicular stomatitis and lymphocytic choriomeningitis virus. Mol Cell Biol. 2005; 25(15):6338–45. https://doi.org/10.1128/MCB.25.15.6338-6345.2005 PMID: 16024773.

77. Vives-Bauza C, Yang L, Manfredi G. Assay of mitochondrial ATP synthesis in animal cells and tissues. Methods Cell Biol. 2007; 80:155–71. https://doi.org/10.1016/S0091-679X(06)80007-5 PMID: 17445693.

78. Wittig I, Braun HP, Schagger H. Blue native PAGE. Nat Protoc. 2006; 1(1):418–28. https://doi.org/10.1038/nprot.2006.62 PMID: 17406264.

79. Malik AN, Czajka A, Cunningham P. Accurate quantification of mouse mitochondrial DNA without co-amplification of nuclear mitochondrial insertion sequences. Mitochondrion. 2016; 29:59–64. https://doi.org/10.1016/j.mito.2016.05.003 PMID: 27181048.

80. Martinez-Bartolome S, Navarro P, Martin-Maroto F, Lopez-Ferrer D, Ramos-Fernandez A, Villar M, et al. Properties of average score distributions of SEQUEST: the probability ratio method. Mol Cell Proteomics. 2008; 7(6):1135–45. Epub 2008/02/28. https://doi.org/10.1074/mcp.M700239-MCP200 PMID: 18303013.

81. Navarro P, Vazquez J. A refined method to calculate false discovery rates for peptide identification using decoy databases. J Proteome Res. 2009; 8(4):1792–6. Epub 2009/08/29. https://doi.org/10.1021/pr800362h PMID: 19714873.

82. Bonzon-Kulichenko E, Garcia-Marques F, Trevisan-Herraz M, Vazquez J. Revisiting peptide identification by high-accuracy mass spectrometry: problems associated with the use of narrow mass precursor windows. J Proteome Res. 2015; 14(2):700–10. Epub 2014/12/17. https://doi.org/10.1021/pr5007284 PMID: 25494653.

83. Navarro P, Trevisan-Herraz M, Bonzon-Kulichenko E, Nunez E, Martinez-Acedo P, Perez-Hernandez D, et al. General statistical framework for quantitative proteomics by stable isotope labeling. Journal of proteome research. 2014; 13(3):1234–47. Epub 2014/02/12. https://doi.org/10.1021/pr4006958 PMID: 24512137.

84. Garcia-Marques F, Trevisan-Herraz M, Martinez-Martinez S, Camafeita E, Jorge I, Lopez JA, et al. A Novel Systems-Biology Algorithm for the Analysis of Coordinated Protein Responses Using Quantitative Proteomics. Mol Cell Proteomics. 2016; 15(5):1740–60. https://doi.org/10.1074/mcp.M115.055905 PMID: 26893027.

85. Calvano SE, Xiao W, Richards DR, Felciano RM, Baker HV, Cho RJ, et al. A network-based analysis of systemic inflammation in humans. Nature. 2005; 437(7061):1032–7. Epub 2005/09/02. https://doi.org/10.1038/nature03985 PMID: 16136080.

86. Ficenec D, Osborne M, Pradines J, Richards D, Felciano R, Cho RJ, et al. Computational knowledge integration in biopharmaceutical research. Brief Bioinform. 2003; 4(3):260–78. Epub 2003/10/30. PMID: 14582520.

87. Huang da W, Sherman BT, Zheng X, Yang J, Imamichi T, Stephens R, et al. Extracting biological meaning from large gene lists with DAVID. Curr Protoc Bioinformatics. 2009; Chapter 13:Unit 13 1. Epub 2009/09/04. https://doi.org/10.1002/0471250953.bi1311s27 PMID: 19728287.

88. Thomas S, Bonchev D. A survey of current software for network analysis in molecular biology. Hum Genomics. 2010; 4(5):353–60. https://doi.org/10.1186/1479-7364-4-5-353 PMID: 20650822.

89. Codrea MC, Nahnsen S. Platforms and Pipelines for Proteomics Data Analysis and Management. Adv Exp Med Biol. 2016; 919:203–15. https://doi.org/10.1007/978-3-319-41448-5_9 PMID: 27975218.

viruses

MDPI

Review

ISG15, a Small Molecule with Huge Implications: Regulation of Mitochondrial Homeostasis

Manuel Albert †, Martina Bécares †, Michela Falqui, Carlos Fernández-Lozano and Susana Guerra *

Department of Preventive Medicine, Public Health and Microbiology, Universidad Autónoma, E-28029 Madrid, Spain; manuel.albert@uam.es (M.A.); martina.becares@uam.es (M.B.); michela.falqui@uam.es (M.F.); carlos.fernandezl@uam.es (C.F.-L.)

* Correspondence: susana.guerra@uam.es; Tel.: +34-91/497-5440; Fax: +34-91/497-5353

† These authors contributed equally.

Received: 26 October 2018; Accepted: 9 November 2018; Published: 13 November 2018

Abstract: Viruses are responsible for the majority of infectious diseases, from the common cold to HIV/AIDS or hemorrhagic fevers, the latter with devastating effects on the human population. Accordingly, the development of efficient antiviral therapies is a major goal and a challenge for the scientific community, as we are still far from understanding the molecular mechanisms that operate after virus infection. Interferon-stimulated gene 15 (ISG15) plays an important antiviral role during viral infection. ISG15 catalyzes a ubiquitin-like post-translational modification termed ISGylation, involving the conjugation of ISG15 molecules to *de novo* synthesized viral or cellular proteins, which regulates their stability and function. Numerous biomedically relevant viruses are targets of ISG15, as well as proteins involved in antiviral immunity. Beyond their role as cellular powerhouses, mitochondria are multifunctional organelles that act as signaling hubs in antiviral responses. In this review, we give an overview of the biological consequences of ISGylation for virus infection and host defense. We also compare several published proteomic studies to identify and classify potential mitochondrial ISGylation targets. Finally, based on our recent observations, we discuss the essential functions of mitochondria in the antiviral response and examine the role of ISG15 in the regulation of mitochondrial processes, specifically OXPHOS and mitophagy.

Keywords: interferon; ubiquitin-like modification; mitochondria; mitophagy; OXPHOS

1. Introduction

1.1. ISG15 Definition

The innate immune response is the first line of defense against microbial and viral infections. Invading microorganisms produce danger- and pathogen-associated molecular patterns that interact with host pattern-recognition receptors, triggering several intracellular signaling cascades that activate nuclear factor *kappa*-B (NF-κB), mitogen-activated protein kinases (MAPKs) and interferon (IFN) regulatory factors (IRFs), resulting in the expression of a broad array of proteins involved in host defense such as type-I IFNs and proinflammatory cytokines [1,2]. The release of type-I IFNs has both autocrine and paracrine effects *via* IFNα/β receptors (IFNARs) on the cell surface. Binding to IFNARs leads to the activation of the Janus kinase-signal transducer and activator of transcription proteins (JAK-STAT) signaling pathway and the formation of the interferon-stimulated gene factor 3 (ISGF3) complex, with the subsequent expression of IFN-stimulated genes [3] that establish an antiviral state and play important roles in determining the host innate and adaptive immune responses [4].

One of the most highly induced genes in the type-I IFN signaling cascade is *ISG15* (interferon-stimulated gene 15), which encodes a small ubiquitin-like protein involved in a post-translational modification

One of the most highly induced genes in the type-I IFN signaling cascade is *ISG15* (interferon-stimulated gene 15), which encodes a small ubiquitin-like protein involved in a post-translational modification (PTM) process termed ISGylation. Through this process, ISG15 covalently binds to a wide range of target proteins [5]. ISG15 exists in three different forms: unconjugated within the cell, conjugated to target proteins, and released into the serum (Figure 1). ISG15 is synthesized as a 17-kDa precursor that is proteolytically processed into a mature form of 15 kDa. This processing exposes a carboxy-terminal LRLRGG motif, required for ISGylation [6] (Figure 1). ISGylation is the result of the coordination of three enzymatic activities-activation, conjugation and ligation—performed by ISG15-activating enzymes (E1), ISG15-conjugating enzymes (E2) and ISG15-ligating enzymes (E3), respectively [7] (Figure 1). Considering the broad substrate selectivity described for ISGylation, and the fact that Herc5 (the major ISG15-ligating enzyme) associates with polyribosomes, it has been established that ISGylation targets proteins undergoing active translation [8]. In the context of viral infection, those newly synthesized proteins are largely viral proteins and cellular proteins involved in the innate immune response.

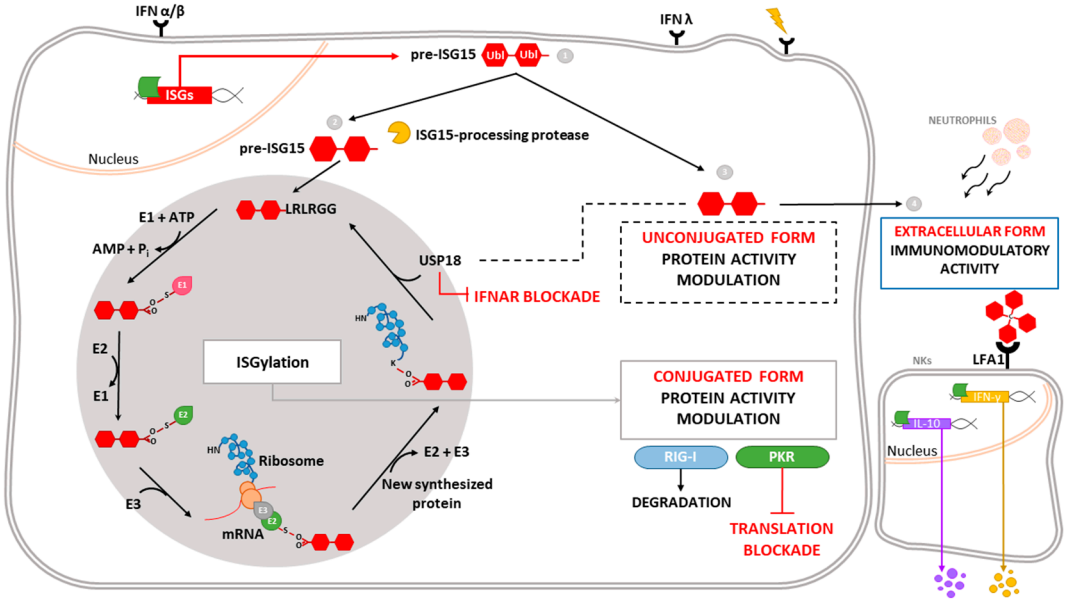

Figure 1. *Intracellular and extracellular activities of ISG15.* Different stimuli trigger the expression of ISG15, which is produced as a precursor of 17 kDa with two ubiquitin-like domains linked by a hinge region (1). Intracellular ISG15 can be processed into its mature form and conjugated to *de novo* synthesized proteins in a process termed ISGylation. ISG15 processing exposes its carboxy-terminal LRLRGG motif, allowing its conjugation to lysine residues in target proteins to modulate their function. In addition, ISGylation is reversible due to the action of the USP18, which also regulates IFNAR-mediated signaling (2). ISG15 can remain unconjugated within the cell, regulating protein activity (3), or be secreted as a cytokine, acting as a chemotactic and stimulating factor for cells (4). Binding of ISG15 to LFA-1 integrin receptor on the surface of NK cells promotes the activation, production and release of IFN-γ and IL-10 from NK cells, respectively. Moreover, extracellular ISG15 is able to form dimers through cysteine residues, to modulate cytokine levels.

ISG15 conjugation to target proteins is a covalent and reversible process through the action of a 43-kDa deISGylase enzyme, ubiquitin-specific protease 18 (USP18) [9,10]. Interestingly, both ISG15 and its conjugating and deconjugating enzymes are upregulated by type-I IFN [9], as well as by other stimuli such as type-II and type-III IFNs [11–13], lipopolysaccharide [14], retinoic acid [15], DNA damage or genotoxic reagents [16]. USP18 not only acts as a deconjugating enzyme, but also as a negative regulator of the type-I IFN pathway (Figure 1), with important implications in antiviral and antibacterial responses, immune cell development, autoimmune diseases and cancer [17]. In humans, ISG15 binds to USP18, increasing its stability and leading to a decrease in IFN-α/β signaling. Consequently, ISG15 deficiency results in low USP18 levels, and therefore a sustained elevation in

for ISG15, which is absent in mice, seems to be predominant in humans, since patients appear not to be more susceptible to viral infections [18,19].

Beyond the above-mentioned forms of ISG15—conjugated to target proteins or unconjugated within the cell—ISG15 is also secreted into the serum, mainly by granulocytes *via* their secretory pathway [20]. Lymphocyte function-associated antigen 1 receptor (LFA1) has recently been identified as the cellular receptor for ISG15 (Figure 1). ISG15 binding to LFA1 triggers the activation of SRC family kinases, promoting IFN-γ and Interleukin-10 (IL-10) secretion in natural killer (NK) cells and, likely, also T-lymphocytes [21]. The role of ISG15 as an inductor of IFN-γ secretion seems to be the basis for the increased susceptibility to mycobacterial diseases in patients lacking a functional form of ISG15 [20]. Secreted ISG15 has also been described to promote NK [22] and dendritic cell [23] maturation, and to act as a chemotactic factor for neutrophils [24]. Along this line, a recent study highlighted the presence of dimeric and multimeric forms of extracellular ISG15 important for its cytokine activity during parasite infection, and speculated on the existence of an unknown ISG15 receptor on dendritic cells that mediates chemotaxis of these cells to the site of infection and IL-1β production [25].

Although there are several features of ISG15 that are shared with ubiquitin, specially its structure, conjugation and deconjugation mechanisms [26], ISGylation has not been shown to stimulate proteasomal degradation of its substrates [10]. Furthermore, some of the ISGylation consequences are exerted by restricting the ubiquitin system, what might be mediated through the conjugation of ISG15 to different E2 and E3 ubiquitin-conjugating enzymes [27], or even through the formation of mixed ubiquitin–ISG15 chains [28]. As a result, ISGylation can decrease the polyubiquitylated proteins levels and downregulate protein turnover by the proteasome system [28]. Additionally, unlike ubiquitin, no poly-ISG15 chains or specific ISG15-interacting motifs have been identified yet.

In the following sections, we discuss the antiviral mechanisms mediated by ISGylation of both viral and cellular proteins, with a focus on mitochondrial proteins, as we recently showed that ISG15 modulates essential mitochondrial metabolic processes such as respiration and mitophagy in macrophages, with important implications for innate immune responses [29].

1.2. Antiviral Role of ISG15 and ISGylation

The antiviral activity associated with ISG15 and/or ISGylation has been widely described since the first observation that *ISG15*-/- mice were more susceptible to viral infections than their wild-type counterparts, albeit the role of ISG15 and ISGylation in viral life cycles is specific to the virus involved [30]. Early studies using *ISG15*-/- mice demonstrated that ISG15 has a protective effect against lethal infection by Influenza virus, Herpes Simplex virus (HSV-1) and Sindbis virus (SINV) [31]. Similarly, mice deficient in UbE1l—the E1 enzyme of ISG15—were also more susceptible to lethal infection by SINV [32]. Moreover, exogenous expression of wild-type ISG15 by recombinant chimeric SINV protected IFNAR-/- mice against systemic and lethal infections, whereas expression of ISG15 mutants unable to conjugate to proteins did not show this protective effect [33], indicating an intrinsic antiviral role for ISGylation. It should be noted that such an antiviral effect could be due to the conjugation of ISG15 to viral and/or cellular proteins. By contrast, free ISG15, but not ISGylation, has been described to promote antiviral responses against Chikungunya virus (CHIKV) infection [34].

To date, an antiviral effect mediated by ISG15 or ISGylation has been described using in vitro and/or in vivo systems for many other DNA and RNA viruses, including Hepatitis B virus [35], Vesicular stomatitis virus [36,37], Respiratory syncytial virus [38,39], Human immunodeficiency virus type 1 (HIV-1) [40], and Ebola virus [27]. The antiviral effect of ISG15 and ISGylation has also been described against viruses of the genera Novirhabdovirus, Birnavirus and Iridovirus in zebrafish, an example of the evolutionary conservation of the antiviral role of ISG15 among vertebrates [41].

Given the importance of the antiviral response governed by ISG15, it is not surprising that viruses have evolved strategies to counteract its antiviral effects. For example, Influenza B virus (IBV) NS1 protein [42], Vaccinia virus E3 protein [43], and Human cytomegalovirus (HCMV) IE1 and PUL26 proteins obstruct ISG15 antiviral action by preventing ISGylation [44]. Similar mechanisms

are also described for Orthonairovirus and Arterivirus OTU-domain-containing proteases [45] and for Coronavirus papain-like proteases (PLpro), which cleave ISG15 from target proteins. Remarkably, a PLpro inhibitor was shown to protect mice from lethal infection in vivo [46]. Surprisingly, it has been reported that ISGylation is necessary for robust production of Hepatitis C virus (HCV), conferring a novel role for ISG15 as a proviral factor that promotes virus production. Indeed, in human hepatocytes, siRNA silencing of ISG15 was sufficient to both inhibit HCV replication and increase IFN expression [47]. Several reports have now highlighted a role for ISG15 in the monitoring of HCV replication in cell cultures, as well as in the maintenance of HCV in liver, and pinpoint ISG15 as among the predictor genes for non-response to IFN therapy [48].

1.3. ISGylated Viral Proteins

Regarding the direct antiviral effect of ISGylation *via* conjugation to viral proteins, perhaps the best-known example is the Influenza A virus (IAV) NS1 protein. This non-structural protein is abundantly expressed in infected cells and acts in multiple stages of the viral cycle, with important roles in IFN antagonism including sequestering double-stranded RNA (dsRNA), inhibiting dsRNA-activated protein kinase (PKR) and contributing to the nuclear export of viral mRNAs while blocking the splicing and export of cellular mRNAs [49]. Seven lysine (K) residues in the NS1 protein were identified as potential target sites of ISGylation [50]. Specifically, ISG15 binding to K41, which is part of the NS1 nuclear-localization signal, prevents its interaction with importin-α, inhibiting the translocation of NS1 to the nucleus and therefore repressing IAV replication and viral RNA processing [51]. Moreover, ISGylation of the IAV NS1 protein blocks its ability to counteract the innate immune response, prevents its interaction with PKR and, therefore, restores IFN-induced antiviral activities against IAV [50].

Beyond NS1, Influenza virus nucleoprotein (NP) and matrix protein (M1) have also been reported as targets of ISG15 conjugation. ISGylated NP hinders the oligomerization of the more abundant unconjugated NP, acting as a dominant-negative inhibitor of NP oligomerization, impeding the formation of viral ribonucleoproteins and causing decreased viral protein synthesis and virus replication [52]. Interestingly, this study also identified a new role for Influenza B virus NS1 in the sequestration of ISGylated viral proteins, especially ISGylated NPs, which is perhaps an evolutionary mechanism to block the antiviral effect of ISGylation.

Another example of ISGylation of a viral protein with antiviral effects is the 2A protease (2Apro) of Coxsackievirus B3 (CVB3). ISG15 conjugation to 2Apro inhibits its ability to cleave the eukaryotic initiation factor eIF4G in cardiomyocytes, hindering the translational shutoff induced by CVB3 infection [53]. Consequently, ISG15 conjugation to CVB3 leads to a reduction in virus titers and limits inflammatory cardiomyopathy, heart failure and lethality [53]. Similarly, ISGylation of the HCMV scaffold protein pUL26 interferes with the viral modulation of the innate immune response. Specifically, ISGylation of pUL26 at K136 and K169 inactivates its function in the downregulation of TNFα-mediated NF-κB activation, suppressing HCMV growth [44]. Finally, another example of an ISGylated viral protein is the Human papillomavirus (HPV) L1 capsid protein. ISGylated L1 proteins were shown to be incorporated into HPV pseudoviruses, resulting in a reduced infectivity; the precise mechanism that mediates this inhibitory effect remains elusive [8].

1.4. ISGylated Cellular Proteins

Knowledge about the impact of host protein ISGylation in virus replication and cell homeostasis is still scant. In contrast to ubiquitylation, the molecular effect of ISG15 conjugation on target proteins is not always clear. Protein ISGylation has been reported to increase protein degradation by selective autophagy [54], but there are also many examples where ISGylation inhibits ubiquitylation, frustrating proteasome-mediated degradation of target proteins [55–57].

With regard to proteins involved in antiviral response, many effectors of IFN signaling such as PKR [58], retinoic acid-inducible gene-I (RIG-I) [59] and *Myxoma* resistance protein 1 (MxA) [60] have been reported to be targets of ISGylation. PKR ISGylation at K69 and K159, both located in the

dsRNA-binding motif, triggers its activation. This modification occurs in the absence of viral RNA and leads to the phosphorylation of eIF2α, preventing protein translation [58] and suggesting that ISGylation might mediate the activation of PKR in response to stressful stimuli beyond viral infection. Further, ISG15 conjugation to RIG-I decreases RIG-I cellular levels and downregulates RIG-I-mediated signaling. Accordingly, ISGylation of RIG-I represents a negative feedback loop that might control the strength of the antiviral response [59]. Interestingly, free ISG15 also regulates RIG-I levels by promoting the interaction between RIG-I and the autophagic cargo receptor p62, mediating RIG-I degradation *via* selective autophagy [61]. The interferon-induced MxA protein is also a target of ISGylation, though the effect of this modification is not clear.

Other proteins involved type-I IFN signaling and regulation, such as components of the JAK-STAT pathway or regulators of signal transduction (e.g., JAK1 and extracellular signal-regulated kinase 1 [ERK1]), are also bound by ISG15, although the functional consequences of ISGylation remain unknown [9,62]. Moreover, interferon regulatory factor 3 (IRF3), STAT1 and the actin-binding protein Filamin B are also targets for ISG15 conjugation, with implications in the development of the innate immune response. IRF3 is ISGylated at K193, K360 and K366, which attenuates its interaction with the peptidyl-prolyl isomerase PIN1, preventing IRF3 ubiquitylation. Thus, ISGylation of IRF3 sustains its activation and enhances IRF3-mediated antiviral responses by inhibiting its degradation [63]. In a similar manner, ISGylation of phosphorylated STAT1 (pSTAT1) inhibits its polyubiquitylation and further proteasomal degradation, supporting sustained STAT1 activation [57]. ISGylation of Filamin B, which acts as a scaffold of IFN signaling mediators, negatively regulates IFNα-induced c-Jun N-terminal kinases (JNK) signaling, preventing apoptosis induction [64].

Beyond antiviral response, ISGylation has been described to block the process of virus budding by interfering with the endosomal sorting complexes required for transport (ESCRT) machinery. For example, ISGylation of CHMP5 triggers its aggregation and the sequestration of the Vps4 cofactor LIP5, impairing the membrane recruitment of Vps4 and its interaction with the Gag budding complex of Avian sarcoma leukosis virus and HIV-1, leading to the inhibition of virus release from the cell [65]. Similarly, ISGylation of tumor susceptibility gene 101 protein (TSG101), another component of the ESCRT sorting complex, inhibits the trafficking of viral hemagglutinin to the cell surface during IAV infection [66], blocking virus release. ISG15 has also been described to inhibit the interaction of HIV-1 Gag protein with TSG101, underscoring a critical role of ISG15 in the IFN-mediated inhibition of HIV-1 budding and release [40]. This sorting mechanism is also used in the generation of exosomes, which are small vesicles secreted to the extracellular environment by most cell types. Interestingly, ISGylation of TSG101 has been recently reported to inhibit exosome secretion [67].

The above examples serve to illustrate the relevance of ISGylation in the induction and regulation of the antiviral response (for a more complete review of ISGylated cellular proteins see Reference [30]), and highlight the complexity of fully understanding the consequences of ISGylation in the regulation of biochemical processes where it is involved. Although the significance of ISGylation of host proteins has been elucidated for only a small set of cellular proteins, ISGylation has a broad target specificity, and there is increasing evidence for its role in regulating many cellular functions. To address this concept, several proteomic studies have been performed to determine ISGylated host proteins. Zhao et al. [60] transfected a tagged ISG15 protein into IFN-stimulated HeLa cells, and used affinity selection to identify 158 ISGylated proteins. In a similar approach, Giannakopoulos et al. [68] used IFN-stimulated USP18-/- mouse embryonic fibroblasts and human U937 cells to detect up to 76 proteins conjugated to endogenously-expressed ISG15. A third proteomic study [69] identified 174 ISGylated cellular proteins in IFN-stimulated A549 human lung adenocarcinoma cells stably expressing FLAG-ISG15. More recently, Peng et al. [70] examined ISGylated proteins in Influenza virus-infected A549 cells, identifying a total of 22 cellular proteins in addition to viral NS1 protein. We have surveyed the proteins identified by these four studies, which rendered up to 330 cellular proteins. Identified proteins include, as previously outlined [8], abundant constitutively expressed proteins as well as diverse interferon-induced proteins. Interestingly, there is only a low degree of overlap between

included in each study, as it is believed that the biological effects of ISGylation are dynamic and cell type/tissue specific [5].

We used DAVID bioinformatics resources [71,72] to determine the subcellular localization of the proteins identified as ISGylation targets in the aforementioned studies, with the aim to obtain a comprehensive picture of the broad range of actions of ISG15. In agreement with a previous report [73], our analysis (Figure 2) shows that ISG15-targeted proteins are found almost throughout the cell, including nucleus, perinuclear space, cytosol, mitochondria, rough endoplasmic reticulum and cell membranes [73]. Moreover, a similar percentage of ISGylation targets were predicted to be located in the nucleus, cytoplasm, extracellular space or as secreted proteins (Figure 2). Interestingly, proteins associated with cytoskeleton and cell junctions represent a significant percentage of the ISG15 target proteins. Other cell structures such as the melanosome or myelin sheath were also represented in the study, perhaps accounting for a specific role of ISGylation in these organelles.

The potential role of ISG15 in mitochondria seems to be relevant, as a recent study predicted that 17% of free ISG15 was localized to mitochondria [13]. In our own analysis of the above proteomic studies, fifty-two ISGylated proteins were predicted to localize to mitochondria, representing about 5% of the total ISG15 target proteins (Figure 2). Further examination of these potentially ISGylated proteins indicate that different mitochondrial processes could be affected by ISG15 conjugation (Table 1). Remarkably, several subunits of the ATP synthase (complex V of the respiratory chain) appear to be ISG15 targets, which may be of relevance as mitochondrial ATP production is the main source of energy for the cell. In line with these observations, our recent work linked ISG15 to the control of the mitochondrial oxidative metabolism in macrophages in the context of viral infection [29]. Based on the evident association between ISG15 and mitochondria, we will briefly review the role of mitochondria as antiviral mediators and targets of ubiquitin-like modifiers, focusing on the current knowledge about ISG15- and ISGylation-mediated regulation of these multifunctional organelles.

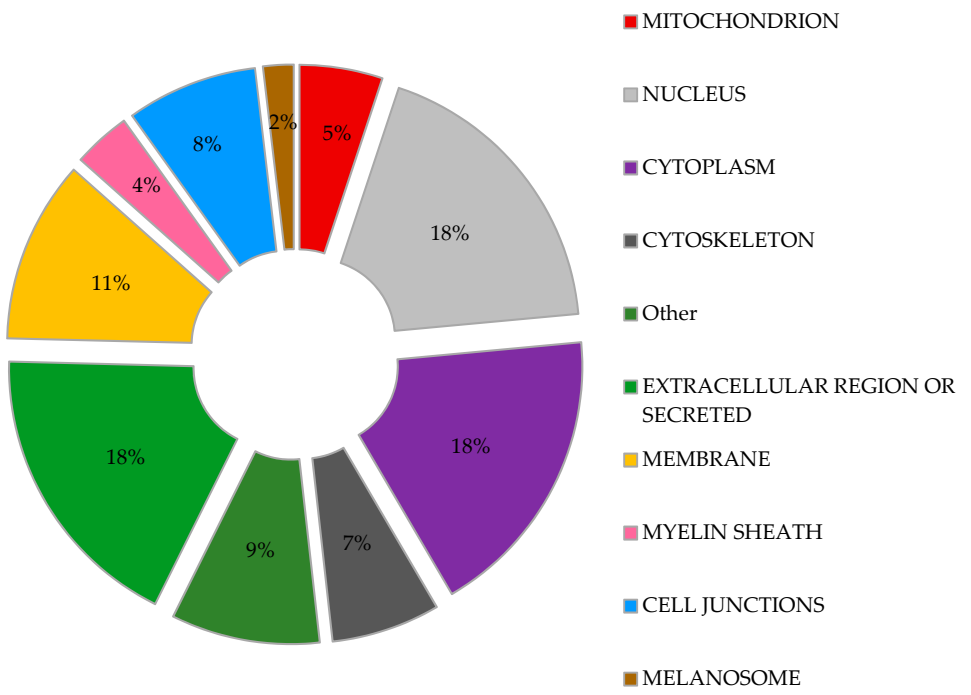

Figure 2. *Predicted subcellular distribution of ISGylated proteins.* Proteins identified as ISGylation targets in different proteomic studies were evaluated for their subcellular location. Percentage of the total ISGylated proteins located in each cellular organelle is shown.

Figure 2. *Predicted subcellular distribution of ISGylated proteins.* Proteins identified as ISGylation targets in different proteomic studies were evaluated for their subcellular location. Percentage of the total ISGylated proteins located in each cellular organelle is shown.

Table 1. ISGylated proteins predicted to locate to mitochondria. Proteins identified as ISGylation targets in different proteomic studies [60,68–70] predicted to locate to mitochondria. Proteins are grouped according to biological functions.

Biological Function	Potentially ISGylated Mitocondrial Proteins
Host-virus interaction	Acyl-CoA thioesterase 8 (ACOT8) [60]
	Complement C1q binding protein (C1QBP) [69]
	Receptor for activated C kinase 1 (RACK1) [60]
	Solute carrier family 25 member 5 (SLC25A5) [69]
	Solute carrier family 25 member 6 (SLC25A6) [69]
	Staphylococcal nuclease and tudor domain containing 1 (SND1) [69]
Negative regulation of apoptotic process	NME/NM23 nucleoside diphosphate kinase 2 (NME2) [69]
	Annexin A1 (ANXA1) [69,70]
	Glutathione S-transferase pi 1 (GSTP1) [60]
	Heat shock protein family A (Hsp70) member 5 (HSPA5) [69]
	Interferon-induced protein with tetratricopeptide repeats 3 (IFIT3) [60]
Positive regulation of protein insertion into mitochondrial membrane involved in apoptotic signaling pathway	Stratifin (SFN) [69]
	Tyrosine 3-monooxygenase/tryptophan 5-monooxygenase activation protein beta (YWHAB) [69]
	Tyrosine 3-monooxygenase/tryptophan 5-monooxygenase activation protein épsilon (YWHAE) [69]
	Tyrosine 3-monooxygenase/tryptophan 5-monooxygenase activation protein gamma (YWHAG) [69]
	Tyrosine 3-monooxygenase/tryptophan 5-monooxygenase activation protein theta (YWHAQ) [69]
	Tyrosine 3-monooxygenase/tryptophan 5-monooxygenase activation protein zeta (YWHAZ) [69]
ATP biosynthetic process	ATP synthase, H+ transporting, mitochondrial F1 complex, alpha subunit 1, cardiac muscle (ATP5A1) [60,69]
	ATP synthase, H+ transporting, mitochondrial F1 complex, beta polypeptide (ATP5B) [60,69]
	ATP synthase, H+ transporting, mitochondrial Fo complex subunit G (ATP5L) [70]
Oxidation-reduction process	Aldehyde dehydrogenase 18 family member A1 (ALDH18A1) [70]
	Fatty acid synthase (FASN) [60,69]
	Glutathione-disulfide reductase (GSR) [69]
	Lactate dehydrogenase B (LDHB) [69]
	Malic enzyme 1 (ME1) [68]
	Peroxiredoxin 1 (PRDX1) [60,69,70]
	Peroxiredoxin 4 (PRDX4) [69]
	Sorbitol dehydrogenase (SORD) [68]
	Superoxide dismutase 1, soluble(SOD1) [69]
	Thioredoxin reductase 1 (TXNRD1) [60,69]
	Thioredoxin (TXN) [69]
Aminoacyl-tRNA synthetase	Alanyl-tRNA synthetase (AARS) [68]
	Glycyl-tRNA synthetase (GARS) [68]
	Phenylalanyl-tRNA synthetase 2, mitocondrial (FARS2) [60]
Tricarboxylic acid cycle	Malate dehydrogenase 1 (MDH1) [69]
	Malate dehydrogenase 2 (MDH2) [69]
Glycolisis	Oxoglutarate dehydrogenase (OGDH) [60]
	Pyruvate kinase, muscle (PKM) [60,69,70]

Table 1. *Cont.*

Biological Function	Potentially ISGylated Mitocondrial Proteins
Chaperone	Chaperonin containing TCP1 subunit 7 (CCT7) [69]
	Heat shock protein 90 alpha family class B member 1 (HSP90AB1) [60,69,70]
	Heat shock protein family A (Hsp70) member 1A (HSPA1A) [60,69]
	Heat shock protein family D (Hsp60) member 1 (HSPD1) [60,69]
Ion channel	Chloride intracellular channel 1 (CLIC1) [60,69]
	Annexin A6 (ANXA6) [69]
Other functions	Creatine kinase, mitochondrial 1B (CKMT1B) [69]
	Ubiquitin-like modifier activating enzyme 1 (UBA1) [69]
	Leucine aminopeptidase 3 (LAP3) [60]
	5-aminoimidazole-4-carboxamide ribonucleotide formyltransferase/IMP cyclohydrolase (ATIC) [60,69]
	clathrin heavy chain (CLTC) [60,69]
	Queuine tRNA-ribosyltransferase accessory subunit 2 (QTRT2) [60]
	Enoyl-CoA hydratase and 3-hydroxyacyl CoA dehydrogenase (EHHADH) [69]
	ATP binding cassette subfamily F member 2 (ABCF2) [60]

2. Mitochondria: Key Organelles in Antiviral Responses

Mitochondria have myriad functions in the cell although they are best known for providing energy in the form of ATP and for controlling metabolism to maintain energy homeostasis. Owing to their endosymbiotic origin, mitochondria have their own genome, a single 16-kb circular DNA which codes for 13mitochondrial proteins, 2 ribosomal RNAs and 22 transfer RNAs [74]. The remainder of mitochondrial proteins are encoded by nuclear DNA and are then transported to the mitochondria through the recognition of amino acid sequences known as mitochondrial targeting signals [75]. As double-membrane organelles, mitochondria have an outer mitochondrial membrane (OMM), where proteins responsible for transport of different molecules are embedded [76]; an intermembrane space (IMS) and an inner mitochondrial membrane (IMM), where electron transport chain (ETC) proteins are localized and oxidative phosphorylation (OXPHOS) and ATP production takes place [77], and a mitochondrial matrix (MM), compartment, where many metabolic pathways occur, such as the tricarboxylic acid cycle, fatty-acid oxidation, synthesis of biomolecules and regulation of apoptosis [78]. The proper development of mitochondrial processes is critical for immune response, as the susceptibility to microbial infections and the risk of systemic inflammatory responses increases considerably when these organelles malfunction [79,80].

Mitochondria are important for antiviral signaling. During RNA-virus infection, viral RNAs are initially recognized by cytoplasmic sensors, mainly RIG-I-like receptors (RLRs) [2], whose interaction with mitochondria is essential for the coordination and development of an adequate antiviral response. The common structure of RLRs consists of a carboxy-terminal regulatory domain, a central RNA helicase domain and amino-terminal caspase recruitment domains (CARDs) [81]. After binding to viral RNA, RLRs trigger IFN-mediated antiviral responses through their interaction with mitochondrial antiviral-signaling protein (MAVS), a CARD-containing OMM protein [82]. The CARD-CARD interaction between RLRs and MAVS causes MAVS polymerization and consequent recruitment of a variety of downstream effectors, including tumor necrosis factor receptor-associated factor family proteins, IKB kinase *epsilon* (IKKε) and TANK binding kinase 1, among others [83]. This "MAVS signalosome" activates NF-κB, IRF3 and IRF7, promoting the expression of type-I IFN and antiviral molecules [84]. Given the central role of MAVS in mitochondrial antiviral signaling, MAVS and both upstream and downstream molecules are under tight regulation to ensure an adequate response [85,86].

Mitochondria are dynamic organelles that undergo constant fusion and fission to regulate their morphology, activity and turnover according to the metabolic needs of the cell [87], and these

mitochondrial dynamics are involved in the regulation of mitochondrial immune functions. Mitofusins and optic atrophy protein 1 are responsible for mitochondrial fusion, whereas the cytosolic GTP-ase dynamin-related protein 1 (Drp1) mediates mitochondrial fission through its interaction with adaptor proteins in the OMM [88,89]. Interestingly, these proteins have been shown to be implicated in the regulation of various mitochondrial immune-relevant processes, such as RLR signaling [83,90,91], apoptosis [92,93], autophagy and mitochondrial bioenergetic conditions [94], which are important mechanisms to combat viral infections.

Mitophagy is a selective autophagic process in which defective mitochondria are engulfed in autophagosomes and eliminated by fusion with lysosomes [95]. Damaged mitochondria constitute a signal for the recruitment of PTEN-induced putative kinase protein 1 (PINK1), which surrounds the mitochondrial surface. The accumulation of PINK1 and its kinase activity promote the translocation of the E3 ubiquitin ligase Parkin from the cytosol to dysfunctional mitochondria, triggering the ubiquitylation of OMM proteins. The formation of ubiquitin chains by Parkin favors the binding of adaptor proteins (e.g., p62 and optineurin), which mediate the interaction with autophagosomes and the further degradation of dysfunctional mitochondria [96,97]. Mitophagy is closely related to mitochondrial dynamics, as mitochondrial fragmentation promotes mitophagy whereas mitochondrial fusion hinders this process [98,99]. Interestingly, defective mitochondria can play either positive or negative roles against viruses. For example, alterations in mitochondrial respiration trigger the production of reactive oxygen species (ROS) which, in addition to being harmful for the cell in high levels, play an important role as second messengers in diverse intracellular signaling pathways [100]. In the context of antiviral signaling, ROS are involved in the regulation of the RLR pathway, potentiating RLR-MAVS signaling and the production of type-I IFN [101]. Because healthy mitochondria are required for an adequate metabolic state and the activation of apoptotic processes [94,102,103], mitophagy must be finely regulated to modulate the mitochondria-mediated antiviral response.

The implications of mitochondria in innate immunity are enormous. We have briefly discussed the interplay between different mitochondrial pathways, such as RLR signaling, mitochondrial dynamics, mitophagy, ROS production and apoptosis, in the protection against viruses. However, mitochondria perform a plethora of functions in the establishment of a defensive state of the cell, which have been thoroughly reviewed by others [85,104–108]. Moreover, the regulation of mitochondrial function is not only carried out by the host, but also by viruses with the aim to shut down defense mechanisms, complete their life cycle and spread [109], underscoring the relevance of mitochondria in antiviral response. Such critical roles of mitochondria in the control of pathogen invasion and maintenance of cellular homeostasis must be strictly coordinated.

2.1. Mitochondria: Targets of Ubiquitin-Like Modifications

As we previously discussed, ubiquitin and ubiquitin-like PTMs are key regulatory processes of the innate and adaptive immune response against viruses, and both processes are finely regulated by mitochondria. In this regard, there is a broad spectrum of PTMs [110], some of which occur within mitochondria, which are responsible for modifying their internal state and function [111,112]. Thus, mitochondria are targets of ubiquitin and ubiquitin-like proteins, such as small ubiquitin-like modifiers (SUMOs) and ISG15.

Ubiquitin is a highly conserved 8.6-kDa protein known as a master regulator of cellular processes. Its covalent conjugation to target proteins has proteolytic and non-proteolytic or regulatory outcomes, which fine-tune protein function and recycling [113]. Indeed, ubiquitylation is essential for the regulation of many mitochondrial processes, such as mitophagy [95,114–116], mitochondrial dynamics [117,118], and mitochondria-related immune signaling [86,119,120], establishing the importance of this modifier in the homeostasis of these organelles.

SUMOs are a family of highly conserved 12-kDa proteins that are essential in eukaryotic cells. Similar to ubiquitin, SUMO conjugation to specific lysine residues of target proteins (SUMOylation)

alters their function, their interaction with other proteins, and their stability [121,122]. Although the major role of SUMOylation is in the regulation of nuclear processes [123], it also targets mitochondria. SUMOs have been proven to be involved in the regulation of mitochondrial dynamics by binding to Drp1 [124], with an important implication in programmed cell death [125–127]. Furthermore, SUMOylation of the mitochondrial oxidative stress sensor DJ-1 results in its stabilization and full activation, reinforcing its protective role against Parkinson's disease [128], where mitochondrial dysfunction has great significance.

ISG15 and Mitochondria

Although ISG15 has been associated with mitochondria, its functions, both free or conjugated to mitochondrial proteins, are still being examined. One exception is the protein Parkin. While not strictly a mitochondrial protein, its translocation to the OMM from the cytoplasm is essential for Parkin-mediated mitophagy [96]. ISG15 conjugation to Parkin enhances its E3 ubiquitin ligase activity and its cytoprotective effect in Parkinson's disease [129], an example of how ISGylation affects mitochondrial processes.

ISG15 and ISGylation for the regulation of mitochondrial metabolism [29]. We undertook a comprehensive analysis of bone marrow-derived macrophages (BMDMs) from wild-type and *ISG15*-/- mice to interrogate how ISG15 and ISGylation could modulate the regulation of mitochondria in the context of stressful stimuli. Monomeric ISG15 and ISGylated proteins were observed in mitochondrial fractions from wild-type BMDMs after type-I IFN pre-treatment, and these proteins were preferentially located to the IMS and IMM (Figure 3). Given their localization, we hypothesized that ISG15 and ISGylation could impact mitochondrial respiratory metabolism, and we focused our study on OXPHOS and ATP production. This analysis revealed that oxygen consumption and ATP production were lower in *ISG15*-/- BMDMs than in equivalent wild-type cells, indicative of defective OXPHOS. In accord with these observations, a clear difference in the distribution of ETC supercomplexes was observed between the two groups, pointing to a possible role for ISG15 in the correct assembly of ETC proteins (Figure 3). As recently reported by Yoshizumi et al. [130] OXPHOS activity is required for RLR-mediated antiviral signaling, and mice with OXPHOS defects showed increased susceptibility to viral infections. Similarly, knockout mice for ISG15 or the ISG15-activating E1 enzyme (Ube1L) were more susceptible to infection with many viruses than wild-type mice [30]. Since the lack of ISG15 seems to cause alterations in OXPHOS, such increase in the sensitivity to viral infections in *ISG15*-/- and Ube1L-/- mice might be explained as a result of defects in RLR-mediated antiviral responses, supporting the role of ISG15 as a regulator of mitochondrial functions. Regarding mitochondrial respiration byproducts, *ISG15*-/- BMDM also produced lower levels of ROS. Because ROS production is tightly controlled by mitochondrial membrane potential [131], low levels of ROS in *ISG15*-/- BMDM might be the result of abnormalities in the transmembrane proton gradient due to the absence of ISG15, and could affect the immune response against viral infections, as discussed earlier. Mitochondrial ROS also participate in the regulation of macrophage polarization [132] and, interestingly, *ISG15*-/- BMDMs displayed mixed features of M1 and M2 phenotypes, suggesting that alterations in mitochondrial OXPHOS could drive changes to immune cell function. Finally, BMDMs lacking ISG15 accumulated non-functional mitochondria with an absence of Parkin, suggesting that ISG15 is also implicated in the regulation of mitophagy, perhaps through the control of Parkin translocation from the cytosol (Figure 3).

Taken together, these findings establish a relevant role for ISG15 and ISGylation in the control of mitochondrial OXPHOS and recycling, at least in murine BMDM, expanding the range of functions of this PTM and underscoring its importance in the regulation of essential cellular processes.

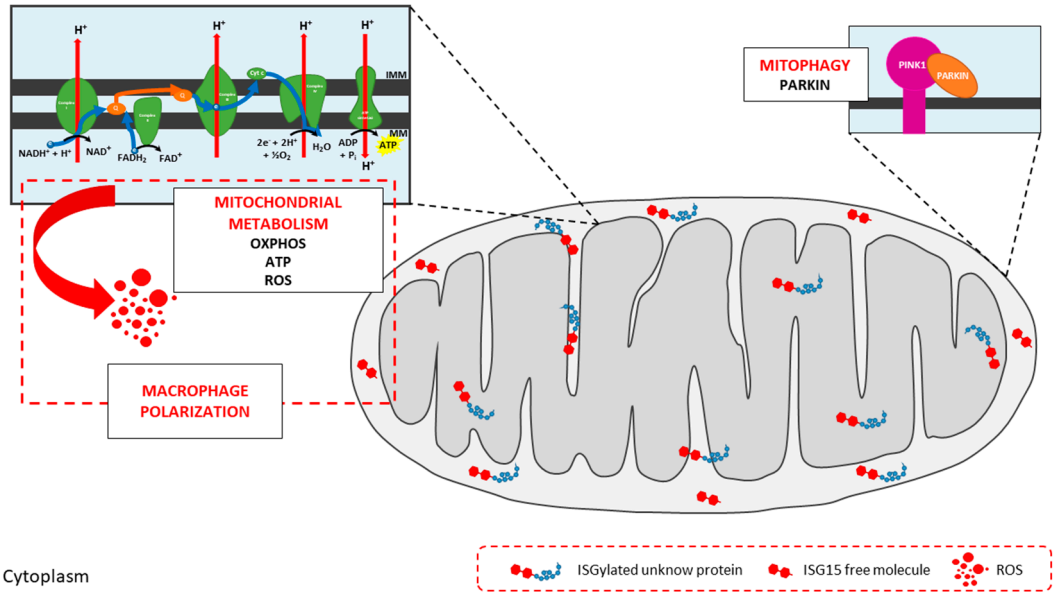

Figure 3. *Impact of ISG15 on mitochondrial activities.* Mitochondria are targets of ISG15 and ISGylation in murine bone marrow-derived macrophages (BMDMs). ISGylated proteins can be found in all mitochondrial localizations, mainly in the mitochondrial intermembrane space (IMS) and inner mitochondrial membrane (IMM), where free ISG15 is also present. ISG15 and ISGylation are involved in the regulation of mitochondrial metabolism. Absence of ISG15 leads to alterations in OXPHOS, with lower oxygen consumption rates and ATP production levels, in addition to aberrant ETC supercomplexes assembly. Such disruption of OXPHOS mechanisms decreases ROS production, with repercussions for macrophage polarization. Mitophagy is also altered in cells lacking ISG15. Finally, *ISG15-/-* BMDM accumulate defective mitochondria and Parkin cannot be found in mitochondrial extracts, suggesting that ISG15 is important during the translocation of Parkin from the cytoplasm to mitochondria.

3. Future Perspectives

The functional significance of PTMs in disease etiology, and the pathologic response to their disruption, is the subject of intense investigation. Many of these reversible modifications act as regulatory mechanisms in mitochondria and show promise for mitochondria-targeted therapeutic strategies. With the advent of mass spectrometry-based screening techniques, there has been a vast increase in our current state of knowledge on mitochondrial PTMs and their protein targets. Detecting ISGylated proteins in different organelles remains challenging, as it typically occurs in only a small portion of the total protein pool of the cell, albeit with essential roles in regulating protein fate and function. Understanding the consequences of ISGylation of mitochondrial proteins will require much work, but should be rewarding not only for developing new strategies to combat viral infections, but also for future applications in other biomedically relevant processes/diseases, for example inflammation, cancer and neurodegeneration.

Funding: This work was supported by grant SAF2014-54623-R and SAF2017-88089-R (funded both by MINISTERIO DE ECONOMÍA, INDUSTRIA Y COMPETIVIDAD, and FEDER/FSE).

Acknowledgments: We thank Diego Sanz for his technical assistance and Kenneth McCreath for reviewing and correcting the manuscript.

Conflicts of Interest: The authors declare no conflicts of interest.

References

1. Iwasaki, A. A virological view of innate immune recognition. *Annu. Rev. Microbiol.* **2012**, *66*, 177–196.
2. Brubaker, S.W.; Bonham, K.S.; Zanoni, I.; Kagan, J.C. Innate immune pattern recognition: A cell biological perspective. *Annu. Rev. Immunol.* **2015**, *33*, 257–290.

References

1. Iwasaki, A. A virological view of innate immune recognition. *Annu. Rev. Microbiol.* **2012**, *66*, 177–196. [CrossRef] [PubMed]
2. Brubaker, S.W.; Bonham, K.S.; Zanoni, I.; Kagan, J.C. Innate immune pattern recognition: A cell biological perspective. *Annu. Rev. Immunol.* **2015**, *33*, 257–290. [CrossRef] [PubMed]
3. Ivashkiv, L.B.; Donlin, L.T. Regulation of type I interferon responses. *Nat. Rev. Immunol.* **2014**, *14*, 36–49. [CrossRef] [PubMed]
4. Raftery, N.; Stevenson, N.J. Advances in anti-viral immune defence: Revealing the importance of the IFN JAK/STAT pathway. *Cell. Mol. Life Sci.* **2017**, *74*, 2525–2535. [CrossRef] [PubMed]
5. Zhang, D.; Zhang, D.E. Interferon-stimulated gene 15 and the protein ISGylation system. *J. Interferon Cytokine Res.* **2011**, *31*, 119–130. [CrossRef] [PubMed]
6. Potter, J.L.; Narasimhan, J.; Mende-Mueller, L.; Haas, A.L. Precursor processing of pro-ISG15/UCRP, an interferon-beta-induced ubiquitin-like protein. *J. Biol. Chem.* **1999**, *274*, 25061–25068. [CrossRef] [PubMed]
7. Durfee, L.A.; Huibregtse, J.M. The ISG15 conjugation system. *Methods Mol. Biol.* **2012**, *832*, 141–149. [PubMed]
8. Durfee, L.A.; Lyon, N.; Seo, K.; Huibregtse, J.M. The ISG15 conjugation system broadly targets newly synthesized proteins: Implications for the antiviral function of ISG15. *Mol. Cell* **2010**, *38*, 722–732. [CrossRef] [PubMed]
9. Malakhov, M.P.; Kim, K.I.; Malakhova, O.A.; Jacobs, B.S.; Borden, E.C.; Zhang, D.E. High-throughput immunoblotting. Ubiquitiin-like protein ISG15 modifies key regulators of signal transduction. *J. Biol. Chem.* **2003**, *278*, 16608–16613. [CrossRef] [PubMed]
10. Villarroya-Beltri, C.; Guerra, S.; Sanchez-Madrid, F. ISGylation—A key to lock the cell gates for preventing the spread of threats. *J. Cell Sci.* **2017**, *130*, 2961–2969. [CrossRef] [PubMed]
11. Taylor, J.L.; D'Cunha, J.; Tom, P.; O'Brien, W.J.; Borden, E.C. Production of ISG-15, an interferon-inducible protein, in human corneal cells. *J. Interferon Cytokine Res.* **1996**, *16*, 937–940. [CrossRef] [PubMed]
12. Cai, B.; Bai, Q.; Chi, X.; Goraya, M.U.; Wang, L.; Wang, S.; Chen, B.; Chen, J.L. Infection with Classical Swine Fever Virus Induces Expression of Type III Interferons and Activates Innate Immune Signaling. *Front. Microbiol.* **2017**, *8*, 2558. [CrossRef] [PubMed]
13. Tecalco Cruz, A.C.; Mejia-Barreto, K. Cell type-dependent regulation of free ISG15 levels and ISGylation. *J. Cell Commun. Signal.* **2017**, *11*, 127–135. [CrossRef] [PubMed]
14. Malakhova, O.; Malakhov, M.; Hetherington, C.; Zhang, D.E. Lipopolysaccharide activates the expression of ISG15-specific protease UBP43 via interferon regulatory factor 3. *J. Biol. Chem.* **2002**, *277*, 14703–14711. [CrossRef] [PubMed]
15. Pitha-Rowe, I.; Hassel, B.A.; Dmitrovsky, E. Involvement of UBE1L in ISG15 conjugation during retinoid-induced differentiation of acute promyelocytic leukemia. *J. Biol. Chem.* **2004**, *279*, 18178–18187. [CrossRef] [PubMed]
16. Jeon, Y.J.; Park, J.H.; Chung, C.H. Interferon-Stimulated Gene 15 in the Control of Cellular Responses to Genotoxic Stress. *Mol. Cells* **2017**, *40*, 83–89. [CrossRef] [PubMed]
17. Honke, N.; Shaabani, N.; Zhang, D.E.; Hardt, C.; Lang, K.S. Multiple functions of USP18. *Cell Death Dis.* **2016**, *7*, e2444. [CrossRef] [PubMed]
18. Zhang, X.; Bogunovic, D.; Payelle-Brogard, B.; Francois-Newton, V.; Speer, S.D.; Yuan, C.; Volpi, S.; Li, Z.; Sanal, O.; Mansouri, D.; et al. Human intracellular ISG15 prevents interferon-alpha/beta over-amplification and auto-inflammation. *Nature* **2015**, *517*, 89–93. [CrossRef] [PubMed]
19. Speer, S.D.; Li, Z.; Buta, S.; Payelle-Brogard, B.; Qian, L.; Vigant, F.; Rubino, E.; Gardner, T.J.; Wedeking, T.; Hermann, M.; et al. ISG15 deficiency and increased viral resistance in humans but not mice. *Nat. Commun.* **2016**, *7*, 11496. [CrossRef] [PubMed]
20. Bogunovic, D.; Byun, M.; Durfee, L.A.; Abhyankar, A.; Sanal, O.; Mansouri, D.; Salem, S.; Radovanovic, I.; Grant, A.V.; Adimi, P.; et al. Mycobacterial disease and impaired IFN-gamma immunity in humans with inherited ISG15 deficiency. *Science* **2012**, *337*, 1684–1688. [CrossRef] [PubMed]
21. Swaim, C.D.; Scott, A.F.; Canadeo, L.A.; Huibregtse, J.M. Extracellular ISG15 Signals Cytokine Secretion through the LFA-1 Integrin Receptor. *Mol. Cell* **2017**, *68*, 581–590. [CrossRef] [PubMed]

22. D'Cunha, J.; Knight, E., Jr.; Haas, A.L.; Truitt, R.L.; Borden, E.C. Immunoregulatory properties of ISG15, an interferon-induced cytokine. *Proc. Natl. Acad. Sci. USA* **1996**, *93*, 211–215. [CrossRef] [PubMed]
23. Padovan, E.; Terracciano, L.; Certa, U.; Jacobs, B.; Reschner, A.; Bolli, M.; Spagnoli, G.C.; Borden, E.C.; Heberer, M. Interferon stimulated gene 15 constitutively produced by melanoma cells induces e-cadherin expression on human dendritic cells. *Cancer Res.* **2002**, *62*, 3453–3458. [PubMed]
24. Owhashi, M.; Taoka, Y.; Ishii, K.; Nakazawa, S.; Uemura, H.; Kambara, H. Identification of a ubiquitin family protein as a novel neutrophil chemotactic factor. *Biochem. Biophys. Res. Commun.* **2003**, *309*, 533–539. [CrossRef] [PubMed]
25. Napolitano, A.; van der Veen, A.G.; Bunyan, M.; Borg, A.; Frith, D.; Howell, S.; Kjaer, S.; Beling, A.; Snijders, A.P.; Knobeloch, K.P.; et al. Cysteine-Reactive Free ISG15 Generates IL-1beta-Producing CD8alpha(+) Dendritic Cells at the Site of Infection. *J. Immunol.* **2018**, *201*, 604–614. [CrossRef] [PubMed]
26. Takeuchi, T.; Iwahara, S.; Saeki, Y.; Sasajima, H.; Yokosawa, H. Link between the ubiquitin conjugation system and the ISG15 conjugation system: ISG15 conjugation to the UbcH6 ubiquitin E2 enzyme. *J. Biochem.* **2005**, *138*, 711–719. [CrossRef] [PubMed]
27. Okumura, A.; Pitha, P.M.; Harty, R.N. ISG15 inhibits Ebola VP40 VLP budding in an L-domain-dependent manner by blocking Nedd4 ligase activity. *Proc. Natl. Acad. Sci. USA* **2008**, *105*, 3974–3979. [CrossRef] [PubMed]
28. Fan, J.B.; Arimoto, K.; Motamedchaboki, K.; Yan, M.; Wolf, D.A.; Zhang, D.E. Identification and characterization of a novel ISG15-ubiquitin mixed chain and its role in regulating protein homeostasis. *Sci. Rep.* **2015**, *5*, 12704. [CrossRef] [PubMed]
29. Baldanta, S.; Fernandez-Escobar, M.; Acin-Perez, R.; Albert, M.; Camafeita, E.; Jorge, I.; Vazquez, J.; Enriquez, J.A.; Guerra, S. ISG15 governs mitochondrial function in macrophages following vaccinia virus infection. *PLoS Pathog.* **2017**, *13*, e1006651. [CrossRef] [PubMed]
30. Perng, Y.C.; Lenschow, D.J. ISG15 in antiviral immunity and beyond. *Nat. Rev. Microbiol.* **2018**, *16*, 423–439. [CrossRef] [PubMed]
31. Lenschow, D.J.; Lai, C.; Frias-Staheli, N.; Giannakopoulos, N.V.; Lutz, A.; Wolff, T.; Osiak, A.; Levine, B.; Schmidt, R.E.; Garcia-Sastre, A.; et al. IFN-stimulated gene 15 functions as a critical antiviral molecule against influenza, herpes, and Sindbis viruses. *Proc. Natl. Acad. Sci. USA* **2007**, *104*, 1371–1376. [CrossRef] [PubMed]
32. Giannakopoulos, N.V.; Arutyunova, E.; Lai, C.; Lenschow, D.J.; Haas, A.L.; Virgin, H.W. ISG15 Arg151 and the ISG15-conjugating enzyme UbE1L are important for innate immune control of Sindbis virus. *J. Virol.* **2009**, *83*, 1602–1610. [CrossRef] [PubMed]
33. Lenschow, D.J.; Giannakopoulos, N.V.; Gunn, L.J.; Johnston, C.; O'Guin, A.K.; Schmidt, R.E.; Levine, B.; Virgin, H.W.T. Identification of interferon-stimulated gene 15 as an antiviral molecule during Sindbis virus infection in vivo. *J. Virol.* **2005**, *79*, 13974–13983. [CrossRef] [PubMed]
34. Werneke, S.W.; Schilte, C.; Rohatgi, A.; Monte, K.J.; Michault, A.; Arenzana-Seisdedos, F.; Vanlandingham, D.L.; Higgs, S.; Fontanet, A.; Albert, M.L.; et al. ISG15 is critical in the control of Chikungunya virus infection independent of UbE1L mediated conjugation. *PLoS Pathog.* **2011**, *7*, e1002322. [CrossRef] [PubMed]
35. Kim, J.H.; Luo, J.K.; Zhang, D.E. The level of hepatitis B virus replication is not affected by protein ISG15 modification but is reduced by inhibition of UBP43 (USP18) expression. *J. Immunol.* **2008**, *181*, 6467–6472. [CrossRef] [PubMed]
36. Ritchie, K.J.; Hahn, C.S.; Kim, K.I.; Yan, M.; Rosario, D.; Li, L.; de la Torre, J.C.; Zhang, D.E. Role of ISG15 protease UBP43 (USP18) in innate immunity to viral infection. *Nat. Med.* **2004**, *10*, 1374–1378. [CrossRef] [PubMed]
37. Knobeloch, K.P.; Utermohlen, O.; Kisser, A.; Prinz, M.; Horak, I. Reexamination of the role of ubiquitin-like modifier ISG15 in the phenotype of UBP43-deficient mice. *Mol. Cell. Biol.* **2005**, *25*, 11030–11034. [CrossRef] [PubMed]
38. Moore, E.C.; Barber, J.; Tripp, R.A. Respiratory syncytial virus (RSV) attachment and nonstructural proteins modify the type I interferon response associated with suppressor of cytokine signaling (SOCS) proteins and IFN-stimulated gene-15 (ISG15). *Virol. J.* **2008**, *5*, 116. [CrossRef] [PubMed]

39. Gonzalez-Sanz, R.; Mata, M.; Bermejo-Martin, J.; Alvarez, A.; Cortijo, J.; Melero, J.A.; Martinez, I. ISG15 Is Upregulated in Respiratory Syncytial Virus Infection and Reduces Virus Growth through Protein ISGylation. *J. Virol.* **2016**, *90*, 3428–3438. [CrossRef] [PubMed]
40. Okumura, A.; Lu, G.; Pitha-Rowe, I.; Pitha, P.M. Innate antiviral response targets HIV-1 release by the induction of ubiquitin-like protein ISG15. *Proc. Natl. Acad. Sci. USA* **2006**, *103*, 1440–1445. [CrossRef] [PubMed]
41. Langevin, C.; van der Aa, L.M.; Houel, A.; Torhy, C.; Briolat, V.; Lunazzi, A.; Harmache, A.; Bremont, M.; Levraud, J.P.; Boudinot, P. Zebrafish ISG15 exerts a strong antiviral activity against RNA and DNA viruses and regulates the interferon response. *J. Virol.* **2013**, *87*, 10025–10036. [CrossRef] [PubMed]
42. Yuan, W.; Krug, R.M. Influenza B virus NS1 protein inhibits conjugation of the interferon (IFN)-induced ubiquitin-like ISG15 protein. *EMBO J.* **2001**, *20*, 362–371. [CrossRef] [PubMed]
43. Guerra, S.; Caceres, A.; Knobeloch, K.P.; Horak, I.; Esteban, M. Vaccinia virus E3 protein prevents the antiviral action of ISG15. *PLoS Pathog.* **2008**, *4*, e1000096. [CrossRef] [PubMed]
44. Kim, Y.J.; Kim, E.T.; Kim, Y.E.; Lee, M.K.; Kwon, K.M.; Kim, K.I.; Stamminger, T.; Ahn, J.H. Consecutive Inhibition of ISG15 Expression and ISGylation by Cytomegalovirus Regulators. *PLoS Pathog.* **2016**, *12*, e1005850. [CrossRef] [PubMed]
45. Frias-Staheli, N.; Giannakopoulos, N.V.; Kikkert, M.; Taylor, S.L.; Bridgen, A.; Paragas, J.; Richt, J.A.; Rowland, R.R.; Schmaljohn, C.S.; Lenschow, D.J.; et al. Ovarian tumor domain-containing viral proteases evade ubiquitin- and ISG15-dependent innate immune responses. *Cell Host Microbe* **2007**, *2*, 404–416. [CrossRef] [PubMed]
46. Deng, X.; Agnihothram, S.; Mielech, A.M.; Nichols, D.B.; Wilson, M.W.; StJohn, S.E.; Larsen, S.D.; Mesecar, A.D.; Lenschow, D.J.; Baric, R.S.; et al. A chimeric virus-mouse model system for evaluating the function and inhibition of papain-like proteases of emerging coronaviruses. *J. Virol.* **2014**, *88*, 11825–11833. [CrossRef] [PubMed]
47. Arnaud, N.; Dabo, S.; Akazawa, D.; Fukasawa, M.; Shinkai-Ouchi, F.; Hugon, J.; Wakita, T.; Meurs, E.F. Hepatitis C virus reveals a novel early control in acute immune response. *PLoS Pathog.* **2011**, *7*, e1002289. [CrossRef] [PubMed]
48. Chen, L.; Li, S.; McGilvray, I. The ISG15/USP18 ubiquitin-like pathway (ISGylation system) in hepatitis C virus infection and resistance to interferon therapy. *Int. J. Biochem. Cell Biol.* **2011**, *43*, 1427–1431. [CrossRef] [PubMed]
49. Marc, D. Influenza virus non-structural protein NS1: Interferon antagonism and beyond. *J. Gen. Virol.* **2014**, *95*, 2594–2611. [CrossRef] [PubMed]
50. Tang, Y.; Zhong, G.; Zhu, L.; Liu, X.; Shan, Y.; Feng, H.; Bu, Z.; Chen, H.; Wang, C. Herc5 attenuates influenza A virus by catalyzing ISGylation of viral NS1 protein. *J. Immunol.* **2010**, *184*, 5777–5790. [CrossRef] [PubMed]
51. Zhao, C.; Hsiang, T.Y.; Kuo, R.L.; Krug, R.M. ISG15 conjugation system targets the viral NS1 protein in influenza A virus-infected cells. *Proc. Natl. Acad. Sci. USA* **2010**, *107*, 2253–2258. [CrossRef] [PubMed]
52. Zhao, C.; Sridharan, H.; Chen, R.; Baker, D.P.; Wang, S.; Krug, R.M. Influenza B virus non-structural protein 1 counteracts ISG15 antiviral activity by sequestering ISGylated viral proteins. *Nat. Commun.* **2016**, *7*, 12754. [CrossRef] [PubMed]
53. Rahnefeld, A.; Klingel, K.; Schuermann, A.; Diny, N.L.; Althof, N.; Lindner, A.; Bleienheuft, P.; Savvatis, K.; Respondek, D.; Opitz, E.; et al. Ubiquitin-like protein ISG15 (interferon-stimulated gene of 15 kDa) in host defense against heart failure in a mouse model of virus-induced cardiomyopathy. *Circulation* **2014**, *130*, 1589–1600. [CrossRef] [PubMed]
54. Nakashima, H.; Nguyen, T.; Goins, W.F.; Chiocca, E.A. Interferon-stimulated gene 15 (ISG15) and ISG15-linked proteins can associate with members of the selective autophagic process, histone deacetylase 6 (HDAC6) and SQSTM1/p62. *J. Biol. Chem.* **2015**, *290*, 1485–1495. [CrossRef] [PubMed]
55. Desai, S.D.; Haas, A.L.; Wood, L.M.; Tsai, Y.C.; Pestka, S.; Rubin, E.H.; Saleem, A.; Nur, E.K.A.; Liu, L.F. Elevated expression of ISG15 in tumor cells interferes with the ubiquitin/26S proteasome pathway. *Cancer Res.* **2006**, *66*, 921–928. [CrossRef] [PubMed]
56. Liu, M.; Li, X.L.; Hassel, B.A. Proteasomes modulate conjugation to the ubiquitin-like protein, ISG15. *J. Biol. Chem.* **2003**, *278*, 1594–1602. [CrossRef] [PubMed]

57. Ganesan, M.; Poluektova, L.Y.; Tuma, D.J.; Kharbanda, K.K.; Osna, N.A. Acetaldehyde Disrupts Interferon Alpha Signaling in Hepatitis C Virus-Infected Liver Cells by Up-Regulating USP18. *Alcohol. Clin. Exp. Res.* **2016**, *40*, 2329–2338. [CrossRef] [PubMed]
58. Okumura, F.; Okumura, A.J.; Uematsu, K.; Hatakeyama, S.; Zhang, D.E.; Kamura, T. Activation of double-stranded RNA-activated protein kinase (PKR) by interferon-stimulated gene 15 (ISG15) modification down-regulates protein translation. *J. Biol. Chem.* **2013**, *288*, 2839–2847. [CrossRef] [PubMed]
59. Kim, M.J.; Hwang, S.Y.; Imaizumi, T.; Yoo, J.Y. Negative feedback regulation of RIG-I-mediated antiviral signaling by interferon-induced ISG15 conjugation. *J. Virol.* **2008**, *82*, 1474–1483. [CrossRef] [PubMed]
60. Zhao, C.; Denison, C.; Huibregtse, J.M.; Gygi, S.; Krug, R.M. Human ISG15 conjugation targets both IFN-induced and constitutively expressed proteins functioning in diverse cellular pathways. *Proc. Natl. Acad. Sci. USA* **2005**, *102*, 10200–10205. [CrossRef] [PubMed]
61. Du, Y.; Duan, T.; Feng, Y.; Liu, Q.; Lin, M.; Cui, J.; Wang, R.F. LRRC25 inhibits type I IFN signaling by targeting ISG15-associated RIG-I for autophagic degradation. *EMBO J.* **2018**, *37*, 351–366. [CrossRef] [PubMed]
62. Malakhova, O.A.; Yan, M.; Malakhov, M.P.; Yuan, Y.; Ritchie, K.J.; Kim, K.I.; Peterson, L.F.; Shuai, K.; Zhang, D.E. Protein ISGylation modulates the JAK-STAT signaling pathway. *Genes Dev.* **2003**, *17*, 455–460. [CrossRef] [PubMed]
63. Shi, H.X.; Yang, K.; Liu, X.; Liu, X.Y.; Wei, B.; Shan, Y.F.; Zhu, L.H.; Wang, C. Positive regulation of interferon regulatory factor 3 activation by Herc5 via ISG15 modification. *Mol. Cell. Biol.* **2010**, *30*, 2424–2436. [CrossRef] [PubMed]
64. Jeon, Y.J.; Choi, J.S.; Lee, J.Y.; Yu, K.R.; Kim, S.M.; Ka, S.H.; Oh, K.H.; Kim, K.I.; Zhang, D.E.; Bang, O.S.; et al. ISG15 modification of filamin B negatively regulates the type I interferon-induced JNK signalling pathway. *EMBO Rep.* **2009**, *10*, 374–380. [CrossRef] [PubMed]
65. Pincetic, A.; Kuang, Z.; Seo, E.J.; Leis, J. The interferon-induced gene ISG15 blocks retrovirus release from cells late in the budding process. *J. Virol.* **2010**, *84*, 4725–4736. [CrossRef] [PubMed]
66. Sanyal, S.; Ashour, J.; Maruyama, T.; Altenburg, A.F.; Cragnolini, J.J.; Bilate, A.; Avalos, A.M.; Kundrat, L.; Garcia-Sastre, A.; Ploegh, H.L. Type I interferon imposes a TSG101/ISG15 checkpoint at the Golgi for glycoprotein trafficking during influenza virus infection. *Cell Host Microbe* **2013**, *14*, 510–521. [CrossRef] [PubMed]
67. Villarroya-Beltri, C.; Baixauli, F.; Mittelbrunn, M.; Fernandez-Delgado, I.; Torralba, D.; Moreno-Gonzalo, O.; Baldanta, S.; Enrich, C.; Guerra, S.; Sanchez-Madrid, F. ISGylation controls exosome secretion by promoting lysosomal degradation of MVB proteins. *Nat. Commun.* **2016**, *7*, 13588. [CrossRef] [PubMed]
68. Giannakopoulos, N.V.; Luo, J.K.; Papov, V.; Zou, W.; Lenschow, D.J.; Jacobs, B.S.; Borden, E.C.; Li, J.; Virgin, H.W.; Zhang, D.E. Proteomic identification of proteins conjugated to ISG15 in mouse and human cells. *Biochem. Biophys. Res. Commun.* **2005**, *336*, 496–506. [CrossRef] [PubMed]
69. Wong, J.J.; Pung, Y.F.; Sze, N.S.; Chin, K.C. HERC5 is an IFN-induced HECT-type E3 protein ligase that mediates type I IFN-induced ISGylation of protein targets. *Proc. Natl. Acad. Sci. USA* **2006**, *103*, 10735–10740. [CrossRef] [PubMed]
70. Peng, Q.-S.; Li, G.-P.; Sun, W.-C.; Yang, J.-B.; Quan, G.-H.; Liu, N. Analysis of ISG15-Modified Proteins from A549 Cells in Response to Influenza Virus Infection by Liquid Chromatography-Tandem Mass Spectrometry. *Chin. J. Anal. Chem.* **2016**, *44*, 850–856. [CrossRef]
71. Huang, D.W.; Sherman, B.T.; Lempicki, R.A. Systematic and integrative analysis of large gene lists using DAVID bioinformatics resources. *Nat. Protoc.* **2009**, *4*, 44–57. [CrossRef] [PubMed]
72. Huang, D.W.; Sherman, B.T.; Lempicki, R.A. Bioinformatics enrichment tools: Paths toward the comprehensive functional analysis of large gene lists. *Nucleic Acids Res.* **2009**, *37*, 1–13. [CrossRef] [PubMed]
73. Austin, K.J.; Carr, A.L.; Pru, J.K.; Hearne, C.E.; George, E.L.; Belden, E.L.; Hansen, T.R. Localization of ISG15 and conjugated proteins in bovine endometrium using immunohistochemistry and electron microscopy. *Endocrinology* **2004**, *145*, 967–975. [CrossRef] [PubMed]
74. Shadel, G.S.; Clayton, D.A. Mitochondrial DNA maintenance in vertebrates. *Annu. Rev. Biochem.* **1997**, *66*, 409–435. [CrossRef] [PubMed]
75. Neupert, W.; Herrmann, J.M. Translocation of proteins into mitochondria. *Annu. Rev. Biochem.* **2007**, *76*, 723–749. [CrossRef] [PubMed]
76. Becker, T.; Wagner, R. Mitochondrial Outer Membrane Channels: Emerging Diversity in Transport Processes. *Bioessays* **2018**, *40*, e1800013. [CrossRef] [PubMed]

77. Papa, S.; Martino, P.L.; Capitanio, G.; Gaballo, A.; De Rasmo, D.; Signorile, A.; Petruzzella, V. The oxidative phosphorylation system in mammalian mitochondria. *Adv. Exp. Med. Biol.* **2012**, *942*, 3–37. [PubMed]
78. Cannino, G.; Ciscato, F.; Masgras, I.; Sanchez-Martin, C.; Rasola, A. Metabolic Plasticity of Tumor Cell Mitochondria. *Front. Oncol.* **2018**, *8*, 333. [CrossRef] [PubMed]
79. Singer, M. The role of mitochondrial dysfunction in sepsis-induced multi-organ failure. *Virulence* **2014**, *5*, 66–72. [CrossRef] [PubMed]
80. Shinde, A.; Luo, J.; Bharathi, S.S.; Shi, H.; Beck, M.E.; McHugh, K.J.; Alcorn, J.F.; Wang, J.; Goetzman, E.S. Increased mortality from influenza infection in long-chain acyl-CoA dehydrogenase knockout mice. *Biochem. Biophys. Res. Commun.* **2018**, *497*, 700–704. [CrossRef] [PubMed]
81. Kawai, T.; Akira, S. The roles of TLRs, RLRs and NLRs in pathogen recognition. *Int. Immunol.* **2009**, *21*, 317–337. [CrossRef] [PubMed]
82. Seth, R.B.; Sun, L.; Ea, C.K.; Chen, Z.J. Identification and characterization of MAVS, a mitochondrial antiviral signaling protein that activates NF-kappaB and IRF 3. *Cell* **2005**, *122*, 669–682. [CrossRef] [PubMed]
83. Koshiba, T.; Yasukawa, K.; Yanagi, Y.; Kawabata, S. Mitochondrial membrane potential is required for MAVS-mediated antiviral signaling. *Sci. Signal.* **2011**, *4*, ra7. [CrossRef] [PubMed]
84. Hou, F.; Sun, L.; Zheng, H.; Skaug, B.; Jiang, Q.X.; Chen, Z.J. MAVS forms functional prion-like aggregates to activate and propagate antiviral innate immune response. *Cell* **2011**, *146*, 448–461. [CrossRef] [PubMed]
85. Jin, H.S.; Suh, H.W.; Kim, S.J.; Jo, E.K. Mitochondrial Control of Innate Immunity and Inflammation. *Immune Netw.* **2017**, *17*, 77–88. [CrossRef] [PubMed]
86. Liu, B.; Gao, C. Regulation of MAVS activation through post-translational modifications. *Curr. Opin. Immunol.* **2018**, *50*, 75–81. [CrossRef] [PubMed]
87. Friedman, J.R.; Nunnari, J. Mitochondrial form and function. *Nature* **2014**, *505*, 335–343. [CrossRef] [PubMed]
88. Lee, H.; Yoon, Y. Mitochondrial fission: Regulation and ER connection. *Mol. Cells* **2014**, *37*, 89–94. [CrossRef] [PubMed]
89. Tilokani, L.; Nagashima, S.; Paupe, V.; Prudent, J. Mitochondrial dynamics: Overview of molecular mechanisms. *Essays Biochem.* **2018**, *62*, 341–360. [CrossRef] [PubMed]
90. Castanier, C.; Garcin, D.; Vazquez, A.; Arnoult, D. Mitochondrial dynamics regulate the RIG-I-like receptor antiviral pathway. *EMBO Rep.* **2010**, *11*, 133–138. [CrossRef] [PubMed]
91. Onoguchi, K.; Onomoto, K.; Takamatsu, S.; Jogi, M.; Takemura, A.; Morimoto, S.; Julkunen, I.; Namiki, H.; Yoneyama, M.; Fujita, T. Virus-infection or 5'ppp-RNA activates antiviral signal through redistribution of IPS-1 mediated by MFN1. *PLoS Pathog.* **2010**, *6*, e1001012. [CrossRef] [PubMed]
92. Arnoult, D. Mitochondrial fragmentation in apoptosis. *Trends Cell Biol.* **2007**, *17*, 6–12. [CrossRef] [PubMed]
93. Castanier, C.; Arnoult, D. Mitochondrial dynamics during apoptosis. *Med. Sci.* **2010**, *26*, 830–835.
94. Schrepfer, E.; Scorrano, L. Mitofusins, from Mitochondria to Metabolism. *Mol. Cell* **2016**, *61*, 683–694. [CrossRef] [PubMed]
95. Pickles, S.; Vigie, P.; Youle, R.J. Mitophagy and Quality Control Mechanisms in Mitochondrial Maintenance. *Curr. Biol.* **2018**, *28*, R170–R185. [CrossRef] [PubMed]
96. Youle, R.J.; Narendra, D.P. Mechanisms of mitophagy. *Nat. Rev. Mol. Cell Biol.* **2011**, *12*, 9–14. [CrossRef] [PubMed]
97. Gkikas, I.; Palikaras, K.; Tavernarakis, N. The Role of Mitophagy in Innate Immunity. *Front. Immunol.* **2018**, *9*, 1283. [CrossRef] [PubMed]
98. Chan, D.C. Mitochondria: Dynamic organelles in disease, aging, and development. *Cell* **2006**, *125*, 1241–1252. [CrossRef] [PubMed]
99. Twig, G.; Shirihai, O.S. The interplay between mitochondrial dynamics and mitophagy. *Antioxid. Redox Signal.* **2011**, *14*, 1939–1951. [CrossRef] [PubMed]
100. Hamanaka, R.B.; Chandel, N.S. Mitochondrial reactive oxygen species regulate cellular signaling and dictate biological outcomes. *Trends Biochem. Sci.* **2010**, *35*, 505–513. [CrossRef] [PubMed]
101. Tal, M.C.; Sasai, M.; Lee, H.K.; Yordy, B.; Shadel, G.S.; Iwasaki, A. Absence of autophagy results in reactive oxygen species-dependent amplification of RLR signaling. *Proc. Natl. Acad. Sci. USA* **2009**, *106*, 2770–2775. [CrossRef] [PubMed]
102. Elmore, S. Apoptosis: A review of programmed cell death. *Toxicol. Pathol.* **2007**, *35*, 495–516. [CrossRef] [PubMed]

103. Osellame, L.D.; Blacker, T.S.; Duchen, M.R. Cellular and molecular mechanisms of mitochondrial function. *Best Pract. Res. Clin. Endocrinol. Metab.* **2012**, *26*, 711–723. [CrossRef] [PubMed]
104. Weinberg, S.E.; Sena, L.A.; Chandel, N.S. Mitochondria in the regulation of innate and adaptive immunity. *Immunity* **2015**, *42*, 406–417. [CrossRef] [PubMed]
105. Mills, E.L.; Kelly, B.; O'Neill, L.A.J. Mitochondria are the powerhouses of immunity. *Nat. Immunol.* **2017**, *18*, 488–498. [CrossRef] [PubMed]
106. Sandhir, R.; Halder, A.; Sunkaria, A. Mitochondria as a centrally positioned hub in the innate immune response. *Biochim. Biophys. Acta Mol. Basis Dis.* **2017**, *1863*, 1090–1097. [CrossRef] [PubMed]
107. Angajala, A.; Lim, S.; Phillips, J.B.; Kim, J.H.; Yates, C.; You, Z.; Tan, M. Diverse Roles of Mitochondria in Immune Responses: Novel Insights Into Immuno-Metabolism. *Front. Immunol.* **2018**, *9*, 1605. [CrossRef] [PubMed]
108. Banoth, B.; Cassel, S.L. Mitochondria in innate immune signaling. *Transl. Res.* **2018**, *202*, 52–68. [CrossRef] [PubMed]
109. Anand, S.K.; Tikoo, S.K. Viruses as modulators of mitochondrial functions. *Adv. Virol.* **2013**, *2013*, 738794. [CrossRef] [PubMed]
110. Vu, L.D.; Gevaert, K.; De Smet, I. Protein Language: Post-Translational Modifications Talking to Each Other. *Trends Plant Sci.* **2018**. [CrossRef] [PubMed]
111. Marquez, J.; Lee, S.R.; Kim, N.; Han, J. Post-Translational Modifications of Cardiac Mitochondrial Proteins in Cardiovascular Disease: Not Lost in Translation. *Korean Circ. J.* **2016**, *46*, 1–12. [CrossRef] [PubMed]
112. Nesci, S.; Trombetti, F.; Ventrella, V.; Pagliarani, A. Post-translational modifications of the mitochondrial F1FO-ATPase. *Biochim. Biophys. Acta Gen. Subj.* **2017**, *1861*, 2902–2912. [CrossRef] [PubMed]
113. Komander, D.; Rape, M. The ubiquitin code. *Annu. Rev. Biochem.* **2012**, *81*, 203–229. [CrossRef] [PubMed]
114. Zimmermann, M.; Reichert, A.S. How to get rid of mitochondria: Crosstalk and regulation of multiple mitophagy pathways. *Biol. Chem.* **2017**, *399*, 29–45. [CrossRef] [PubMed]
115. Desai, S.; Juncker, M.; Kim, C. Regulation of mitophagy by the ubiquitin pathway in neurodegenerative diseases. *Exp. Biol. Med.* **2018**, *243*, 554–562. [CrossRef] [PubMed]
116. Harper, J.W.; Ordureau, A.; Heo, J.M. Building and decoding ubiquitin chains for mitophagy. *Nat. Rev. Mol. Cell Biol.* **2018**, *19*, 93–108. [CrossRef] [PubMed]
117. Escobar-Henriques, M.; Langer, T. Dynamic survey of mitochondria by ubiquitin. *EMBO Rep.* **2014**, *15*, 231–243. [CrossRef] [PubMed]
118. Ali, S.; McStay, G.P. Regulation of Mitochondrial Dynamics by Proteolytic Processing and Protein Turnover. *Antioxidants* **2018**, *7*, 15.
119. Heaton, S.M.; Borg, N.A.; Dixit, V.M. Ubiquitin in the activation and attenuation of innate antiviral immunity. *J. Exp. Med.* **2016**, *213*, 1–13. [CrossRef] [PubMed]
120. Liu, J.; Qian, C.; Cao, X. Post-Translational Modification Control of Innate Immunity. *Immunity* **2016**, *45*, 15–30. [CrossRef] [PubMed]
121. Johnson, E.S. Protein modification by SUMO. *Annu. Rev. Biochem.* **2004**, *73*, 355–382. [CrossRef] [PubMed]
122. Enserink, J.M. Regulation of Cellular Processes by SUMO: Understudied Topics. *Adv. Exp. Med. Biol.* **2017**, *963*, 89–97. [PubMed]
123. Zhao, X. SUMO-Mediated Regulation of Nuclear Functions and Signaling Processes. *Mol. Cell* **2018**, *71*, 409–418. [CrossRef] [PubMed]
124. Harder, Z.; Zunino, R.; McBride, H. Sumo1 conjugates mitochondrial substrates and participates in mitochondrial fission. *Curr. Biol.* **2004**, *14*, 340–345. [CrossRef] [PubMed]
125. Guo, C.; Hildick, K.L.; Luo, J.; Dearden, L.; Wilkinson, K.A.; Henley, J.M. SENP3-mediated deSUMOylation of dynamin-related protein 1 promotes cell death following ischaemia. *EMBO J.* **2013**, *32*, 1514–1528. [CrossRef] [PubMed]
126. Prudent, J.; Zunino, R.; Sugiura, A.; Mattie, S.; Shore, G.C.; McBride, H.M. MAPL SUMOylation of Drp1 Stabilizes an ER/Mitochondrial Platform Required for Cell Death. *Mol. Cell* **2015**, *59*, 941–955. [CrossRef] [PubMed]
127. Choi, S.G.; Kim, H.; Jeong, E.I.; Lee, H.J.; Park, S.; Lee, S.Y.; Lee, H.J.; Lee, S.W.; Chung, C.H.; Jung, Y.K. SUMO-Modified FADD Recruits Cytosolic Drp1 and Caspase-10 to Mitochondria for Regulated Necrosis. *Mol. Cell. Biol.* **2017**, *37*, e00254-16. [CrossRef] [PubMed]

128. Guerra de Souza, A.C.; Prediger, R.D.; Cimarosti, H. SUMO-regulated mitochondrial function in Parkinson's disease. *J. Neurochem.* **2016**, *137*, 673–686. [CrossRef] [PubMed]
129. Im, E.; Yoo, L.; Hyun, M.; Shin, W.H.; Chung, K.C. Covalent ISG15 conjugation positively regulates the ubiquitin E3 ligase activity of parkin. *Open Biol.* **2016**, *6*. [CrossRef] [PubMed]
130. Yoshizumi, T.; Imamura, H.; Taku, T.; Kuroki, T.; Kawaguchi, A.; Ishikawa, K.; Nakada, K.; Koshiba, T. RLR-mediated antiviral innate immunity requires oxidative phosphorylation activity. *Sci. Rep.* **2017**, *7*, 5379. [CrossRef] [PubMed]
131. Berry, B.J.; Trewin, A.J.; Amitrano, A.M.; Kim, M.; Wojtovich, A.P. Use the Protonmotive Force: Mitochondrial Uncoupling and Reactive Oxygen Species. *J. Mol. Biol.* **2018**, *430*, 3873–3891. [CrossRef] [PubMed]
132. He, C.; Carter, A.B. The Metabolic Prospective and Redox Regulation of Macrophage Polarization. *J. Clin. Cell. Immunol.* **2015**, *6*, 371. [CrossRef] [PubMed]